2012

Geochemistry of the Mesoarchean Fiskenaesset anorthosite complex and associated tonalite-trondhjemite-granodiorite (TTG) gneisses, southwestern Greenland

Hua Huang
University of Windsor

Geochemistry of the Mesoarchean Fiskenæsset anorthosite complex and associated tonalite-trondhjemite-granodiorite (TTG) gneisses, southwestern Greenland

By
Hua Huang

A Dissertation
Submitted to the Faculty of Graduate Studies
through Earth and Environmental Sciences
in Partial Fulfillment of the Requirements for
the Degree of Doctor of Philosophy at the
University of Windsor

Windsor, Ontario, Canada
2012

Geochemistry of the Mesoarchean Fiskenæsset anorthosite complex and associated tonalite-trondhjemite-granodiorite (TTG) gneisses, southwestern Greenland

by

Hua Huang

APPROVED BY:

Dr. J. Brenan, External Examiner
University of Toronto

Dr. J. Gauld
Department of Chemistry and Biochemistry

Dr. J. Gagnon
Department of Earth and Environmental Sciences

Dr. I. Samson
Department of Earth and Environmental Sciences

Dr. B. Fryer, Co-Advisor
Great Lakes Institute for Environmental Research

Dr. A. Polat, Co-Advisor
Department of Earth and Environmental Sciences

Dr. C. Senn, Chair of Defense
Department of Psychology and Women's Studies Program

16 May 2012

Declaration of Co-Authorship / Previous Publication

I. Co-Authorship Declaration

I hereby declare that this thesis incorporates material that is result of joint research, as follows:

The collaboration occurs in Chapter 2, 3 and 4 of this dissertation. These chapters contain material that is in press, in review and in preparation for publication. Field work was carried out with the co-operation of Ali Polat and with help from Ali Polat, Brian J. Fryer, Peter W.U. Appel and Brian F. Windley contributed to the thesis through criticism and revision of the original versions of the manuscripts. Field observations, laboratory analyses, data interpretation, key ideas and manuscript preparation were performed by the author.

I am aware of the University of Windsor Senate Policy on Authorship and I certify that I have properly acknowledged the contribution of other researchers to my thesis, and have obtained written permission from each of the co-author(s) to include the above material(s) in my thesis.

I certify that, with the above qualification, this thesis, and the research to which it refers, is the product of my own work.

II. Declaration of Previous Publication

This thesis includes 3 original papers that in press, in review and in preparation for publication. for publication in peer reviewed journals, as follows:

Thesis Chapter	Publication title/full citation	Publication status*
Chapter 2	**Hua Huang** (60%), Ali Polat (25%), Brian J. Fryer (8%), Peter W.U. Appel(2%) and Brian F. Windley (5%), Geochemistry of the Mesoarchean Fiskenæsset	In Press (Chemical Geology)

	Complex at Majorqap qâva, SW Greenland: Evidence for two different magma compositions	
Chapter 3	**Hua Huang** (65%), Brian J. Fryer (25%), Ali Polat (10%), Trace element chemistry of primary igneous hornblende, clinopyroxene and plagioclase from the Fiskenæsset Complex on Majorqap qâva, SW Greenland	In Preparation
Chapter 4	**Hua Huang** (65%), Ali Polat (25%), Brian J. Fryer (10%), Origin of the Archean tonalite–trondhjemite–granodiorite (TTG) suites and granites in the Fiskenæsset region, southern West Greenland: implication for the continental growth	In press (Gondwana Research)

I certify that I have obtained a written permission from the copyright owner(s) to include the above published material(s) in my thesis. I certify that the above material describes work completed during my registration as graduate student at the University of Windsor.

I declare that, to the best of my knowledge, my thesis does not infringe upon anyone's copyright nor violate any proprietary rights and that any ideas, techniques, quotations, or any other material from the work of other people included in my thesis, published or otherwise, are fully acknowledged in accordance with the standard referencing practices. Furthermore, to the extent that I have included copyrighted material that surpasses the bounds of fair dealing within the meaning of the Canada Copyright Act, I certify that I have obtained a written permission from the copyright owner(s) to include such material(s) in my thesis.

I declare that this is a true copy of my thesis, including any final revisions, as approved by my thesis committee and the Graduate Studies office, and that this thesis has not been submitted for a higher degree to any other University or Institution.

Abstract

This study presents new field, petrographic, and high precision geochemical data for the Mesoarchean Fiskenæsset Complex and spatially associated Mesoarchean to Neoarchean tonalite-trondhjemite-granodiorite (TTG) gneisses, in southwestern Greenland.

On the basis of textural evidence, whole-rock geochemical data, and the trace element compositions of hornblende, plagioclase and clinopyroxene, it is suggested that hornblende has a magmatic origin. On the basis of whole-rock major and trace element characteristics and the trace element compositions of hornblende grains, two distinct geochemical suites (Suite A and Suite B) are recognized in the Fiskenæsset Complex. Field observations, whole-rock geochemistry, and hornblende, plagioclase and clinopyroxene trace element compositions indicate that the Fiskenæsset Complex originated through fractionation of olivine, pyroxene and hornblende, and late crystallization of plagioclase. Injection of new mafic magmas into variably solidified anorthositic magmas and crystal mushes resulted in the formation of leucogabbros via magma mixing. The rocks of the Fiskenæsset Complex are characterized arc signature, consistent with a subduction zone geodynamic setting. The occurrence of magmatic hornblende throughout the sequence is consistent with a hydrous mantle source.

Orthogneisses in the Fiskenæsset region are composed of an older suite of metamorphosed TTGs, and a younger suite of high-K granites. The TTGs have high Al_2O_3, Na_2O and Sr but low Y contents. They also have highly fractionated REE patterns, enrichment of Sr and Pb, and depletion of Nb and Ti. The geochemical characteristics of the TTGs can be explained by partial melting of hydrous basalts at the base of a thickened oceanic island arc, leaving a rutile-bearing eclogitic residue. Field observations and geochemical modelling suggest that the spatially and temporarily associated tholeiitic basalts (now amphibolites) in the Fiskenæsset region might have been the sources of TTG melts.

The high-K granites have steep REE patterns and display variably negative Eu anomalies. Relatively high K_2O/Na_2O ratios in the granodiorites indicate that they were the source of the granites. Delamination of the eclogitic residue led to the loss of the lower crust and thereby triggering the subsequent basaltic underplating. Melting of the granodiorites in response to the basaltic underplating resulted in the generation of high-K granitic melts.

Acknowledgements

I would like to thank my dissertation advisors Dr. Ali Polat and Dr. Brian J. Fryer. They have been incredibly patient with me over the years and encouraged me even when I led myself to understand the details of the research project. I would like to thank Dr. Ali Polat again, for keeping me on the right track. I would like to thank the Geological Survey of Denmark and Greenland (GEUS), particularly Dr. Peter.W.U. Appel, Dr. Jochen Kolb and Dr. Per Kalvig.

I am highly grateful to my ex-supervisor Dr. Shan Gao who showed me the way of geochemical research.

I would like to thank the committee member. Especially, I am highly grateful to Dr Iain Samson who helped me identifying minerals in the section for many times.

I would like to thank the Department of Earth and Environmental Sciences for providing me with the opportunity to gain valuable teaching experience as a teaching assistant. I would also like to thank all the faculty, staff members and graduate students in the Department of Earth and Environmental Sciences for their support.

I would like to acknowledge two special people who made incredible sacrifices for me. My wife had to part with my company for many years when I moved to Windsor and my son gave me some fun for relaxing. I am so thankful for their support through the years. This accomplishment is really for the two of them.

Thanks to Dr. Zhaoping Yang, Mr. J.C. Barrett and Dr. Mohamed El-Sayed Shaheen for their help during ICP-MS and LA-ICP-MS analyses. Thanks to Ms. Sharon Lackie for her help in using environmental scanning electron microscope.

Table of Contents

List of Tables

List of Figures

CHAPER 1

Introduction

1.1. Background on Archean anorthosites

Anorthosites characterized by calcic (usually >An_{80}) plagioclase occur in most Archean cratons (Ashwal, 1993; Ashwal et al., 1994; Phinney et al., 1988). Archean anorthosites constitute major part of large layered igneous complexes, with relatively thin ultramafic sequence and thick gabbroic–anorthositic units. In the field, Archean anorthosites are usually intruded by granitoid gneisses. The origin of Archean anorthosites is a longstanding problem (Ashwal, 1993; Ashwal et al., 1994; Phinney et al., 1988; and references therein). The traditional view has been that Archean anorthosites form from the residual liquid following the crystallization of olivine and pyroxene from an anhydrous basaltic melt (Ashwal, 1993; Ashwal et al., 1994; Phinney et al., 1988). However, studies on the anorthosite complexes, especially those from the Archean high-grade gneiss complexes in SW Greenland, revealed the involvement of hydrous parental magmas in the generation of the anorthosite complexes, which is indicated by the primary crystallization of hornblende (Windley et al. 1973; Windley and Smith 1974; Polat et al., 2009, 2010, 2011a, 2012; Rollinson, 2010; Hoffmann et al., 2012).

The Fiskenæsset Complex is one of the calcic anorthosite layered complexes which are well exposed in the Archean craton of SW Greenland (Fig. 1.1). The best-preserved stratigraphic section of the Fiskenæsset Complex is located at Majorqap qâva. Although pervious studies on the mineral chemistry were conducted on rocks from Majorqap qâva (Myers and Platt, 1977), the lack of high precision of trace element geochemical data (e.g., Nb, Ta, V, Co, Sc, Pr, Er, Ho) used to distinguish between different geodynamic settings have hampered the attempts to understand the generation of Archean anorthosites. In order to improve our understanding of the petrogenesis of Archean anorthosites, I have characterized in detail the field, petrographic, and geochemical signatures of the

Fiskenæsset Complex at Majorqap qâva in the Fiskenæsset region of SW Greenland (Fig. 1.1). This study reports detailed field and petrographic observations, whole-rock major and trace element geochemical data, and mineral trace element geochemical data for the anorthosites, leucogabbros, gabbros, hornblendites, pyroxenites, dunites, and peridotites of the Fiskenæsset Complex at Majorqap qâva, to understand its petrogenesis and geodynamic setting.

1.2. Background on Archean tonalite-trondhjemite-granodiorite suites (TTGs)

TTGs are extensively widespread in the Archean cratons and they represent the largest portion (>80%) of preserved Archean continental crust (Martin et al., 2005). Understanding the origin of Archean TTGs is important for determining the origin of continental crust and assessing the nature of the geodynamic processes that were operative in the Archean. The key geochemical characteristics of Archean TTGs include strong fractionation of light rare-earth elements (LREE) from heavy rare-earth elements (HREE), high Sr/Y and La/Yb and negative Ti-Nb-Ta anomalies (Martin et al., 2005 and references therein). The origin of these geochemical variations is still under debate. For instance, researchers have proposed that the geochemical features of Archean TTGs are either a result of partial melting of garnet-bearing amphibolite or a result of partial melting of rutile-bearing eclogite (Martin, 1994; Sen and Dunn, 1994; Rapp and Watson, 1995; Martin, 1999; Rapp et al., 1999; Foley et al., 2002; Klemme et al., 2002; Rapp et al., 2003; Xiong, 2006; Foley, 2008; Hoffmann et al., 2011). Accordingly, a variety of melt generation scenarios have been proposed based upon the trace element composition of TTGs, including subducted oceanic crust, the lower portion of thickened arc crust, and mafic roots of an oceanic plateau (Jahn et al., 1981; Martin, 1994; Rapp and Watson, 1995; Martin, 1999; Smithies, 2000; Foley et al., 2002; Whalen et al., 2002; Rapp et al., 2003; Martin et al., 2005; Bédard, 2006; Moyen and Stevens, 2006).

In the Fiskenæsset region, as in many Archean terrains, the granitoid plutons

including TTGs and granites are closely associated with tholeiitic volcanics and the Fiskenæsset Complex. On a regional scale, the predominant granitoid gneisses occupy over 80% of the region (Myers, 1976; Myers, 1985). However, geochemical investigations focusing the widespread granitoid gneisses bordering the Fiskenæsset Complex are scarce. As a result, the petrogenesis of the granitoid plutons is not yet well constrained. In this study I have investigated the geochemistry of the Fiskenæsset granitoid rocks to address the nature of the protolith, the conditions of granitoid genesis, and understand the formation of Archean continental crust.

1.3. Background on the Fiskenæsset Complex and associated orthogneisses of the Fiskenæsset region, SW Greenland

The Fiskenæsset Complex and associated orthogneisses are located in the Archean craton of SW Greenland. Archean (ca. 3.8-2.7 Ga) TTG orthogneisses containing many layers of amphibolite and anorthosite, both up to ca. 2 km thick, together with rare meta-sedimentary rocks, dominate the Archean craton of SW Greenland (e.g., Bridgwater et al., 1976; Friend and Nutman, 2005a; Garde, 2007; Friend et al., 2009). Geological, geochronological and geochemical studies in the Archean crust in SW Greenland have established four Eoarchean, two Mesoarchean, and two Neoarchean terranes (Nutman et al., 2004; Friend and Nutman, 2005a, b; Nutman and Friend, 2007; Windley and Garde, 2009). However, from the perspective of metamorphic facies, Windley and Garde (2009) divided the Archean craton of SW Greenland into six Mesoarchean to Neoarchean crustal blocks. From south to north these include the Ivittuut, Kvanefjord, Bjørnesund, Sermilik, Fiskefjord, and Maniitsoq blocks. The Fiskenæsset region is located in the Bjørnesund block. The Fiskenæsset region consists of ~80% granitoid orthogneisses, ~15% amphibolites, and ~5% Fiskenæsset Complex including anorthosite, leucogabbro, gabbro and ultramafic rocks (peridotite, dunite, pyroxenite, hornblendite) (Kalsbeek and Myers, 1973; Windley and Smith, 1974; Myers, 1985; Windley and Garde, 2009; Polat et al.,

2011b). The Fiskenæsset Complex is one of the most well-exposed Archean anorthosite complexes in the world (Windley et al., 1973; Myers, 1985;). Within the Fiskenæsset Complex, one of the best-preserved stratigraphic sequences is at Majorqap qava, which have been used as a model for the Archean anorthosite petrogenesis. The Fiskenæsset Complex is composed of six major lithostratigraphic units which are, from the bottom to the top: Lower Gabbro (50 m), Ultramafic (40 m), Lower leucogabbro (50 m), Middle gabbro (40 m), Upper Leucogabbro (60 m), and Anorthosite (250 m) Units (Myers, 1985).

The oldest rocks in the Fiskenæsset region are amphibolites which were derived from tholeiitic volcanic rocks and locally contain well-preserved remnants of pillow structures. The Fiskenæsset Complex was emplaced into these basic metavolcanic rocks (Escher and Myers, 1975; V.J. van Hinsberg and B.F. Windley in Keulen et al., 2011). The subsequent granitoid gneisses with TTG affinity intruded into the metavolcanic amphibolites and the Fiskenæsset Complex as sheet-like body (Steenfelt et al., 2005; Næraa and Scherstén, 2008; Friend et al., 2009; Huang et al., 2012). At Majorqap qâva a large number of hornblenditic pegmatite pipes and dykes transect the part of the Fiskenæsset Complex (Myers, 1985). At several localities on Qeqertarssuatsiaq island and in the Itise area ultramafic layers are cross cut by a network of thin hornblendite veins (Polat et al., 2012).

Three major fold phases including an early large scale recumbent fold and two late sets of folds with steep axial surfaces at high angles to each other resulted in spectacular km-scale fold interference patterns (Kalsbeek and Myers, 1973; Windley and Smith, 1974; Myers, 1985).

During Mesoarchean to Neoarchean (ca. 2.85-2.66 Ga), a large portion of the Fiskenæsset region was affected by the regional high grade metamorphism, locally up to granulite facies and underwent retrogression to amphibolite facies (Black et al., 1973; Moorbath and Pankhurst, 1976; Riciputi et al., 1990; McGregor and Friend, 1992).

Herr et al. (1967) reported a Re–Os age of 3.08±0.07 Ga from the molybdenites in the Fiskenæsset anorthosite. Gancarz (1976) acquired a Pb-Pb isochron age of 2.75 Ga from plagioclase and hornblende separates from the Fiskenæsset anorthosites and leucogabbros. A five-point mixed whole-rock and mineral Sm-Nd isochron age of 2.86±0.05 Ga were acquired for the time of primary crystallization of the Fiskenæsset Complex. Anorthosites, leucogabbros, gabbros and ultramafic rocks from the Fiskenæsset Complex on Qeqertarssuatsiaq island have yielded 2.97±0.02 Ga and 2.94±0.03 Ga Sm-Nd and Pb-Pb isotope regression ages, respectively, (Polat et al., 2010). Zircons from a hornblenditic pegmatite pipe intruding part of the Fiskenæsset Complex on Majorqap qâva yielded a $^{207}Pb/^{206}Pb$ age of 2.87 Ga, and the inherited zircons are ca. 2.95 Ga old, which is in agreement with the Sm-Nd and Pb-Pb intrusion age of the Fiskenæsset Complex (Keulen et al. 2010). A Rb/Sr whole-rock age of 2.88 Ga was reported for the orthogneisses intruding the Fiskenæsset Complex (Moorbath and Pankhurst, 1976). Zircon studies from two granitoid gneisses samples surrounding the Fiskenæsset Complex in the Sinarssuk area indicate that granitoid gneisses are at least ca. 2.95 Ga old (Polat et al., 2010). Inherited zircons from these two samples have older ages from 3.2 to 3.0 Ga and the metamorphic zircons of overgrowth and recrystallization yield younger ages between 2.94 and 2.65 Ga (Polat et al., 2010).

1.4. Objectives

The main objective of this study to understand the origin of the Fiskenæsset Complex and spatially associated orthogneisses in SW Greenland. This study uses new field and petrographic observations, whole-rock major and trace element geochemical data and mineral trace element geochemical data from the Fiskenæsset Complex and associated orthogneisses of the Fiskenæsset region to better constrain:

1. The geochemical characteristics of rocks from the Fiskenæsset Complex
2. The chemostratigraphy of the Fiskenæsset Complex

3. The trace element mineral chemistry of hornblende, clinopyroxene and plagioclase from the Fiskenæsset Complex

4. The significance of the hornblende in the formation of the Fiskenæsset Complex

5. Tectonic settings in which the Fiskenæsset Complex formed

6. The nature of the mantle source from which the Fiskenæsset Complex was derived

7. The chemical composition and the source of TTG gneisses

8. The geochemical relationship between the amphibolites and TTG gneisses

9. The geodynamic setting of the TTG gneisses

10. The role of Archean anorthosite and the orthogneisses in continental crust growth and mantle evolution in SW Greenland

1.5. Outline of thesis structure

This thesis consists of 5 chapters. Each of the core chapters is presented in paper format which results in some repetition in the analytical procedure, geological background and references.

Chapter 1 is the introduction for the thesis.

Chapter 2 presents high precision major and trace element geochemical data for the six major stratigraphic units of the Fiskenæsset Complex at Majorqap qâva, SW Greenland. The geochemical data were used to understand the primary magmatic geochemical signatures. Detailed field work and petrographic observations together with the whole-rock geochemical data indicate hornblende is a primary magmatic mineral which precipitated from hydrous magmas. Geochemical reversals, defined by increased bulk rock Mg#, Cr, Ni and HREE concentrations, mainly occur in the Middle Gabbro Unit. Combined with the whole-rock major and trace element geochemical data, two distinct geochemical suites (Suites A and B) were recognized. This Chapter has been accepted by Chemical Geology. It is currently under revision.

Chapter 3 discusses trace element geochemistry of hornblende, clinopyroxene and

plagioclase and demonstrates that all the minerals retain their primary geochemical signature. The presence of two distinct petrogenetic suites of rocks from the six units of the Majorqap qâva section has been further confirmed using trace element chemistry of hornblende. HREE-depleted hornblende occurs in the earlier Suite A, whereas HREE-enriched hornblende appears in the later Suite B. This chapter is in preparation and will be submitted to Geochimica et Cosmochimica Acta in two to three weeks.

Chapter 4 discusses the field and geochemical characteristics of orthogneisses in the Fiskenæsset region. The orthogneisses are composed of main TTGs and minor high-K granites. The TTGs are considered as a result of partial melting of amphibolite with rutile-bearing eclogite residue on the basis of their geochemical characteristics and the trace element modeling. The late high-K granites are interpreted as the product of partial melting of granodiorites during mafic magma underplating. This chapter was accepted as a research article in Gondwana Research and is in press now (published online).

Chapter 5 presents a summary of the study.

1.6. References

Ashwal, L.D., Jacobsen, S.B., Myers, J.S., Kalsbeek, F., Goldstein, S.J., 1989. Sm-Nd age of the Fiskenæsset Anorthosite Complex, West Greenland. Earth and Planetary Science Letters 91(3-4): 261-270.

Ashwal, L.D., 1993. Anorthosites. Minerals and Rocks Series, 21. Springer-Verlag, Berlin, 422 pp.

Ashwal, L.D., Myers, J.S., Condie, K.C., 1994. Chapter 8 Archean anorthosites, Developments in Precambrian Geology. Elsevier, pp. 315-355.

Black, L.P., Moorbath, S., Pankhurs.Rj, Windley, B.F., 1973. $^{207}Pb/^{206}Pb$ whole Rock Age of the Archaean Granulite Facies Metamorphic Event in West Greenland. Nature-Physical Science 244(134): 50-53.

Bédard, J.H., 2006. A catalytic delamination-driven model for coupled genesis of Archaean crust and sub-continental lithospheric mantle. Geochimica et Cosmochimica

Acta 70(5): 1188-1214.

Bridgwater, D., Keto, L., McGregor, V.R., Myers, J.S., 1976. Archaean gneiss complex of Greenland. In: Escher, A., Watt, W.S. (Eds.), Geology of Greenland. Geological Survey of Greenland, Copenhagen, pp. 19-75.

Escher, J.C., Myers, J.S., 1975. New evidence concerning the original relationships of early Precambrian volcanics and anorthosites in the Fiskenæsset region, southern West Greenland. Bulletin Grønlands Geologiske Undersøgelse 75: 72-76.

Foley, S., Tiepolo, M., Vannucci, R., 2002. Growth of early continental crust controlled by melting of amphibolite in subduction zones. Nature 417(6891): 837-840.

Foley, S., 2008. A trace element perspective on Archean crust formation and on the presence or absence of Archean subduction. Geological Society of America Special Papers 440: 31-50.

Friend, Clark R.L., Nutman, Allen P., 2005a. Complex 3670–3500 Ma Orogenic Episodes Superimposed on Juvenile Crust Accreted between 3850 and 3690 Ma, Itsaq Gneiss Complex, Southern West Greenland. The Journal of Geology 113(4): 375-397.

Friend, C.R.L., Nutman, A.P., 2005b. New pieces to the Archaean terrane jigsaw puzzle in the Nuuk region, southern West Greenland: steps in transforming a simple insight into a complex regional tectonothermal model. Journal of the Geological Society 162(1): 147-162.

Friend, C.R.L., Nutman, A.P., Baadsgaard, H., Duke, M.J.M., 2009. The whole rock Sm-Nd 'age' for the 2825 Ma Ikkattoq gneisses (Greenland) is 800 Ma too young: Insights into Archaean TTG petrogenesis. Chemical Geology 261(1-2): 61-75.

Garde, A.A., 1997. Accretion and evolution of an Archaean high-grade grey gneissamphibolite complex: the Fiskefjord area, southern West Greenland. Geology of Greenland Survey Bulletin 177.

Hoffmann, J.E., Münker, C., Næraa, T., Rosing, M.T., Herwartz, D., Garbe-Schönberg, D., Svahnberg, H., 2011. Mechanisms of Archean crust formation inferred from

high-precision HFSE systematics in TTGs. Geochimica et Cosmochimica Acta 75(15): 4157-4178.

Hoffmann, J.E., Svahnberg, H., Piazolo, S., Scherstén, A., Münker, C., 2012. The geodynamic evolution of Mesoarchean anorthosite complexes inferred from the Naajat Kuuat Complex, southern West Greenland. Precambrian Research 196–197(0): 149-170.

Huang, H., Polat, A., Fryer, B.J., 2012. Origin of Archean tonalite–trondhjemite–granodiorite (TTG) suites and granites in the Fiskenæsset region, southern West Greenland: Implications for continental growth. Gondwana Research doi:10.1016/j.gr.2011.12.001.

Jahn, B.M., Glikson, A.Y., Peucat, J.J., Hickman, A.H., 1981. REE geochimistry and isotopic data of Archean silicic volcanics and granitoids from the Pilbara Block, Western Australia: implications for the early crustal evolution. Geochimica et Cosmochimica Acta 45(9): 1633-1652.

Kalsbeek, F., Myers, J.S., 1973. The geology of the Fiskenæsset region. Rapport Grønlands Geologiske Undersøgelse 51: 5-18.

Keulen, N., Naeraa, T., Kokfelt, T.F., Schumacher, J.C., Scherstén, A., 2010. Zircon record of the igneous and metamorphic history of the Fiskenæsset anorthosite complex in southern West Greenland. Geological Survey of Denmark and Greenland Bulletin(20): 67-70. Keulen, N., Kokfelt, T.F., the homogenisation team, 2011. A seamless, digital, internet-based geological map of South-West and southern West Greenland, 1:100 000, 61°30′ – 64°. http://geuskort.geus.dk/gisfarm/svgrl.jsp. Copenhagen: Geological Survey of Denmark and Greenland.

Klemme, S., Blundy, J.D., Wood, B.J., 2002. Experimental constraints on major and trace element partitioning during partial melting of eclogite. Geochimica et Cosmochimica Acta 66(17): 3109-3123.

Martin, H., 1994. Chapter 6 The Archean Grey Gneisses and the Genesis of Continental

Crust. In: Condie, K.C. (Ed.), Developments in Precambrian Geology. Elsevier, pp. 205-259.

Martin, H., 1999. Adakitic magmas: modern analogues of Archaean granitoids. Lithos 46(3): 411-429.

Martin, H., Smithies, R.H., Rapp, R., Moyen, J.F., Champion, D., 2005. An overview of adakite, tonalite-trondhjemite-granodiorite (TTG), and sanukitoid: relationships and some implications for crustal evolution. Lithos 79(1-2): 1-24.

McGregor, V.R., Friend, C.R.L., 1992. Late Archean Prograde Amphibolite- to Granulite-Facies Relations in the Fiskenæsset Region, Southern West Greenland. The Journal of Geology 100(2): 207-219.

Moorbath, S., Pankhurst, R.J., 1976. Further rubidium-strontium age and isotope evidence for the nature of the late Archaean plutonic event in West Greenland. Nature 262(5564): 124-126.

Moyen, J.F., Stevens, G., 2006. Experimental constraints on TTG petrogenesis: Implications for Archean geodynamics. In: Benn, K., Mareschal, J.C., Condie, K.C. (Eds.), Archean Geodynamics and Environments. Geophysical Monograph Series, pp. 149-175.

Myers, J.S., 1976. Granitoid sheets, thrusting, and Archean crustal thickening in West Greenland. Geology 4(5): 265-268.

Myers, J.S., Platt, R.G., 1977. Mineral chemistry of layered Archaean anorthosite at Majorqap qava, near Fiskenæsset, southwest Greenland. Lithos 10(1): 59-72.

Myers, J.S., 1985. Stratigraphy and structure of the Fiskenæsset complex, southernWest Greenland. Bulletin Grønlands Geologiske Undersøgelse 150: 1-72.

Naeraa, T., Scherstén, A., 2008. New zircon ages from the Tasiusarsuaq terrane, southern West Greenland. Geological Survey of Denmark and Greenland Bulletin(15): 73-76.

Nutman, A.P., Friend, C.R.L., Barker, S.L.L., McGregor, V.R., 2004. Inventory and assessment of Palaeoarchaean gneiss terrains and detrital zircons in southern West

Greenland. Precambrian Research 135(4): 281-314.

Nutman, A.P., Friend, C.R.L., 2007. Adjacent terranes with ca. 2715 and 2650 Ma high-pressure metamorphic assemblages in the Nuuk region of the North Atlantic Craton, southern West Greenland: Complexities of Neoarchaean collisional orogeny. Precambrian Research 155(3–4): 159-203.

Phinney, W.C., Morrison, D.A., Maczuga, D.E., 1988. Anorthosites and related megacrystic units in the evolution of Archean crust. Journal of Petrology 29(6): 1283-1323.

Polat, A., Appel, P.W.U., Fryer, B., Windley, B., Frei, R., Samson, I.M., Huang, H., 2009. Trace element systematics of the Neoarchean Fiskenæsset anorthosite complex and associated meta-volcanic rocks, SW Greenland: Evidence for a magmatic arc origin. Precambrian Research 175(1-4): 87-115.

Polat, A., Frei, R., Scherstén, A., Appel, P.W.U., 2010. New age (ca. 2970 Ma), mantle source composition and geodynamic constraints on the Archean Fiskenæsset anorthosite complex, SW Greenland. Chemical Geology 277(1-2): 1-20.

Polat, A., Fryer, B.J., Appel, P.W.U., Kalvig, P., Kerrich, R., Dilek, Y., Yang, Z., 2011a. Geochemistry of anorthositic differentiated sills in the Archean (~ 2970 Ma) Fiskenæsset Complex, SW Greenland: Implications for parental magma compositions, geodynamic setting, and secular heat flow in arcs. Lithos 123(1-4): 50-72.

Polat, A., Appel, P.W.U., Fryer, B.J., 2011b. An overview of the geochemistry of Eoarchean to Mesoarchean ultramafic to mafic volcanic rocks, SW Greenland: Implications for mantle depletion and petrogenetic processes at subduction zones in the early Earth. Gondwana Research 20, 255-283.

Polat, A., Fryer, B.J., Samson, I.M., Weisener, C., Appel, P.W.U., Frei, R., Windley, B.F., 2012. Geochemistry of ultramafic rocks and hornblendite veins in the Fiskenæsset layered anorthosite complex, SW Greenland: Evidence for hydrous upper mantle in the Archean. Precambrian Research doi:10.1016/j.precamres.2011.11.013.

Rapp, R.P., Watson, E.B., 1995. Dehydration melting of metabasalt at 8-32 kbar: Implications for continental growth and crust-mantle recycling. Journal of Petrology 36(4): 891-931.

Rapp, R.P., Shimizu, N., Norman, M.D., 2003. Growth of early continental crust by partial melting of eclogite. Nature 425(6958): 605-609.

Riciputi, L.R., Valley, J.W., McGregor, V.R., 1990. Conditions of Archean granulite metamorphism in the Godthab-Fiskenaesset region, southern West Greenland. Journal of Metamorphic Geology 8(2): 171-190.

Rollinson, H., 2010. Coupled evolution of Archean continental crust and subcontinental lithospheric mantle. Geology 38(12): 1083-1086.

Rollinson, H., Reid, C., Windley, B., 2010. Chromitites from the Fiskenæsset anorthositic complex, West Greenland: clues to late Archaean mantle processes. Geological Society, London, Special Publications 338(1): 197-212.

Sen, C., Dunn, T., 1994. Dehydration melting of a basaltic composition amphibolite at 1.5 and 2.0 GPa: implications for the origin of adakites. Contributions to Mineralogy and Petrology 117(4): 394-409.

Steenfelt, A., Garde, A.A., Moyen, J.-F., 2005. Mantle wedge involvement in the petrogenesis of Archaean grey gneisses in West Greenland. Lithos 79(1-2): 207-228.

Windley, B.F., Herd, R.K., Bowden, A.A., 1973. The Fiskenæsset complex,West Greenland, Part 1. A preliminary study of the stratigraphy, petrology, and whole-rock chemistry from Qeqertarssuatsiaq Bulletin Grønlands Geologiske Undersøgelse 106: 80.

Windley, B.F., Smith, J.V., 1974. The Fiskenæsset Complex, West Greenland,Part II: General mineral chemistry from Qeqertarssuatsiaq. Bulletin Grønlands Geologiske Undersøgelse 108: 1-54.

Windley, B.F., Garde, A.A., 2009. Arc-generated blocks with crustal sections in the North Atlantic craton of West Greenland: Crustal growth in the Archean with modern

analogues. Earth-Science Reviews 93(1-2): 1-30.

Xiong, X.-L., 2006. Trace element evidence for growth of early continental crust by melting of rutile-bearing hydrous eclogite. Geology 34(11): 945-948.

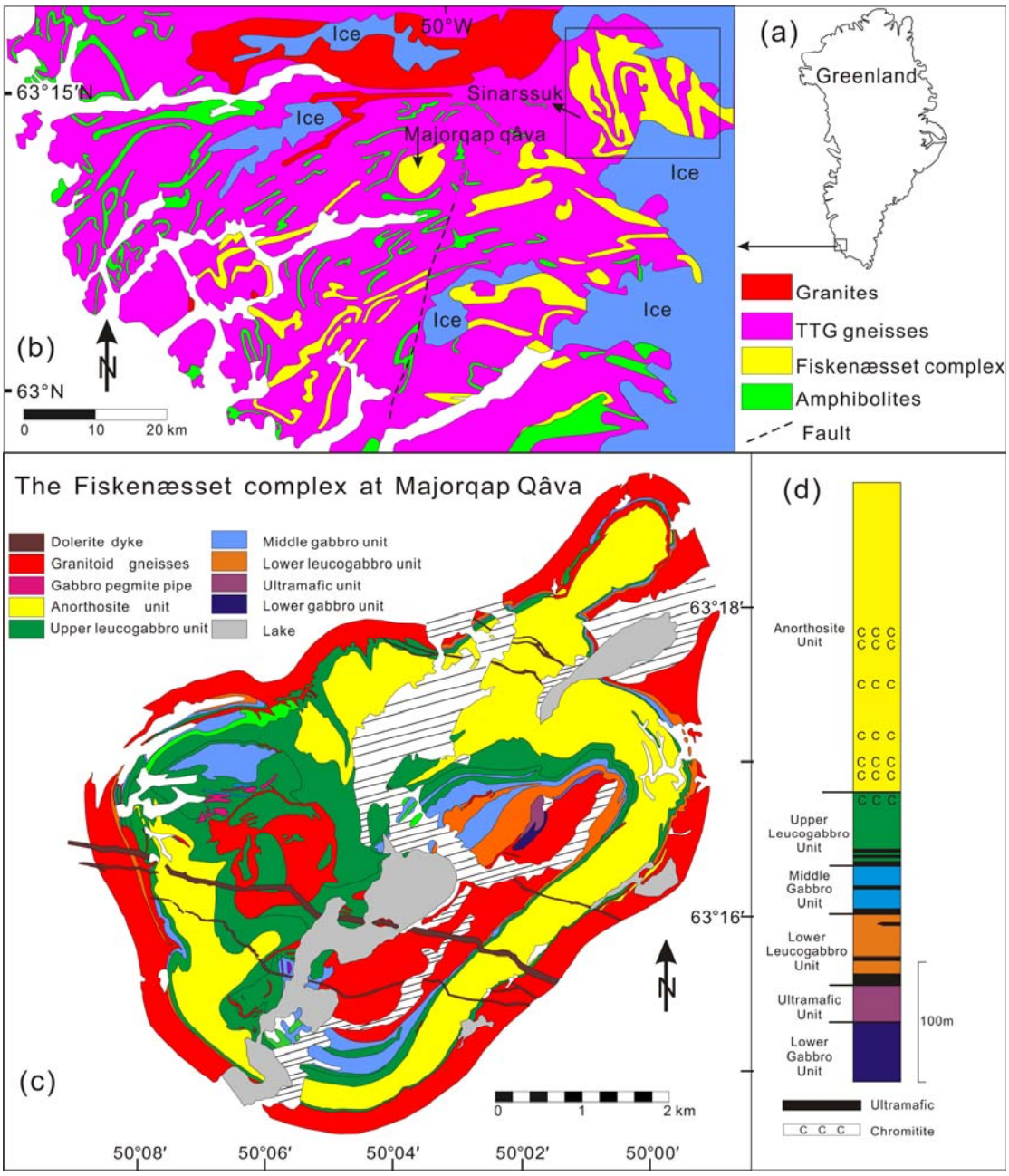

Fig 1.1. (a) General location of the study area in Greenland. (b) Simplified geological map of the Fiskenæsset region (after Myers, 1976)**.** (c) Simplified geological map of the Majorqap qâva outcrop of the Fiskenæsset Complex (after Myers, 1985). (d) Simplified stratigraphic succession of the Fiskenæsset Complex compiled from a number of outcrops (after Myers, 1985). The diagonal lines represent the Quaternary deposits.

CHAPTER 2

Geochemistry of the Mesoarchean Fiskenæsset Complex at Majorqap qâva, SW Greenland: Evidence for two different magma compositions

2.1. Introduction

Archean layered intrusions in high-grade gneissic terranes are predominantly composed of anorthosites, leucogabbros, gabbros, and peridotites; anorthosites are the major component (Windley and Smith, 1976; Ashwal, 1993; Ashwal et al., 1994; Myers, 1988; Phinney et al., 1988). Although subsequent tonalite–trondhjemite–granodiorite (TTG) intrusions have removed most of their stratigraphy, and deformation and metamorphism have modified many original structures, the primary igneous mineralogy, textures, structures, and contact relationships are still surprisingly well preserved in several complexes. Anorthosites are best known from the Archean high-grade gneiss complexes in SW Greenland, Canada, Australia, India, and South Africa (Hor et al., 1975; Phinney et al., 1988; Myers, 1985, 1988; Kinny et al., 1988; Ashwal, 1993; Ashwal et al., 1994; Barton et al., 1996; Sajeev et al., 2009; Hoffman et al., 2012). Modern equivalents of Archean anorthosites are found in xenoliths brought up from the magma chambers of extant island arcs as in the Lesser Antilles (e.g. Kiddle et al., 2010), and in Paleozoic analogs in New Zealand (Gibson and Ireland, 1999).

Calcic anorthosite layered complexes are particularly widespread in the Archean craton of SW Greenland (Fig. 2.1), where they provide important constraints on petrogenetic and geodynamic processes that operated in the early Earth (Windley and Smith, 1974; Myers, 1985; Ashwal, 1993; Polat et al., 2009, 2010; Hoffmann et al., 2011). Despite their abundance, only the Fiskenæsset and Naajat Kuuat complexes have been intensively investigated (e.g., Windley et al. 1973; Windley and Smith 1974; Henderson et al. 1976; Myers and Platt 1977; Weaver et al. 1981; Myers 1985; Ashwal et al. 1989;

Polat et al., 2009, 2010, 2011a,b; Hoffmann et al., 2012).

The best-preserved stratigraphic section of the Fiskenæsset Complex is at Majorqap qâva (Myers, 1985) (Fig. 2.1), where primary magmatic and structural features are remarkably well developed (Figs. 2.2 and 2.3). Although some early studies of the mineral chemistry were conducted on rocks from Majorqap qâva (Myers and Platt, 1977), today we are able to undertake much higher precision analyses of several petrogenetically important elements (e.g., Nb, Ta, U, Th, V, Co, Sc, Pr, Er, Ho), which enable us to distinguish between different magma types that are diagnostic of specific geodynamic environments such as mid-ocean ridges, ocean islands and subduction zones.

This paper presents new whole-rock geochemical data from all major stratigraphic units of the Mesoarchean Fiskenæsset Complex at Majorqap qâva, as a result of our extensive new field work on the complex in this region (Fig. 2.1; Supplementary Fig. 2. 1). In addition, we report new high precision trace element data for hornblendes from three units: Lower Gabbro, Ultramafic, and Middle Gabbro. New geochemical data reveal the presence of two distinct suites derived from differentiation of primary magmas that originated from different sources in a Mesoarchean sub-arc mantle wedge.

2.2. Regional geology, field characteristics, metamorphism, and geochronology

The Fiskenæsset region consists of ~80% granitoid orthogneiss, ~15% amphibolite, and ~5% anorthosite, leucogabbro, gabbro and ultramafic rocks including peridotite, dunite, pyroxenite, and hornblendite (Kalsbeek and Myers, 1973; Windley and Smith, 1974; Myers, 1985; Windley and Garde, 2009; Polat et al., 2011a). Most of the Fiskenæsset region underwent granulite facies metamorphism and subsequent amphibolite facies retrogression (Pidgeon and Kalsbeek, 1978; Riciputi et al., 1990; McGregor and Friend, 1992). However, for descriptive simplicity in this study igneous names are used for all rocks in the Fiskenæsset Complex without the prefix “meta”.

The Fiskenæsset Complex, where best preserved, retains a primary, igneous, layered

stratigraphy (Myers, 1985). Main geological characteristics and field relationships of the complex at Majorqap qâva are presented in Figs. 2.2 and 2.3. The complex was intruded mostly by sheets of TTG composition (Steenfelt et al., 2005; Næraa and Scherstén, 2008; Friend et al., 2009; Huang et al., 2011). These intrusions were deformed and metamorphosed into the regional orthogneisses during Mesoarchean-Neoarchean tectonothermal events (Myers, 1985; Polat et al., 2010). Contacts between the host orthogneisses and the Fiskenæsset Complex and amphibolites are marked mainly by shear zones (Figs. 2a and b). In spite of three phases of isoclinal folding, and amphibolite to granulite facies metamorphism, much of the Fiskenæsset Complex locally retains cumulate textures, phase layering, mineral grading, channel deposits, and cross-cutting relationships (Figs. 2 and 3; Windley et al., 1973; Myers, 1976, 1985; Ghisler, 1976; Polat et al., 2009, 2011a, b). A variety of field, geochemical, and isotopic data indicate that the Fiskenæsset Complex was emplaced into Archean oceanic crust (Escher and Myers, 1975; Peck and Valley, 1996).

Three major episodes of isoclinal to tight folding of all rocks resulted in spectacular km-scale recumbent F_1 isoclines, fold interference patterns, and associated thrusts (Kalsbeek and Myers, 1973; Windley and Smith, 1974; Myers, 1985). Subsequently, the protoliths of the TTG gneisses intruded the Fiskenæsset Complex during large-scale isoclinal F_2 folding. Finally, large-scale F_3 folds refolded the F_1 and F_2 structures, giving rise to fold interference patterns (Kalsbeek and Myers, 1973; Myers, 1985). However, all stages of the deformation were heterogeneous leaving rocks that range from undeformed to extremely deformed.

The best-preserved stratigraphic sequence of the Fiskenæsset Complex is at Majorqap qâva. A generalized stratigraphic log (Fig. 2.1d) was based on a major study at Majorqap qâva (Myers, 1985). In ascending order, there are six major lithostratigraphic units: Lower Gabbro (50 m), Ultramafic (40 m), Lower Leucogabbro (50 m), Middle Gabbro (40 m), Upper Leucogabbro (60 m), Anorthosite (250 m) (Fig. 2.1d) (Myers,

1985).

An important observation relevant to the discussion below of the geochemical evidence for two magmatic suites in the complex is the fact that the layered rocks in most of the major units are transected by a variety of anorthositic, gabbroic, and ultramafic dykes and sills, which are up to about two metres wide. An intense swarm of hornblendite sills intruded layered dunites and peridotites of the Ultramafic Unit with a 60 cm-wide hornblendite sill every one metre (Figs. 2.2 and 2.3). These sills can be distinguished from cumulate layers by their thin discordant contacts, apophyses, and xenoliths of dunite.

The Lower Gabbro Unit includes the most deformed rocks among the sampled stratigraphic units of the complex. It is strongly foliated and extensively recrystallized (see also Myers, 1985). Accordingly, it is difficult to recognize its protolith in the field.

Mineral grading and magmatic layers are particularly well preserved in the Ultramafic and Middle Gabbro Units (Figs. 2.2 and 2.3). The Middle Gabbro Unit displays interfingered gabbros and leucogabbros with rounded and wavy contacts (Fig. 2.3a). In the Middle Gabbro Unit gabbros contain rounded inclusions of leucogabbros; and leucogabbros, in turn, have gabbroic inclusions; these field relationships may have resulted from magma mixing. The Upper Leucogabbro Unit contains large plagioclase crystals enclosed in a hornblende matrix (Figs. 2.3b and c), as well as slump structures (Fig. 3d; see also Myers, 1985).

Molybdenites in Fiskenæsset anorthosite yielded a Re–Os age of 3080±70 Ma (Herr et al., 1967). Gancarz (1976) reported a Pb–Pb isochron age of 2750 Ma from plagioclase and hornblende that were separated from Fiskenæsset anorthosites and leucogabbros. Ashwal et al. (1989) argued that a five-point mixed whole-rock and mineral Sm-Nd isochron age of 2.86±0.05 Ga represents the time of primary crystallization of the Fiskenæsset Complex. Anorthosites, leucogabbros, gabbros and ultramafic rocks of the complex have 2973±28 Ma and 2945±36 Ma Sm-Nd and Pb-Pb isotope regression ages,

respectively, interpreted as the most likely magmatic age for the complex (Polat et al., 2010). A hornblenditic pegmatite pipe (Myers, 1985) that transects part of the complex at Majorqap qâva has a $^{207}Pb/^{206}Pb$ zircon age of 2.87 Ga, and its oldest zircon grains are ca. 2.95 Ga, which is in agreement with the Sm-Nd and Pb-Pb intrusion age of the complex (Keulen et al. 2010).

2.3. Petrography

Modal abundances of minerals in selected samples from all lithological units at Majorqap qâva are presented in Table 2.1. Photomicrographs of these units are given in Supplementary Figs. 2.2-2.4. Accordingly, only a petrographic summary presented here.

Gabbros of the Lower Gabbro Unit consist of fine-grained plagioclase and hornblende with an equigranular texture (Supplementary Fig. 2.2a). Hornblendites of the Lower Gabbro Unit consist of >90% hornblende (Table 2.1; Supplementary Fig. 2.2b).

The Ultramafic Unit is composed of peridotite, hornblendite, dunite, and pyroxenite; the most common rock types are peridotites and hornblendites. The dunites of the Ultramafic Unit consist of olivine (~90%), clinopyroxene (5-10%) and accessory (<2%) spinel, magnetite, and chromite (Table 2.1; Supplementary Figs. 2.2c and d). The peridotites consist of olivine (50 – 60%), clinopyroxene (10-30%), orthopyroxene (5-10%) and accessory (<5%) spinel, magnetite, and chromite (Table 2.1; Supplementary Fig. 2.2e). The hornblendites are very similar to the hornblendites of the Lower Gabbro Unit (Table 2.1; Supplementary Fig. 2.2f). One pyroxenite is composed of clinopyroxene (70-80%) and orthopyroxene (20-30%).

Leucogabbros of the Lower Leucogabbro Unit are made up of plagioclase and hornblende of which plagioclase is the dominant phase, amounting to 70-80% by volume (Table 2.1; Supplementary Figs. 2.2g and h). Hornblende occurs as separate interstitial crystals between plagioclase grains (Supplementary Figs. 2.2g and h).

The Middle Gabbro Unit contains gabbros, peridotites, hornblendites, and

anorthosites. The gabbros consist of equal amounts of plagioclase and hornblende with minor orthopyroxene (Table 2.1; Supplementary Figs. 2.3a and b). The peridotites are composed of olivine, orthopyroxene, hornblende, spinel and magnetite in various portions (Table 2.1; Supplementary Fig. 2.3c and d). The hornblendite consists of >85% hornblende (grain size about 1-1.5 mm) and minor plagioclase (Table 2.1; Supplementary Figs. 2.3e and f). Hornblendes are in sharp mutual contact (Supplementary Fig. 2.3e), and plagioclase occurs as interstitial grains between them (Supplementary Fig. 2.3f). The anorthosites contain plagioclase (90 – 95%) and hornblende (5 – 10%) (Table 2.1; Supplementary Fig. 2.3h), the hornblende occurs as individual granules or aggregates of grains along plagioclase-plagioclase boundaries.

Leucogabbros of the Upper Leucogabbro Unit have a similar mineral composition and texture to the leucogabbros of the Lower Leucogabbro Unit (Table 2.1). Subhedral and anhedral plagioclases (1-1.5 mm) constitute a framework of cumulus minerals, with hornblende filling the interstices between them (Supplementary Figs. 2.4a and b). Plagioclase displays some degree of recrystallization and alteration Supplementary Fig. 2.4c). The rocks are typically dominated by equilibrium textures with straight grain boundaries and triple junctions (Supplementary Fig. 2.4d).

Anorthosites of the Anorthosite Unit are petrographically very similar to the anorthosites of the Middle Gabbro Unit. Plagioclase, the most abundant phase (90 – 95%), is twinned and unzoned (Supplementary Fig. 2.4e; Table 2.1). Hornblendes (5 – 10%) form individual granules or granular aggregates along plagioclase-plagioclase grain boundaries. Locally, chromite occurs as an inclusion within hornblende, or it includes hornblende grains (Supplementary Figs. 2.4f-h).

2.4. Sampling and analytical methods

2.4.1. Sampling

Seventy-three samples were collected from the Majorqap qâva sequence (Fig. 2.1c;

Supplementary Fig. 2.1) in order to cover a wide range of rock types and to obtain a meaningful distribution of samples throughout the stratigraphic section. Samples were collected from least-altered and least-deformed outcrops. The weight of the samples varied between 2 and 3 kg. Global Positioning System (GPS) coordinates for the samples are presented in Supplementary Tables 2.1-2.6. For regional correlations, our samples are extrapolated to the simplified stratigraphic sections of Myers (1985) (Supplementary Fig 2.1). Given three phases of deformation and lateral changes in lithology, the locations of samples on the simplified stratigraphic sequence (Supplementary Fig. 2.1) should be taken as approximate. For a detailed stratigraphic description of the Fiskenæsset Complex at Majorqap qâva, see Myers (1985).

The Lower Gabbro Unit, particularly its lower part, contains lenses of melanocratic amphibolite or gabbro, which grades into 'normal' gabbro with increasing plagioclase content. Although samples 508961, 508962, 508964 and 507973 are defined as melanocratic gabbro in the field, they are petrographically and geochemically comparable to hornblendites. Therefore, they are classified as hornblendites (see Table 2.1; Supplementary Table 2.1).

2.4.2. Whole-rock analyses

Analyzed samples have grain sizes between 1 mm and 1 cm. Accordingly, to be representative of the whole-rocks, pulverized samples ranged from 300 to 500 g. They were powdered using an agate mill at Activation Laboratories Ltd. (ACTLABS), Canada. Major and some trace elements (Sc, Zr and V) were analyzed on a Thermo Jarrel-Ash ENVIRO II ICP-OES. Samples were fused at 1000°C in an induction furnace with a flux of lithium metaborate and lithium tetraborate. The molten beads were dissolved in a solution of 5% HNO_3 containing an internal standard, and mixed continuously until complete dissolution. Loss on ignition (LOI) was determined by measuring weight loss upon heating to 1100°C over a three hour period. Totals of major element oxides are

100±1 wt.% with an analytical precision of 1–2% for most major elements. The analytical precision for Sc, Zr and V is better than 10%.

Trace elements including transition metals (Ni, Co and Cr), REE, HFSE, and LILE were analyzed by a high-sensitivity Thermo Elemental X7 Series II ICP-MS in the Great Lakes Institute for Environmental Research (GLIER), University of Windsor, Canada, following the protocols of Jenner et al. (1990). Sample dissolution was conducted under clean lab conditions with doubly distilled acids. Approximately 100 – 130 mg of sample powder was used for acid digestion. Samples were dissolved in Teflon bombs in a concentrated mixture of HF-HNO_3 at a temperature of 120°C for 4 days and then further attacked with 50% HNO_3 until no solid residue was left. International standards BHVO-2 and BCR-2 were used as reference materials to estimate analytical precision. The results of standard analyses and recommended values are given in Table 2.2.

Mg-numbers (Mg#) were calculated as the molar ratio of $Mg^{2+}/(Mg^{2+}+Fe^{2+})$. Samples were normalized to chondrites and normal mid-ocean ridge basalt (N-MORB); the normalization values are from Taylor and McLennan (1985) and Hofmann (1988), respectively. Europium (Eu/Eu*), Ce (Ce/Ce*), Nb (Nb/Nb*), Ti (Ti/Ti*), Zr (Zr/Zr*), Pb (Pb/Pb*) and Sr (Sr/Sr*) anomalies were calculated with respect to the neighboring immobile elements, following the method of Taylor and McLennan (1985).

2.4.3. Mineral trace element analyses

A total of 32 hornblende grains in four samples (one gabbro and three hornblendites) from the Lower Gabbro, Ultramafic, and Middle Gabbro Units were analyzed for transition metals (V, Cr, Co, Ni), LILE (Rb, Ba), Th, U, HFSE (Nb, Ta, Zr, Hf) and REE (La-Lu). Minerals analyzed for trace elements were selected using an Environmental Scanning Electron Microscope (EDAX FEI Quanta 200 FEG Environmental SEM) equipped with an Energy Dispersive X-ray Spectrometry (EDS) at the Great Lakes Institute for Environmental Research (GLIER), University of Windsor, Canada. Trace

element analyses were carried out using femtosecond (fs) laser ablation-inductively coupled plasma-mass spectrometry (LA-ICP-MS) (Shaheen et al., 2008). Before LA-ICP-MS measurements, hornblende grains in polished samples (about 0.1 mm thick) were analyzed by SEM to check for homogeneity and to determine Ca concentrations that were used as an internal standard. Analytical results of the replicate NIST 612 standard used in calibrations are shown in Table 2.3.

2.5. Geochemical results

2.5.1. Whole-rock analyses

Major and trace element data for the analyzed rocks are presented in Supplementary Tables 2.1-2.6. A summary of significant compositional values and element ratios for the analyzed rocks in each stratigraphic unit of the Fiskenæsset Complex at Majorqap qâva is given in Table 2.4.

2.5.1.1. Lower Gabbro Unit

This unit is made up of gabbros and hornblendites. The gabbros have 43.0–50.8 wt.% SiO_2, 5.2–8.6 wt.% MgO, and 11.0–14.3 wt.% Al_2O_3 (Fig. 2.4; Table 2.4; Supplementary Table 2.1). They have Mg-numbers between 35 to 55 and near-chondritic CaO/Al_2O_3 (0.80-1.04) ratios (Table 2.4). On chondrite-normalized REE and N-MORB-normalized trace element diagrams, they have the following characteristics: (1) depleted to moderately enriched LREE patterns (La/Sm_{cn}=0.46-1.68); (2) flat to moderately depleted HREE patterns (Gd/Yb_{cn}=1.08-1.58); (3) small negative to positive Eu anomalies; (4) enrichments of Th and U; (5) positive Pb and Sr anomalies; (6) negative anomalies of Nb and Zr; and (7) positive Ti anomalies (Figs. 2.5a and b; Supplementary Table 2.1).

Hornblendites have small ranges of SiO_2 (48.8-49.8 wt.%), Al_2O_3 (7.6-8.7 wt.%), Fe_2O_3 (14.3-16.1 wt.%), MgO (9.8-11.9 wt.%), CaO (11.2-12.8 wt.%), Na_2O (1.4-1.8

wt.%), and K_2O (0.2-0.7 wt.%). They have Mg-numbers between 57 and 62, and high CaO/Al_2O_3 (1.37-1.69) ratios. They also have high Ni (179-331 ppm), Co (67-74 ppm), and Cr (488-873 ppm) contents (Table 4; Supplementary Table 2.1). The hornblendites display moderately depleted to slightly enriched LREE patterns (La/Sm_{cn}=0.76-1.10), strongly depleted HREE patterns (Gd/Yb_{cn}=1.52-1.61), and minor negative Eu anomalies. N-MORB-normalized trace-element patterns are characterized by enrichments in Th and U, depletions of Nb and Zr, and positive Pb, Sr, and Ti anomalies (Figs. 2.5c and d; Supplementary Table 2.1; Table 2.4).

2.5.1.2. Ultramafic Unit

The Ultramafic Unit consists of hornblendites, peridotites, dunites, and pyroxenites. Compared with the hornblendites of the Lower Gabbro Unit, hornblendites of this unit have relatively high MgO (12.3-18.2 wt.%), Ni (311-653 ppm), and Cr (918-1694 ppm) contents (Fig. 2.4; Supplementary Table 2.2; Table 2.4). They have Mg-numbers between 60 and 69, and high CaO/Al_2O_3 (1.58-2.00) (Supplementary Table 2.2). Chondrite- and N-MORB-normalized trace-element patterns of hornblendites are similar to those of the hornblendites of the Lower Gabbro Unit (Figs. 2.5e and f).

Peridotites are characterized by 22.5-31.4 wt.% MgO, 1.5-3.8 wt.% Al_2O_3, 1053-1812 ppm Ni, and 946-1822 ppm Cr. CaO/Al_2O_3 (2.13-5.16) ratios are super-chondritic and Al_2O_3/TiO_2 (2.4-8.9) ratios are strongly sub-chondritic (Fig. 2.4; Table 2.4; Supplementary Table 2.2). The peridotites are depleted in LREE (La/Sm_{cn}=0.31-0.76) and HREE (Gd/Yb_{cn} =1.67-2.55) and have negative Eu anomalies (Eu/Eu*=0.43-0.93). They have the following trace element characteristics on an N-MORB-normalized trace-element diagram: (1) enrichments of Th and U over LREE; (2) depletions of Nb and Zr; and (3) positive Pb and Ti anomalies (Figs. 2.5g and h; Supplementary Table 2.2; Table 2.4).

One dunite sample has the highest MgO (37.2 wt.%), but the lowest CaO (1.6 wt.%)

and Al_2O_3 (0.6 wt.%) contents. It has low REE contents and its trace element pattern is similar to that of the peridotites (Figs. 2.5i and j; Supplementary Table 2.2; Table 2.4).

One pyroxenite sample is siliceous SiO_2=53.4 wt.% and has the highest Mg-number (Mg#=83). Its REE and trace element patterns resemble those of the LREE-enriched hornblendites in the Lower Gabbro Unit (Figs. 2.5k and l; Supplementary Table 2.2; Table 2.4).

2.5.1.3. Lower Leucogabbro Unit

Leucogabbros have high contents of Al_2O_3 (23.3-30.7 wt.%) and CaO (12.4-17.2 wt.%) and low Fe_2O_3 (1.3-7.5 wt.%) and MgO (0.9-9.2 wt.%) (Fig. 2.4; Supplementary Table 2.3; Table 2.4). Mg-numbers are variably high (Mg#=57-74). On chondrite- and N-MORB-normalized trace element diagrams, they have the following characteristics: (1) strongly enriched LREE patterns (La/Sm_{cn}=1.81-6.92) with one exceptional sample (508992; La/Sm_{cn}=0.63); (2) slightly enriched to strongly depleted HREE patterns (Gd/Yb_{cn}=0.80-1.77); (3) large positive Eu anomalies (Eu/Eu*=1.33-5.68); (4) enrichments in Th and U; (5) positive Pb and Sr anomalies; (6) negative anomalies of Nb with one outlier sample; and (7) negative to positive Ti anomalies (Figs. 2.6a and b; Supplementary Table 2.3; Table 2.4).

Two anorthosite breccia samples are characterized by significantly high CaO and Al_2O_3 contents, but extremely low MgO. One sample has a large positive Ce anomaly (Ce/Ce*=1.78). Their N-MORB-normalized trace element patterns are comparable to those of the HREE-depleted leucogabbros of the Lower Leucogabbro Unit (Figs. 2.6c and d; Supplementary Table 2.3; Table 2.4).

One gabbro sample has similar geochemical characteristics to the gabbros of the Lower Gabbro Unit (Supplementary Table 2.3; Figs. 2.6e and f; Table 2.4).

2.5.1.4. Middle Gabbro Unit

This unit contains gabbros, anorthosites, hornblendites, and peridotites (Supplementary Table 2.4; Table 2.4). The gabbros have 46.2-48.0 wt.% SiO_2, with high MgO (8.9-13.19 wt.%), Al_2O_3 (12.7-19.2 wt.%), and CaO (12.8-15.7 wt.%). Mg-numbers (74-78) are relatively high. CaO/Al_2O_3 (0.81-1.02) ratios are close to the chondritic value (Fig. 2.4; Supplementary Table 2.4; Table 2.4). They also have high Ni (175-323 ppm) and Cr (882-1600 ppm) concentrations. They display depleted to enriched LREE (La/Sm_{cn}=0.36-6.32) and slightly enriched to flat HREE (Gd/Yb_{cn}=0.73-0.99) patterns. Europium anomalies (Eu/Eu*=1.01-1.60) are mainly positive (Supplementary Table 2.4; Table 2.4). On an N-MORB-normalized trace element diagram, they have the following characteristics: (1) enrichments of Th and U; (2) positive Pb and Sr anomalies; (3) negative anomalies of Nb; and (4) negative anomalies of Ti (Figs. 2.6g and h; Supplementary Table 2.4; Table 2.4).

Anorthosites have high contents of CaO (17.2-17.7 wt.%) and Al_2O_3 (30.2-32.4 wt.%) contents, but low MgO (0.9-1.9 wt.%), Fe_2O_3 (1.7-2.1 wt.%), Ni (20-50 ppm), and Cr (95-174 ppm) contents (Supplementary Table 2.4; Table 2.4). They are enriched in LREE (La/Sm_{cn}=1.98-2.75), slightly depleted in HREE (Gd/Yb_{cn}=1.15-1.16) and display positive Eu (Eu/Eu*=2.30-4.80) anomalies (Figs. 2.6i and j). The N-MORB-normalized trace element patterns of the anorthosites of the Middle Gabbro Unit are similar to those of the anorthosite breccias of the Lower Leucogabbro Unit (Fig. 2.6; Supplementary Tables 2.3 and 2.4; Table 2.4).

Hornblendites have high MgO (13.4-20.8 wt.%) and Ni (369-688 ppm) concentrations. Al_2O_3 (7.3-17.9 wt.%) is variably high. They have Mg-numbers between 67 and 76, and a moderate range of CaO/Al_2O_3 (1.58-2.00) (Supplementary Table 2.4; Table 2.4). They possess depleted to enriched LREE (La/Sm_{cn}=0.45-2.76) and enriched to flat HREE (Gd/Yb_{cn}=0.77-0.98) patterns (Fig. 2.6k). They have negative to positive Eu and Ce anomalies, and the following trace-element characteristics: (1) enrichments in Th and U; (2) depletion of Nb; and (3) large positive Pb anomalies (Figs. 2.6k and l; Table

2.4).

Two peridotite samples have high contents of MgO (29.7-34.5 wt.%) and relatively high Al_2O_3 (4.3-7.6 wt.%) (Supplementary Table 2.4; Table 2.4). The peridotites are enriched to slightly depleted in LREE (La/Sm_{cn}=0.68-1.78) and have enriched HREE (Gd/Yb_{cn}=0.57-0.61) patterns and positive to negative Eu anomalies. Their N-MORB-normalized trace-element patterns resemble those of the hornblendites of the Middle Gabbro Unit (Figs. 2.6m and n).

2.5.1.5. Upper Leucogabbro Unit

The upper leucogabbros have high Al_2O_3 (25.6-31.2 wt.%) and CaO (14.7-16.8 wt.%) but low Fe_2O_3 (2.1-6.5 wt.%) and MgO (2.0-6.5 wt.%) contents. Mg-numbers (Mg#=64-67) are high (Fig. 2.4; Supplementary Table 2.5). Their trace element characteristics are broadly similar to those of the leucogabbros of the Lower Leucogabbro Unit (Figs. 2.7a and b; Supplementary Table 2.5; Table 2.4).

One anorthosite dyke has a high MgO (4.8 wt.%) content, a high Mg-number (68), and a trace element pattern that resembles the patterns of the anorthositic breccias of the Lower Leucogabbro Unit (Figs. 2.7c and d).

Two hornblendite samples have similar chemical characteristics as the hornblendites of the Middle Gabbro unit (Figs. 2.7e and f; Supplementary Table 2.5; Table 2.4).

2.5.1.6. Anorthosite Unit

Anorthosites have high Al_2O_3 (30.3-33.1 wt.%) and CaO (13.9-19.1 wt.%) but low MgO (0.2-1.9 wt.%), Fe_2O_3 (0.7-2.6 wt.%), Ni (8-58 ppm), and Cr (8-118 ppm) contents (Supplementary Table 2.6; Table 2.4). They have variable Mg-numbers (27 to 62) (Supplementary Table 2.6; Table 2.4). The chondrite-normalized diagrams show strong positive Eu anomalies (Eu/Eu*=1.46-8.72) and enrichments in LREE

(La/Sm_{cn}=1.27-35.55) and depletions in HREE (Gd/Yb_{cn}=1.12-2.71) (Fig. 2.7g). They have the following trace element characteristics: (1) enrichments in Th and U; (2) positive Pb and Sr anomalies; (3) negative anomalies of Nb, with one outlier; (4) negative to positive Zr anomalies; and (5) negative to positive Ti anomalies (Figs. 2.7g and h; Supplementary Table 2.6; Table 2.4).

Three anorthosite samples between the Upper Leucogabbro and Anorthosite Units have high Al_2O_3 (30.3-32.7 wt.%) and CaO (16.6-17.1 wt.%) but low Fe_2O_3 (1.1-1.7 wt.%) and MgO (0.6-1.7 wt.%) contents. Mg-numbers for these anorthosites are variably high (Mg#=52-67) (Table 2.4). Trace element patterns resemble those of the anorthosite of the Anorthosite Unit (Figs. 7i and j; Supplementary Table 2.6; Table 2.4).

2.5.2. Hornblende trace element compositions

Four samples, one from the Lower Gabbro Unit (508973), one from the Ultramafic Unit (508983), and two from the Middle Gabbro Unit (508931, 508915), were selected for hornblende trace element analyses (Supplementary Table 2.7).

2.5.2.1. Lower Gabbro Unit

All hornblende grains in sample 508973 have coherent chondrite-normalized REE and N-MORB-normalized extended trace element patterns, consistent with a homogeneous composition (Fig. 2.8; Supplementary Table 2.7). They have slightly convex-upward LREE (La/Sm_{cn}=0.91-1.21) patterns and moderately depleted HREE (Gd/Yb_{cn}=1.39-1.50) values (Fig. 2.8; Supplementary Table 2.7). These patterns are similar to that of respective whole-rock sample (Fig. 2.8a). On N-MORB-normalized diagram, hornblendes have the following characteristics: (1) enrichments of Rb, Ba and U over Th and Nb; (2) enrichments of Rb and Ba relative to REE; (3) enrichment of La over Nb and Ta; (4) strong positive Pb anomalies; and (5) large negative anomalies of Zr and Hf (Fig. 2.8b; Supplementary Table 2.7). Nb/Ta and Zr/Hf ratios are consistently

sub-chondritic.

2.5.2.2. Ultramafic Unit

Sample 508983 also displays a homogeneous trace element composition (Supplementary Table 2.7), and trace element patterns are similar to that of sample 508973 (Fig. 2.8c). Hornblendes of the Ultramafic Unit have higher Cr (1450-1850 vs. 625-803 ppm), Ni (386-517 ppm), and Co (80-91 vs. 67-75 ppm) contents than those of the Lower Gabbro Unit (sample 508973). In contrast, they have lower V, HFSE (Zr, Hf, Y, Nb, Ta), REE, Th, and U than their counterparts in the Lower Gabbro Unit (sample 508973). Zr/Hf ratios are consistently sub-chondritic, whereas Nb/Ta ratios are sub-chondritic to super-chondritic.

2.5.2.3. Middle Gabbro Unit

Two samples, one hornblendite (508915) and one gabbro (508931), from the Middle Gabbro Unit were analyzed for trace elements (Supplementary Table 2.7). Hornblende grains in both samples have uniform compositions. In the gabbro they have consistently higher Cr, V and Ba but lower Rb, Zr, and Nb contents (Supplementary Table 2.7). Both samples share sub-chondritic Nb/Ta and Zr/Hf ratios. On chondrite- and N-MORB-normalized diagrams, the hornblendes in the Middle Gabbro Unit display the following features: (1) enrichments of Rb and U over Th, Nb and LREE; (2) depleted LREE (La/Sm_{cn}=0.26-0.36) patterns; (3) enriched HREE (Gd/Yb_{cn}=0.64-0.80) patterns; (4) large positive Pb anomalies; and (5) small negative Zr and Hf anomalies (Figs. 2.8e and f). Hornblendes in gabbro have small positive whereas hornblendes in the hornblendite possess moderately negative Eu anomalies (Figs. 2.8e and g). Hornblendes from the Lower Gabbro and Middle Gabbro Units plot in two widely separated fields on La/Sm_{cn} vs. Gd/Yb_{cn} and Gd/Yb_{cn} and Nd/Zr_{pm} diagrams (Fig. 2.9). Hornblendes of the Ultramafic Unit plot next to those of the Lower Gabbro Unit (Fig. 2.9).

2.6. Discussion

2.6.1. Alteration and element mobility

Post-magmatic hydrothermal alteration and metamorphism can modify primary magmatic compositions to a large extent (Lahaye et al., 1995; Polat and Hofmann, 2003; Ordóñez-Calderón et al., 2008). This applies particularly to our samples collected from the Fiskenæsset Complex, which was deformed and metamorphosed during several tectonothermal events (Windley et al., 1973; Windley and Smith, 1974; Myers and Platt, 1977; Pidgeon and Kalsbeek, 1978; Myers, 1985; McGregor and Friend, 1992; Polat et al., 2010). Although the samples selected for chemical analyses are relatively unaltered, post-magmatic tectonothermal events may have affected the geochemistry of the Fiskenæsset anorthosites, gabbros, leucogabbros, hornblendites, and peridotites. To assess the effects of alteration on the original chemistry of the Fiskenæsset Complex, we adopt the alteration criteria of Polat and Hofmann (2003). Only three samples have loss on ignition (LOI) values >2 wt.% with a maximum of 3.1 wt.%, which suggests that the rocks have not been strongly hydrated or carbonated. However, dehydration of the Fiskenæsset Complex during granulite facies metamorphism cannot be ruled out. Samples having large Ce anomalies ($Ce/Ce^* < 0.85$ and $Ce/Ce^* > 1.15$) are considered as variably altered. For example, anorthosite sample 508906 has a large negative Ce anomaly ($Ce/Ce^*=0.70$) and is extremely enriched in LREE ($La/Sm_{cn}=35.5$). In comparison, the other anorthosites have $La/Sm_{cn}<12$. Accordingly, these samples have been designated as altered and not used in the petrogenetic interpretation (Supplementary Table 2.1-2.6).

REE and HFSE are generally immobile during alteration and metamorphism, which is indicated by the coherent N-MORB- and chondrite-normalized patterns. LILE (Pb and Sr) can be mobilized during metamorphism and hydrothermal alteration (Lahaye et al., 1995; Polat and Hofmann, 2003). However, on N-MORB-normalized trace element diagrams, they also display limited variation, suggesting these elements were relatively immobile on the whole-rock scale. Strong evidence for the limited mobility of trace

elements, particularly REE and HFSE, in samples reported in this study, is provided by the following features: (1) similarities between trace element patterns of whole-rocks and hornblende grains in the same samples (Fig. 2.8); and (2) coherent trace element patterns, including LILE, REE and HFSE, exhibited by hornblende grains analyzed in four samples (Fig. 2.8; Supplementary Table 2.7).

2.6.2. Evaluation of crustal contamination

Negative Nb anomalies in the studied rocks could reflect either mantle source characteristics or be features of continental crust contamination. Several lines of evidence preclude contamination of the Fiskenæsset Complex by continental crust during magma emplacement: (1) there is no field evidence that the Fiskenæsset Complex was emplaced into older continental crust (see Myers, 1985, and references therein); (2) all the samples have <50.9 wt.% SiO_2 except the pyroxenite that has 53.4 wt.% SiO_2, which suggests that they have not assimilated continental crust; (3) there are no correlations between SiO_2 abundances and contamination-sensitive elements and ratios (e.g., Th, Zr, La, Ni, La/Sm_{cn}, Nb/Nb*, Zr/Zr*); (4) many samples have low total REE, which are distinct from Archean continental crust (see Taylor and McLennan, 1995); and (5) Nd isotopes do not show a large scatter (see Polat et al., 2010).

Alternatively, negative Nb anomalies could have resulted from fractionation of Fe-Ti-rich minerals, such as ilmenite or amphibole (cf., Hoffmann et al., 2012). We agree with Hoffmann et al. (2012) that negative Nb anomalies can be generated by the fractionation of Fe-Ti phases. The origin of these anomalies in the Fiskenæsset Complex, however, is attributed mainly to subduction zone processes, rather than mineral fractionation, for the following three main reasons: (1) negative Nb anomaly is a ubiquitous feature of all types of cumulates, including peridotites, dunites, and hornblendites, in the complex (Polat et al., 2009, 2011a, c); (2) there is no correlation between Nb and Ti anomalies (Figs. 2.5-2.7; Supplementary Tables 2.1-2.6); and (3) in all

hornblende grains analyzed for this study, on N-MORB-normalized diagrams Nb is depleted relative to Rb, Ba, U, Pb, and La, which are typically enriched in subduction-derived fluids or melts. On the other hand, the magnitude of Nb anomalies in the Fiskenæsset cumulates is likely to have been affected to some extent by the fractionation of Fe-Ti oxides and hornblende.

2.6.3. Magmatic versus metamorphic minerals and geochemical signatures

Despite multiple phases of deformation and amphibolite to granulite facies metamorphism, igneous mineralogy and textures are well preserved in the Fiskenæsset Complex (Windley et al., 1973; Windley and Smith, 1974; Myers and Platt, 1977; Myers, 1985; Polat et al., 2009). Myers and Platt (1977) analyzed plagioclase, amphibole, olivine and spinel grains for major elements in samples from Majorqap qâva. Results of this study indicate that the anorthite content in plagioclase decreases, with stratigraphic height, from An_{98-94} to An_{90-75} (see also Windley and Smith, 1974). Hornblende grains exhibit upward Fe enrichment in the stratigraphy. Variations in hornblende and plagioclase compositions were attributed to magma differentiation (e.g., fractionation of forsteritic olivine and anorthitic plagioclase) rather than the effect of metamorphism.

Photomicrographs in Supplementary Figs. 2.2-2.4 indicate that the primary magmatic textures and minerals, including olivine, pyroxene, plagioclase, hornblende and chromite, are well preserved in the complex. The origin of hornblendes in the Fiskenæsset Complex has been controversial (see Polat et al., 2009, 2011c and references therein therein); either an igneous origin (Windley et al., 1973; Polat et al., 2009; Windley and Garde, 2009; Rollinson et al., 2010), or a metamorphic origin replacing mainly pyroxene (Myers, 1985).

On the basis of petrographic observations, we suggest the majority of hornblende grains at Majorqap qâva originated as an igneous mineral, although we recognize that they may have also experienced some recrystallization during metamorphism. The

general absence of relicts of pyroxene within hornblende suggests that hornblendes are igneous in origin. The most convincing petrographic evidence for an igneous origin of hornblendes in the Fiskenæsset Complex is found in undeformed chromite cumulates in the Sinarssuk area (Figs. 2.1b and 2.10). In these cumulates, hornblende occurs both as an interstitial mineral and as small rounded inclusions in chromite (Cr-Fe-Fe-spinel) grains (Fig. 2.10). There is no obvious sign of recrystallization of chromite and hornblende grains, implying that hornblende and chromite crystallized simultaneously from the same magma.

Ashwal et al. (1989) showed that the REE patterns for a plagioclase separate from a leucogabbro resemble the REE pattern for a whole-rock sample of anorthosite from an adjacent zone. Trace element patterns of hornblendes from the Lower Gabbro, Ultramafic, and Middle Gabbro Units are similar to those of their respective whole-rock samples (Fig. 2.8). These observations imply that substantial redistribution of REE and HFSE on the sample scale did not occur during metamorphism. Collectively, geochemical signatures preserved in least-altered whole-rock samples (see Supplementary Tables 2.1-2.6) and those in hornblende grains in four selected samples (Supplementary Table 2.7) are interpreted as magmatic.

2.6.4. Evidence for two geochemical magma suites

Plots of whole-rock MgO vs. TiO_2, CaO, Fe_2O_3, MnO and Al_2O_3 suggest that the Fiskenæsset Complex was crystallized from at least two types of parental magmas, generating two suites of rocks (hereafter referred to as Suites A and B). Suite A consists of gabbros of the Lower Gabbro Unit, hornblendites of the Lower Gabbro and Ultramafic Units, and peridotites and pyroxenites of the Ultramafic Unit. Suite B comprises leucogabbros of the Lower Leucogabbro Unit, gabbros of the Middle Gabbro Unit, and leucogabbros of the Upper Leucogabbro Unit. For the least-altered samples, two distinctly different trends are seen (Fig. 2.4). Suite A is characterized by high TiO_2, Fe_2O_3

and MnO, whereas Suite B displays high CaO and Al_2O_3 contents. Distinction between Suites A and B is also clearly seen on plots of Mg-number versus TiO_2, CaO, Fe_2O_3, MnO, Al_2O_3, Ni, and Co (not shown). On N-MORB-normalized trace element diagrams, Suite A is characterized by higher concentrations of virtually all incompatible elements, whereas Suite B is characterized by lower concentrations. Additionally, the majority of samples in Suite A have positive Ti anomalies, whereas most samples in Suite B have negative Ti anomalies (Figs. 2.5-2.7; Supplementary Tables 2.1-2.6). Positive and negative Ti anomalies are likely to reflect the accumulation and fractionation (removal) of Ti-bearing minerals (e.g., ilmenite, Ti-rich magnetite, Ti-bearing amphibole), respectively, in the magmas of these suites.

Hornblende grains in the Lower Gabbro and Ultramafic Units (Suite A) and the Middle Gabbro (Suite B) Unit have different trace element patterns and fall into two separate fields on La/Sm_{cn} vs. Gd/Yb_{cn} and Gd/Yb_{cn} vs. Nd/Zr_{cn} diagrams (Fig. 2.9; Supplementary Table 2.7). Collectively, in addition to whole-rock geochemical data, the trace element systematics of hornblendes in gabbros and hornblendites provide compelling evidence for the presence of two distinct suites of rocks at Majorqap qâva, stemming from differentiation of two compositionally distinct parental magmas. Given their distinct trace element compositions, these parental magmas appear to have been derived from different mantle sources. Given that all rock types in the Fiskenæsset Complex have similar initial Nd isotopic signatures (Polat et al., 2010), compositional differences in the sources of Suites A and B were probably generated by subduction-related metasomatism shortly before their melting. Because of the cumulative nature of the Fiskenæsset Complex, compositions of the parental magmas cannot be reliably constrained using the whole-rock and hornblende data alone presented in this study. The results of this study concur with the two major cycles of crystal deposition proposed by Myers (1985).

Irvine (1974) interpreted Alaskan-type ultramafic complexes (olivine

clinopyroxenite, hornblende-magnetite clinopyroxenite, peridotite, dunite, and hornblendite) associated with hornblende-anorthosite (plagioclase An_{98-90}) pegmatites on Duke Island as the product of crystallization of a hydrous magma. Sisson et al. (1996) reported hornblende gabbros with subsidiary ultramafic olivine hornblendite, plagioclase hornblendite and plagioclase-rich hornblende gabbro from the Sierra Nevada batholith at Onion Valley, which they suggested formed from a hydrous melt. The field relationships at Majorqap qâva indicate that the Fiskenæsset Complex is very similar to Alaskan-type ultramafic complexes and hornblende-anorthosite on Duke Island and to the hornblende-rich gabbro and associated rocks at Onion Valley. It is therefore likely that the Fiskenæsset Complex crystallized from hydrous magmas.

2.6.5. Geodynamic significance

From field observations that demonstrate the widespread spatial association of the Fiskenæsset Complex and bordering mafic volcanic rocks (now amphibolite), Weaver et al. (1982) pointed out that the meta-volcanic amphibolites have an ocean floor trace element chemistry, and Myers (1985) suggested that the Fiskenæsset Complex was emplaced into oceanic crust. The Fiskenæsset amphibolites and cumulates have the geochemical characteristics of a MORB-Island-Arc-Basalt signature, which further confirms that the Fiskenæsset Complex was emplaced into oceanic crust (Polat et al., 2009, 2011a, b, c).

Rocks of both Suites A and B share the depletion of Nb relative to Th, U, LREE, Pb, and Sr, indicating that negative Nb anomalies reflect mainly mantle source characteristics rather than mineral fractionation processes (Figs. 2.5-2.7; Supplementary Tables 2.1-2.6). More compelling evidence for a subduction zone origin for the Fiskenæsset Complex is provided by the trace element compositions of hornblendes in gabbros and hornblendites in both Suites A and B. Both suites are strongly enriched in Rb, Ba, U and Pb relative to HFSE (Nb, Ta, Zr, Hf, Y), consistent with a subduction zone origin (Saunders et al., 1991;

Pearce and Parkinson, 1993; Murphy, 2007).

2.7. Conclusions

1. This study reports extensive whole-rock major and trace element data for all major stratigraphic units of the Mesoarchean (ca. 2.97 Ga) Fiskenæsset Complex at Majorqap qâva, SW Greenland. The units that were sampled for whole-rock analyses include the Lower Gabbro, Ultramafic, Lower Leucogabbro, Middle Gabbro, Upper Leucogabbro, and Anorthosite. In addition, hornblendes in samples from the Lower Gabbro, Middle Gabbro and Ultramafic Units were analyzed for trace elements.

2. Hornblende is an abundant mineral in the Fiskenæsset rocks, including hornblendites, peridotites, gabbros, leucogabbros, and anorthosites. It occurs mainly as an interstitial igneous mineral to olivine, orthopyroxene, clinopyroxene, and chromite. It also occurs as abundant inclusions in chromites. The occurrence of hornblende as both an interstitial mineral and inclusions in the Fiskenæsset cumulates is attributed to crystallization of this mineral from hydrous magmas.

3. On the basis of whole-rock and mineral data, the rocks of the Fiskenæsset Complex are divisible into two distinct suites (Suites A and B) that originated from the differentiation of two different parental magmas. The REE and HFSE systematics of these suites suggest different mantle sources for the parental magmas. Both field and geochemical data indicate a variable amount of mixing between the two magma types.

4. The N-MORB-normalized trace-element patterns of both magma suites are consistent with a subduction zone geodynamic setting. Despite some degree of recrystallization, the majority of hornblende grains appear to have retained their magmatic geochemical signatures. Coherent trace element patterns including Rb, Ba, Th, U, Pb, Nb, Ta, Zr, Hf and REE in hornblendes suggest that these elements were relatively immobile on a grain scale during metamorphism. Enrichments of Rb, Ba, U, Pb, and LREE relative to Nb, Ta, Zr, and Hf in hornblendes provide compelling evidence for the formation of the

Fiskenæsset Complex in a supra-subduction zone geodynamic setting.

2.8. Acknowledgments

Two anonymous reviewers are acknowledged for their constructive comments, which have resulted in significant improvements to the paper. The research was supported by NSERC grants to A. Polat and B. Fryer, and the fieldwork by the Bureau of Minerals and Petroleum in Nuuk and the Geological Survey of Denmark and Greenland (GEUS). A. Polat thanks Mr. Tekin Demir for helping his family during fieldwork in Greenland. We thank S. Weatherly, A. Dziggel, J. Kolb, P. Kalvig, A., Kisters, and O. Dahl for discussions of geological problems in various contexts.

2.9. References

Ashwal, L.D., Jacobsen, S.B., Myers, J.S., Kalsbeek, F., Goldstein, S.J., 1989. Sm-Nd age of the Fiskenæsset Anorthosite Complex, West Greenland. Earth and Planetary Science Letters 91, 261-270.

Ashwal, L.D., 1993. Anorthosites. Minerals and Rocks Series, 21. Springer-Verlag, Berlin, 422 pp.

Ashwal, L.D., Myers, J.S., Condie, K.C., 1994. Chapter 8 Archean anorthosites, Developments in Precambrian Geology. Elsevier, pp. 315-355.

Barton, J.M., 1986. The Messina layered intrusion, Limpopo belt, South Africa: an example of in-situ contamination of an Archean anorthosite complex by continental crust. Precambrian Research 78, 139-150.

Escher, J.C., Myers, J.S., 1975. New evidence concerning the original relationships of early Precambrian volcanics and anorthosites in the Fiskenæsset region, southern West Greenland. Bulletin Grønlands Geologiske Undersøgelse 75, 72-76.

Friend, C.R.L., Nutman, A.P., Baadsgaard, H., Duke, M.J.M., 2009. The whole rock Sm–Nd 'age' for the 2825 Ma Ikkattoq gneisses (Greenland) is 800 Ma too young: Insights into Archaean TTG petrogenesis. Chemical Geology 261, 62-76.

Gancarz, A.J., 1976. Isotopic systematic in Archean rocks, west Greenland, PhD thesis, California Institute of Technology, Pasadena, pp. 378.

Ghisler, M., 1976. The Geology, Mineralogy and Geochemistry of the Pre-Orogenic Archean Stratiform Chromite Deposits at Fiskenæsset, West Greenland. Monograph Series Mineral Deposits, 14, pp. 156.

Gibson, G.M., Ireland, T.R., 1999. Black Giants anorthosite, New Zealand: a Paleozoic analogue of Archean stratform anorthosites and implications for the formation of Archean high-grade gneiss terranes. Geology 27, 131-134.

Hawkesworth, C.J., Turner, S.P., McDermott, F., Peate, D.W., van Calsteren, P., 1997. U-Th Isotopes in Arc Magmas: Implications for Element Transfer from the Subducted Crust. Science 276, 551-555.

Henderson, P., Fishlock, S. J., Laul, J.C., Cooper, T.D., Conrad, R.L., Boynton, W.V., Schmitt, R.A., 1976. Rare earth element abundances in rocks and minerals from the Fiskenæsset Complex, West Greenland. Earth and Planetary Science Letters 30, 37-49.

Herr, W., Wolfle, R., Eberhardt, P., Kopp, E., 1967. Development and recent application of the Re/Os dating method. In: Radioactive Dating and Methods of Low-Level Counting, International Atomic Energy Agency, Vienna, pp. 499-508.

Hoffmann, J.E., Svahnberg, H., Piazolo, S., Scherstén, A., Münker, C., 2011. The geodynamic evolution of Mesoarchean anorthosite complexes inferred from the Naajat Kuuat Complex, southern West Greenland. Precambrian Research 196-197, 149-170.

Hofmann, A.W., 1988. Chemical differentiation of the Earth: the relationship between mantle, continental crust, and oceanic crust. Earth and Planetary Science Letters 90, 297-314.

Hor, A.K., Hutt, D.K., Smith, J.V., Wakefield, J., Windley, B.F., 1975. Petrochemistry and

mineralogy of early Precambrian anorthositic rocks of the Limpopo belt, South Africa. Lithos 8, 297-310.

Huang, H., Polat, Fryer, B.J., 2011. Origin of the Archean tonalite–trondhjemite–granodiorite (TTG) suites and granites in the Fiskenæsset region, southern West Greenland: implication for the continental growth. Gondwana Research doi:10.1016/j.gr.2011.12.001.

Irvine, T.N., 1974. Petrology of the Duke Island Ultramafic Complex, Southeastern Alaska. Geological Society of America, Memoirs,138, 240 pp.

Jenner, G.A., Longerich, H.P., Jackson, S.E., Fryer, B.J., 1990. ICP-MS -- A powerful tool for high-precision trace-element analysis in Earth sciences: Evidence from analysis of selected U.S.G.S. reference samples. Chemical Geology 83, 133-148.

Kalsbeek, F., Myers, J.S., 1973. The geology of the Fiskenæsset region. Rapport GrønlandsGeologiske Undersøgelse 51, pp. 5-18.

Keulen, N., Næraa, T., Kokfelt, T.P., Schumacher, J.C., Scherstén, A., 2010. Zircon record of the igneous and metamorphic history of the Fiskenæsset anorthosite complex in southern West Greenland. In: Bennike, O., Garde, A.A., Watt, W.S., (Eds.), Review of Survey Activities 2009. Geological Survey of Denmark and Greenland Bulletin 20, 67-70.

Keulen, N., Kokfelt, T.F., the homogenisation team, 2011. A seamless, digital, internet-based geological map of South-West and southern West Greenland, 1:100 000, 61°30′ – 64°. http://geuskort.geus.dk/gisfarm/svgrl.jsp. Copenhagen: Geological Survey of Denmark and Greenland.

Kiddle, E.J., Edwards, B.R., Loughlin, S.C., Petterson, M., Sparks, R.S.J., Voight, B., 2010 Crustal structure beneath Montserrat, Lesser Antilles, constrained by xenoliths, seismic velocity and petrology. Geophysical Research Letters 37, LOOE11, doi:10, 1029/2009GL042145.

Kinny, P.D., Williams, I.S., Froude, D.O., Ireland, T.R., Compston, W., 1988. Early

Archean zircon ages from orthogneisses and anorthosites at Mount Narryer, Western Australia. Precambrian Research 38, 325-341.

Lahaye, Y. et al., 1995. The influence of alteration on the trace-element and Nd isotopic compositions of komatiites. Chemical Geology 126, 43-64.

McGregor, V.R., Friend, C.R.L., 1992. Late Archean prograde amphibolite- to granulite-facies relations in the Fiskenæsset region, Southern West Greenland. Journal of Geology 100, 207-219.

Müntener, O., Kelemen, P., Grove, T., 2001. The role of H_2O during crystallization of primitive arc magmas under uppermost mantle conditions and genesis of igneous pyroxenites: an experimental study. Contributions to Mineralogy and Petrology 141, 643-658.

Murphy, J.B., 2007. Arc magmatism II: geochemical and isotopic characteristics. Geoscience Canada 34, 7-35.

Myers, J.S., 1976. Channel deposits of peridotite, gabbro and chromitite from turbidity currents in the stratiform Fiskenæsset anorthosite complex, southwest Greenland. Lithos 9, 181-291.

Myers, J.S., 1985. Stratigraphy and structure of the Fiskenæsset complex, southernWest Greenland. Bulletin Grønlands Geologiske Undersøgelse 150, pp. 1-72.

Myers, J.S., 1988. Oldest known terrestrial anorthosite at Mount Narryer, Western Australia. Precambrian Research 38, 309-323.

Myers, J.S., Platt, R.G., 1977. Mineral chemistry of layered Archaean anorthosite at Majorqap qava, near Fiskenæsset, southwest Greenland. Lithos 10, 59-72.

Næraa, T., Scherstén, A., 2008. New zircon ages from the Tasiusarsuaq terrane, southern West Greenland. Geological Survey of Denmark and Greenland Bulletin 15, 73-76.

Ordóñez-Calderón, J.C., Polat, A., Fryer, B.J., Gagnon, J.E., Raith, J.G., Appel, P.W.U., 2008. Evidence for HFSE and REE mobility during calc-silicate metasomatism,

Mesoarchean (~3075 Ma) Ivisaartoq greenstone belt, southern West Greenland. Precambrian Research 161, 317-340.

Pearce, J.A., Parkinson, I.J., 1993. Trace element models for mantle melting: application to volcanic arc petrogenesis. In: Prichard, H.M., Alabster, T., Harris, N.B.W., Nearly C.R. (eds.), Magmatic Processes and Plate Tectonics, Geological Society Special Publication 76, 373-403.

Peck, W.H., Valley, J.W., 1996. The Fiskenaesset Anorthosite complex: Stable isotope evidence for shallow emplacement into Archean ocean crust. Geology 24, 523-526.

Phinney, W.C., Morrison, D.A., Maczuga, D.E., 1988. Anorthosites and related megacrystic units in the evolution of Archean crust. Journal of Petrology 29, 1283-1323.

Pidgeon, R.T., Kalsbeek, F., 1978. Dating of igneous and metamorphic events in the Fiskenaesset region of southern west Greenland. Canadian Journal of Earth Sciences 15, 2021-2025.

Polat, A., Hofmann, A.W., 2003. Alteration and geochemical patterns in the 3.7-3.8 Ga Isua greenstone belt, West Greenland. Precambrian Research 126, 197-218.

Polat, A., Appel, P.W.U., Fryer, B., Windley, B., Frei, R., Samson, I.M., Huang, H., 2009. Trace element systematics of the Neoarchean Fiskenæsset anorthosite complex and associated meta-volcanic rocks, SW Greenland: Evidence for a magmatic arc origin. Precambrian Research 175, 87-115.

Polat, A., Frei, R., Schersten, A., Appel, P.W.U., 2010. New age (ca. 2970Ma), mantle source composition and geodynamic constraints on the Archean Fiskenæsset anorthosite complex, SW Greenland. Chemical Geology 277, 1-20.

Polat, A., Fryer, B., Appel, P.W.U., Kalvig, P., Kerrich, R., Dilek, Y., Yang, Z., 2011a. Geochemistry of anorthositic differentiated sills in the Archean (~ 2970 Ma) Fiskenæsset Complex, SW Greenland: Implications for parental magma compositions, geodynamic setting, and secular heat flow in arcs. Lithos 123, 50-72.

Polat, A., Appel, P.W.U., Fryer, B.J., 2011b. An overview of the geochemistry of Eoarchean to Mesoarchean ultramafic to mafic volcanic rocks, SW Greenland: Implications for mantle depletion and petrogenetic processes at subduction zones in the early Earth. Gondwana Research 20, 255-283.

Polat, A., Fryer, B., Samson, I.M., Weisener, C., Appel, P.W.U., Frei, R., Brian F. Windley, B.F., 2011c. Geochemistry of ultramafic rocks and hornblendite veins in the Fiskenæsset layered anorthosite complex, SW Greenland: Evidence for hydrous upper mantle in the Archean. Precambrian Research, doi: 10.1016/j.precamres.2011.11.013.

Riciputi, L.R., Valley, J.W., McGregor, V.R., 1990. Conditions of Archean granulite metamorphism in the Godthab-Fiskenaesset region, southern West Greenland. Journal of Metamorphic Geology 8, 171-190.

Rollinson, H., Reid, C., Windley, B., 2010. Chromitites from the Fiskenæsset anorthositic complex, West Greenland: clues to late Archaean mantle processes. Geological Society, London, Special Publications 338, 197-212.

Sajeev, K., Windley, B.F., Connolly, J.A.D., Kon, Y., 2009. Retrogressed eclogite (20 kbar, 1020°C) from the Neoproterozoic Palghat-Cauvery suture zone, southern India. Precambrian Research 171, 23-36.

Saunders, A.D., Norry, M.J., Tarney, J., 1991. Fluid influence on the trace element compositions of subduction zone magmas. Philosophical Transactions of Royal Society London A., 335, 377-392.

Shaheen, M., Gagnon, J.E., Yang, Z., Fryer, B.J., 2008. Evaluation of the analytical performance of femtosecond laser ablation inductively coupled plasma mass spectrometry at 785 nm with glass reference materials. J. Anal. At. Spectrom., 23: 1610-1621.

Sisson, T.W., Grove, T.L., Coleman, D.S., 1996. Hornblende gabbro sill complex at Onion Valley, California, and a mixing origin for the Sierra Nevada batholith. Contributions to Mineralogy and Petrology 126, 81-108.

Steenfelt, A., Garde, A.A., Moyen, J.F., 2005. Mantle wedge involvement in the petrogenesis of Archaean grey gneisses in West Greenland. Lithos 79, 207-228.

Taylor, S.R., McLennan, S.M., 1985. The Continental Crust: Its Composition and Evolution. Blackwell, Oxford, 312 pp.

Taylor, S.R., McLennan, S.M., 1995. The geochemical evolution of the continental crust. Reviews of Geophysics 33, 241-265.

Weaver, B.L., Tarney, J., Windley, B., 1981. Geochemistry and petrogenesis of the Fiskenæsset anorthosite complex, southern West Greenland: Nature of the parent magma. Geochimica et Cosmochimica Acta 45, 711-725.

Weaver, B.L., Tarney, J., Windley, B.F., Leake, B.E., 1982. Geochemistry and petrogenesis of Archaean metavolcanic amphibolites from Fiskenaesset, S. W. Greenland. Geochimica et Cosmochimica Acta 46, 2203-2215.

Windley, B.F., Garde, A.A., 2009. Arc-generated blocks with crustal sections in the North Atlantic craton of West Greenland: Crustal growth in the Archean with modern analogues. Earth-Science Reviews 93, 1-30.

Windley, B.F., Herd, R.K., Bowden, A.A., 1973 The Fiskenæsset complex, West Greenland, Part I: A preliminary study of the stratigraphy, petrology, and whole-rock chemistry from Qeqertarssuatsiaq. Bulletin Grønlands Geologiske Undersøgelse 106, pp. 1-80.

Windley, B.F., Smith, J.V., 1974. The Fiskenæsset Complex, West Greenland,Part II: General mineral chemistry from Qeqertarssuatsiaq. Bulletin Grønlands Geologiske Undersøgelse 108, pp. 1-54.

Windley, B.F., Smith, J.V. 1976. Archean high grade complexes and modern continental margins. Nature 260, 671-675.

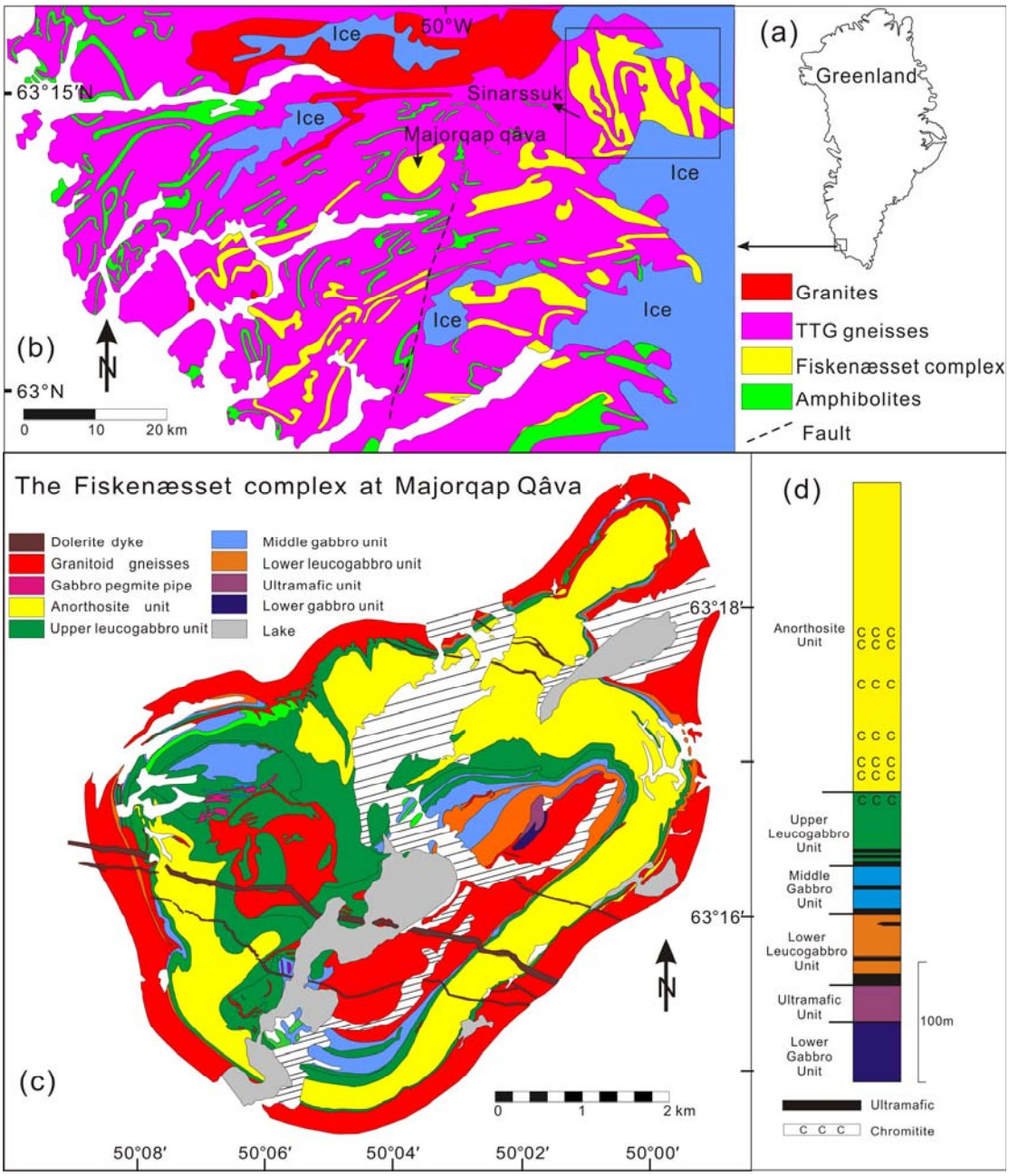

Fig 2.1. (a) General location of the study area in Greenland. (b) Simplified geological map of the Fiskenæsset region (after Myers, 1976)**.** (c) Simplified geological map of the Majorqap qâva outcrop of the Fiskenæsset Complex (after Myers, 1985). (d) Simplified stratigraphic succession of the Fiskenæsset Complex compiled from a number of outcrops (after Myers, 1985). The diagonal lines represent the Quaternary deposits.

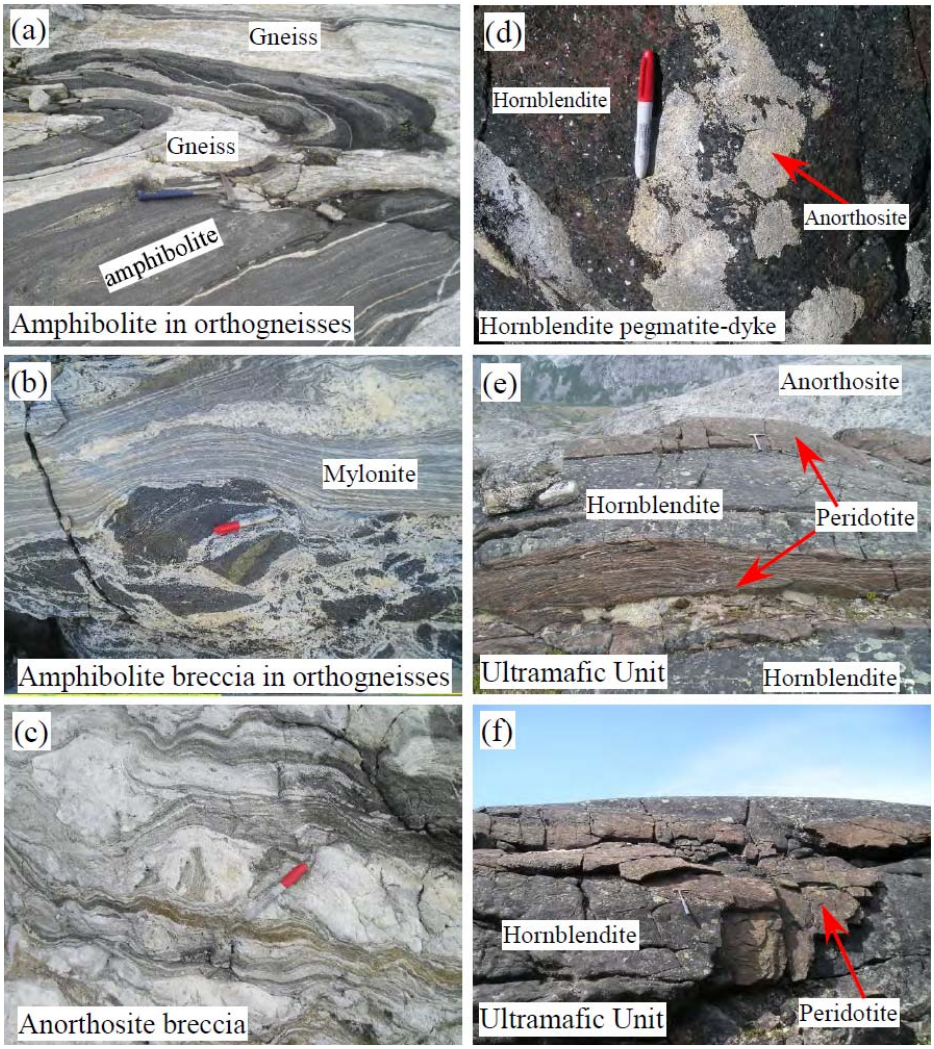

Fig 2.2. Field photographs illustrating the lithological characteristics and field relationships of the Fiskenæsset Complex in the Majorqap qâva area (except Fig. 2a). (a) A contact between orthogneiss and amphibolites, displaying fragments of amphibolites within mylonitic orthogneisses (from the Sinarssuk area). (b) A brecciated anorthosite outcrop at the contact between the Fiskenæsset Complex and orthogneisses. (c) Hornblendite pegmatite (dyke) cutting across the Upper Leucogabbro Unit. (d) Peridotite and hornblendite sills in the Ultramafic Unit. Distant anorthosites are seen in the upper right part of the photograph. (e) Olivine-rich cumulate layers within the Ultramafic Unit. (f) Mineral-graded magmatic layering in the Middle Gabbro Unit.

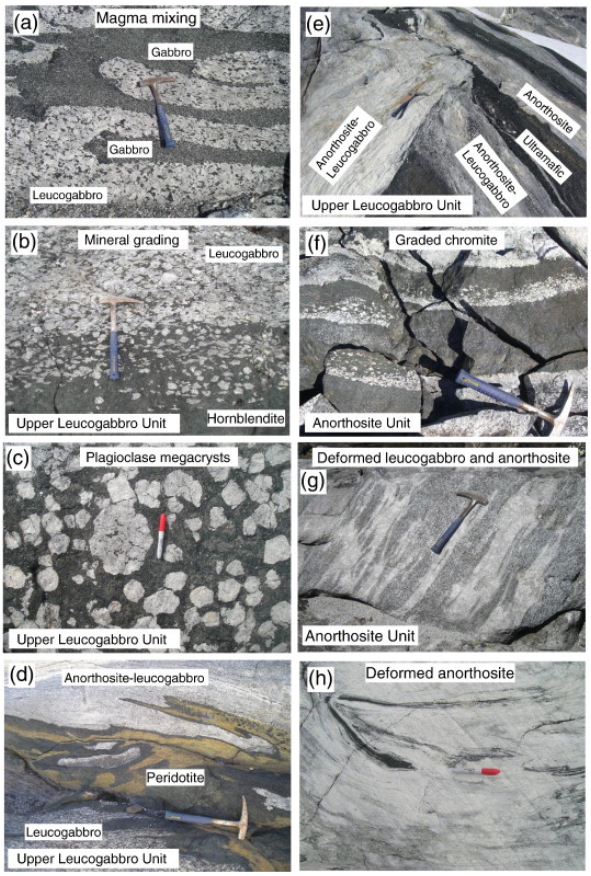

Fig 2.3. Field photographs illustrating the lithological characteristics and field relationships of the Fiskenæsset Complex at Majorqap qâva. (a) An outcrop of interfingered gabbros and leucogabbros, with wavy contacts, in the Middle Gabbro Unit. Gabbros contain rounded leucogabbro inclusion; in turn, leucogabbros enclose gabbro inclusions (not shown). (b) Mineral grading in the Upper Leucogabbro Unit. The outcrop consists mainly of plagioclase and hornblende. (c) Large plagioclase crystals in the Upper Leucogabbro Unit. The outcrop consists mainly of plagioclase and hornblende. (d) Interfingered peridotite, leucogabbro, and anorthosite in the Upper Leucogabbro Unit (from Polat et al., 2009). (e) An anorthositic dyke cross-cutting the leucogabbros and ultramafic layers with sharp contacts in the Upper Leucogabbro Unit (from Polat et al., 2009). (f) Graded chromite layers in the Anorthosite Unit. (g) Leucogabbroic streaks in anorthosite in the Anorthosite Unit. (h) Deformed (folded) anorthosite in the Anorthosite Unit.

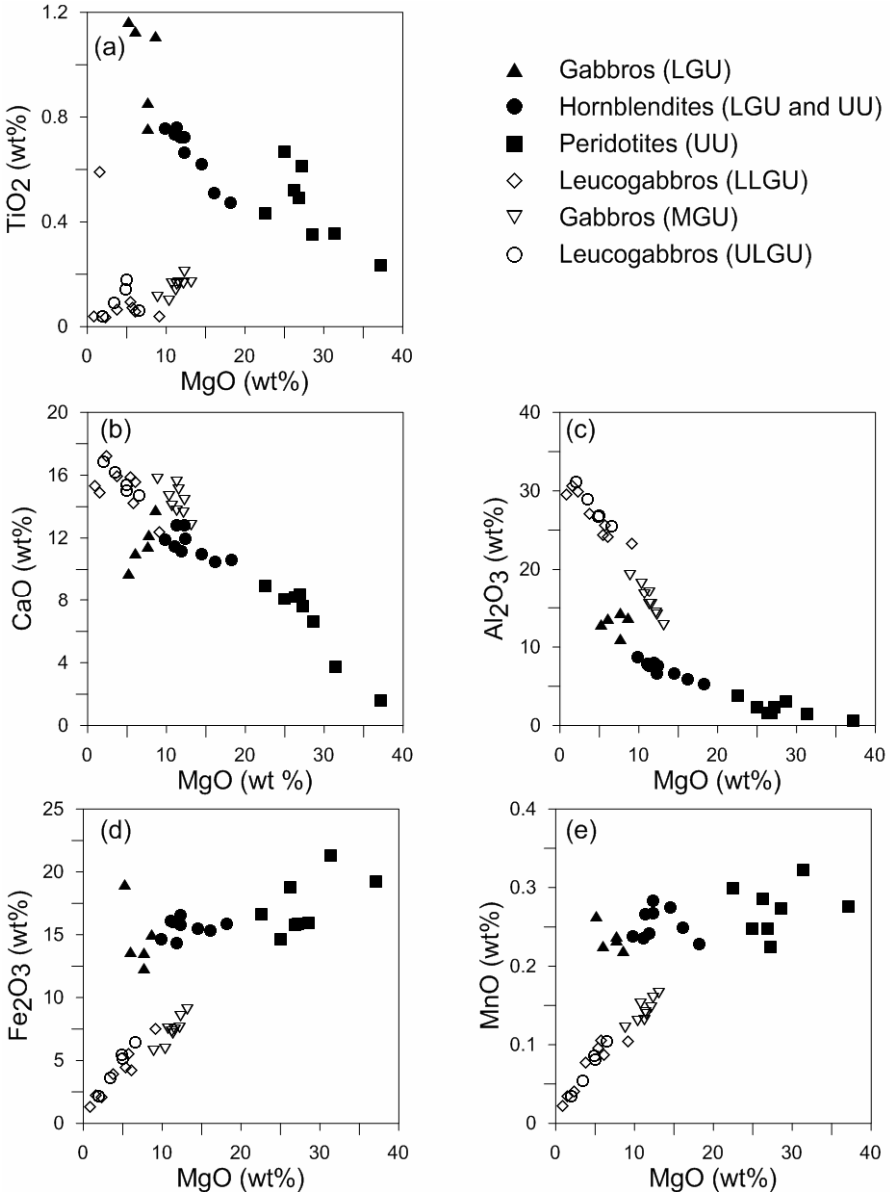

Fig. 2.4. TiO_2, CaO, Fe_2O_3, MnO and Al_2O_3 versus MgO variation diagrams for the Lower Gabbro Unit (LGU), Ultramafic Unit (UU), Lower Leucogabbro Unit (LLGU), Middle Gabbro Unit (MGU), and Upper Leucogabbro Gabbro (ULGU) Unit of the Fiskenæsset Complex.

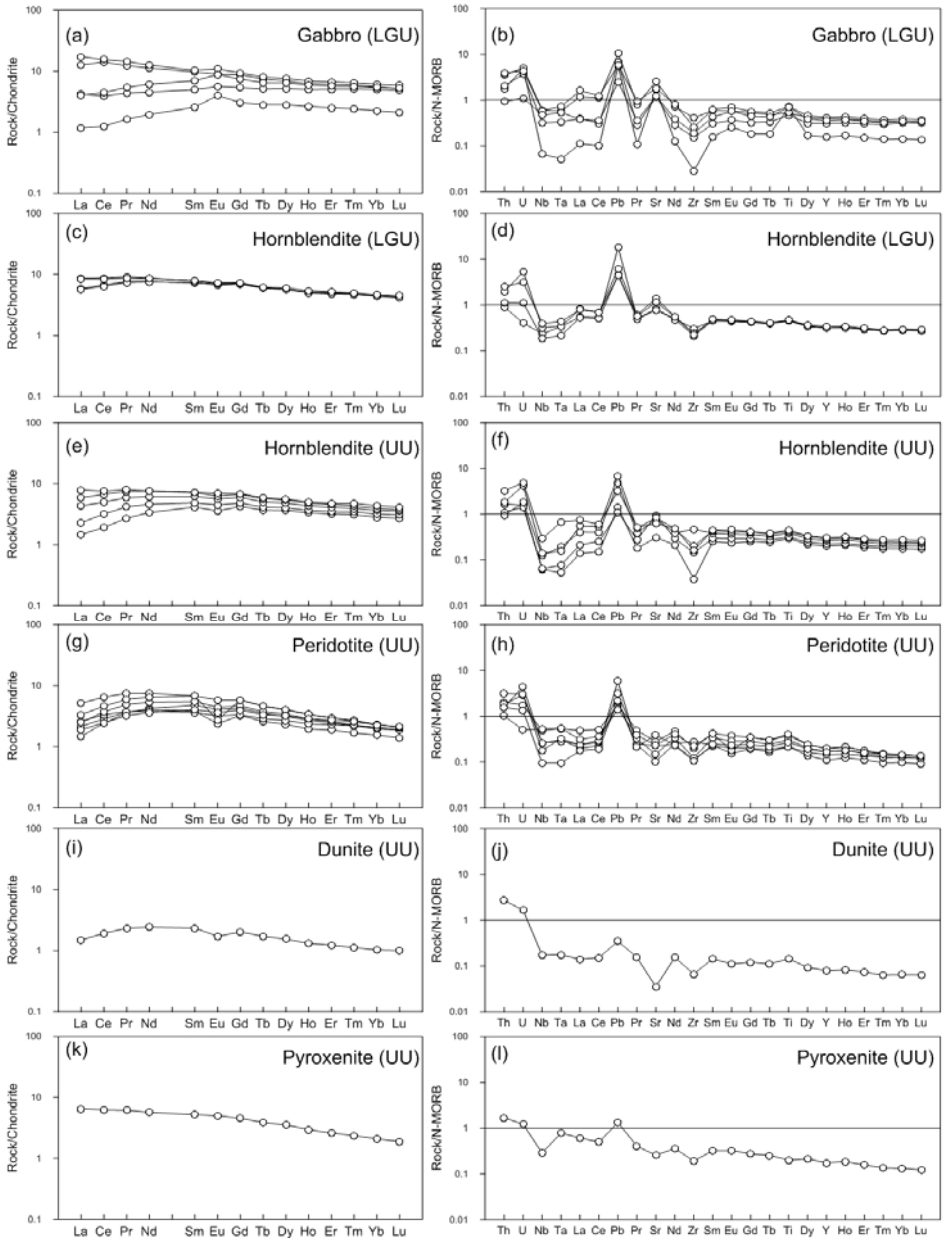

Fig. 2.5. Chondrite-normalized REE and N-MORB-normalized extended trace element diagrams for gabbro and hornblendite samples of the Lower Gabbro Unit (LGU) and for hornblendite, peridotite, dunite and pyroxenite samples of the Ultramafic Unit (UU). Chondrite normalization values are from Taylor and McLennan (1985) and N-MORB normalization values from Hofmann (1988).

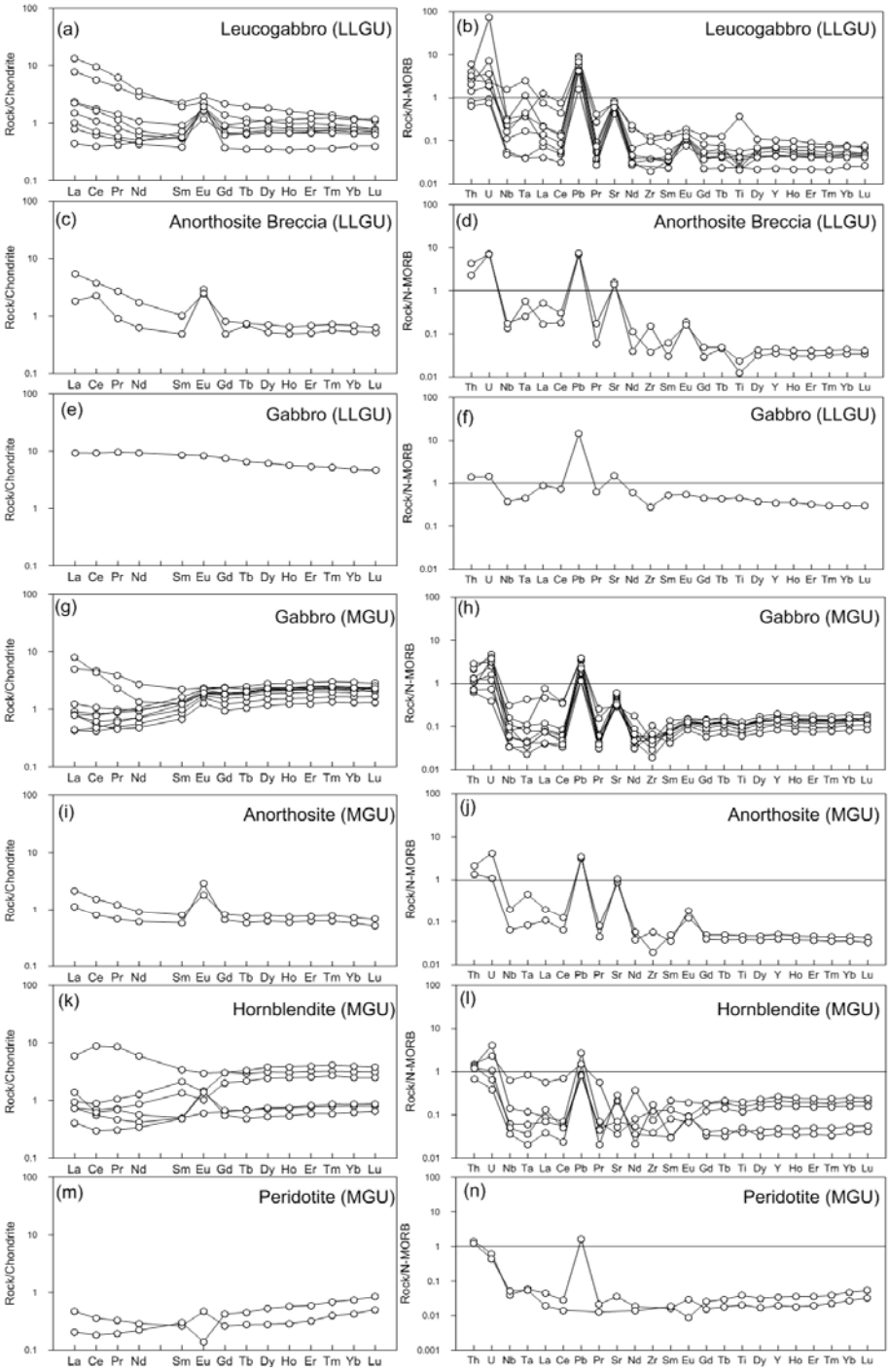

Fig. 2.6. Chondrite-normalized REE and N-MORB-normalized extended trace element diagrams for leucogabbro, anorthosite breccia, and gabbro samples of the Lower Leucogabbro Unit (LLGU) and for gabbro, anorthosite, hornblendite and peridotite samples of the Middle Gabbro Unit (MGU). Chondrite normalization values are from Taylor and McLennan (1985) and N-MORB normalization values from Hofmann (1988).

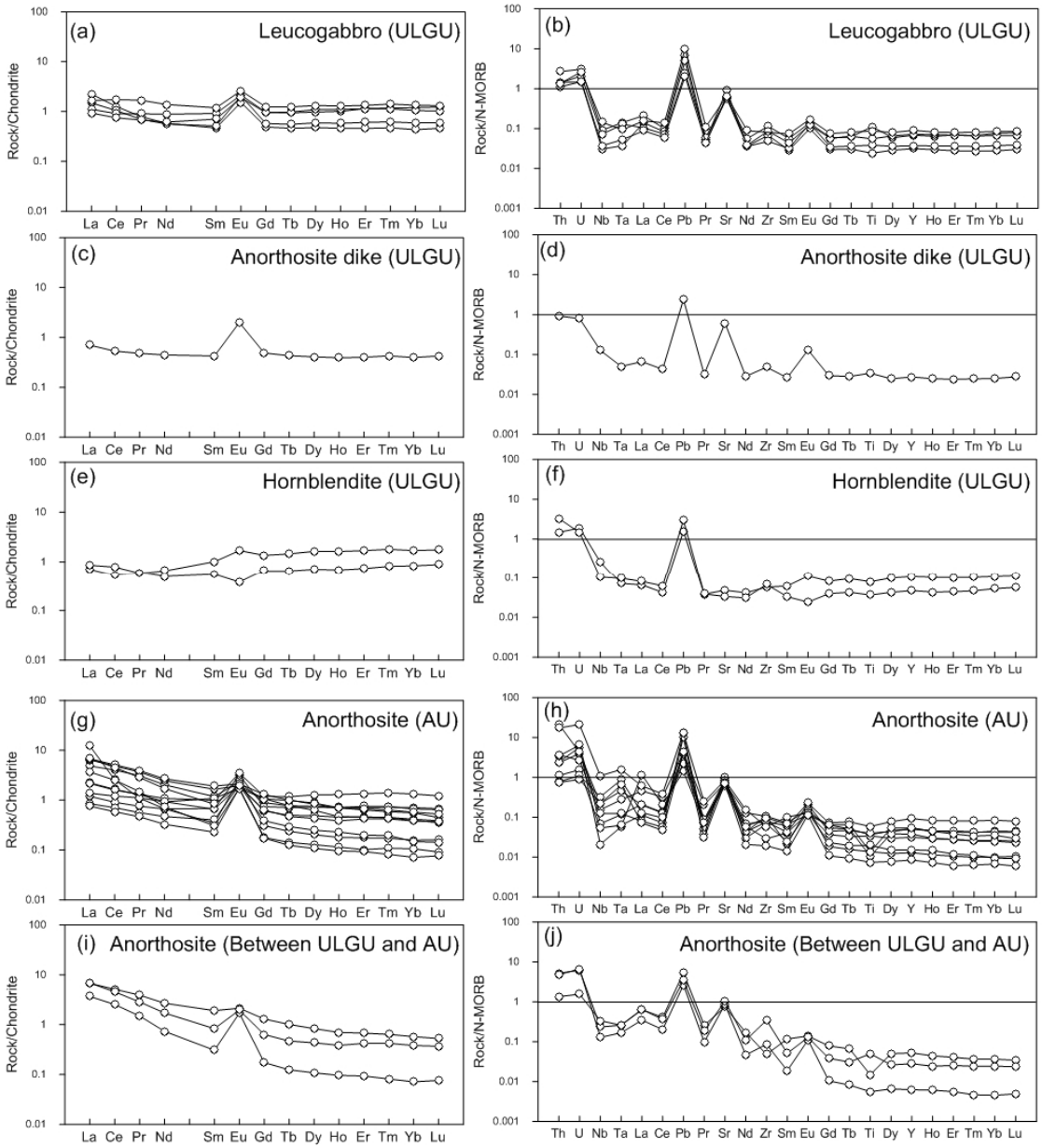

Fig. 2.7. Chondrite-normalized REE and N-MORB-normalized extended trace element diagrams for leucogabbro, anorthosite dike, and hornblendite samples from the Upper Leucogabbro Unit (ULGU) and the Anorthosite Unit (AU). Chondrite normalization values are from Taylor and McLennan (1985) and N-MORB normalization values from Hofmann (1988).

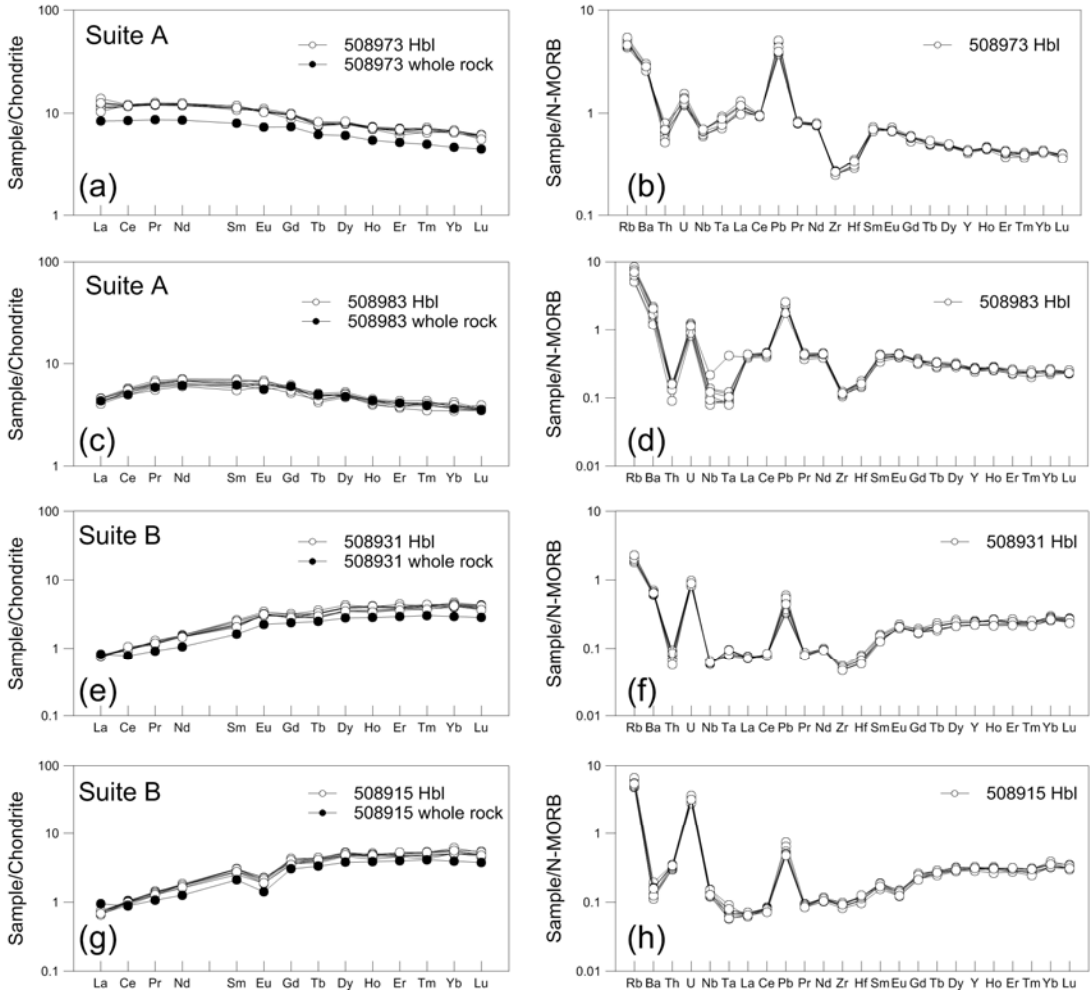

Fig. 2.8. Chondrite-normalized REE and N-MORB-normalized extended trace element diagrams for hornblendes in hornblendites of Ultramafic Units (UMU), and hornblendes in hornblendite and gabbro samples from the Middle Gabbro Unit (MGU). Chondrite normalization values are from Taylor and McLennan (1985) and N-MORB normalization values from Hofmann (1988).

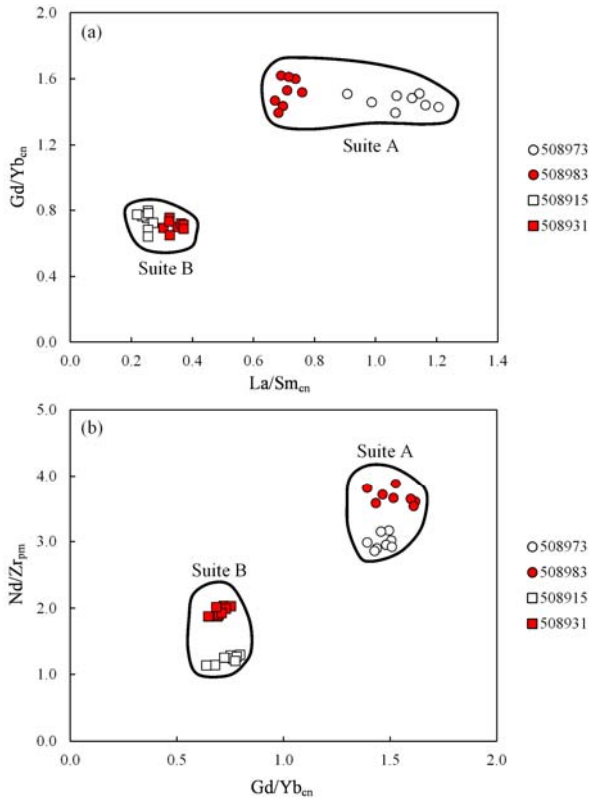

Fig. 2.9. (a) La/Sm_{cn} vs. Gd/Yb_{cn} and (b) Gd/Yb_{cn} vs. Nb/Zr_{pm} diagrams for hornblendes in the Ultramafic, Lower Gabbro, and Middle Gabbro Units. Chondrite normalization values are from Taylor and McLennan (1985) and N-MORB normalization values from Hofmann (1988).

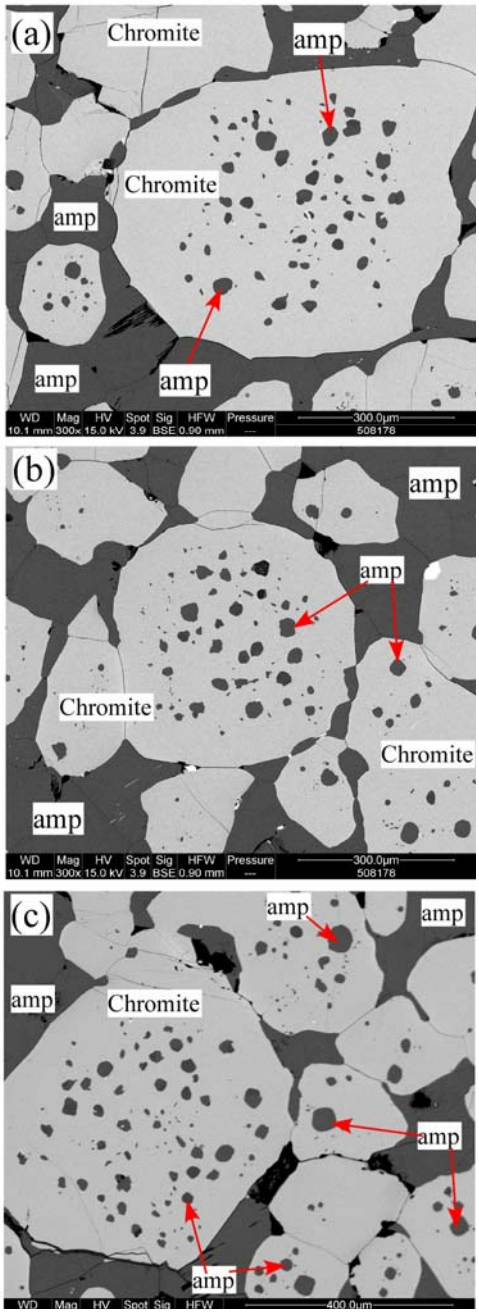

Fig. 2.10. (a-c) Scanning electron microscope (SEM) backscatter electron (BSE) images of Chromite (Cr-Fe-Al-spinel) cumulates in an ultramafic layer of the Fiskenæsset Complex at Sinarssuk. Chromite cumulates contain amphibole grains as inclusions and an interstitial phase. The presence of amphibole (Mg-hornblende) as a primary igneous mineral implies a hydrous magmatic source.

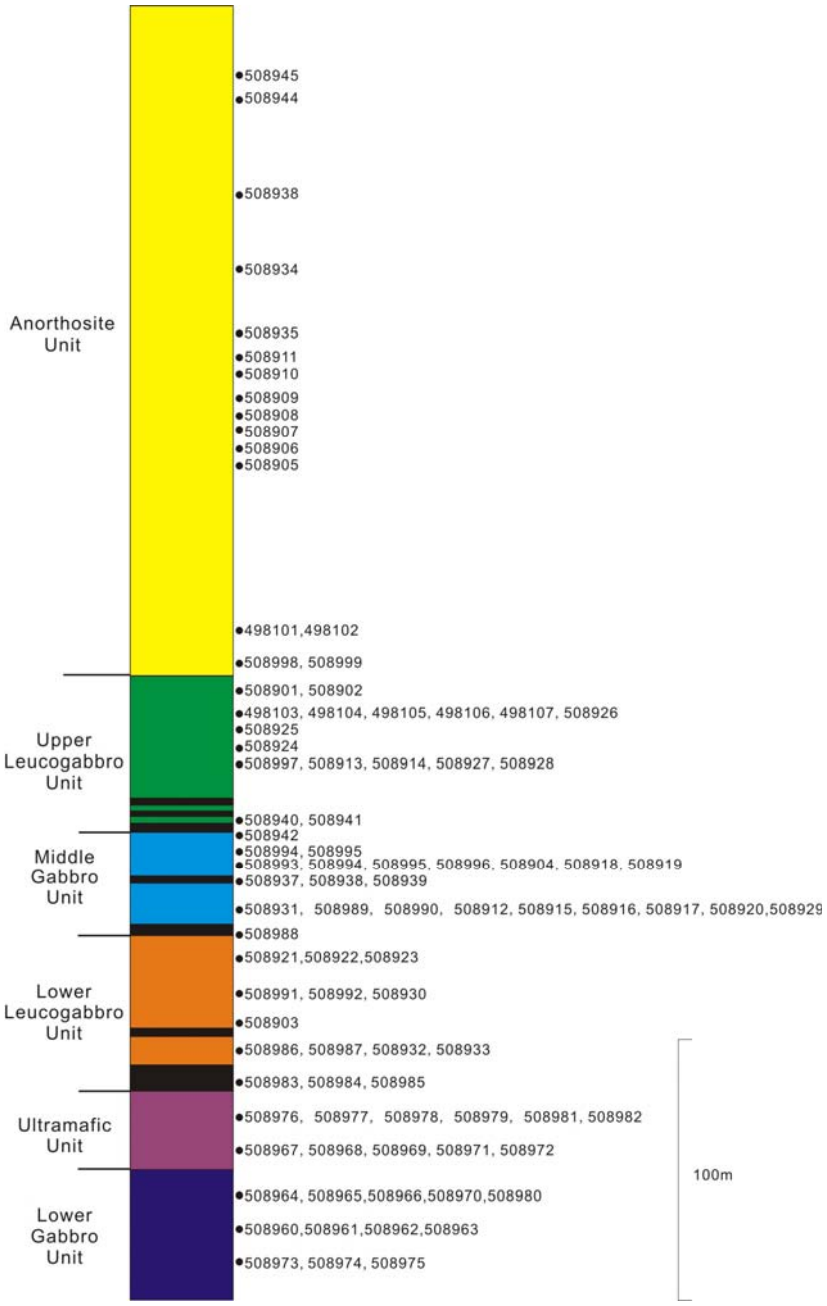

Supplementary Fig 2.1. Sample positions on the generalized stratigraphic section of the Fiskenæsset Complex.

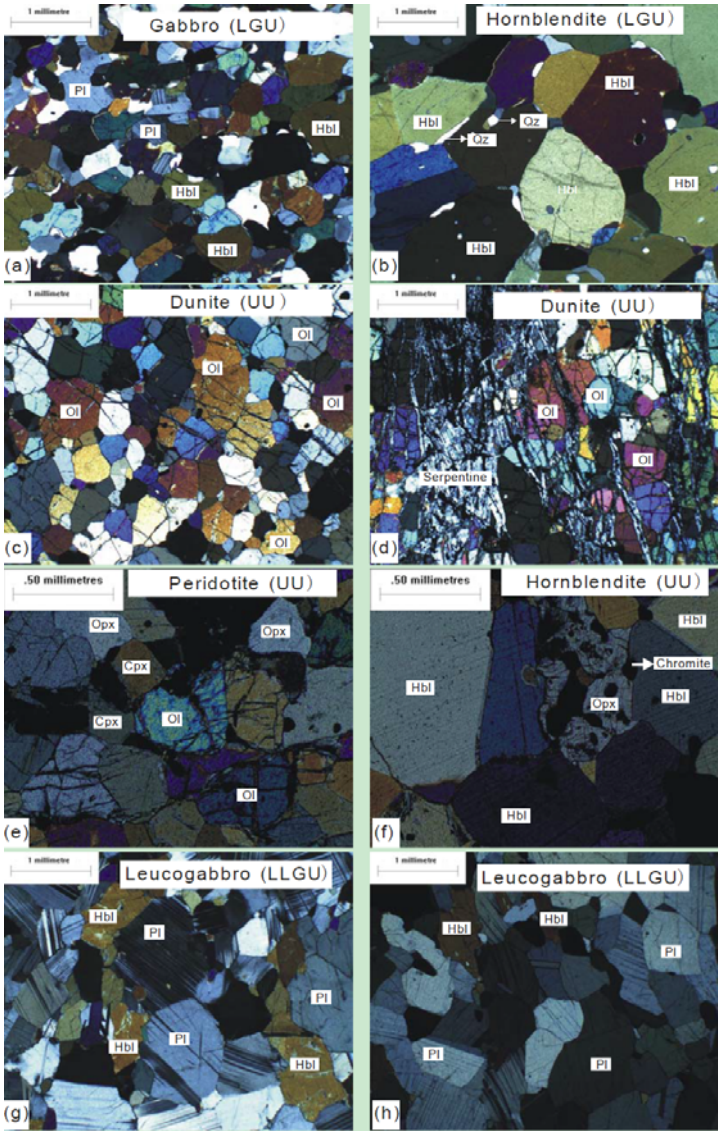

Supplementary Fig 2.2. Photomicrographs of the Lower Gabbro (LGU) Unit, Ultramafic Unit (UU) and Lower Leucogabbro Unit (LLGU) of the Fiskenæsset Complex. (a) Gabbro with metamorphic plagioclase and hornblende. (b) Hornblendite with hornblende and quartz. (c) Dunite with olivine. (d) Dunite with olivine and serpentine. (e) Peridotite with olivine, orthopyroxene and clinopyroxene. (f) Hornblendite with hornblende, relict orthopyroxene and chromite. (g) Typical equilibrium texture with triple junctions with interfacial angles close to 120° in leucogabbro with plagioclase and hornblende. (h) Leucogabbro with plagioclase and hornblende. (Pl: plagioclase, Hbl: hornblende, Qz: quartz, Ol: olivine, Cpx: clinopyroxene, Opx: orthopyroxene).

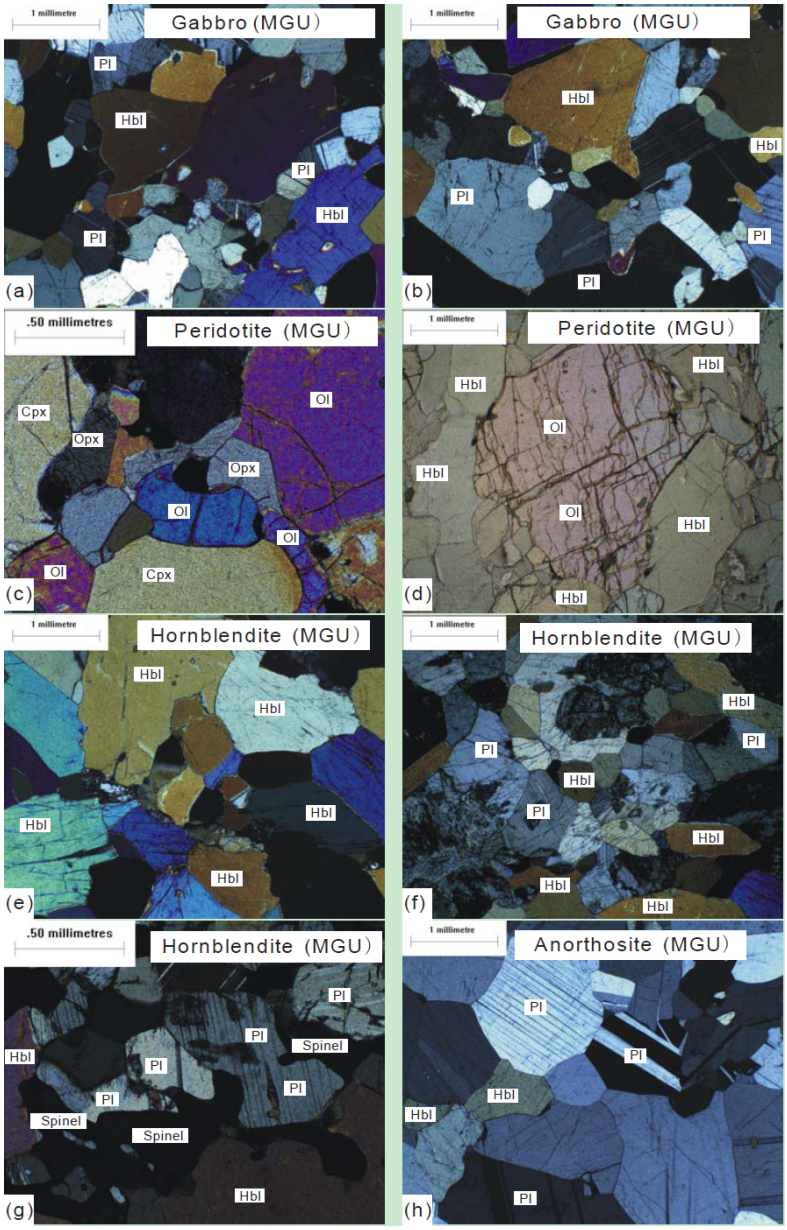

Supplementary Fig 2.3. Photomicrographs of rocks in the Middle Gabbro Unit (MGU) of the Fiskenæsset Complex. (a) Gabbro with plagioclase and hornblende. (b) Gabbro with plagioclase and hornblende. (c) Peridotite with olivine, orthopyroxene and hornblende. (d) Peridotite with olivine and hornblende. (e) Hornblendite. (f) Hornblendite with minor plagioclase. (g) Plagioclase-spinel corona in hornblendite. (h) Anorthosite with minor hornblende. (Pl: plagioclase, Hbl: hornblende, Ol: olivine, Cpx: clinopyroxene, Opx: orthopyroxene).

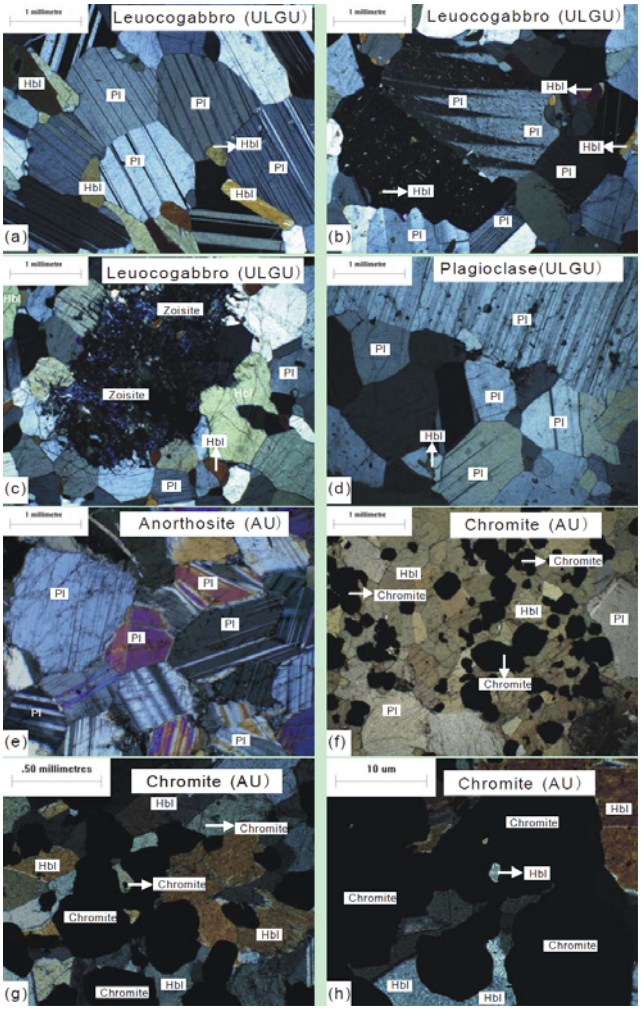

Supplementary Fig 2.4. Photomicrographs of the Upper Leucogabbro Unit (ULGU) and Anorthosite Unit rocks in the Fiskenæsset Complex. (a) Typical equilibrium texture with triple junctions with interfacial angles close to 120° in leucogabbro with plagioclase and minor hornblende. (b) Leucogabbro with twinned plagioclase and hornblende. Plagioclases contain tiny hornblende inclusions. (c) Leucogabbro with plagioclase (altered to zoisite) and hornblende. (d) Recrystallized plagioclases with stable equilibrium triple junctions and planar grain boundaries in Leucogabbro. (e) Anorthosite with plagioclase. (f) A chromite-rich layer in anorthosite. (g) Chromite inclusions in hornblende in anorthosite. (h) Hornblende inclusion in chromite in chromitite. (Pl: plagioclase, Hbl: hornblende, Ol: olivine, Cpx: clinopyroxene, Opx: orthopyroxene).

Table 2.1 Modal abundances of minearals for selected samples in the Fiskenæsset Complex at Majorqap qâva

Sample	Mineral composition	Rock name	Unit
508961	Pyroxene (10-15%), hornblende (80-85%), opaque (0-5%)	Pyroxene hornblendite	Lower Gabbro
508963	Pyroxene (0-3%), plagioclase (5-10%), hornblende (80-85%)	Hornblendite	Lower Gabbro
508974	Plagioclase (30-40%), hornblende (40-50%), pyroxene (20-30%)	Gabbro	Lower Gabbro
508968	Olivine (90-95%), pyroxene (0-2%), serpentine (0-3%), opaque (0-2%)	Dunite	Ultramafic
508971	Olivine (10-15%), pyroxene (70-85%), serpentine (0-3%), opaque (5-10%)	Peridotite	Ultramafic
508972	Olivine (10-15%), pyroxene (70-85%)	Peridotite	Ultramafic
508976	Hornblende (75-80%), pyroxene (25-30%)	Pyroxene hornblendite	Ultramafic
508978	Pyroxene (60-70%), olivine (30-40%), opaque (0-5%)	Peridotite	Ultramafic
508979	Pyroxene (95-98%), opaque (2-3%)	Pyroxenite	Ultramafic
508981	Pyroxene (0-3%), hornblende (90-95%), opaque (0-5%)	Hornblendite	Ultramafic
508983	Hornblende (100%)	Hornblendite	Ultramafic
508985	Pyroxene (25-30%), plagioclase (10-15%), hornblende (60-65%)	Hornblendite	Ultramafic
508903	Plagioclase (75-85%), hornblende (15-20%), biotite (0-2%)	Leucogabbro	Lower Leucogabbro
508921	Plagioclase (70-80%), hornblende (20-30%)	Leucogabbro	Lower Leucogabbro
508930	Plagioclase (90-95%), hornblende (0-5%)	Leucogabbro	Lower Leucogabbro
508986	Plagioclase (60-70%), hornblende (20-30%)	Leucogabbro	Lower Leucogabbro
508917	Plagioclase (30-40%), hornblende (60-70%), pyroxene (0-5%)	Gabbro	Middle Gabbro
508918	Olivine (15-20%), pyroxene (10-15%), hornblende (60-70%), opaque (5-7%)	Olivine-pyroxene hornblendtie	Middle Gabbro
508920	Plagioclase (20-30%), hornblende (70-80%)	Leucogabbro	Middle Gabbro
508929	Pyroxene (2-6%), hornblende (75-85%), spinel (10-15%)	Pyroxene hornblendite	Middle Gabbro
508931	Plagioclase (30-40%), hornblende (60-70%)	Gabbro	Middle Gabbro
508937	Pyroxene (0-5%), hornblende (95-100%)	Hornblendite	Middle Gabbro
508938	Olivine (10-15%), pyroxene (5-10%), hornblende (70-80%), opaque (0-5%)	Olivine-pyroxene hornblendtie	Middle Gabbro
508939	Olivine (70-80%), pyroxene (0-5%), hornblende (15-20%), spinel (2-5%)	Peridotite	Middle Gabbro
508988	Olivine (70-80%), pyroxene (10-15%), hornblende (10-15%), spinel (5-7%)	Peridotite	Middle Gabbro
508989	Plagioclase (30-40%), hornblende (60-70%), zoisite (5-10%)	Gabbro	Middle Gabbro

Table 2.1 (continued)

Sample	Mineral composition	Rock name	Unit
508990	Plagioclase (30-40%), hornblende (60-70%)	Gabbro	Middle Gabbro
508993	Plagioclase (5-15%), pyroxene(4-8%), hornblende (75-85%), spinel (0-2%)	Pyroxene hornblendite	Middle Gabbro
508904	Plagioclase (30-40%), hornblende (50-60%)	Gabbro	Middle Gabbro
508915	Plagioclase (5-15%), hornblende (85-90%)	Hornblendite	Middle Gabbro
508916	Plagioclase (90-95%), hornblende (0-5%)	Anorthosite	Middle Gabbro
508901	Chromite (50-60%), hornblende (30-40%), biotite (0-5%)	Chromititte	Upper Leucogabbro-Anorthosite
508914	Plagioclase (70-80%), hornblende (20-30%), zoisite (5-10%)	Leucogabbro	Upper Leucogabbro
508925	Plagioclase (70-80%), hornblende (20-30%)	Leucogabbro	Upper Leucogabbro
508926	Plagioclase (70-80%), hornblende (20-30%)	Leucogabbro	Upper Leucogabbro
508927	Plagioclase (75-85%), hornblende (20-25%)	Leucogabbro	Upper Leucogabbro
508928	Plagioclase (75-85%), hornblende (20-25%)	Leucogabbro	Upper Leucogabbro
508940	Plagioclase (70-80%), hornblende (20-30%), biotite (5-10%)	Leucogabbro	Upper Leucogabbro
508941	Hornblende (95-100%)	Hornblendite	Upper Leucogabbro
508908	Chromite (40-50%), plagioclase (5-10%), hornblende (30-40%), biotite (0-5%)	Chromititte	Anorthosite
508935	Chromite (40-50%),plagioclase (15-20%), hornblende (30-40%)	Chromititte	Anorthosite
508998	Plagioclase (100%)	Anorthosite	Anorthosite
508999	Plagioclase (100%)	Anorthosite	Anorthosite

Table 2.2
Measured and recommended trace element concentrations (ppm) for USGS BHVO-2 and BCR-2.

	BHVO-2		BCR-2	
Element	Measured (n=34)	Recommanded	Measured (n=9)	Recommanded
Cr	226	280	27	18
Co	46	45	36	37
Ni	186	119	91	
Rb	8.90	9.8	40.83	48
Sr	388	389	350	346
Y	23	26	30	37
Zr	159	172	177	188
Nb	13.9	18	9.2	
Ba	126	130	669	683
La	15	15	24	25
Ce	36	38	51	53
Pr	5.1		6.3	
Nd	23	25	26	28
Sm	5.8	6.2	5.9	
Eu	2.0		1.7	2
Gd	6.1	6.3	6.0	6.8
Tb	0.89	0.9	0.92	
Dy	5.07		5.56	
Ho	0.93	1.04	1.11	
Er	2.49		3.24	
Tm	0.32		0.45	
Yb	1.9	2	2.9	3.5
Lu	0.27	0.28	0.43	
Ta	0.9	1.4	0.5	
Pb	3.3		12.0	
Th	1.5	1.2	6.1	6.2
U	0.48		1.46	1.69

Table 2.3

Measured and recommended trace element concentrations (ppm) for NIST 612.

Element	Measured (n=56)	Recommended	RSD (%)
V	39.31	39.22	2.5
Cr	40.02	39.88	3.6
Co	35.31	35.26	2.1
Ni	38.96	38.44	11.5
Rb	31.71	31.63	2.6
Y	38.28	38.25	1.8
Zr	36.03	35.99	1.7
Nb	38.12	38.06	2.0
Ba	37.80	37.74	1.7
La	35.81	35.77	1.4
Ce	38.41	38.35	1.7
Pr	37.24	37.16	1.4
Nd	35.25	35.24	1.3
Sm	36.76	36.72	1.2
Eu	34.46	34.44	0.9
Gd	36.94	36.95	1.4
Tb	35.93	35.92	1.3
Dy	35.96	35.97	1.3
Ho	37.88	37.87	1.3
Er	37.41	37.43	1.5
Tm	37.56	37.55	1.5
Yb	39.93	39.95	1.8
Lu	37.69	37.71	1.4
Hf	34.76	34.77	1.5
Ta	39.78	39.77	1.1
Pb	39.16	38.96	4.0
Th	37.21	37.23	1.7
U	37.20	37.15	2.1

Table 2.4 Summary of significant compositional values and element ratios for rocks in the Fiskenæsset Complex at Majorqap qâva.

	Gabbro (LGU)	Hornblendite (LGU)	Hornblendites (UU)	Peridotites (UU)	Leucogabbros (LLGU)	Anorthosite (LLGU)	Gabbro (MGU)
	n=5	n=4	n=5	n=7	n=8	n=1	n=9
SiO_2	43.0-50.8	48.8-49.8	45.8-46.8	40.1-46.8	43.7-48.8	43.1	46.3-48.0
Al_2O_3	11.0-14.3	7.6-8.7	5.3-7.6	1.5-3.8	23.3-30.7	30.1	12.7-19.2
Fe_2O_3	12.3-19.0	14.3-16.1	15.3-16.5	14.6-21.3	1.3-7.5	2.2	5.7-9.1
MnO	0.2-0.3	0.2-0.3	0.23-0.28	0.22-.0.32	0.02-0.11	0.06	0.12-0.17
MgO	5.2-8.6	9.8-11.9	12.3-18.2	22.5-31.4	0.9-9.2	0.2	8.9-13.1
CaO	9.7-13.8	11.2-12.8	10.5-12.8	3.7-.8.9	12.4-17.2	22.2	12.8-15.7
TiO_2	0.8-1.2	0.7-0.8	0.5-0.7	0.4-0.7	0.03-0.59	0.04	0.10-0.21
Mg#	35-55	57-62	60-69	73-78	57-74	13	74-78
Cr	27-173	488-872	914-1694	946-1822	66-798	41	882-1600
Ni	85-146	179-331	311-653	1053-1812	26-331	16	175-323
CaO/Al_2O_3	0.8-1.0	1.4-1.7	1.58-2.00	2.13-5.16	0.49-0.65	0.74	0.81-1.02
Al_2O_3/TiO_2	11.0-19.0	9.9-11.5	9.9-11.6	3.16-8.86	52-880	791	68-189
La/Sm cn	0.5-1.7	0.8-1.1	0.35-1.09	0.31-0.76	0.63-6.92	5.38	0.36-6.32
Gd/Yb cn	1.08-1.54	1.52-1.61	1.51-1.70	1.67-2.55	0.80-1.77	1.19	0.73-0.99
La/Yb cn	0.53-2.83	1.28-1.95	0.52-1.81	0.76-2.25	0.38-15.20	7.95	0.18-3.78
Eu/Eu*	0.97-1.42	0.92-0.97	0.85-0.99	0.43-0.93	1.33-5.68	2.7	1.01-1.60
Sr/Nd	21-122	15-24	11-30	4-16	32-203	127	16-181
Th/La	0.05-0.28	0.03-0.06	0.04-0.17	0.04-0.17	0.17-1.09	0.4	0.18-0.87
Nb/Nb*	0.15-0.8	0.24-0.33	0.13-0.20	0.16-0.94	0.08-1.13	0.12	0.11-0.41
Ti/Ti*	1.17-3.88	1.21-.1.27	1.18-1.27	1.24-1.55	0.33-3.12	0.52	0.72-0.85
Pb/Pb*	5.4-53.3	7.1-34.9	4.1-13.2	3.5-25.0	14.4-143.3	32.4	10.8-107.3
Sr/Sr*	1.9-12.9	1.4-2.2	1.1-3.1	0.4-1.6	2.3-18.5	9.9	1.3-18.0

Table 2.4 (continued)

	Hornblendite (MGU)	Anorthosite (MGU)	Peridotites (MGU)	Leucogabbros (ULGU)	Anorthosite(ULGU)	Anorthosite
	n=3	n=2	n=2	n=5	n=1	n=15
SiO_2	34.4-45.8	45.9-46.0	39.9-41.6	44.2-45.7	44.9	42.5-50.8
Al_2O_3	7.3-14.5	30.9-32.4	4.3-7.6	25.6-31.2	28.1	28.1-33.2
Fe_2O_3	12.5-20.6	1.7-2.1	15.8-18.2	2.1-6.5	4.6	0.7-4.6
MnO	0.19-0.22	0.03-0.04	0.24-0.25	0.03-0.10	0.1	0.01-0.07
MgO	19.1-20.8	0.9-1.9	29.7-34.5	2.0-6.5	4.8	0.2-4.8
CaO	5.9-10.1	17.2-17.7	2.7-4.3	14.7-16.8	15	13.9-22.2
TiO_2	0.19-0.36	0.1	0.03-0.06	0.04-0.18	0.1	0.01-0.10
Mg#	67-76	51-65	76-81	64-67	68	13.2-67
Cr	1571-6117	95-174	128-303	21-356	38	8-174
Ni	463-668	20-50	1158-1227	75-253	156	8-156
CaO/Al_2O_3	0.41-1.39	0.5-0.6	0.56-0.63	0.54-0.58	0.53	0.43-0.74
Al_2O_3/TiO_2	23-47	412-531	68-231	149-799	512	342-3629
La/Sm cn	0.45-1.48	2-2.8	0.68-1.78	1.21-4.76	1.65	1.27-12.02
Gd/Yb cn	0.77-0.81	1.1-1.2	0.57-0.61	0.81-1.13	1.24	0.90-2.71
La/Yb cn	0.24-0.93	2.0-3.1	0.27-1.10	0.89-5.16	1.78	1.63-51.60
Eu/Eu*	0.56-1.07	2.3-4.8	0.39-1.77	2.15-3.78	4.37	1.35-8.72
Sr/Nd	5-18	132-250	13-19	67-233	219	44-305
Th/La	0.30-0.49	0.5-0.6	0.78-1.31	0.42-0.65	0.66	0.06-2.66
Nb/Nb*	0.19-0.41	0.17-0.31	0.16-0.34	0.07-0.31	0.51	0.08-1.03
Ti/Ti*	0.80-5.08	0.97-1.02	1.17-1.27	0.82-1.85	1.29	0.23-1.77
Pb/Pb*	16.8-38.0	31.5-65.7	66.0	38.1-97.3	65.4	13.2-227.1
Sr/Sr*	0.5-1.6	11.1-23	1.3-1.7	5.8-19.2	20.5	3.5-26.9

AU: Anorthosite Unit; ULGU: Upper Leucogabbro Unit; MGU: Middle Gabbro Unit; LGU: Lower Gabbro Unit; LLGU: Lower Leucogabbro Unit; UU: Ultramafic Unit

cn: chondrite -normalized

Supplementary Table 2.1

Major (wt.%) and trace (ppm) element concentrations and significant element ratios for rocks in the Lower Gabbro Unit.

	Gabbros					Hornblendites			
Sample	508963	508966	508974	508975	508980	508961	508962	508964	508973
SiO_2	43.0	47.7	50.8	48.5	49.8	48.8	49.6	49.1	49.8
Al_2O_3	13.8	14.3	11.0	12.8	13.6	7.9	7.6	8.0	8.7
Fe_2O_3	15.0	12.3	13.6	19.0	13.6	16.1	16.0	14.3	14.6
MnO	0.22	0.23	0.24	0.26	0.23	0.24	0.27	0.24	0.24
MgO	8.6	7.7	7.7	5.2	6.0	11.1	11.3	11.9	9.8
CaO	13.8	12.2	11.5	9.7	11.1	11.5	12.8	11.2	11.9
Na_2O	1.3	2.5	2.6	3.0	2.9	1.4	1.4	1.5	1.8
K_2O	1.0	0.6	0.7	0.9	0.4	0.3	0.2	0.7	0.6
TiO_2	1.1	0.8	0.9	1.2	1.1	0.7	0.8	0.7	0.8
P_2O_5		0.05	0.08	0.08	0.06	0.04	0.04	0.06	0.06
LOI	1.1	0.4	0.2	-0.2	0.2	0.6	0.5	0.8	0.1
Total	98.8	98.6	99.2	100.5	99.0	98.6	100.4	98.4	98.3
Mg#	53	55	53	35	47	58	58	62	57
Sc	52	52	34	24	46	37	42	35	37
Zr	3	16	43	27	20	32	22	25	23
V	540	313	225	259	339	224	243	203	223
Cr	68	152	173	27	53	607	673	873	488
Co	66	48	61	67	48	70	71	74	67
Ni	132	129	146	85	93	217	220	331	179
Ga	24	23	39	48	39	17	16	18	31
Rb	23.4	3.6	5.2	6.8	3.2	2.6	2.6	4.5	5.5
Sr	169	120	259	185	125	83	78	146	122
Y	5.5	11.2	14.2	15.1	12.7	11.1	11.3	11.2	12.2
Nb	0.23	1.10	2.12	2.07	1.66	0.82	0.65	1.12	1.37
Cs	0.43	0.02	0.10	0.03	0.03	0.03	0.04	0.03	0.05
Ba	46	28	53	75	23	17	17	24	38
La	0.43	1.54	4.64	6.33	1.48	2.15	2.08	3.16	3.08
Ce	1.20	3.76	13.47	14.88	4.27	6.45	6.15	8.35	8.10
Pr	0.22	0.60	1.68	1.96	0.74	1.05	1.01	1.26	1.18
Nd	1.38	3.23	8.01	8.94	4.32	5.46	5.37	6.20	6.08
Sm	0.60	1.15	2.25	2.37	1.61	1.69	1.71	1.81	1.83
Eu	0.35	0.49	0.78	0.94	0.77	0.60	0.58	0.61	0.63
Gd	0.93	1.65	2.67	2.87	2.26	2.12	2.15	2.18	2.25
Tb	0.16	0.30	0.43	0.46	0.38	0.34	0.35	0.35	0.36
Dy	1.07	1.97	2.63	2.90	2.46	2.15	2.18	2.14	2.30
Ho	0.23	0.42	0.53	0.59	0.50	0.44	0.43	0.43	0.46
Er	0.63	1.26	1.51	1.66	1.42	1.25	1.22	1.20	1.29
Tm	0.09	0.18	0.21	0.23	0.20	0.17	0.17	0.17	0.18
Yb	0.56	1.24	1.37	1.51	1.34	1.13	1.10	1.09	1.15
Lu	0.08	0.19	0.20	0.22	0.20	0.16	0.16	0.16	0.17
Ta	0.01	0.06	0.11	0.14	0.10	0.06	0.04	0.07	0.08
Pb	2.7	3.4	5.1	2.9	1.2	8.9	2.2	3.1	2.1
Th	0.34	0.38	0.66	0.74	0.17	0.17	0.21	0.36	0.47
U	0.35	0.26	0.36	0.31	0.08	0.03	0.08	0.38	0.22
CaO/Al_2O_3	1.00	0.85	1.04	0.76	0.81	1.46	1.69	1.40	1.37
Al_2O_3/TiO_2	12.4	19.0	12.9	11.0	12.0	10.7	9.9	11.0	11.5
La/Sm_{cn}	0.46	0.84	1.30	1.68	0.58	0.80	0.76	1.10	1.06
Gd/Yb_{cn}	1.35	1.08	1.58	1.54	1.37	1.52	1.58	1.61	1.59
La/Yb_{cn}	0.53	0.84	2.29	2.83	0.75	1.29	1.28	1.95	1.81
Eu/Eu*	1.42	1.08	0.97	1.10	1.23	0.97	0.92	0.94	0.95
Ce/Ce*	0.90	0.92	1.13	0.99	0.95	1.00	0.99	0.98	0.99
Sr/Nd	122	37	32	21	29	15	15	24	20
Th/La	0.28	0.10	0.05	0.05	0.04	0.03	0.03	0.04	0.06
Zr/Zr*	0.21	0.52	0.63	0.36	0.47	0.65	0.45	0.46	0.43
Nb/Nb*	0.15	0.35	0.29	0.23	0.80	0.33	0.24	0.25	0.28
Ti/Ti*	3.88	1.45	1.17	1.47	1.71	1.25	1.27	1.22	1.21
Pb/Pb*	53.3	22.9	11.0	5.4	6.9	34.9	9.2	9.6	7.1
Sr/Sr*	12.9	3.7	3.0	1.9	3.0	1.5	1.4	2.2	1.9
North	63° 16' 28.2"	63° 16' 33.8"	63° 16' 26.3"	63° 16' 27.1"	63° 16' 30.2"	63° 16' 28.5"	63° 16' 28.5"	63° 16' 29.4"	63° 16' 26.3"
West	50° 01' 23.4"	50° 01' 25.1"	50° 01' 27.1"	50° 01' 25.8"	50° 01' 26.0"	50° 01' 27.3"	50° 01' 27.3"	50° 01' 22.7"	50° 01' 27.1"

cn: chondrite -normalized

Supplementary Table 2.2

Major (wt.%) and trace (ppm) element concentrations and significant element ratios for rocks in the Ultramafic Unit.

	Hornblendites					Peridotites			
Sample	508981	508985	508983	508976	508977	508978	508984	508969	508967
SiO_2	45.8	50.1	48.3	48.5	46.7	44.5	44.7	40.1	43.2
Al_2O_3	5.3	5.9	6.7	6.6	7.6	2.3	1.6	1.5	3.1
Fe_2O_3	15.9	15.3	15.5	15.8	16.5	15.9	18.8	21.3	15.9
MnO	0.23	0.25	0.27	0.27	0.28	0.22	0.29	0.32	0.27
MgO	18.2	16.2	14.5	12.3	12.4	27.2	26.3	31.4	28.6
CaO	10.6	10.5	11.0	12.8	12.0	7.6	8.2	3.7	6.6
Na_2O	0.7	0.7	1.1	1.2	1.2	0.5	0.3	0.3	0.6
K_2O	0.2	0.1	0.4	0.5	0.6	0.1	0.1	0.1	0.1
TiO_2	0.5	0.5	0.6	0.7	0.7	0.6	0.5	0.4	0.4
P_2O_5		0.01	0.03	0.03	0.04	0.02	0.01	0.03	
LOI	1.5	0.2	1.0	0.7	1.0	0.3	-0.9	0.1	0.6
Total	98.9	99.7	99.3	99.3	99.0	99.2	99.9	99.2	99.4
Mg#	69	68	65	61	60	77	73	74	78
Sc	31	34	34	37	36	22	23	14	22
Zr	4	15	49	21	17	21	7	8	12
V	178	170	190	208	217	132	132	80	109
Cr	1694	1318	1222	914	918	1525	1404	946	1677
Co	101	88	87	84	85	122	124	168	135
Ni	653	498	481	311	341	1483	1173	1812	1559
Ga	17	21	22	23	26	13	9	2	8
Rb	2.7	8.7	8.2	3.0	5.9	0.9	0.3	1.0	3.1
Sr	33	100	79	85	62	30	12	12	24
Y	7.3	8.1	9.5	10.4	10.9	7.2	5.5	3.9	5.3
Nb	0.22	0.22	0.43	0.49	1.02	1.71	0.28	0.91	0.93
Cs	0.04	0.91	0.09	0.06	0.14	0.02	0.02	0.09	0.20
Ba	7	15	16	17	19	4	2	2	7
La	0.54	0.84	1.58	2.15	2.91	1.89	0.54	0.78	0.95
Ce	1.84	3.03	4.77	6.40	7.21	6.19	2.30	2.72	3.20
Pr	0.37	0.57	0.81	1.02	1.09	1.03	0.49	0.50	0.51
Nd	2.39	3.28	4.35	5.40	5.43	5.33	2.99	2.84	2.67
Sm	0.96	1.12	1.42	1.64	1.68	1.57	1.10	0.88	0.84
Eu	0.31	0.39	0.49	0.55	0.61	0.51	0.35	0.21	0.28
Gd	1.30	1.47	1.83	2.05	2.10	1.77	1.30	0.99	1.02
Tb	0.21	0.24	0.29	0.33	0.34	0.27	0.20	0.15	0.17
Dy	1.39	1.54	1.82	2.05	2.12	1.51	1.19	0.88	1.02
Ho	0.28	0.31	0.37	0.41	0.43	0.29	0.23	0.17	0.20
Er	0.79	0.87	1.02	1.14	1.18	0.74	0.61	0.47	0.57
Tm	0.11	0.12	0.14	0.15	0.17	0.09	0.08	0.06	0.08
Yb	0.70	0.79	0.90	0.98	1.08	0.57	0.48	0.38	0.49
Lu	0.10	0.12	0.13	0.14	0.16	0.08	0.07	0.05	0.07
Ta	0.01	0.01	0.04	0.03	0.13	0.10	0.02	0.06	0.05
Pb	0.69	0.54	2.33	3.32	1.60	0.86		2.87	1.03
Th	0.31	0.21	0.18	0.34	0.61	0.38	0.34	0.30	0.35
U	0.11	0.10	0.13	0.30	0.35	0.13	0.04	0.32	0.21
CaO/Al_2O_3	2.00	1.77	1.65	1.95	1.58	3.29	5.01	2.53	2.13
Al_2O_3/TiO_2	11.2	11.6	10.7	9.9	10.5	3.8	3.2	4.2	8.9
La/Sm cn	0.35	0.47	0.70	0.83	1.09	0.76	0.31	0.56	0.71
Gd/Yb cn	1.51	1.52	1.64	1.70	1.57	2.53	2.20	2.11	1.67
La/Yb cn	0.52	0.72	1.19	1.49	1.81	2.25	0.76	1.39	1.30
Eu/Eu*	0.85	0.93	0.93	0.91	0.99	0.93	0.90	0.67	0.92
Ce/Ce*	0.96	1.03	0.99	1.01	0.95	1.04	1.05	1.01	1.07
Sr/Nd	14	30	18	16	11	6	4	4	9
Th/La	0.17	0.07	0.04	0.05	0.08	0.06	0.15	0.11	0.11
Zr/Zr*	0.16	0.49	1.22	0.44	0.35	0.45	0.24	0.31	0.50
Nb/Nb*	0.13	0.13	0.20	0.14	0.19	0.49	0.16	0.46	0.39
Ti/Ti*	1.27	1.23	1.25	1.18	1.25	1.41	1.55	1.43	1.24
Pb/Pb*	8.5	4.1	12.1	13.2	5.8	3.5		25.0	8.2
Sr/Sr*	1.5	3.1	1.8	1.5	1.1	0.6	0.4	0.4	0.9
North	63° 16' 31.7"	63° 16' 35.5"	63° 16' 34.2"	63° 16' 27.2"	63° 16' 28.4"	63° 16' 32.5"	63° 16' 35.2"	63° 16' 28.4"	63° 16' 28.7"
West	50° 01' 30.0"	50° 01' 28.9"	50° 01' 27.5"	50° 01' 31.2"	50° 01' 29.1"	50° 01' 26.8"	50° 01' 27.5"	50° 01' 24.6"	50° 01' 25.2"

Supplementary Table 2.2 (continued)

	Peridotites			Dunite	Pyroxenite
Sample	508971	508982	508972	508968	508979
SiO_2	45.0	46.8	45.2	39.3	53.4
Al_2O_3	1.6	2.3	3.8	0.6	2.1
Fe_2O_3	15.8	14.6	16.6	19.2	8.6
MnO	0.25	0.25	0.30	0.28	0.18
MgO	26.9	25.0	22.5	37.2	21.3
CaO	8.4	8.1	8.9	1.6	10.9
Na_2O	0.4	0.5	0.7	0.1	0.4
K_2O	0.1	0.2	0.2	0.1	0.1
TiO_2	0.5	0.7	0.4	0.2	0.3
P_2O_5	0.01	0.02	0.01	0.01	
LOI	1.0	0.7	0.6	1.3	1.2
Total	99.9	99.2	99.3	99.8	98.6
Mg#	77	77	73	79	83
Sc	21	23	28	13	23
Zr	13	23	11	7	20
V	115	134	154	54	83
Cr	1602	1599	1822	1395	833
Co	128	109	127	167	66
Ni	1469	1343	1053	2483	774
Ga	10	11	14	4	10
Rb	0.7	1.1	1.1	0.7	1.0
Sr	16	23	41	4	28
Y	6.0	7.1	6.0	2.8	6.2
Nb	0.63	1.86	0.34	0.61	1.01
Cs	0.03	0.02	0.01	0.12	0.07
Ba	3	3	7	7	2
La	0.91	1.22	0.69	0.55	2.38
Ce	3.56	4.38	2.35	1.83	5.98
Pr	0.67	0.82	0.44	0.32	0.85
Nd	3.82	4.62	2.59	1.73	4.04
Sm	1.26	1.56	0.92	0.54	1.21
Eu	0.38	0.24	0.32	0.15	0.44
Gd	1.42	1.79	1.21	0.62	1.40
Tb	0.22	0.27	0.19	0.10	0.22
Dy	1.29	1.53	1.23	0.59	1.35
Ho	0.24	0.29	0.24	0.11	0.25
Er	0.63	0.74	0.67	0.30	0.65
Tm	0.08	0.10	0.09	0.04	0.08
Yb	0.51	0.57	0.56	0.25	0.52
Lu	0.07	0.08	0.08	0.04	0.07
Ta	0.06	0.10	0.02	0.03	0.15
Pb	1.52	0.69	1.06	0.17	0.65
Th	0.59	0.19	0.29	0.51	0.32
U	0.22	0.04	0.10	0.12	0.09
CaO/Al_2O_3	5.16	3.51	2.36	2.88	5.29
Al_2O_3/TiO_2	3.3	3.5	8.7	2.4	6.4
La/Sm cn	0.45	0.49	0.47	0.64	1.24
Gd/Yb cn	2.28	2.55	1.75	1.98	2.17
La/Yb cn	1.22	1.45	0.83	1.46	3.09
Eu/Eu*	0.88	0.43	0.91	0.78	1.02
Ce/Ce*	1.07	1.03	1.00	1.02	0.99
Sr/Nd	4	5	16	2	7
Th/La	0.17	0.04	0.13	0.28	0.05
Zr/Zr*	0.37	0.53	0.44	0.45	0.56
Nb/Nb*	0.21	0.94	0.18	0.28	0.28
Ti/Ti*	1.36	1.52	1.30	1.41	0.86
Pb/Pb*	10.1	3.7	10.7	2.3	2.9
Sr/Sr*	0.4	0.5	1.6	0.2	0.6
North	63° 16' 31.1"	63° 16' 34.7"	63° 16' 31.5"	63° 16' 28.9"	63° 16' 32.5"
West	50° 01' 26.0"	50° 01' 30.2"	50° 01' 26.4"	50° 01' 24.4"	50° 01' 26.8"

cn: chondrite -normalized

Supplementary Table 2.3

Major (wt.%) and trace (ppm) element concentrations and significant element ratios for rocks in the Lower Leucogabbro Unit.

	Leucogabbros								Gabbro
Sample	508903	508922	508923	508930	508986	508987	508991	508992	508970
SiO_2	45.5	43.7	47.7	48.8	46.7	47.0	45.1	46.6	50.9
Al_2O_3	25.7	23.3	30.7	29.5	24.2	27.0	29.9	24.4	9.3
Fe_2O_3	5.5	7.5	2.2	1.3	4.2	3.9	2.1	4.4	13.9
MnO	0.11	0.10	0.03	0.02	0.09	0.08	0.04	0.10	0.25
MgO	5.8	9.2	1.5	0.9	6.1	3.8	2.3	5.4	9.3
CaO	14.2	12.4	14.9	15.3	15.6	16.0	17.2	15.8	12.1
Na_2O	1.2	1.3	2.0	1.9	1.2	1.4	1.0	1.1	2.1
K_2O	0.5	0.2	0.8	0.2	0.4	0.2	0.2	0.1	0.8
TiO_2	0.07	0.04	0.59	0.04	0.06	0.07	0.03	0.09	0.74
P_2O_5	0.01		0.02	0.01		0.01	0.15	0.02	0.06
LOI	1.2	1.1	0.4	0.4	0.7	0.4	0.6	0.8	0.5
Total	99.7	98.8	100.9	98.4	99.1	99.8	98.6	98.9	100
Mg#	67	71	58	57	74	66	69	71	57
Sc	9	3	7	6	21	20	14	28	36
Zr	10		13	10	4	2			29
V	34	15	53	21	57	79	32	91	217
Cr	96	66	136	98	798	489	151	366	455
Co	34	51	10	5	25	20	11	23	63
Ni	196	331	57	26	128	63	60	102	163
Ga	29	22	46	36	29	33	45	33	32
Rb	52.9	6.0	53.4	5.8	5.0	3.5	8.8	4.8	18.2
Sr	84	44	84	80	66	72	78	61	166
Y	2.10	0.82	3.74	2.45	1.59	1.63	1.58	2.60	12.52
Nb	1.14	0.19	5.53	0.80	0.39	0.56	1.05	0.17	1.33
Cs	6.21	0.81	1.87	0.47	0.15	0.15	0.69	0.63	0.27
Ba	54	7	100	73	16	9	18	7	43
La	0.86	0.29	2.90	4.90	0.55	0.37	0.81	0.16	3.44
Ce	1.72	0.59	5.42	9.17	1.04	0.68	1.56	0.37	8.90
Pr	0.19	0.07	0.58	0.86	0.11	0.08	0.16	0.06	1.33
Nd	0.76	0.31	2.10	2.53	0.44	0.35	0.52	0.34	6.68
Sm	0.21	0.09	0.52	0.45	0.12	0.13	0.13	0.16	1.98
Eu	0.15	0.18	0.25	0.20	0.10	0.17	0.14	0.17	0.73
Gd	0.27	0.11	0.66	0.42	0.20	0.21	0.19	0.28	2.30
Tb	0.05	0.02	0.11	0.07	0.04	0.04	0.04	0.06	0.38
Dy	0.33	0.14	0.69	0.41	0.26	0.28	0.26	0.43	2.34
Ho	0.07	0.03	0.14	0.08	0.06	0.06	0.06	0.10	0.47
Er	0.20	0.09	0.37	0.24	0.17	0.18	0.17	0.30	1.33
Tm	0.03	0.01	0.05	0.03	0.03	0.03	0.02	0.04	0.18
Yb	0.20	0.10	0.30	0.22	0.17	0.19	0.16	0.28	1.18
Lu	0.03	0.02	0.04	0.03	0.03	0.03	0.02	0.04	0.17
Ta	0.08	0.01	0.48	0.07	0.03	0.08	0.22	0.01	0.09
Pb	4.45	0.78	3.09	3.96	3.98	2.61	3.31	2.05	6.97
Th	0.75	0.15	0.49	1.14	0.59	0.26	0.38	0.12	0.26
U	5.13	0.07	0.16	0.13	0.25	0.14	0.51	0.05	0.10
CaO/Al_2O_3	0.55	0.53	0.49	0.52	0.64	0.59	0.58	0.65	1.30
Al_2O_3/TiO_2	362	597	52	797	417	410	880	262	13
La/Sm cn	2.55	2.08	3.51	6.92	2.80	1.81	3.90	0.63	1.10
Gd/Yb cn	1.09	0.93	1.77	1.57	0.95	0.88	0.94	0.80	1.58
La/Yb cn	2.93	2.00	6.55	15.20	2.17	1.32	3.44	0.38	1.98
Eu/Eu*	1.89	5.68	1.33	1.42	2.00	3.16	2.77	2.38	1.04
Ce/Ce*	0.99	0.96	0.98	1.05	0.98	0.93	1.03	0.91	0.97
Sr/Nd	111	145	40	32	152	203	149	179	25
Th/La	0.87	0.53	0.17	0.23	1.09	0.71	0.47	0.74	0.03
Zr/Zr*	1.55		0.77	0.59	1.07	0.58			0.50
Nb/Nb*	0.35	0.22	1.13	0.08	0.17	0.44	0.46	0.29	0.34
Ti/Ti*	0.84	1.09	3.12	0.33	0.87	0.91	0.51	0.86	1.15
Pb/Pb*	78.9	39.3	17.8	14.4	118.5	114.9	68.4	143.3	20.7
Sr/Sr*	9.3	12.8	3.3	2.3	12.7	18.3	11.6	18.5	2.4
North	63° 17' 10.3"	63° 17' 10.6"	63° 17' 04.6"	63° 16' 36.4"	63° 16' 32.2"	63° 16' 31.4"	63° 16' 36.2"	63° 16' 36.3"	63° 16' 30.3"
West	50° 05' 32.3"	50° 06' 06.5"	50° 06' 36.5"	50° 07' 37.0"	50° 01' 36.5"	50° 01' 44.4"	50° 02' 18.4"	50° 02' 24.3"	50° 01' 25.8"

Supplemer Supplementary Table 2.3 (continued)

	Anorthosite breccias	
Sample	508932	508933[a]
SiO_2	43.1	42.2
Al_2O_3	30.1	31.7
Fe_2O_3	2.2	0.8
MnO	0.06	0.04
MgO	0.2	0.0
CaO	22.2	23.7
Na_2O	1.1	0.2
K_2O		0.1
TiO_2	0.04	0.02
P_2O_5	0.03	0.01
LOI	1.9	2.1
Total	101.0	100.9
Mg#	13	9
Sc	2	2
Zr	4	16
V	13	12
Cr	41	176
Co	2	1
Ni	16	5
Ga	36	35
Rb	0.7	3.8
Sr	157	177
Y	1.64	1.24
Nb	0.62	0.47
Cs	0.09	0.12
Ba	4	10
La	2.00	0.67
Ce	3.66	2.18
Pr	0.37	0.12
Nd	1.24	0.44
Sm	0.23	0.11
Eu	0.21	0.25
Gd	0.25	0.15
Tb	0.04	0.04
Dy	0.27	0.20
Ho	0.06	0.04
Er	0.17	0.13
Tm	0.03	0.02
Yb	0.17	0.13
Lu	0.02	0.02
Ta	0.05	0.11
Pb	3.68	3.44
Th	0.81	0.43
U	0.50	0.52
CaO/Al_2O_3	0.74	0.75
Al_2O_3/TiO_2	791	1583
La/Sm cn	5.38	3.76
Gd/Yb cn	1.19	0.92
La/Yb cn	7.95	3.42
Eu/Eu*	2.70	5.95
Ce/Ce*	1.00	1.78
Sr/Nd	127	398
Th/La	0.22	0.20
Zr/Zr*	0.46	4.46
Nb/Nb*	0.12	0.21
Ti/Ti*	0.52	0.33
Pb/Pb*	32.4	67.7
Sr/Sr*	9.9	32.2
North	63° 16' 34.9"	63° 16' 34.5"
West	50° 07' 09.3"	50° 07' 13.3"

cn: chondrite -normalized. [a]Altered

Supplementary Table 2.4

Major (wt.%) and trace (ppm) element concentrations and significant element ratios for rocks in the Middle Gabbro Unit.

	Gabbros								
Sample	508904	508912	508917	508920	508931	508989	508990	508994	508995
SiO_2	46.8	47.4	46.3	47.9	46.5	48.0	47.0	46.6	47.7
Al_2O_3	16.8	12.7	15.5	14.3	14.1	19.2	18.1	17.1	15.4
Fe_2O_3	7.5	9.1	7.4	7.6	8.5	5.7	5.9	7.3	7.2
MnO	0.15	0.17	0.14	0.15	0.16	0.12	0.13	0.13	0.14
MgO	10.7	13.1	11.6	12.2	12.3	8.9	10.4	11.3	11.3
CaO	14.0	12.8	15.1	13.6	14.4	15.7	14.6	13.7	15.6
Na_2O	0.9	1.0	0.8	0.9	0.9	0.6	0.7	1.0	0.8
K_2O	0.2	0.4	0.1	0.2	0.1	0.1	0.2	0.3	0.1
TiO_2	0.17	0.17	0.17	0.16	0.21	0.11	0.10	0.14	0.16
P_2O_5	0.01			0.01	0.01			0.02	
LOI	1.1	1.5	1.2	1.4	2.0	1.4	1.9	2.6	1.4
Total	98.3	98.3	98.2	98.3	99.2	99.8	99.1	100.1	99.8
Mg#	74	74	75	76	74	75	78	75	76
Sc	46	47	46	49	52	37	37	40	52
Zr	6	5	5	4	3	11	7	2	5
V	147	157	151	153	181	119	108	127	163
Cr	1218	1413	1104	1186	1153	882	911	978	1600
Co	52	60	55	51	56	37	40	50	46
Ni	271	323	275	283	273	175	212	261	266
Ga	19	19	18	17	18	26	25	27	24
Rb	3.0	5.3	4.3	3.2	5.6	1.8	8.6	6.0	3.2
Sr	49	31	34	42	32	56	62	37	32
Y	5.2	5.8	5.3	5.0	6.7	3.5	2.8	4.4	5.2
Nb	0.28	1.10	0.19	0.55	0.39	0.12	0.11	0.34	0.21
Cs	0.24	0.26	0.24	0.19	1.17	0.48	1.60	0.23	0.58
Ba	9	25	6	16	11	4	13	12	4
La	0.46	1.84	0.34	2.92	0.30	0.16	0.29	0.29	0.16
Ce	1.02	4.54	0.79	4.20	0.74	0.40	0.51	0.58	0.45
Pr	0.14	0.54	0.12	0.32	0.13	0.07	0.06	0.09	0.08
Nd	0.69	1.95	0.67	0.97	0.75	0.40	0.34	0.50	0.52
Sm	0.30	0.51	0.31	0.29	0.37	0.20	0.16	0.23	0.28
Eu	0.19	0.20	0.17	0.16	0.20	0.14	0.11	0.15	0.17
Gd	0.57	0.74	0.58	0.54	0.72	0.38	0.29	0.47	0.56
Tb	0.11	0.13	0.11	0.11	0.14	0.08	0.06	0.10	0.12
Dy	0.83	0.91	0.85	0.79	1.06	0.57	0.44	0.72	0.88
Ho	0.18	0.20	0.19	0.18	0.24	0.13	0.10	0.16	0.20
Er	0.56	0.62	0.57	0.55	0.73	0.39	0.31	0.50	0.59
Tm	0.08	0.09	0.08	0.08	0.11	0.06	0.05	0.07	0.09
Yb	0.54	0.60	0.57	0.52	0.73	0.41	0.32	0.48	0.59
Lu	0.08	0.09	0.09	0.08	0.11	0.06	0.05	0.10	0.09
Ta	0.02	0.08	0.01	0.02	0.02	0.00	0.01	0.01	0.01
Pb	0.85	1.65	0.57	1.92	1.77	0.57	1.88	1.22	1.08
Th	0.40	0.41	0.25	0.54	0.21	0.12	0.23	0.14	0.13
U	0.33	0.29	0.18	0.22	0.11	0.03	0.09	0.27	0.05
CaO/Al_2O_3	0.83	1.01	0.97	0.95	1.02	0.82	0.81	0.81	1.01
Al_2O_3/TiO_2	102	76	92	87	68	170	189	125	96
La/Sm cn	0.96	2.27	0.69	6.32	0.51	0.51	1.18	0.79	0.36
Gd/Yb cn	0.86	0.99	0.82	0.85	0.81	0.75	0.73	0.78	0.78
La/Yb cn	0.57	2.07	0.40	3.78	0.28	0.26	0.62	0.40	0.18
Eu/Eu*	1.42	1.01	1.24	1.25	1.15	1.59	1.60	1.43	1.29
Ce/Ce*	0.96	1.07	0.92	1.02	0.89	0.90	0.89	0.85	0.93
Sr/Nd	71	16	51	44	43	142	181	74	62
Th/La	0.87	0.22	0.73	0.18	0.69	0.74	0.80	0.47	0.83
Zr/Zr*	0.82	0.31	0.68	0.47	0.35	2.46	1.88	0.36	0.81
Nb/Nb*	0.16	0.31	0.16	0.11	0.38	0.22	0.11	0.41	0.35
Ti/Ti*	0.79	0.72	0.79	0.83	0.77	0.78	0.85	0.77	0.73
Pb/Pb*	23.2	10.8	18.9	16.9	59.4	35.4	107.3	54.6	57.5
Sr/Sr*	6.8	1.3	5.1	3.2	4.5	14.7	18.0	7.5	6.6
North	63° 17' 09.1"	63° 16' 57.7"	63° 16' 44.7"	63° 16' 53.3"	63° 16' 37.5"	63° 16' 37.8"	63° 16' 36.8"	63° 16' 41.1"	63° 16' 43.0"
West	50° 05' 40.5"	50° 04' 21.6"	50° 07' 22.0"	50° 07' 02.1"	50° 07' 27.1"	50° 01' 59.1"	50° 02' 03.2"	50° 02' 28.7"	50° 02' 15.8"

Supplementary Table 2.4 (continued)

	Anorthosites		Hornblendites					
Sample	508916	508942	508937[a]	508915	508938	508918	508929[a]	508993[a]
SiO_2	46.0	45.9	48.79	45.83	45.47	34.35	42.33	43.63
Al_2O_3	30.9	32.4	8.78	7.26	8.83	14.48	17.86	17.68
Fe_2O_3	2.1	1.7	11.2	13.01	12.49	20.63	11.67	10.3
MnO	0.04	0.03	0.20	0.19	0.21	0.22	0.17	0.14
MgO	1.9	0.9	15.8	19.14	20.5	20.77	15.85	13.99
CaO	17.2	17.7	11.94	10.11	9.84	5.87	9.86	10.42
Na_2O	1.3	0.9	0.9	1.02	1.08	0.65	0.93	1
K_2O	0.1	0.1	0.22	0.21	0.1	0.15	0.14	0.2
TiO_2	0.08	0.06	0.25	0.32	0.19	0.36	0.08	0.06
P_2O_5	0.02		0.02			0.01		
LOI	0.6	1.3	1.5	1.6	1.29	0.13	1.12	1.76
Total	100.1	101.0	99.57	98.7	100	97.62	100	99.18
Mg#	65	51	74	74	76	67	73	73
Sc	9	7	61	70	53	19	8	18
Zr	2	6	8	13	4	26		18
V	38	30	194	238	155	257	59	59
Cr	174	95	1619	1571	1721	6117	1187	147
Co	12	7	71	104	90	165	94	77
Ni	50	20	369	498	463	688	559	478
Ga	30	31	15	11	11	22	18	23
Rb	2.8	4.4	3.6	8.5	3.4	2.2	0.9	6.1
Sr	86	107	5	4	7	5	22	29
Y	1.8	1.4	7.6	9.5	5.7	1.7	1.3	1.7
Nb	0.72	0.22	2.18	0.50	0.22	0.21	0.17	0.12
Cs	0.19	0.44	0.07	0.29	0.08	0.14	0.03	0.49
Ba	6	7	6	3	5	3	2	5
La	0.80	0.41	2.21	0.35	0.27	0.27	0.51	0.15
Ce	1.49	0.75	8.48	0.85	0.66	0.53	0.59	0.29
Pr	0.17	0.09	1.17	0.15	0.10	0.06	0.09	0.04
Nd	0.65	0.43	4.21	0.90	0.61	0.30	0.40	0.24
Sm	0.18	0.13	0.79	0.49	0.31	0.12	0.12	0.11
Eu	0.16	0.25	0.26	0.12	0.09	0.05	0.13	0.12
Gd	0.25	0.20	0.94	0.93	0.62	0.19	0.17	0.21
Tb	0.04	0.03	0.17	0.19	0.13	0.04	0.03	0.04
Dy	0.29	0.23	1.19	1.44	0.94	0.27	0.20	0.29
Ho	0.06	0.05	0.26	0.33	0.21	0.06	0.05	0.06
Er	0.19	0.15	0.79	0.99	0.63	0.19	0.15	0.20
Tm	0.03	0.02	0.11	0.15	0.10	0.03	0.02	0.03
Yb	0.17	0.14	0.78	0.97	0.62	0.20	0.15	0.21
Lu	0.02	0.02	0.12	0.14	0.09	0.03	0.02	0.03
Ta	0.09	0.02	0.16	0.02	0.01	0.01	0.01	0.00
Pb	1.54	1.69	0.74	1.31	0.42	0.58	0.39	0.72
Th	0.40	0.26	0.28	0.26	0.24	0.26	0.22	0.13
U	0.30	0.08	0.17	0.29	0.05	0.14	0.08	0.03
CaO/Al_2O_3	0.56	0.55	1.36	1.39	1.11	0.41	0.55	0.59
Al_2O_3/TiO_2	412	531	36	23	47	40	218	281
La/Sm cn	2.75	1.98	1.76	0.45	0.55	1.48	2.76	0.85
Gd/Yb cn	1.16	1.15	0.98	0.77	0.81	0.79	0.91	0.78
La/Yb cn	3.10	2.01	1.91	0.24	0.29	0.93	2.24	0.48
Eu/Eu*	2.30	4.80	0.92	0.56	0.62	1.07	2.76	2.42
Ce/Ce*	0.95	0.91	1.24	0.88	0.93	0.95	0.63	0.84
Sr/Nd	132	250	1	5	12	18	54	121
Th/La	0.27	0.34	0.03	0.30	0.37	0.49	0.37	0.45
Zr/Zr*	0.36	1.58	0.27	1.22	0.57	8.73		6.78
Nb/Nb*	0.31	0.17	0.67	0.41	0.21	0.19	0.13	0.22
Ti/Ti*	0.97	1.02	0.80	0.88	0.80	5.08	1.59	0.87
Pb/Pb*	31.5	65.7	2.4	38.0	16.8	32.1	17.0	67.0
Sr/Sr*	11.1	23.0	0.1	0.5	1.3	1.6	4.7	12.3
North	63° 16' 42.2"	63° 16' 44.1"	63° 16' 57.1"	63° 16' 42.2"	63° 16' 57.1"	63° 16' 48.6"	63° 16' 47.0"	63° 16' 38.8"
West	50° 07' 24.3"	50° 07' 22.2"	50° 06' 51.0"	50° 07' 24.3"	50° 06' 51.0"	50° 07' 16.2"	50° 05' 46.7"	50° 02' 24.9"

Supplementary Table 2.4 (continued)

	Peridotites	
Sample	508939	508988
SiO_2	39.92	41.6
Al_2O_3	7.62	4.3
Fe_2O_3	18.17	15.8
MnO	0.25	0.24
MgO	29.68	34.5
CaO	4.3	2.7
Na_2O	0.47	0.14
K_2O	0.14	0.05
TiO_2	0.03	0.06
P_2O_5		
LOI	0.23	-0.38
Total	100.8	99.01
Mg#	76	81
Sc	10	23
Zr		
V	25	57
Cr	128	303
Co	150	158
Ni	1227	1158
Ga	7	7
Rb	1.1	0.3
Sr	4	2
Y	0.7	1.2
Nb	0.14	0.18
Cs	0.03	0.02
Ba	3	1
La	0.17	0.07
Ce	0.34	0.17
Pr	0.04	0.03
Nd	0.21	0.16
Sm	0.06	0.07
Eu	0.04	0.01
Gd	0.08	0.13
Tb	0.02	0.03
Dy	0.11	0.20
Ho	0.02	0.05
Er	0.08	0.15
Tm	0.01	0.02
Yb	0.11	0.19
Lu	0.02	0.03
Ta	0.01	0.01
Pb	0.80	
Th	0.27	0.23
U	0.04	0.03
CaO/Al_2O_3	0.56	0.63
Al_2O_3/TiO_2	231	68
La/Sm cn	1.78	0.68
Gd/Yb cn	0.61	0.57
La/Yb cn	1.10	0.27
Eu/Eu*	1.77	0.39
Ce/Ce*	0.91	0.91
Sr/Nd	19	13
Th/La	0.78	1.31
Zr/Zr*		
Nb/Nb*	0.16	0.34
Ti/Ti*	1.17	1.27
Pb/Pb*	66.0	
Sr/Sr*	1.7	1.3
North	63° 16' 54.6"	63° 16' 35.0"
West	50° 06' 55.4"	50° 01' 54.7"

cn: chondrite -normalized. [a]Altered

Supplementary Table 2.5
Major (wt.%) and trace (ppm) element concentrations and significant element ratios for rocks in the Upper Leucogabbro Unit.

	Leucogabbros					Anorthosite dyke	Hornblendites	
Sample	508924	508925	508926	508927	508928	508940	508941[a]	508919
SiO_2	44.6	44.3	44.2	45.7	45.4	44.9	46.4	34.2
Al_2O_3	31.2	25.6	26.9	28.9	26.7	28.1	12.3	16.8
Fe_2O_3	2.1	6.5	5.2	3.6	5.4	4.6	10.0	18.5
MnO	0.03	0.10	0.08	0.05	0.09	0.07	0.19	0.23
MgO	2.0	6.5	5.0	3.5	4.9	4.8	15.4	25.3
CaO	16.8	14.7	15.0	16.2	15.4	15.0	11.3	4.7
Na_2O	1.21	1.1	1.16	1.28	1.25	1.0	1.4	0.3
K_2O	0.09	0.19	0.12	0.11	0.24	0.8	0.3	0.1
TiO_2	0.04	0.06	0.18	0.09	0.14	0.1	0.1	0.1
P_2O_5	0.01			0.01	0.01	0.01	0.01	
LOI	0.75	0.98	0.77	0.29	0.79	1.0	1.6	0.1
Total	98.9	100.0	98.6	99.6	100.4	100.4	99.0	100.3
Mg#	65	67	66	66	64	68	75	73
Sc	4	9	4	17	16	3	38	9
Zr	7	5	12	9		5	6	7
V	19	35	48	54	77	17	121	56
Cr	52	225	21	356	115	38	814	114
Co	14	39	31	20	32	26	72	148
Ni	75	253	191	98	157	156	398	592
Ga	27	25	24	26	27	30	14	15
Rb	2.6	6.8	4.6	1.6	6.7	144.2	8.8	1.1
Sr	95	60	61	67	66	69	5	4
Y	1.1	1.3	2.4	2.6	3.2	1.0	3.8	1.7
Nb	0.32	0.11	0.25	0.13	0.50	0.44	0.92	0.36
Cs	0.43	1.48	1.20	0.31	0.57	16.97	0.23	0.05
Ba	12	14	5	7	5	36	6	3
La	0.82	0.55	0.41	0.34	0.61	0.26	0.26	0.31
Ce	1.20	0.99	0.87	0.71	1.67	0.51	0.50	0.75
Pr	0.11	0.10	0.12	0.09	0.23	0.07	0.08	0.08
Nd	0.41	0.40	0.63	0.44	0.99	0.32	0.47	0.35
Sm	0.11	0.12	0.21	0.16	0.27	0.10	0.23	0.12
Eu	0.13	0.18	0.19	0.16	0.23	0.17	0.15	0.03
Gd	0.15	0.18	0.29	0.29	0.38	0.15	0.42	0.20
Tb	0.03	0.03	0.05	0.06	0.07	0.02	0.08	0.04
Dy	0.18	0.23	0.37	0.41	0.50	0.16	0.62	0.27
Ho	0.04	0.05	0.09	0.09	0.11	0.03	0.14	0.06
Er	0.11	0.15	0.28	0.28	0.33	0.10	0.42	0.18
Tm	0.02	0.02	0.04	0.04	0.05	0.02	0.06	0.03
Yb	0.11	0.15	0.30	0.26	0.33	0.10	0.42	0.21
Lu	0.02	0.02	0.05	0.04	0.05	0.02	0.07	0.03
Ta	0.03	0.01	0.02	0.01	0.02	0.01	0.01	0.02
Pb	3.44	2.40	1.22	1.00	4.87	1.17	0.77	1.45
Th	0.50	0.27	0.26	0.21	0.25	0.17	0.28	0.61
U	0.22	0.10	0.15	0.11	0.19	0.06	0.14	0.10
CaO/Al_2O_3	0.54	0.57	0.56	0.56	0.58	0.53	0.92	0.28
Al_2O_3/TiO_2	799	412	149	325	191	512	96	284
La/Sm cn	4.76	2.90	1.21	1.32	1.39	1.65	0.70	1.59
Gd/Yb cn	1.13	0.98	0.81	0.90	0.93	1.24	0.80	0.79
La/Yb cn	5.16	2.53	0.93	0.89	1.24	1.78	0.42	1.02
Eu/Eu*	3.17	3.78	2.28	2.32	2.15	4.37	1.44	0.63
Ce/Ce*	0.95	1.02	0.91	0.94	1.04	0.92	0.82	1.11
Sr/Nd	233	150	97	153	67	219	12	11
Th/La	0.61	0.49	0.65	0.61	0.42	0.34	0.55	1.96
Zr/Zr*	2.06	1.43	2.05	2.10		1.76	1.13	2.10
Nb/Nb*	0.12	0.07	0.19	0.12	0.31	0.51	0.84	0.20
Ti/Ti*	0.82	1.06	1.85	0.85	1.08	1.29	0.82	0.85
Pb/Pb*	97.3	79.4	38.1	39.8	80.2	65.4	39.1	60.3
Sr/Sr*	19.3	13.1	9.3	14.1	5.9	20.5	1.2	1.0
North	63° 17' 02.9"	63° 17' 01.7"	63° 16' 44.3"	63° 16' 40.6"	63° 16' 41.8"	63° 16' 49.2"	63° 16' 44.5"	63° 16' 50.9"
West	50° 05' 45.8"	50° 05' 55.3"	50° 06' 02.4"	50° 06' 04.0"	50° 05' 51.2"	50° 07' 15.4"	50° 07' 22.1"	50° 07' 10.3"

cn: chondrite -normalized. [a] Altered

Supplementary Table 2.6

Major (wt.%) and trace (ppm) element concentrations and significant element ratios for rocks in the Anorthosite Unit.

	Anorthosites								
Sample	508905	508906[a]	508907	508936	508944	508945	508998	498101	498102
SiO_2	46.6	46.5	45.6	42.5	46.7	47.2	50.8	46.5	45.4
Al_2O_3	30.7	31.0	32.6	30.7	33.1	32.5	30.7	32.2	33.2
Fe_2O_3	2.3	1.4	1.4	2.6	0.8	1.0	0.8	1.2	0.7
MnO	0.04	0.03	0.02	0.05	0.02	0.03	0.02	0.02	0.01
MgO	1.9	0.3	0.8	0.9	0.6	0.4	0.2	1.0	0.2
CaO	16.4	19.1	17.3	19.8	15.7	16.9	14.4	13.9	17.5
Na_2O	1.6	0.3	1.4	0.8	1.8	1.7	2.9	1.9	1.5
K_2O	0.1	0.1	0.1	0.1	0.6	0.1	0.3	1.3	0.0
TiO_2	0.06	0.02	0.06	0.06	0.03	0.10	0.02	0.02	0.01
P_2O_5	0.01			0.02		0.02	0.05		
LOI	0.4	0.4	0.5	1.9	1.0	0.6	0.5	1.6	0.4
Total	99.9	99.1	99.7	99.4	100.3	100.5	100.6	99.6	99.0
Mg#	62	27	55	42	58	45	34	62	36
Sc	2	1	4	2		3		1	1
Zr	11	11	3	8	7	8	6	10	2
V	14	10	19	17	7	14		8	8
Cr	43	31	118	28	47	37	15	15	8
Co	11	3	5	10	3	3	2	5	3
Ni	58	20	28	46	25	10	8	28	16
Ga	28	33	30	33	33	29	54	47	43
Rb	3.6	0.6	1.4	3.8	35.8	1.1	26.8	126.4	3.8
Sr	73	65	71	100	101	86	85	74	71
Y	1.8	0.5	1.1	1.8	0.5	3.3	1.4	1.9	0.3
Nb	0.54	0.07	0.24	0.19	0.43	0.77	3.81	1.14	0.77
Cs	0.36	0.09	0.62	1.06	3.63	0.28	0.90	2.32	0.31
Ba	21	2	8	17	80	13	24	30	4
La	1.78	4.52	0.82	0.44	0.31	0.79	2.36	0.51	0.28
Ce	3.85	2.46	1.58	0.87	0.68	1.53	4.63	1.16	0.56
Pr	0.42	0.15	0.18	0.10	0.08	0.18	0.50	0.15	0.06
Nd	1.45	0.48	0.66	0.47	0.33	0.77	1.74	0.66	0.23
Sm	0.27	0.08	0.15	0.16	0.09	0.23	0.38	0.25	0.05
Eu	0.20	0.23	0.17	0.28	0.17	0.30	0.17	0.15	0.15
Gd	0.27	0.09	0.19	0.23	0.12	0.37	0.33	0.32	0.05
Tb	0.04	0.01	0.03	0.04	0.02	0.07	0.05	0.06	0.01
Dy	0.29	0.08	0.19	0.28	0.10	0.49	0.24	0.33	0.05
Ho	0.06	0.02	0.04	0.06	0.02	0.11	0.04	0.06	0.01
Er	0.18	0.04	0.11	0.19	0.05	0.34	0.11	0.16	0.03
Tm	0.03	0.01	0.02	0.03	0.01	0.05	0.02	0.02	0.00
Yb	0.18	0.04	0.10	0.16	0.04	0.33	0.10	0.14	0.03
Lu	0.03	0.01	0.01	0.02	0.01	0.05	0.01	0.02	0.00
Ta	0.05	0.01	0.02	0.01	0.02	0.09	0.30	0.17	0.12
Pb	2.06	0.70	1.10	6.47	5.08	1.99	6.52	1.92	2.06
Th	0.43	0.45	0.64	0.21	0.68	4.07	3.21	0.14	0.14
U	0.28	0.40	0.46	0.11	0.19	0.30	1.50	0.08	0.06
CaO/Al_2O_3	0.53	0.61	0.53	0.64	0.48	0.52	0.47	0.43	0.53
Al_2O_3/TiO_2	519	1411	593	480	1034	342	1805	1462	2770
La/Sm cn	4.10	35.55	3.39	1.75	2.10	2.16	3.90	1.27	3.33
Gd/Yb cn	1.26	1.95	1.46	1.12	2.61	0.90	2.71	1.89	1.68
La/Yb cn	6.84	78.07	5.36	1.80	5.73	1.63	16.36	2.48	7.21
Eu/Eu*	2.27	8.01	3.06	4.48	5.05	3.19	1.46	1.64	8.72
Ce/Ce*	1.04	0.70	0.97	0.96	1.03	0.95	1.00	0.97	0.99
Sr/Nd	50	136	107	210	303	112	49	112	305
Th/La	0.11	0.18	0.40	0.24	1.01	2.66	0.69	0.12	0.25
Zr/Zr*	1.09	3.49	0.59	1.82	2.47	1.18	0.46	1.53	1.12
Nb/Nb*	0.15	0.01	0.08	0.15	0.23	0.11	0.34	1.03	0.95
Ti/Ti*	0.76	0.98	1.10	0.87	1.16	0.76	0.24	0.23	0.87
Pb/Pb*	16.4	11.8	21.2	220.0	227.1	38.8	43.6	46.8	111.1
Sr/Sr*	4.0	10.3	8.8	19.1	26.9	9.9	3.9	9.9	24.9
North	63° 17' 05.7"	63° 17' 04.7"	63° 17' 05.6"	63° 16' 29.4"	63° 16' 30.8"	63° 16' 28.9"	63° 16' 58.6"	63° 17' 00.9"	63° 17' 01.1"
West	50° 05' 03.0"	50° 04' 03.0"	50° 04' 44.3"	50° 07' 00.9"	50° 07' 13.1"	50° 07' 19.1"	50° 01' 32.5"	50° 01' 43.9"	50° 01' 55.5"

cn: chondrite -normalized. [a]Altered. [b]Between Upper Leucogabbro and Anorthosite Unit.

Supplementary Table 2.6 (continued)

Sample	508909[b]	508910[b]	508934[b]
SiO_2	46.8	46.8	43.8
Al_2O_3	31.8	32.7	30.3
Fe_2O_3	1.5	1.1	1.7
MnO	0.02	0.01	0.03
MgO	0.9	0.6	1.7
CaO	16.6	17.1	16.9
Na_2O	1.7	1.7	1.5
K_2O	0.1	0.1	0.4
TiO_2	0.02	0.01	0.08
P_2O_5	0.02		
LOI	0.3	0.5	3.1
Total	99.5	100.5	99.5
Mg#	55	52	67
Sc	1		1
Zr	5	9	36
V	10		11
Cr	68	42	31
Co	7	5	7
Ni	58	34	54
Ga	30	27	35
Rb	3.1	2.7	23.3
Sr	84	97	118
Y	1.9	0.2	1.0
Nb	0.82	0.45	1.17
Cs	0.27	0.19	1.00
Ba	20	11	56
La	2.48	1.35	2.52
Ce	4.90	2.42	4.34
Pr	0.54	0.20	0.39
Nd	1.91	0.52	1.22
Sm	0.44	0.07	0.19
Eu	0.19	0.15	0.17
Gd	0.40	0.05	0.19
Tb	0.06	0.01	0.03
Dy	0.32	0.04	0.16
Ho	0.06	0.01	0.03
Er	0.17	0.02	0.10
Tm	0.02	0.00	0.02
Yb	0.14	0.02	0.09
Lu	0.02	0.00	0.01
Ta	0.05	0.03	0.05
Pb	2.59	1.30	1.68
Th	0.97	0.90	0.25
U	0.44	0.47	0.11
CaO/Al_2O_3	0.52	0.52	0.56
Al_2O_3/TiO_2	1323	3629	374
La/Sm cn	3.53	12.02	8.25
Gd/Yb cn	2.26	2.43	1.66
La/Yb cn	11.75	51.60	17.94
Eu/Eu*	1.35	7.37	2.71
Ce/Ce*	1.00	1.08	1.03
Sr/Nd	44	186	97
Th/La	0.20	0.37	0.06
Zr/Zr*	0.34	2.91	4.63
Nb/Nb*	0.13	0.10	0.36
Ti/Ti*	0.26	0.76	1.77
Pb/Pb*	16.3	18.9	13.2
Sr/Sr*	3.5	12.6	7.3
North	63° 17' 00.6"	63° 16' 58.6"	63° 16' 31.3"
West	50° 04' 38.2"	50° 04' 41.7"	50° 07' 10.0"

Supplementary Table 2.7

Trace element concentrations (ppm) and significant element ratios for hornblendes in Lower Gabbro Unit (MGU), Ultramafic Unit (UU), and Middle Gabbro Unit (MGU)

	Suite A															
	508973 Hornblendite (LGU)								508983 Hornblendite (UU)							
	hb1	hb2	hb3	hb4	hb5	hb6	hb7	hb8	hb1	hb2	hb3	hb4	hb5	hb6	hb7	hb8
V	264	263	255	264	232	240	242	225	203	208	203	203	191	190	178	190
Cr	792	757	803	539	683	792	625	705	1720	1848	1757	1839	1338	1575	1446	1512
Co	75	75	74	74	73	74	72	67	87	86	91	86	85	81	80	81
Ni	179	176	172	189	166	172	169	164	430	431	446	517	507	429	386	398
Rb	6.81	6.21	6.46	6.32	5.44	6.08	5.75	5.57	9.74	10.55	8.46	6.65	6.40	9.61	8.07	8.91
Y	15.32	15.00	15.30	14.53	15.02	15.14	15.27	15.64	9.88	9.55	9.15	9.08	8.59	9.64	9.22	9.34
Zr	27.46	25.64	26.18	26.34	26.49	28.04	27.66	27.99	12.66	12.43	11.85	11.48	10.89	12.79	11.57	12.05
Nb	2.320	2.164	2.159	2.079	2.413	2.431	2.434	2.353	0.46	0.48	0.75	0.31	0.28	0.37	0.33	0.42
Ba	41.40	36.36	39.98	36.65	37.89	35.74	39.18	35.46	29.68	30.43	21.17	18.45	16.53	25.52	23.65	28.54
La	3.799	4.094	4.128	4.243	4.502	4.691	4.602	5.101	1.691	1.640	1.523	1.539	1.490	1.655	1.587	1.667
Ce	11.592	11.104	11.178	11.094	11.297	11.469	11.338	11.568	5.506	5.374	5.269	5.017	4.749	5.214	5.035	5.300
Pr	1.738	1.648	1.682	1.671	1.634	1.695	1.671	1.692	0.937	0.887	0.847	0.820	0.759	0.874	0.850	0.898
Nd	8.882	8.704	8.842	8.439	8.382	8.712	8.659	8.581	5.033	4.770	4.574	4.483	4.266	4.846	4.811	4.922
Sm	2.701	2.472	2.699	2.572	2.595	2.602	2.597	2.730	1.626	1.517	1.422	1.346	1.265	1.493	1.441	1.576
Eu	0.906	0.960	0.899	0.896	0.925	0.888	0.892	0.912	0.589	0.595	0.529	0.560	0.517	0.534	0.564	0.572
Gd	2.892	3.046	2.911	2.689	2.992	2.921	2.982	2.914	1.743	1.800	1.890	1.737	1.575	1.798	1.723	1.661
Tb	0.468	0.457	0.442	0.434	0.447	0.440	0.476	0.444	0.280	0.276	0.255	0.244	0.257	0.296	0.283	0.287
Dy	3.015	3.042	3.092	2.977	2.977	3.067	3.146	3.102	1.869	1.896	1.844	1.780	1.865	2.010	1.929	1.914
Ho	0.598	0.600	0.609	0.593	0.619	0.628	0.613	0.613	0.375	0.367	0.336	0.359	0.347	0.382	0.373	0.365
Er	1.725	1.653	1.742	1.527	1.638	1.774	1.737	1.694	1.034	1.020	0.928	0.967	0.918	1.079	0.952	1.028
Tm	0.244	0.229	0.257	0.233	0.247	0.248	0.242	0.248	0.146	0.142	0.151	0.144	0.124	0.155	0.138	0.145
Yb	1.588	1.685	1.652	1.597	1.671	1.679	1.635	1.688	0.984	1.039	0.966	0.899	0.859	0.923	0.933	0.987
Lu	0.227	0.227	0.235	0.221	0.225	0.225	0.211	0.231	0.137	0.139	0.135	0.132	0.134	0.150	0.136	0.137
Hf	1.018	0.911	0.860	0.866	0.920	1.034	0.998	1.034	0.503	0.504	0.505	0.426	0.484	0.518	0.439	0.476
Ta	0.147	0.137	0.141	0.146	0.164	0.172	0.168	0.178	0.022	0.023	0.079	0.017	0.018	0.016	0.015	0.020
Pb	2.123	2.454	2.461	2.384	1.789	1.867	1.928	1.882	1.174	1.251	1.200	1.097	1.132	1.144	0.877	1.251
Th	0.097	0.105	0.115	0.125	0.134	0.122	0.129	0.150	0.027	0.026	0.028	0.025	0.017	0.031	0.024	0.030
U	0.094	0.086	0.089	0.100	0.110	0.085	0.098	0.089	0.088	0.080	0.085	0.068	0.057	0.071	0.063	0.081
La/Sm_{cn}	0.91	1.07	0.99	1.06	1.12	1.16	1.14	1.21	0.67	0.70	0.69	0.74	0.76	0.72	0.71	0.68
Gd/Yb_{cn}	1.51	1.50	1.46	1.39	1.48	1.44	1.51	1.43	1.47	1.43	1.62	1.60	1.52	1.61	1.53	1.39
La/Nb_{pm}	1.47	1.70	1.72	1.84	1.68	1.74	1.70	1.95	3.33	3.10	1.82	4.41	4.84	4.06	4.38	3.53
Rb/Nb_{pm}	8.2	8.0	8.3	8.5	6.3	6.9	6.6	6.6	59.22	61.48	31.14	58.76	64.18	72.77	68.72	58.27
Ba/Nb_{pm}	4.51	4.25	4.68	4.46	3.97	3.72	4.07	3.81	16.42	16.14	7.09	14.84	15.09	17.59	18.33	16.99
Pb/Ce_{pm}	4.50	5.42	5.40	5.27	3.89	3.99	4.17	3.99	5.23	5.71	5.59	5.37	5.85	5.38	4.27	5.79
Nd/Zr_{pm}	3.02	3.17	3.15	2.99	2.95	2.90	2.92	2.86	3.71	3.58	3.60	3.64	3.65	3.53	3.88	3.81
Zr/Hf	27.0	28.1	30.4	30.4	28.8	27.1	27.7	27.1	25.2	24.6	23.5	27.0	22.5	24.7	26.3	25.3
Nb/Ta	15.8	15.8	15.3	14.2	14.7	14.1	14.5	13.2	21.1	20.5	9.6	18.8	15.5	22.9	21.4	21.6

Supplementary Table 2.7 Continued.

	Suite B															
	508915 Hornblendite								508931 Gabbro							
	hb1	hb2	hb3	hb4	hb5	hb6	hb7	hb8	hb1	hb2	hb3	hb4	hb5	hb6	hb7	hb8
V	160	154	160	169	164	174	167	145	297	333	325	360	284	304	269	348
Cr	663	375	1155	1114	638	406	908	827	2514	3179	2701	3162	2311	2349	2183	3048
Co	64	61	61	64	63	61	59	58	60	58	59	61	54	55	52	60
Ni	271	266	285	290	289	289	273	278	230	247	240	252	224	227	222	256
Rb	6.60	6.09	8.13	6.19	6.52	8.27	7.00	6.84	2.27	2.52	2.90	2.53	2.54	2.42	2.58	2.88
Y	10.74	11.04	11.37	11.01	10.20	11.33	11.52	11.06	9.01	8.71	7.97	8.03	8.68	8.74	8.55	7.86
Zr	8.91	9.16	9.50	9.22	8.51	10.19	10.19	9.58	5.57	5.25	4.83	4.83	5.20	5.16	5.25	4.84
Nb	0.423	0.427	0.461	0.489	0.453	0.533	0.522	0.449	0.210	0.200	0.209	0.205	0.226	0.207	0.205	0.212
Ba	1.71	1.54	2.66	1.80	1.73	2.24	2.21	2.17	8.35	8.55	9.70	8.84	8.76	8.89	9.09	8.91
La	0.256	0.274	0.257	0.256	0.244	0.240	0.273	0.250	0.284	0.276	0.275	0.269	0.287	0.296	0.290	0.271
Ce	1.014	0.986	0.945	0.978	0.923	0.964	0.945	0.863	0.943	0.939	0.960	0.963	0.897	0.948	0.916	1.007
Pr	0.185	0.196	0.174	0.191	0.176	0.191	0.183	0.174	0.170	0.174	0.166	0.166	0.178	0.158	0.163	0.164
Nd	1.234	1.260	1.259	1.249	1.140	1.309	1.240	1.163	1.119	1.069	1.054	1.051	1.110	1.066	1.056	1.046
Sm	0.647	0.700	0.701	0.644	0.579	0.705	0.690	0.631	0.599	0.506	0.489	0.533	0.571	0.512	0.573	0.471
Eu	0.186	0.198	0.195	0.175	0.164	0.181	0.182	0.165	0.298	0.270	0.271	0.263	0.276	0.261	0.280	0.274
Gd	1.206	1.140	1.254	1.169	1.109	1.315	1.243	1.071	0.974	0.911	0.865	0.915	0.977	0.915	0.846	0.856
Tb	0.226	0.227	0.245	0.243	0.215	0.251	0.256	0.237	0.207	0.187	0.164	0.162	0.186	0.188	0.191	0.174
Dy	1.813	1.829	1.926	1.823	1.757	2.010	1.945	1.842	1.636	1.514	1.382	1.328	1.481	1.492	1.521	1.331
Ho	0.395	0.387	0.403	0.432	0.355	0.414	0.417	0.407	0.344	0.357	0.308	0.299	0.338	0.337	0.348	0.289
Er	1.147	1.200	1.257	1.190	1.138	1.238	1.293	1.311	1.106	0.997	0.952	0.927	0.989	0.964	1.015	0.899
Tm	0.173	0.162	0.182	0.172	0.151	0.191	0.187	0.186	0.147	0.153	0.134	0.148	0.147	0.141	0.156	0.132
Yb	1.252	1.252	1.359	1.238	1.269	1.404	1.511	1.386	1.163	1.080	0.994	1.003	1.105	1.064	1.080	1.033
Lu	0.186	0.191	0.186	0.189	0.174	0.206	0.200	0.182	0.163	0.151	0.155	0.145	0.161	0.146	0.158	0.139
Hf	0.318	0.312	0.357	0.320	0.288	0.336	0.357	0.372	0.235	0.193	0.182	0.179	0.225	0.200	0.197	0.171
Ta	0.011	0.013	0.013	0.012	0.011	0.017	0.015	0.015	0.018	0.018	0.016	0.015	0.015	0.016	0.018	0.018
Pb	0.244	0.363	0.313	0.235	0.264	0.246	0.243	0.231	0.158	0.165	0.292	0.181	0.217	0.242	0.266	0.218
Th	0.056	0.057	0.066	0.064	0.060	0.063	0.065	0.063	0.015	0.016	0.016	0.013	0.012	0.017	0.016	0.010
U	0.216	0.203	0.233	0.238	0.231	0.252	0.258	0.227	0.061	0.068	0.065	0.066	0.057	0.069	0.058	0.063
La/Sm_{cn}	0.26	0.25	0.24	0.26	0.27	0.22	0.26	0.26	0.31	0.35	0.36	0.33	0.32	0.37	0.33	0.37
Gd/Yb_{cn}	0.80	0.75	0.76	0.78	0.72	0.77	0.68	0.64	0.69	0.70	0.72	0.75	0.73	0.71	0.65	0.69
La/Nb_{pm}	0.54	0.58	0.50	0.47	0.49	0.40	0.47	0.50	1.22	1.24	1.18	1.18	1.14	1.29	1.28	1.15
Rb/Nb_{pm}	43.4	39.7	49.0	35.2	40.0	43.1	37.2	42.3	30.0	35.0	38.6	34.3	31.2	32.5	34.9	37.7
Ba/Nb_{pm}	1.02	0.91	1.46	0.93	0.96	1.06	1.07	1.22	10.06	10.79	11.74	10.90	9.78	10.87	11.22	10.62
Pb/Ce_{pm}	5.91	9.03	8.13	5.90	7.03	6.25	6.30	6.58	4.12	4.31	7.48	4.61	5.95	6.25	7.13	5.31
Nd/Zr_{pm}	1.29	1.28	1.24	1.26	1.25	1.20	1.13	1.13	1.87	1.90	2.03	2.03	1.99	1.93	1.88	2.02
Zr/Hf	28.0	29.4	26.6	28.8	29.5	30.3	28.6	25.8	23.7	27.2	26.6	27.0	23.1	25.8	26.6	28.2
Nb/Ta	38.4	33.0	34.5	40.3	40.4	30.6	35.8	29.6	11.4	11.0	12.8	13.9	14.9	13.2	11.2	11.8

CHAPTER 3

Trace element chemistry of primary igneous hornblende, clinopyroxene and plagioclase from the Fiskenæsset Complex on Majorqap qâva, SW Greenland

3.1. Introduction

Archean anorthositic intrusions, which include leucogabbro, gabbro and ultramafic units have been recognized as layered intrusions occurring in Archean terranes and have played a significant role in understanding of geological processes that operated in the early Earth. The intensively investigated Fiskenæsset Complex provides many insights on the petrogenesis of Archean anorthosite (Windley et al., 1973; Windley and Smith, 1974; Henderson et al., 1976; Myers and Platt, 1977; Myers, 1985; Ashwal et al., 1989; Polat et al., 2009, 2010, 2011; Huang et al., submitted). Windley et al. (1973) noted that hornblende is the only ferromagnesian silicate mineral present in most anorthosites and leucogabbros and suggested that hornblende plays an important role in the differentiation of the Fiskenæsset Complex. Myers (1985), however, considered it likely that most hornblende was a metamorphic derivative of pyroxene, given that some hornblende in undeformed leucogabbro encloses older cores of pyroxene. Recent studies on similar anorthosites from southern West Greenland prefer a magmatic origin for hornblende precipitating from a hydrous parental magma (Polat et al., 2009,2011; Windley and Garde, 2009; Rollinson et al., 2010; Hoffmann et al., 2012; Huang et al., submitted). The idea that the hornblende in the Fiskenæsset Complex formed from a hydrous melt is consistent with experimental work (Sisson and Grove, 1993a, b; Müntener et al., 2001). Based on experimental data, Sisson and Grove (1993a, b) and Müntener et al. (2001) emphasized that plagioclase is subordinate to Fe, Mg silicates among the early minerals crystallizing from hydrous basalt melts and that Al_2O_3 largely remains in the melt where its concentration rises with advancing fractionation until plagioclase appears at a later stage. Field and petrographic observations indicate that plagioclase was not involved in

the early evolution of the Fiskenæsset Complex, which is also consistent with the experimental results. Huang et al. (submitted) pointed out that cumulate rocks with strikingly similar mineralogy and textures to the Fiskenæsset Complex are reported from the Onion Valley Complex of the Sierra Nevada batholiths and the Alaskan-type complex on Duke Island and suggested that the Fiskenæsset Complex was produced by multi-stage evolution of hydrous mafic magmas (Irvine, 1974; Sisson et al., 1996).

Even though a broad consensus exists that hornblende is essential for the formation of the Fiskenæsset Complex, disagreement arises on the significance of the magmatic hornblende: whether they came from a primitive liquid as cumulate, from a residual liquid as the intercumulus phase, or through reaction between early cumulate and primitive liquid or conversely with a more evolved melt (Anderson, 1980; Brandriss and Bird, 1999; Coogan et al., 2001; Meurer and Claeson, 2002; Tiepolo et al., 2002; Borghini and Rampone, 2007). Within the Fiskenæsset Complex, one of the well preserved stratigraphic sequences is on Majorqap qâva. Hornblende occurs as major or minor constituents in a wide variety of rocks including gabbbro, hornblendite, peridotite, leucogabbro and anorthosite and it provides a unique opportunity to understand the role of hornblende in the evolution of magmas which generated Fiskenæsset Complex and may help to understand the processes occurring in Archean anorthosite complexes. A fundamental barrier to progress in understanding the petrogenesis of hornblende is the pervasive post intrusion regional metamorphism that may have affected the hornblende. In order to identifying metamorphic effects, we have analyzed the trace element composition of the preserved igneous hornblende, clinopyroxene and plagioclase by femtosecond LA-ICP-MS in the Fiskenæsset Complex. The field observations, the petrography and the consistency of REE and trace element patterns of the igneous hornblende, clinopyroxene and plagioclase demonstrate that these crystals have not been significantly affected by regional metamorphism. Their mineral chemistry, therefore, should reflect the trace element composition of the melt from which they grew.

3.2. Regional geology

The Fiskenæsset Complex including anorthosite, leucogabbro, gabbro and ultramafic rocks is located in the Fiskenæsset region of southern West Greenland (Fig. 3.1). The Fiskenæsset region consists of ~80% granitoid orthogneisses, ~15% amphibolites, and ~5% Fiskenæsset Complex (Kalsbeek and Myers, 1973; Windley and Smith, 1974; Myers, 1985; Windley and Garde, 2009).

The age of the Fiskenæsset Complex is constrained by a Sm-Nd regression age 2973±28 Ma and a Pb-Pb isotope regression age 2945±36 obtained by Polat et al., 2010. A younger $^{207}Pb/^{206}Pb$ zircon age of 2.87 Ga was acquired for a hornblenditic pegmatite pipe transecting part of the Fiskenæsset Complex on Majorqap qâva but the hornblenditic pegmatite pipe has older zircon grains are ca. 2.95 Ga , which is similar to the Sm-Nd and Pb-Pb intrusion age of the Fiskenæsset Complex (Keulen et al., 2010).

The Fiskenæsset Complex was intruded into amphibolites which were originally basaltic lavas, and is still in stratigraphic contact with overlying and underlying 1-2 km-thick (maximum) of amphibolites (Escher and Myers, 1975; V.J. van Hinsberg and Windley, in Keulen et al., 2011). The Fiskenæsset Complex was subsequently intruded by felsic rocks of TTG (tonalite-trondhjemite-granodiorite) suite, which have since been converted to orthogneisses during high grade metamorphism (Naeraa and Scherstén, 2008; Huang et al., 2012).

During Mesoarchean to Neoarchean tectonothermal events, strong deformation and metamorphism transformed these intrusions into the regional orthogneisses (Myers, 1985; Polat et al., 2010). The spectacular km-scale fold interference patterns were a function of three major episodes of isoclinal to tight folding and a complex sequence of fold and fabric development resulted from each episode of deformation (Kalsbeek and Myers, 1973; Windley and Smith, 1974; Myers, 1985). The igneous layering of the Fiskenæsset Complex and meta-volcanic amphibolites were folded together into large recumbent isoclinal, nappe-like F1 folds. Then the protoliths of the TTG gneisses intruded the

Fiskenæsset Complex during a phase of major thrusting associated with large-scale isoclinal F2 folds. Finally, large-scale F3 folds refolded the F1 and F2 structures, giving rise to fold interference patterns.

Between 2.85 and 2.79 Ga, most of the Fiskenæsset Complex underwent granulite facies metamorphism with peak metamorphic conditions in the region reaching about 780°C and 8.9 kbar (~30 km depth) (Black et al., 1973; Moorbath and Pankhurst, 1976; Riciputi et al., 1990; McGregor and Friend, 1992). A zircon U-Pb age of 2.66 Ga was obtained for the end of low-grade amphibolite facies metamorphism of the southern Fiskenæsset region (Pidgeon and Kalsbeek, 1978). Igneous rock names are used without the prefix 'meta' for descriptive simplicity given that most of the Fiskenæsset Complex was metamorphosed to granulite grade and subsequent1y retrogressed to amphibolite facies.

The Fiskenæsset Complex, where best preserved as on Majorqap qâva, retains a primary igneous layered stratigraphy (Myers, 1985). A generalized stratigraphic log (Fig 3. 1d) was based on a major study on Majorqap qâva (Myers, 1985). From bottom to top, there are six major lithostratigraphic Units: Lower Gabbro (50 m), Ultramafic (40 m), Lower Leucogabbro (50 m), Middle Gabbro (40 m), Upper Leucogabbro (60 m), Anorthosite (250 m) (Fig. 3.1d) (Myers, 1985). Given three phases of deformation and lateral changes in lithology, the locations of samples on the measured stratigraphic sequences should be taken as approximate (Fig. 3.1; Supplementary Fig. 3.1).

On the basis of whole rock geochemical characteristics, Huang et al. (submitted) divided the Fiskenæsset Complex into two Suites, A and B. Suite A consists of gabbros of the Lower Gabbro Unit, hornblendites of the Lower Gabbro and Ultramafic Units, peridotites and pyroxenites of the Ultramafic Unit and anorthosites of the Lower Leucogabbro, Middle Gabbro, Upper Leucogabbro and Anorthosite Units. Suite B is composed of leucogabbros of the Lower Leucogabbro Unit, gabbros, hornblendites, and peridotites of the Middle Gabbro Unit, and leucogabbros and hornblendites of the Upper

Leucogabbro Unit. Suite A is HREE depleted whereas Suite B is HREE enriched.

3.3. Petrography

The petrographic descriptions of the Fiskenæsset Complex mainly follow the ascending order of the six lithostratigraphic Units: Lower Gabbro, Ultramafic, Lower Leucogabbro, Middle Gabbro, Upper Leucogabbro, Anorthosite (Fig. 3.1d) (Myers, 1985).

Gabbro (508974) consists of fine-grained plagioclase, hornblende and clinopyroxene with an equigranular texture; the grain size of plagioclase, hornblende and clinopyroxene is about 0.2-0.5 mm (Fig. 3.2a).

Hornblendite (508973) contains >90% hornblende grains about 1-1.5 mm across (Fig. 3.2b) that are mutually in equilibrium and interstitial plagioclase and clinopyroxene.

Dunite (508968) consists of olivine (~90%), clinopyroxene (5-10%) and accessory minerals (<2%) such as spinel, magnetite, and chromite (Fig. 3.2c). In some places, olivine has been partially altered to serpentine (Fig. 3.2d).

Peridotites (508969 and 598978) are composed of olivine (50–60%), clinopyroxene (10-30%), orthopyroxene (5-10%) and accessory minerals (<5%) such as spinel, magnetite, and chromite (Fig. 3.2e). Olivine has been partially altered to serpentine.
Pyroxenite (508979) contains clinopyroxene (70-80%) and orthopyroxene (20-30%) (Fig. 3.2f).

Hornblendite (508983) consists of pure hornblende with two distinct sizes: euhedral and subhedral large grains (1-2 mm) and small polygonal grains (0.1-0.3 mm) (Fig. 3.2g).

Leucogabbros (508903, 508930 and 508922) are made up of plagioclase (70-80%) and hornblende (20-30%) with subhedral granular textures (Fig. 3.3a). Hornblende occurs as separate interstitial crystals between plagioclase grains. Plagioclase (0.5-1.5

mm), is intensely twinned but unzoned, and has an equilibrium texture with triple junctions displaying interfacial angles close to 120°.

Peridotites (508988 and 508939) are composed of olivine, orthopyroxene, hornblende, spinel and magnetite in various portions (Fig. 3.3b and f). Olivine occurs as large grains with sizes ranging between 1.5-2 mm. Rounded pale green hornblende has a grain size about 1-1.5 mm.

Hornblendite (508915) is made up of over 85% hornblende (grain size about 1-1.5 mm) and minor plagioclase (Fig. 3.3c). Hornblendes are in sharp mutual contact and plagioclase occurs as interstitial grains between them. Green spinel, a minor but common constituent, occurs as sub-euhedral to anhedral grains; smaller grains are included in relict orthopyroxene, and larger ones are associated with hornblende.

Anorthosite (508916) contains plagioclase (90–95%) and hornblende (5–10%) (Fig. 3.3d). Plagioclase is subhedral, twinned and unzoned with a grain size up to 1.5 mm. Hornblendes occur as individual granules or aggregates of grains along plagioclase-plagioclase boundaries.

Gabbros (508931 and 508989) consist of equal amounts of plagioclase and hornblende with minor orthopyroxene (Fig. 3.3e). Hornblende and plagioclase grain size is up to 2 mm. Plagioclase occurs as large crystals, or more commonly as equilibrium granular polygons among hornblendes. Plagioclase exhibits varying degrees of replacement by zoisite. Hornblendes are usually present as large grains or aggregates of granules.

Leucogabbros (508925 and 508926) have a similar mineral composition and texture to the leucogabbros (508903, 508930 and 508922). Subhedral and anhedral plagioclases (1-1.5 mm) constitute a framework of cumulus minerals, with hornblende filling the interstices between them (Fig. 3.3g). The rocks are typically dominated by a well-formed equilibrium texture with straight grain boundaries and triple junctions (Fig. 3.3g).

Anorthosite (508998) consists of almost pure plagioclase, which is twinned and

unzoned (Fig. 3.3h).

3.4. Analytic methods

Major element mineral chemistry was determined using an Environmental Scanning Electron Microscope (EDAX FEI Quanta 200 FEG Environmental SEM) equipped with an Energy Dispersive X-ray Spectrometry (EDS) at the Great Lakes Institute for Environmental Research (GLIER), University of Windsor, Canada. Given that these major element analyses were not determined with mineral standards they are used only for mineral identification and assessment of the compositional variations in analyzed minerals. Trace and ultra-trace element analyses of hornblende, clinopyroxene and plagoiolcase were carried out on selected samples using femtosecond (fs) laser ablation-inductively coupled plasma-mass spectrometry (LA-ICP-MS) at University of Windsor (Shaheen et al. 2008). Before LA-ICP-MS measurements, grains hornblende, clinopyroxene and plagioclase in polished samples (about 0.1 mm in thickness) were analyzed by SEM to check for homogeneity and determine Ca concentrations which were used as an internal standard. Analytical results of the replicate NIST 612 standards used in calibrations are shown in Table 3.1.

Samples were normalized to chondrites and normal mid-ocean ridge basalt (N-MORB); the normalization values are from Taylor and McLennan (1985) and Hofmann (1988), respectively. Europium, Ce, Nb, Ti, Zr, Pb and Sr anomalies were calculated with respect to the neighboring immobile elements, following the method of Taylor and McLennan (1985).

3.5. Mineral chemistry

3.5.1. Mineral chemistry of hornblende

The description of the trace element geochemistry of hornblende mainly following the whole-rock classification of Suite A and Suite B (Huang et al., submitted) with the

addition of an anomalous hornblende grouping for samples that do not fit with their Suite B whole rock chemistry.

3.5.1.1 Suite A

Hornblende from gabbro (508974) has high V (321 ppm), Cr (309 ppm) and Ni (158 ppm) concentrations. It is slightly enriched in LREE (La/Sm_{cn}=1.03) with HREE depletion (Gd/Yb_{cn}=1.42) (Fig. 3.4a; Table 3.2). On a N-MORB-normalized trace element diagram, it has the following characteristics: (1) enrichment of Rb, Ba and U; (2) a positive Pb anomaly (Pb/Pb*= 3.50); (3) a negative Nb (Ta) (Nb/Nb*= 0.80) anomaly and (4) a negative Zr (Hf) (Zr/Zr*= 0.30) anomaly (Fig. 3.4a; Table 3.2). Hornblende from hornblendites (508973 and 508983) have similar chondrite- and N-MORB-normalized trace-element patterns to those of the gabbro (508974) (Fig. 3.4b,c; Table 3.2) but have even greater consistency, for all elements, in between grain chemistry than the gabbro hornblendes.

3.5.1.2 Suite B

Hornblendes from different rock types of Suite B including gabbros (508931 and 508989), leucogabbros (508925 and 508926), peridotite (508988) and hornblendite (508915) have very similar trace element geochemical characteristics. Hornblende has a large range of V (99-315 ppm), Cr (3-2828 ppm) and Ni (237-429 ppm) concentrations. They have depleted LREE (La/Sm_{cn}=0.24-0.42) and slightly enriched HREE (Gd/Yb_{cn}=0.51-0.80) patterns with negative to positive Eu anomalies (Eu/Eu*=0.36-1.87) (Fig. 3.5a, c e, g, i and k; Table 3.2). On a N-MORB-normalized trace element diagram, they show the following characteristics: (1) enrichment of Rb and Ba, (2) positive Pb anomalies (Pb/Pb*=3.28-13.31) and (3) generally slight negative anomalies of Nb (Ta) (Nb/Nb*=0.23–0.91) (Fig. 3.5b, d, f, h, j and i; Table 3.2).

3.5.1.3 Anomalous hornblendes

Hornblende from leucogabbros (508903 and 508930) and anorthosite (508916) have large variations in V (79-305 ppm), Cr (328-2216 ppm) and Ni (200-488 ppm) concentrations. They are depleted in LREE (La/Sm_{cn}=0.55-0.84) (Fig. 3.6a, c and e; Table 3.2). Their N-MORB-normalized trace-element patterns are characterized by enrichment of Rb and U, positive Nb (Ta) anomalies (Nb/Nb*=1.18-2.84), positive and negative Pb anomalies (Pb/Pb*=0.49-5.77) and negative Zr (Hf) anomalies (Zr/Zr*= 0.14-0.67) (Fig. 3. 6b, d and f; Table 3.2).

Hornblende from leucogabbro (508922) exhibits substantial HREE heterogeneity (Gd/Yb_{cn}=0.79-1.63) (Fig. 3.6g and i; Table 3.2). HREE profiles of hornblende are divided into two types: Type 1 hornblende has chondrite-normalized REE and N-MORB-normalized trace element patterns very similar to those of hornblende in leucogabbros (508925 and 508926) (Fig 3.5c and a; Table 3.2). In contrast, the N-MORB-normalized trace element pattern of Type 2 hornblende resembles those of hornblende in the same leucogabbros (508925 and 508926) except for its relative depletion in HREE (Fig. 3.6j; Table 3.2)..

Hornblende from peridotite (508939) possesses enriched LREE (La/Sm_{cn}=1.42) and enriched HREE (Gd/Yb_{cn}=0.56) patterns (Fig. 3.6k; Table 3.2). It has positive Eu anomalies (Eu/Eu*=2.27). On an N-MORB-normalized trace element diagram, it has the following characteristics: (1) positive Pb anomaly (Pb/Pb*=16.16) and (2) negative anomalies of Nb (Ta) (Nb/Nb*=0.37) (Fig. 3.6i; Table 3.2).

3.5.2. Mineral chemistry of clinopyroxene (all from Suite A)

Clinopyroxene from gabbro (508974) has low V (125 ppm), Ni (69 ppm) and Cr (88 ppm) contents. It has low REE contents (e.g. La: 4-5 times La in C1-chondrite; Fig. 3.7a) with depletion of LREE (La/Sm_{cn}=0.85), and the following trace-element characteristics: (1) strong enrichments in Th and U; (2) a strong depletion of Nb (Ta) (Nb/Nb*=0.01);

and (3) large positive Pb (Pb/Pb*=4.03) anomaly (Fig. 3.7b; Table 3.3).

Clinopyroxene from dunite (508968) and peridotites (50869 and 508978) have similar chemical compositions. They have high Ni (667-740 ppm) and Cr (1136-1839 ppm) contents. They are depleted in LREE (La/Sm_{cn}=0.51-0.78) and HREE (Gd/Yb_{cn}=2.04-2.47) and have small negative Eu anomalies (Eu/Eu*=0.72–0.97). The pyroxenite (508979) clinopyroxene is an outlier as it is LREE enriched (La/Sm_{cn}=1.32) (Fig. 3.7c, e, g and i; Table 3.3). The clinopyroxenes from the dunite and peridotites have the following trace element characteristic on an N-MORB-normalized trace-element diagram: (1) enrichments of Rb and U; (2) depletion to enrichment of Nb (Ta) (Nb/Nb*=0.33-1.10), and (3) negative Zr (Zr/Zr*=0.12-0.25) anomalies (Fig. 3.7d, f, h and j; Table 3.3). The pyroxenite clinopyroxene is characterized by a large Ba depletion (Fig. 3.7 j).

3.5.3. Mineral chemistry of plagioclase

The REE patterns of plagioclase are characterized by relative LREE-enrichment and by a consistent positive Eu anomaly except for plagioclase from gabbro (508931) (Fig. 3.8; Table 3.4). In most samples, HREE are below detection. Interestingly, plagioclase from gabbro (508931) has a LREE depleted (La/Sm_{cn}=0.84) and HREE enriched (Gd/Yb_{cn}=0.59) pattern (Fig. 3.8g; Table 3.4). Plagioclase from gabbro (508974) and hornblendite (508973) have the highest Sr (868-1039 ppm), Ba (140-180 ppm) and Pb (12.9-13.3 ppm) concentrations (Table 3.4).

3.6. Discussion

3.6.1. Assessment of alteration and secondary element mobility of trace elements in hornblende, clinopyroxene and plagioclase

A great variety of magmatic textures are well preserved within the Fiskenæsset Complex such as mineral-graded layering, cumulative peridotite, cumulative gabbro and

megacryst plagioclase (see Figs. 3a, 3b, 3f, 3g, 4c in Huang et al., submitted). An intimate interlayering of hornblendite with peridotite, dunite, and pyroxenite in the Ultramafic Unit strongly indicates that little pervasive alteration associated with aqueous fluids has occurred in subsequent structural/metamorphic events. This suggest that it is very likely that the amphiboles were a primary magmatic phase. Dunites, peridotites, pyroxenites and hornblendites are the most primitive magmatic rocks exposed in the Fiskenæsset Complex. Preservation of cumulate textures such as euhedral olivine and pyroxene surrounded by tiny amounts of interstitial Fe-Ti oxides, adcumulative hornblendes without pyroxene relicts clearly indicate that they are igneous cumulates (Fig. 3.2g). Leucogabbros and anorthosites with some percentage of hornblende in the Fiskenæsset Complex exhibit interstitial hornblende between large plagioclase crystals, which represents a typical adcumulate texture (Fig. 3.3d, 3g and 3h). As leucogabbros and anorthosites preserve original magmatic textures this further suggests that hornblende was a primary hydrous phase. Overall, field relations and petrographic observations point out that the principal evolution of the Fiskenæsset Complex was mainly controlled by igneous processes. Whole-rock trace elements of the Fiskenæsset Complex exhibit typical features of subduction-related magmatism such as negative anomalies in HFSE (Nb, Ta and Zr) and enrichment in LILE such as Pb and Sr (Polat et al., 2009, 2012; Huang et al., submitted). Field relations and whole-rock trace element geochemistry indicate that most of the Fiskenæsset Complex was formed by magmatic processes in a supra-subduction environment and, thus, provides crucial information toward the understanding of differentiation processes of hydrous magma which operate above subduction zones (Polat et al., 2009, 2012; Windley and Garde, 2009; Rollinson et al., 2010; Huang et al.,submitted).

In gabbro (508974), there is coexisting hornblende and clinopyroxene. Noticeably, hornblende and clinopyroxene in gabbro (508974) have significantly different trace element compositions (Tables 3.2 and 3.3). Normalization of incompatible trace element

concentrations of hornblende to N-MORB reveals that Ba, Rb and Pb are consistently and markedly enriched. Nb, Ta, Zr and Hf are slightly depleted relative to neighboring REE; their concentrations are significantly higher than in associated clinopyroxene (Fig. 3.9b and d). Niobium abundances in the clinopyroxene are very low. Niobium is also generally relatively immobile, even under amphibolite facies metamorphism (e.g., Weaver and Tarney, 1981). Thus, interaction of an aqueous fluid and clinopyroxene is likely to form hornblende with low Nb abundances. Therefore, it is unlikely that the hornblende was derived from primary clinopyroxene. In addition, hornblende has higher abundances of Nb and Ta than clinopyroxene does, which is consistent with D_{Nb} and D_{Ta} in pyroxenes being more than one order of magnitude lower than D_{Nb} and D_{Ta} for amphibole (e.g., Tiepolo et al. 2007). Similarly, the hornblende preferentially incorporating MREE compared to HREE is interpreted as a primary amphibole signature (Fig. 3.9a) (e.g., Tiepolo et al. 2007). Interestingly, hornblende of hornblendite (508973 and 508983) has very similar chemical characteristics to those of hornblende of gabbro (508974) (Fig. 3.4), which not only indicates the hornblende is of igneous origin but also suggests a genetic link between them. In addition, hornblende from gabbro (508974), and hornblendites (508973 and 508983) have different geochemical compositions from those of clinopyroxene from dunite (508968), peridotites (508969 and 508978) and pyroxenite (508979), which further confirms that hornblende originated from igneous processes (Figs. 3.4 and 3.7). Moreover, clinopyroxene has higher Gd/Yb_{cn} than hornblende, which also excludes the possibility of the hornblende being derived from clinopyroxene (Tables 3.2 and 3.3).

Given a primary magmatic origin, can hornblende preserve its original igneous chemical composition or have post-magmatic events/alteration modified the pristine magmatic trace element compositions. The hornblendes display surprisingly coherent chondrite-normalized REE and N-MORB-normalized trace-element patterns, strongly suggesting that these elements were essentially immobile during metamorphism (Fig.

3.4). Generally, LILE (Rb, Ba and Pb) are mobilized during metamorphism and hydrothermal alteration. However, on N-MORB-normalized trace element diagrams, they also display limited variation, suggesting these elements were relatively immobile on the mineral scale (Fig. 3.4). It is suggested therefore that the hornblendes of gabbro (508974) and hornblendites (508973 and 508983) have preserved their primary igneous chemical characteristics.

There is no significant difference of the geochemistry of the hornblende from different rock types including gabbros (508931 and 508989), leucogabbros (508925 and 508926), peridotite (508988) and hornblendite (508915) (Fig. 3.5). Such features are considered as a strong evidence for hornblende from all these rocks having crystallized at the same time from the same parent magma. An alternative hypothesis could have hornblende formation reflecting interaction of the gabbroic crystal mush with an infiltrating aqueous fluid of igneous origin. Michard (1989) has studied the REE content of hydrothermal fluids from a number of geothermal fields and found that the hydrothermal fluids are usually LREE enriched. However, hornblende preserves significant LREE depletion (La/Sm_{cn}=0.24-0.42) (Fig. 3.5; Table 3.2), and this argues against the involvement of a LREE-rich externally derived component. A further argument against involvement of an aqueous fluid is the lack of clinopyroxene reaction rims and coronas of hornblende on pyroxene. LREE enriched amphiboles derived from interaction between clinopyroxene and hydrothermal fluids have been found in the Northern Apennine olivine gabbros and the oceanic gabbros from the MARK area (Tribuzio et al. 2000; Gillis and Meyer 2001; Coogan et al. 2001). These hydrothermal amphiboles usually occur as rims on clinopyroxene and interstitial grains to clinopyroxene. By contrast, granular hornblende that is interstitial to plagioclase in leucogabbros (508925 and 508926) and main cumulate mineral in gabbros (508931 and 508989), peridotite (508988) and hornblendite (508915) indicate an igneous origin, having crystallized from a magmatic melt. The similarity of the trace element patterns of

the studied hornblendes indicate that the hornblende may have largely conserved their trace element contents during the late metamorphism and thus retained the geochemical signature of the original hornblende. The intra and inter-crystal homogeneity of the hornblende which is indicated by the coherent chondrite-normalized REE and N-MORB-normalized trace element diagrams and the generally very low relative standard deviations of multiple grain analyses further confirm that the hornblende likely retained its magmatic trace element signature (Fig. 3.5).

Hornblende from leucogabbros (508903 and 508930) and anorthosite (508916) have extremely high absolute concentrations of incompatible elements like Nb, Zr and REE (Fig. 3.6b, d and f; Table 3.2), which suggests that the hornblende crystallized from igneous liquids rather than derived from interaction between gabbroic assemblages and aqueous fluids at subsolidus conditions (Tribuzio et al. 2000; Gillis and Meyer 2001; Coogan et al. 2001). As previously stated, hornblende does not present any evidence for mobilization of trace elements including the LILE as a consequence of metamorphism. Therefore, it is suggested that the hornblende chemistry is primary.

Hornblende from leucogabbro (508922) has distinct heterogeneity of HREE (Fig. 3.6g and i). Unequivocally, Type 1 hornblende crystallized from the same parent melt as the magmatic liquid which generated the hornblende of gabbros (508931 and 508989), leucogabbros (508925 and 508926), peridotite (508988) and hornblendite (508915) (Figs. 3.5 and 3.6h). Types 1 and 2 are virtually indistinguishable with respect to the most of the trace elements, suggesting that HREE may provide additional insights into crystallization history (Figs. 3.5 and 3.6j).

Hornblende from the peridotite (508939) possesses an enriched LREE (La/Sm_{cn}=1.41) and enriched HREE (Gd/Yb_{cn}=0.56) pattern (Fig. 3.6k). As mentioned above, the LREE enrichment characteristic may indicate an involvement of an aqueous fluid in the formation of the hornblende. However, petrographic observation shows that hornblende occurs as oikocrysts enclosing olivine without pyroxene in peridotite

(508939) (Fig. 3.3f), which argues against a hydrothermal origin for the hornblende. It is more plausible that the hornblende is of magmatic origin which is indicted by its petrographical and geochemical homogeneity. No convincing evidence of trace element mobilization following the postmagmatic process was observed during this study.

On the basis of the field and petrographic observations, we conclude that (1) the hornblende developed during magmatic processes, and (2) no metamorphic process have affected the trace element compositions including those generally mobile LILE contained in the hornblende. Similarly, we suggest the clinopyroxene and the plagioclase retained their igneous geochemical signatures.

3.6.2. Evidence for two suites of magmas in the Fiskenæsset Complex on Majorqap qâva

Based on the whole-rock Gd/Yb_{cn}, Huang et al. (submitted) divided the Fiskenæsset Complex on Majorqap qâva into two suites: Suite A ($Gd/Yb_{cn}>1$) and Suite B ($Gd/Yb_{cn}<1$). The differences between Suite A and Suite B are also evident in terms of their hornblende trace element chemistry. In particular, the hornblende from Suite A is readily distinguished from the hornblende from Suite B by its higher REE abundances and its depletion in HREE (Fig. 3.10). Distinction between both suites is also clearly shown in Gd/Yb_{cn} vs. La/Yb_{cn} plot of hornblende (Fig. 3.11). Hornblende from Suite A is characterized by depletion of HREE ($Gd/Yb_{cn}>1$), whereas hornblende from Suite B shows the enrichment of HREE ($Gd/Yb_{cn}<1$).

However, the anomalous hornblendes from leucogabbros (508903, 508922 and 508930), anorthosite (508916) and peridotite (508939) are not included in Figs 3.10 and 3.11) and suggests some additional complications that will be explored in further work.

3.7. Conclusion

1. Field observations, petrographic observations and the consistency of REE and trace element patterns of the igneous hornblende, clinopyroxene and plagioclase indicate that

the crystals preserve their primary igneous geochemical characteristics despite a complex post emplacement history.

2. New geochemical data for hornblende from the gabbroic rocks in Fiskenæsset Complex on Majorqap qâva show two distinct petrogenetic suites. The geologically earlier Suite A is characterized by hornblende with depletion of HREE ($Gd/Yb_{cn}>1$). The later Suite B contains hornblende with HREE enrichment ($Gd/Yb_{cn}<1$).

3.8. Acknowledgments

The research was supported by NSERC grants to A. Polat and B. Fryer, and the field work by the Bureau of Minerals and Petroleum in Nuuk and the Geological Survey of Denmark and Greenland (GEUS).

3.9 Reference

Anderson, A.T., 1980. Significance of hornblende in calc-alkaline andesites and basalts. American Mineralogist 65(9-10): 837-851.

Ashwal, L.D., Jacobsen, S.B., Myers, J.S., Kalsbeek, F., Goldstein, S.J., 1989. Sm-Nd Age of the Fiskenæsset anorthosite Complex, West Greenland. Earth and Planetary Science Letters 91(3-4): 261-270.

Ashwal, L.D., 1993. Anorthosites. Minerals and Rocks Series, 21. Springer-Verlag, Berlin, 422 pp.

Black, L.P., Moorbath, S., Pankhurs.Rj, Windley, B.F., 1973. $^{207}Pb/^{206}Pb$ whole Rock Age of the Archaean Granulite Facies Metamorphic Event in West Greenland. Nature-Physical Science 244(134): 50-53.

Borghini, G., Rampone, E., 2007. Postcumulus processes in oceanic-type olivine-rich cumulates: the role of trapped melt crystallization versus melt/rock interaction. Contributions to Mineralogy and Petrology 154(6): 619-633.

Brandriss, M.E., Bird, D.K., 1999. Effects of H_2O on Phase Relations during

Crystallization of Gabbros in the Kap Edvard Holm Complex, East Greenland. Journal of Petrology 40(6): 1037-1064.

Coogan, L.A., Wilson, R.N., Gillis, K.M., MacLeod, C.J., 2001. Near-solidus evolution of oceanic gabbros: insights from amphibole geochemistry. Geochimica et Cosmochimica Acta 65(23): 4339-4357.

Escher, J.C., Myers, J.S., 1975. New evidence concerning the original relationships of early Precambrian volcanics and anorthosites in the Fiskenæsset region, southern West Greenland. Bulletin Grønlands Geologiske Undersøgelse 75, 72-76.

Greene, A.R., DeBari, S.M., Kelemen, P.B., Blusztajn, J., Clift, P.D., 2006. A detailed geochemical study of island arc crust: the Talkeetna Arc section, south-central Alaska. Journal of Petrology 47(6): 1051-1093.

Henderson, P., Fishlock, S.J., Laul, J.C., Cooper, T.D., Conard, R.L., Boynton, W.V., Schmitt, R.A., 1976. Rare earth element abundances in rocks and minerals from the Fiskenæsset Complex, West Greenland. Earth and Planetary Science Letters 30(1): 37-49.

Hoffmann, J.E., Svahnberg, H., Piazolo, S., Scherstén, A., Münker, C., 2012. The geodynamic evolution of Mesoarchean anorthosite complexes inferred from the Naajat Kuuat Complex, southern West Greenland. Precambrian Research 196–197(0): 149-170.

Hofmann, A.W., 1988. Chemical differentiation of the Earth: the relationship between mantle, continental crust, and oceanic crust. Earth and Planetary Science Letters 90(3): 297-314.

Huang, H., Polat, A., Fryer, B.J., Peter, W.U.A., Windley, B.F., submitted. Geochemistry of the Mesoarchean Fiskenæsset Complex at Majorqap qâva, SW Greenland: Evidence for two different magma compositions. (Submited to Chemical Geology).

Huang, H., Polat, A., Fryer, B.J., 2012. Origin of Archean tonalite–trondhjemite–granodiorite (TTG) suites and granites in the Fiskenæsset

region, southern West Greenland: Implications for continental growth. Gondwana Research doi:10.1016/j.gr.2011.12.001.

Irvine, T.N., 1974. Petrology of the Duke Island Ultramafic Complex, Southeastern Alaska. Geological Society of America, Memoirs,138, 240 pp.

Kalsbeek, F., Myers, J.S., 1973. The geology of the Fiskenæsset region. Rapport GrønlandsGeologiske Undersøgelse 51: 5-18.

Keulen, N., Naeraa, T., Kokfelt, T.F., Schumacher, J.C., Scherstén, A., 2010. Zircon record of the igneous and metamorphic history of the Fiskenæsset anorthosite complex in southern West Greenland. Geological Survey of Denmark and Greenland Bulletin(20): 67-70.

Keulen, N., Kokfelt, T.F., the homogenisation team, 2011. A seamless, digital, internet-based geological map of South-West and southern West Greenland, 1:100 000, 61°30′ – 64°. http://geuskort.geus.dk/gisfarm/svgrl.jsp. Copenhagen: Geological Survey of Denmark and Greenland.

Langmuir, C.H., 1989. Geochemical consequences of in situ crystallization. Nature 340(6230): 199-205.

McGregor, V.R., Friend, C.R.L., 1992. Late Archean Prograde Amphibolite- to Granulite-Facies Relations in the Fiskenæsset Region, Southern West Greenland. The Journal of Geology 100(2): 207-219.

Meurer, W.P., Claeson, D.T., 2002. Evolution of Crystallizing Interstitial Liquid in an Arc-Related Cumulate Determined by LA ICP-MS Mapping of a Large Amphibole Oikocryst. Journal of Petrology 43(4): 607-629.

Michard, A., 1989. Rare earth element systematics in hydrothermal fluids. Geochimica et Cosmochimica Acta, 53(3): 745-750.

Moorbath, S., Pankhurst, R.J., 1976. Further rubidium-strontium age and isotope evidence for the nature of the late Archaean plutonic event in West Greenland. Nature 262(5564): 124-126.

Müntener, O., Kelemen, P., Grove, T., 2001. The role of H_2O during crystallization of primitive arc magmas under uppermost mantle conditions and genesis of igneous pyroxenites: an experimental study. Contributions to Mineralogy and Petrology 141(6): 643-658.

Myers, J.S., Platt, R.G., 1977. Mineral chemistry of layered Archaean anorthosite at Majorqap qava, near Fiskenæsset, southwest Greenland. Lithos 10(1): 59-72.

Myers, J.S., 1985. Stratigraphy and structure of the Fiskenæsset complex, southernWest Greenland. Bulletin Grønlands Geologiske Undersøgelse 150: 1-72.

Naeraa, T., Scherstén, A., 2008. New zircon ages from the Tasiusarsuaq terrane, southern West Greenland. Geological Survey of Denmark and Greenland Bulletin(15): 73-76.

Phinney, W.C., Morrison, D.A., Maczuga, D.E., 1988. Anorthosites and related megacrystic units in the evolution of Archean crust. Journal of Petrology 29(6): 1283-1323.

Pidgeon, R.T., Kalsbeek, F., 1978. Dating of igneous and metamorphic events in the Fiskenæsset region of southern west Greenland. Canadian Journal of Earth Sciences 15(12): 2021-2025.

Polat, A., Appel, P.W.U., Fryer, B., Windley, B., Frei, R., Samson, I.M., Huang, H., 2009. Trace element systematics of the Neoarchean Fiskenæsset anorthosite complex and associated meta-volcanic rocks, SW Greenland: Evidence for a magmatic arc origin. Precambrian Research 175(1-4): 87-115.

Polat, A., Frei, R., Schersten, A., Appel, P.W.U., 2010. New age (ca. 2970Ma), mantle source composition and geodynamic constraints on the Archean Fiskenæsset anorthosite complex, SW Greenland. Chemical Geology 277(1-2): 1-20.

Polat, A., Fryer, B.J., Appel, P.W.U., Kalvig, P., Kerrich, R., Dilek, Y., Yang, Z., 2011. Geochemistry of anorthositic differentiated sills in the Archean (~ 2970 Ma) Fiskenæsset Complex, SW Greenland: Implications for parental magma compositions, geodynamic setting, and secular heat flow in arcs. Lithos 123(1-4): 50-72.

Riciputi, L.R., Valley, J.W., McGregor, V.R., 1990. Conditions of Archean granulite metamorphism in the Godthab-Fiskenæsset region, southern West Greenland. Journal of Metamorphic Geology 8(2): 171-190.

Rollinson, H., Reid, C., Windley, B., 2010. Chromitites from the Fiskenæsset anorthositic complex, West Greenland: clues to late Archaean mantle processes. Geological Society, London, Special Publications 338(1): 197-212.

Scoates, J.S., 2000. The Plagioclase–Magma Density Paradox Re-examined and the Crystallization of Proterozoic Anorthosites. Journal of Petrology 41(5): 627-649.

Shaheen, M., Gagnon, J.E., Yang, Z., Fryer, B.J., 2008. Evaluation of the analytical performance of femtosecond laser ablation inductively coupled plasma mass spectrometry at 785 nm with glass reference materials. J. Anal. At. Spectrom., 23: 1610-1621.

Sisson, T.W., Grove, T.L., 1993a. Experimental investigations of the role of H_2O in calc-alkaline differentiation and subduction zone magmatism Contributions to Mineralogy and Petrology 113(2): 143-166.

Sisson, T.W., Grove, T.L., 1993b. Temperatures and H_2O contents of low-MgO high-alumina basalts. Contributions to Mineralogy and Petrology 113(2): 167-184.

Sisson, T.W., Grove, T.L., Coleman, D.S., 1996. Hornblende gabbro sill complex at Onion Valley, California, and a mixing origin for the Sierra Nevada batholith. Contributions to Mineralogy and Petrology 126(1-2): 81-108.

Taylor, S.R., McLennan, S.M., 1985. The Continental Crust: Its Composition and Evolution. Blackwell,Oxford, 312 pp.

Tiepolo, M.T., Tribuzio, R.T., Vannucci, R.V., 2002. The compositions of mantle-derived melts developed during the Alpine continental collision. Contributions to Mineralogy and Petrology 144(1): 1-15.

Tiepolo, M., Oberti, R., Zanetti, A., Vannucci, R., Foley, S.F., 2007. Trace-Element Partitioning Between Amphibole and Silicate Melt. Reviews in Mineralogy and

Geochemistry, 67(1): 417-452.

Tribuzio, R., Tiepolo, M., Thirlwall, M.F., 2000. Origin of titanian pargasite in gabbroic rocks from the Northern Apennine ophiolites (Italy): insights into the late-magmatic evolution of a MOR-type intrusive sequence. Earth and Planetary Science Letters, 176(3–4): 281-293.

Weaver, B.L., Tarney, J., 1981. Chemical changes during dyke metamorphism in high-grade basement terrains. Nature, 289(5793): 47-49.

Windley, B.F., Herd, R.K., Bowden, A.A., 1973 The Fiskenæsset complex, West Greenland, Part I: A preliminary study of the stratigraphy, petrology, and whole-rock chemistry from Qeqertarssuatsiaq. Bulletin Grønlands Geologiske Undersøgelse 106: 1-80.

Windley, B.F., Smith, J.V., 1974. The Fiskenæsset Complex, West Greenland,Part II: General mineral chemistry from Qeqertarssuatsiaq. Bulletin Grønlands Geologiske Undersøgelse 108: 1-54.

Windley, B.F., Garde, A.A., 2009. Arc-generated blocks with crustal sections in the North Atlantic craton of West Greenland: Crustal growth in the Archean with modern analogues. Earth-Science Reviews 93(1-2): 1-30.

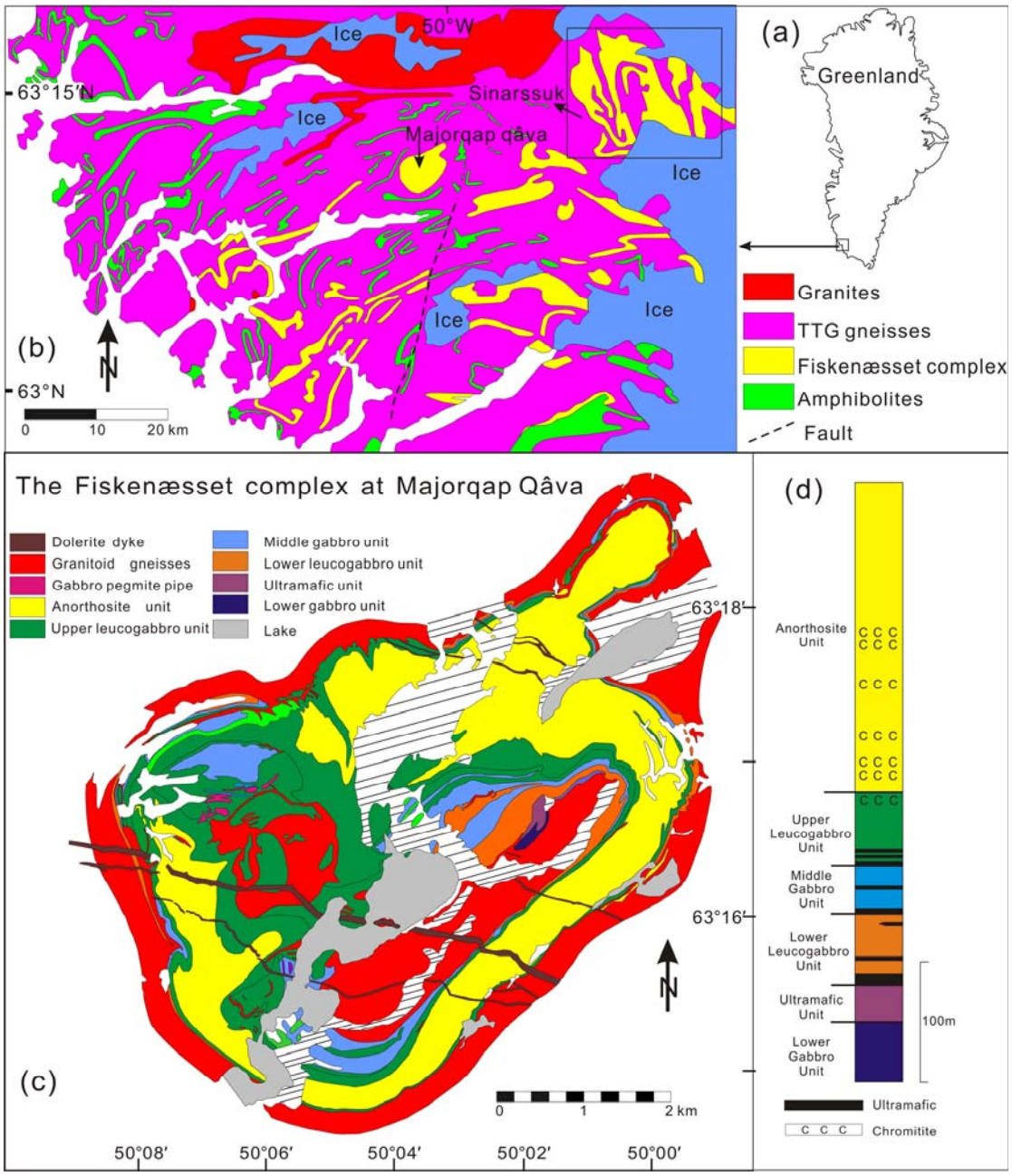

Fig 3.1. (a) General location of the study area in Greenland. (b) Simplified geological map of the Fiskenæsset region (after Myers, 1976). (c) Simplified geological map of the Majorqap qâva outcrop of the Fiskenæsset Complex (after Myers, 1985). (d) Simplified stratigraphic succession of the Fiskenæsset Complex compiled from a number of outcrops (after Myers, 1985). The diagonal lines represent the Quaternary deposits.

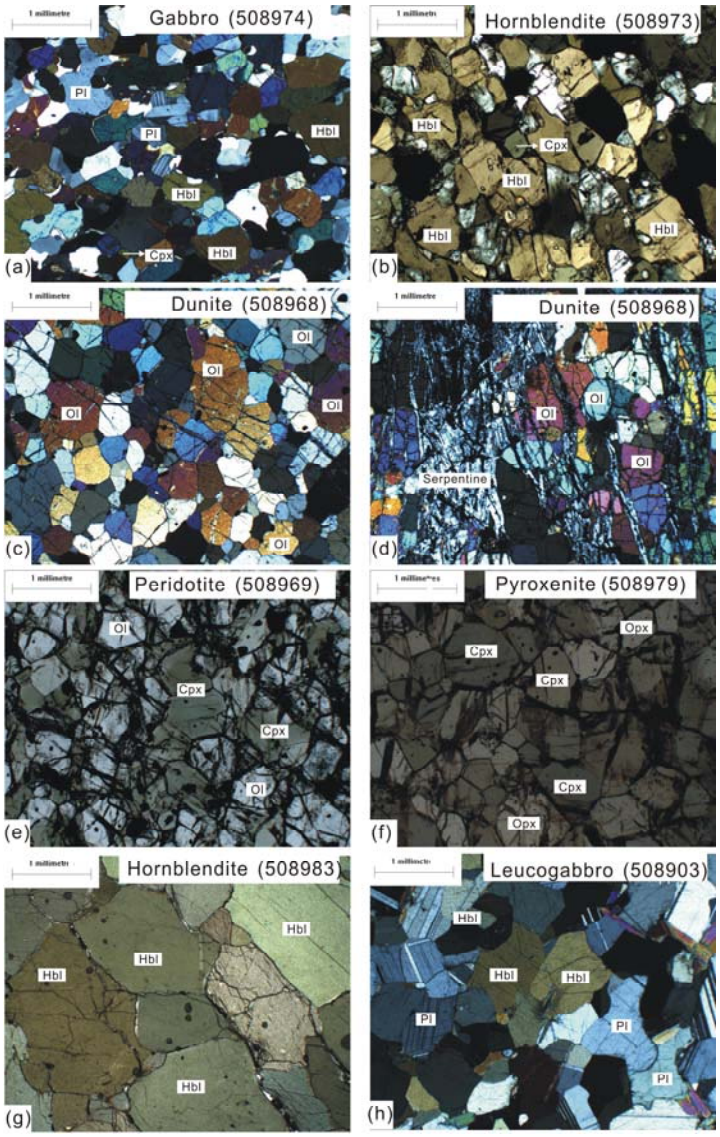

Fig 3.2. Photomicrographs of typical rocks of the Fiskenæsset Complex. (a) Gabbro (508974) with metamorphic plagioclase, hornblende and clinopyroxene. (b) Hornblendite (508973) with hornblende and clinopyroxene. (c) Dunite (508968) with olivine. (d) Dunite (508968) with olivine and serpentine. (e) Peridotite (508969) with olivine and clinopyroxene. (f) Pyroxenite (508979) with orthopyroxene and clinopyroxene. (g) Hornblendite (508983) with hornblende. (h) Leucogabbro (508903) with plagioclase and hornblende. (Pl: plagioclase, Hbl: hornblende, Ol: olivine, Cpx: clinopyroxene, Opx: orthopyroxene).

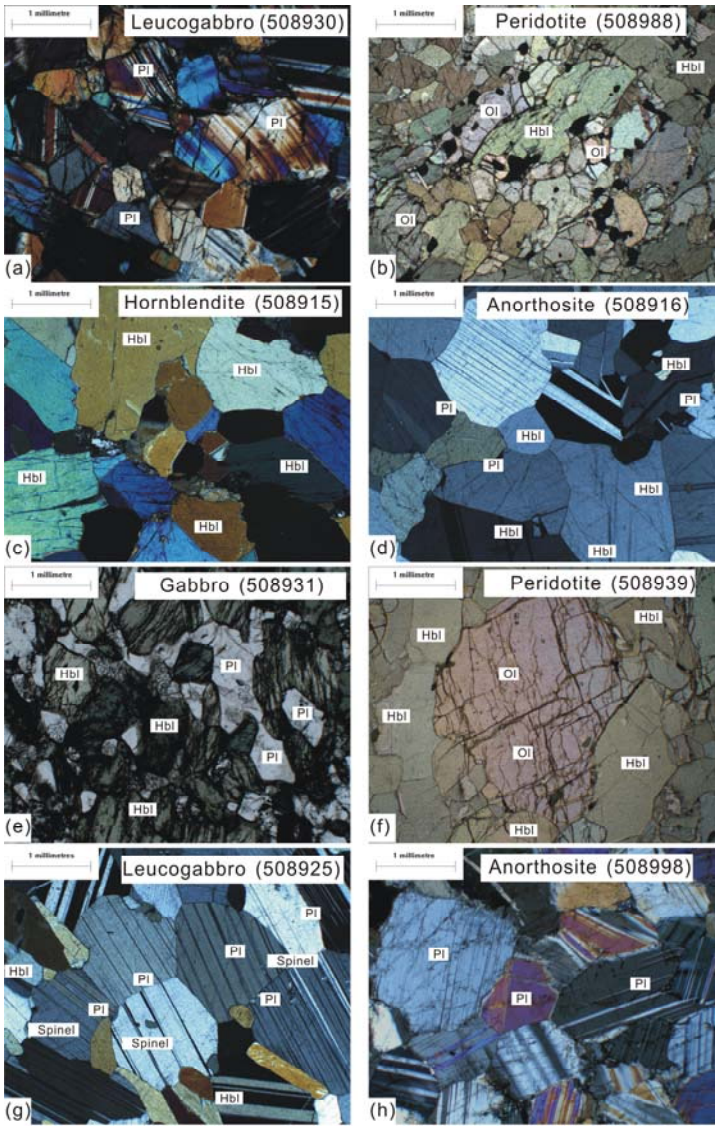

Fig 3.3. Photomicrographs of typical rocks of the Fiskenæsset Complex. (a) Leucogabbro (508930) with plagioclase and hornblende. (b) Peridotite (508988) with olivine and hornblende. (c) Hornblendite (508915) with hornblende. (d) Anorthosite (508915) with minor hornblende. (e) Gabbro (508931) with plagioclase and hornblende. (f) Peridotite (508939) with olivine and hornblende. (g) Leucogabbro (508925) with plagioclase and hornblende. (h) Anorthosite with minor plagioclase. (Pl: plagioclase, Hbl: hornblende, Ol: olivine, Cpx: clinopyroxene, Opx: orthopyroxene).

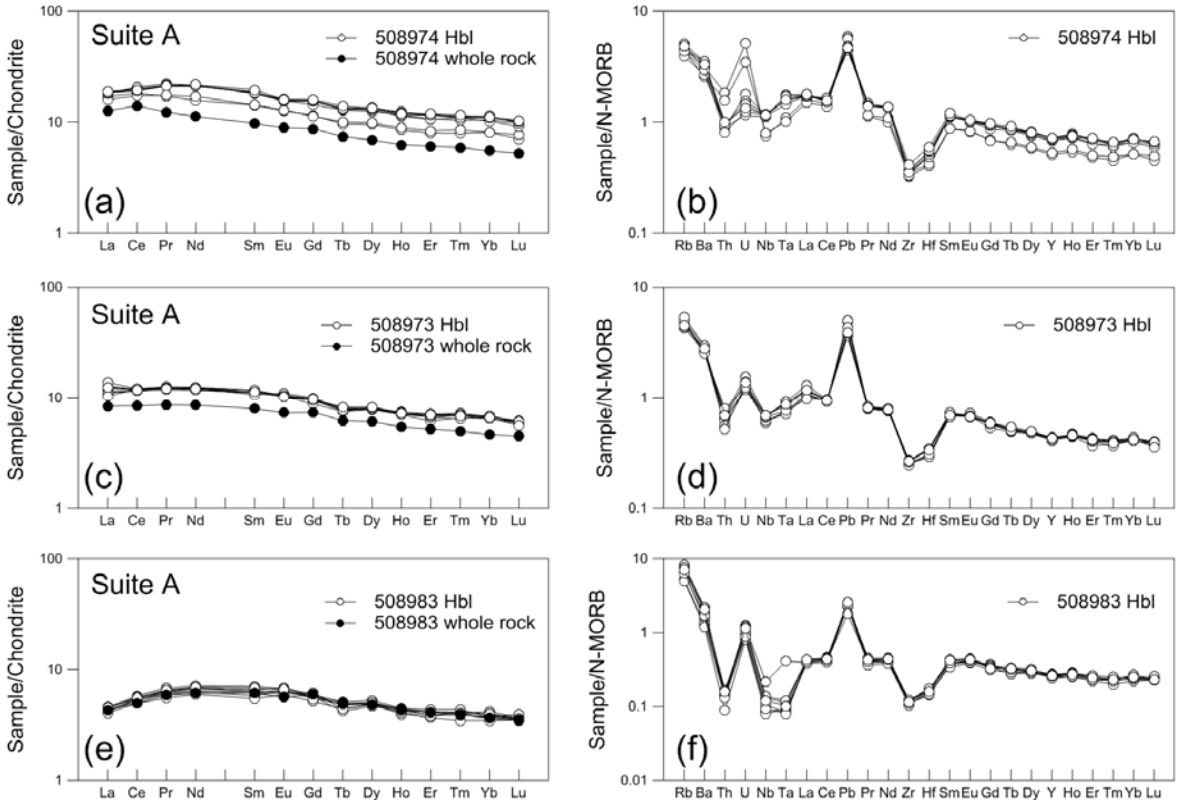

Fig 3.4. Chondrite-normalized REE and N-MORB-normalized trace element patterns for hornblende from gabbro (508974), and hornblendites (508973 and 508983) (Suite A).

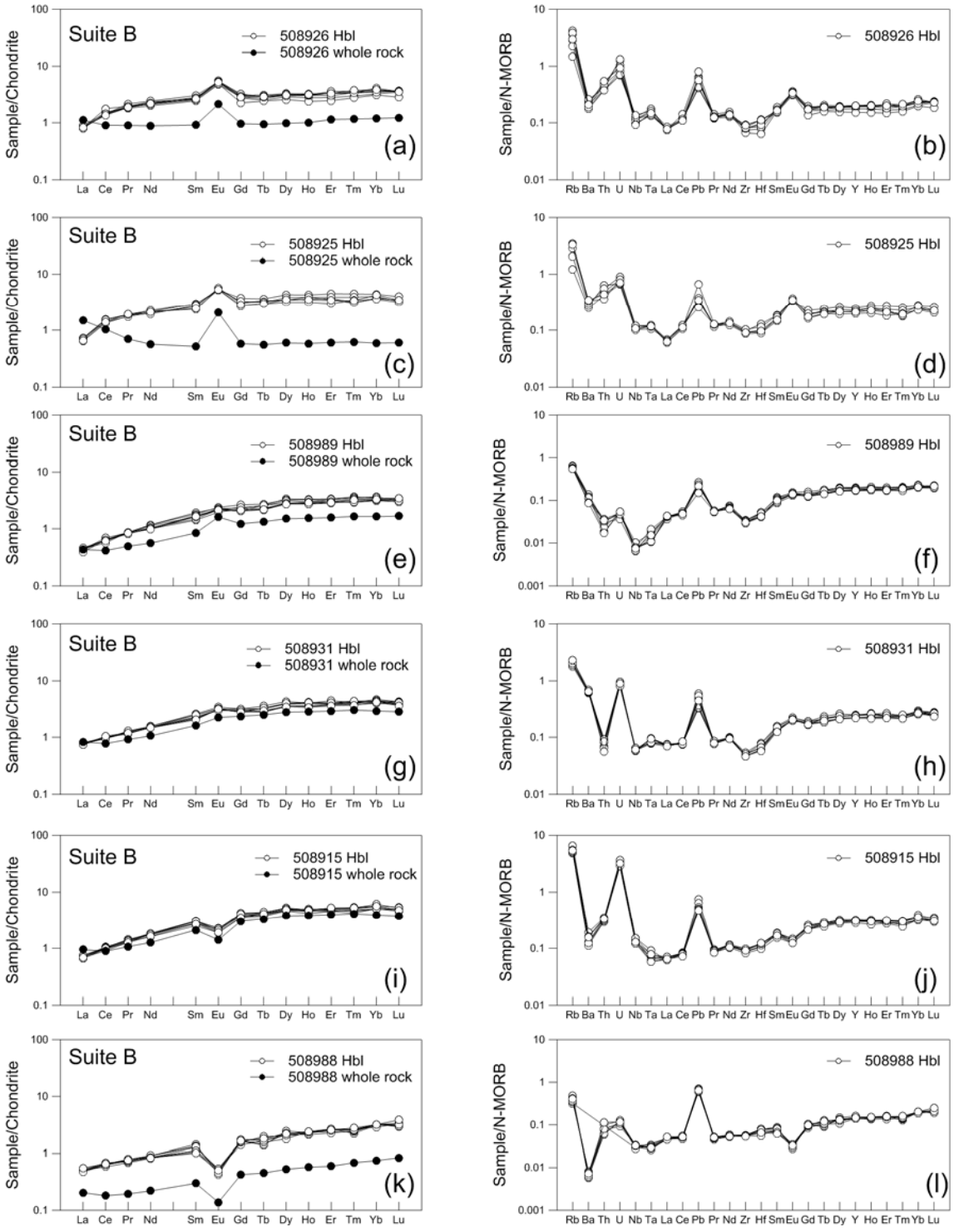

Fig 3.5. Chondrite-normalized REE and N-MORB-normalized trace element patterns for hornblende from gabbros (508931 and 508989), leucogabbros (508925 and 508926), peridotite (508988), and hornblendite (508915) (Suite B).

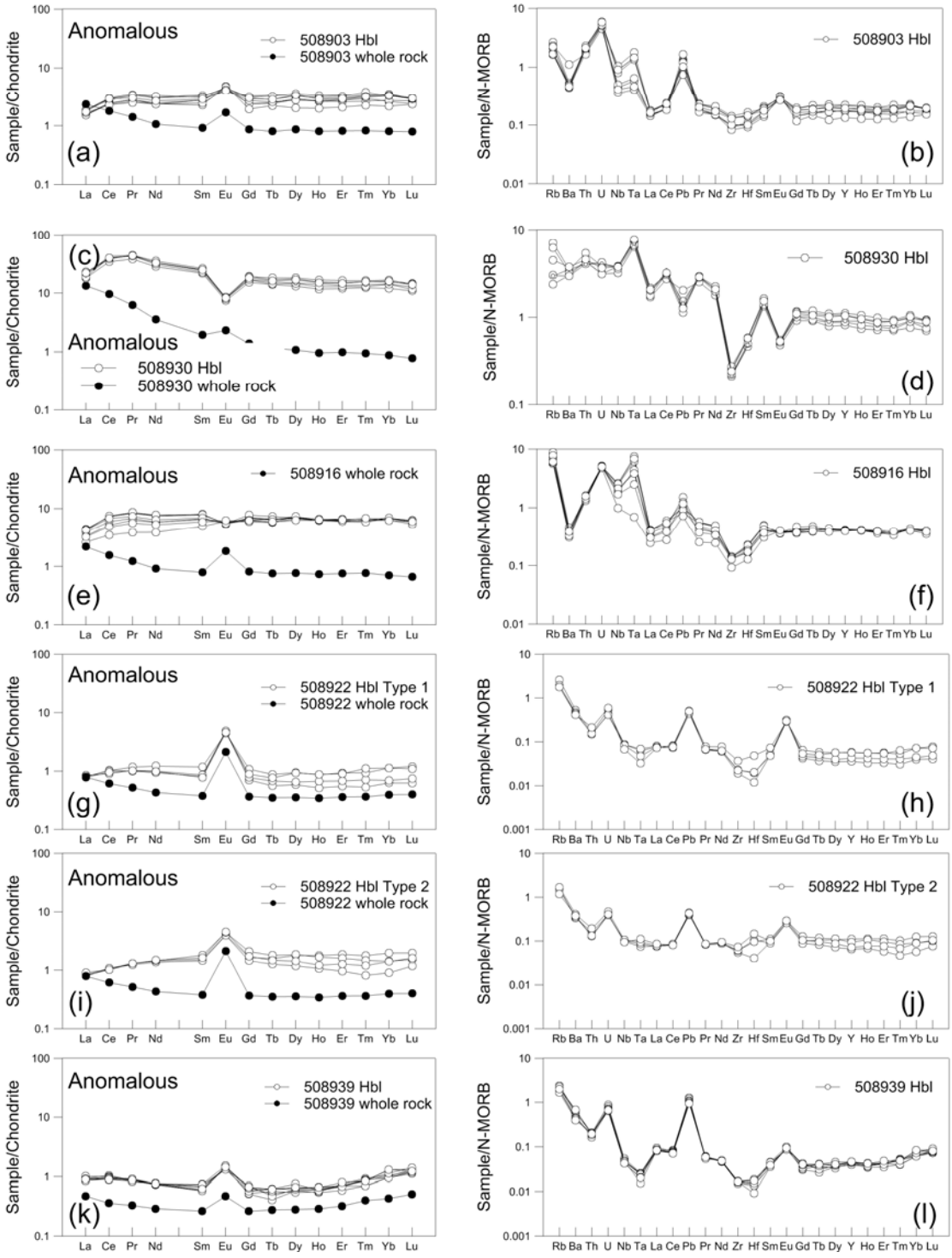

Fig 3.6. Chondrite-normalized REE and N-MORB-normalized trace element patterns for hornblende from leucogabbros (508903, 508930 and 508922) anorthosite (508916), and peridotite (508939) (Anomalous hornblendes).

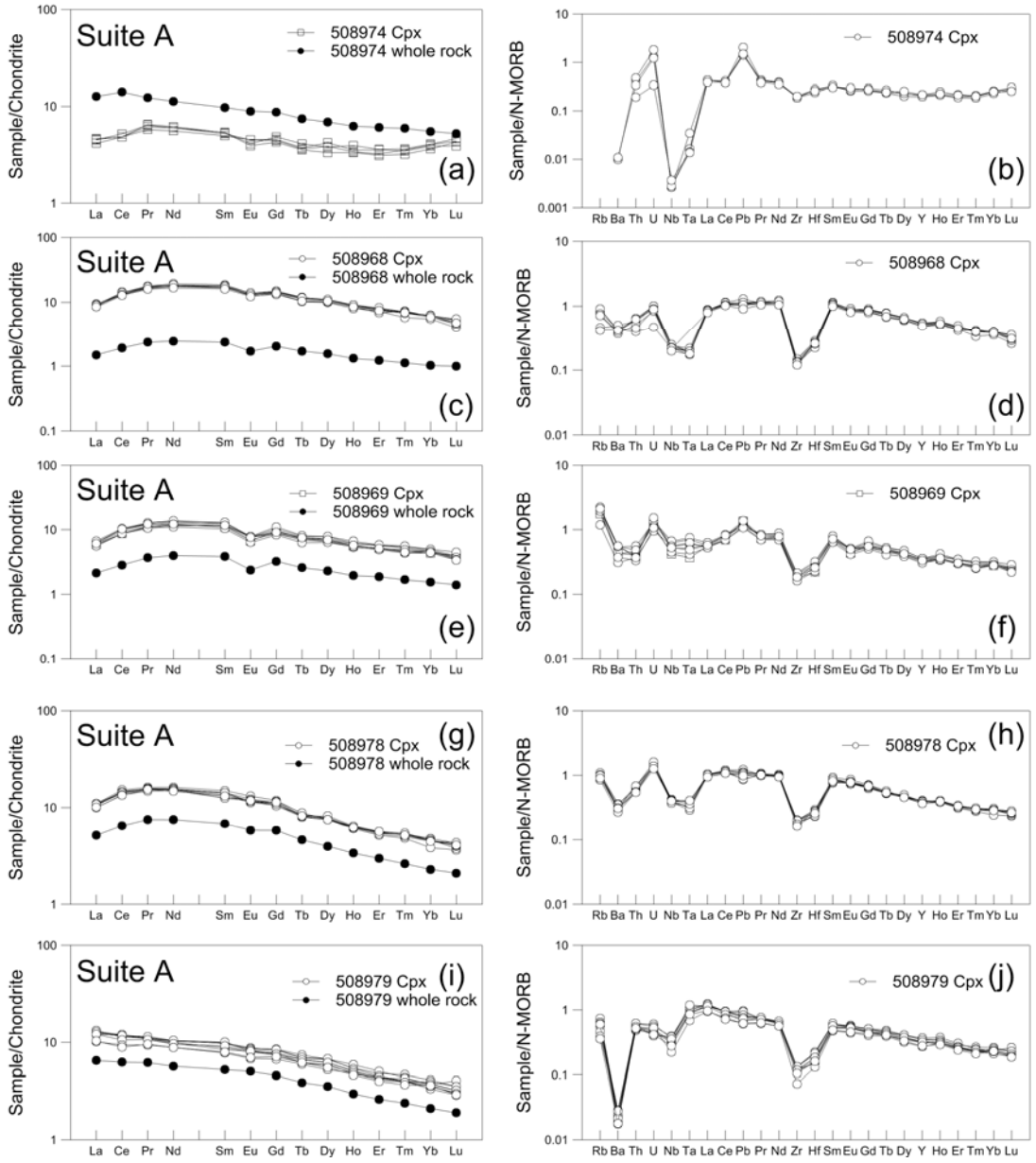

Fig 3.7. Chondrite-normalized REE and N-MORB-normalized trace element patterns for clinopyroxene from gabbro (508974), dunite (508968), peridotites (50869 and 508978) and pyroxenite (508979) (Suite A).

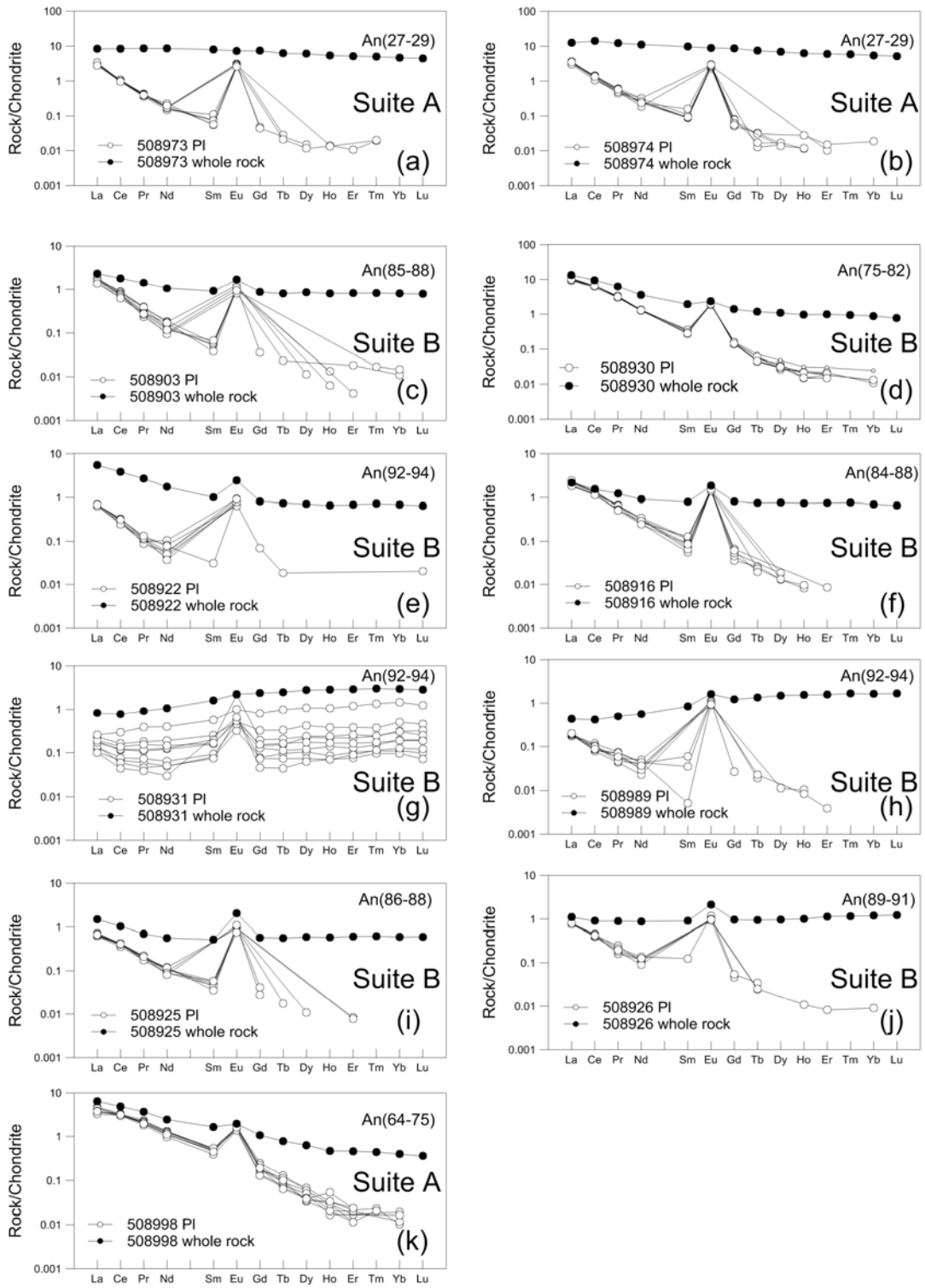

Fig 3.8. Chondrite-normalized REE patterns for plagioclase.

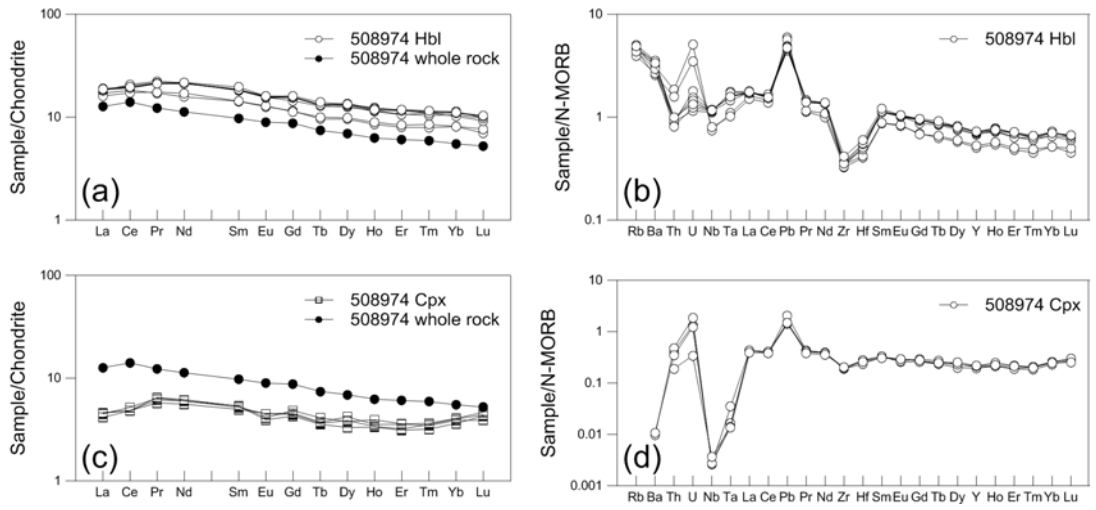

Fig 3.9. Chondrite-normalized REE and N-MORB-normalized trace element patterns for hornblende and clinopyroxene from gabbro (508974).

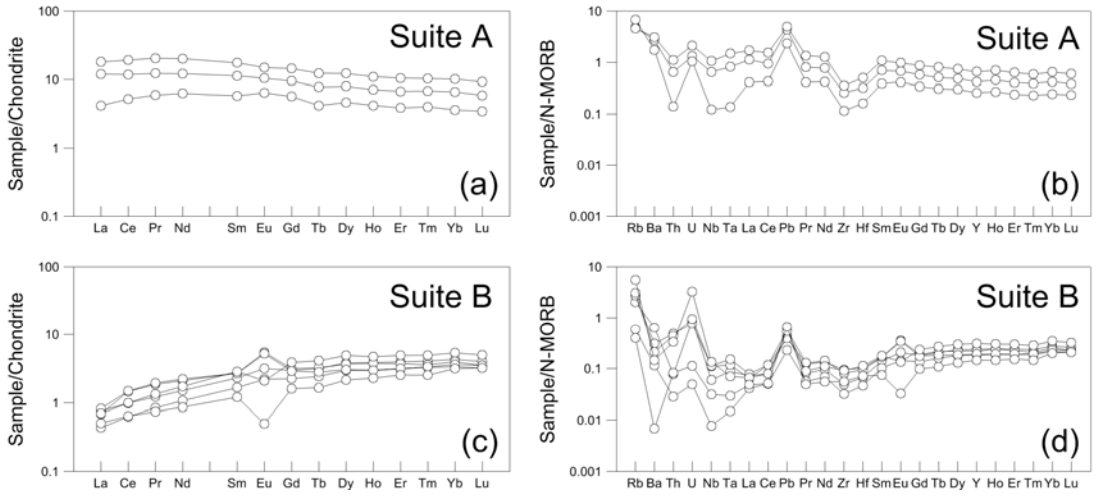

Fig 3.10. Chondrite-normalized REE and N-MORB-normalized trace element patterns for hornblende of Suite A and Suite B.

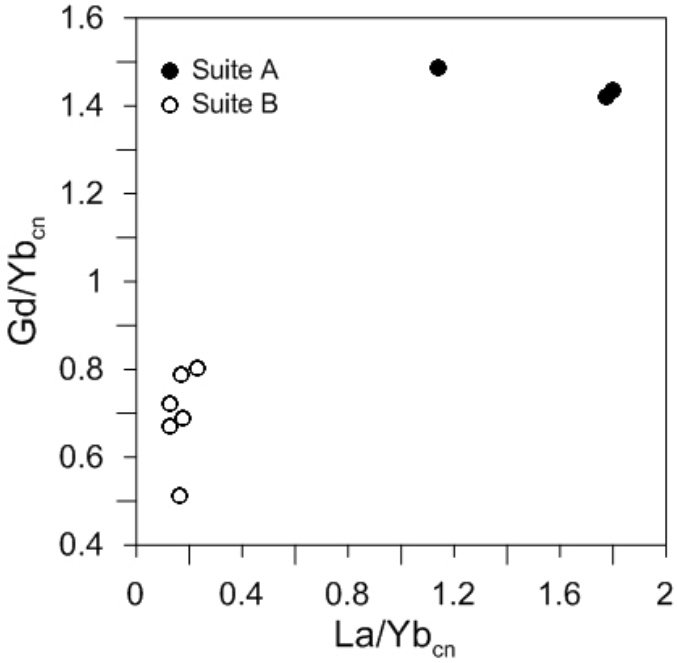

Fig 3.11. La/Yb$_{cn}$ versus Gd/Yb$_{cn}$ variation diagram for hornblende.

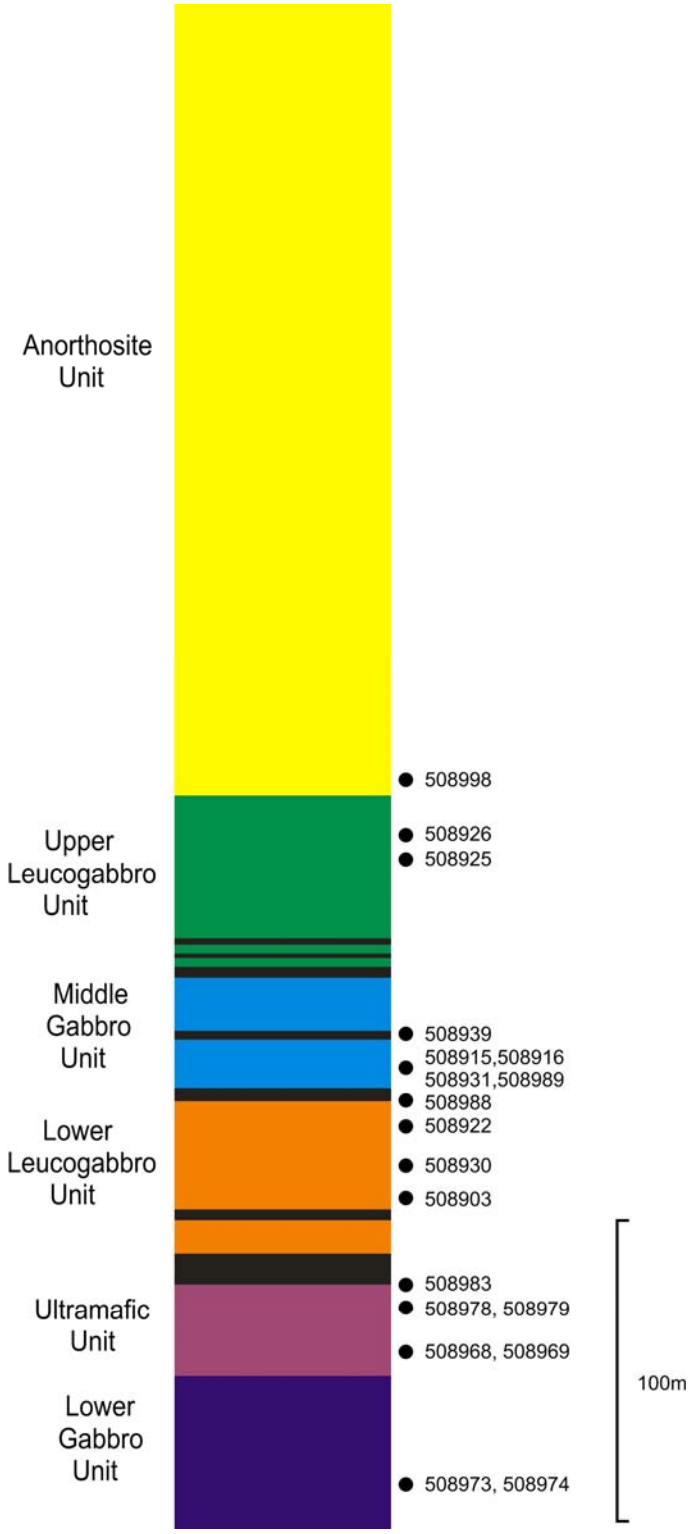

Supplementary Fig. 3.1. Sample positions on the general section.

Table 3.1
Measured and recommended trace element concentrations (ppm) for Nist 612.

	Nist 612 (Hornblende and Clinopyroxene)				Nist 612 (Plagioclase)		
Elemen	Measured (n=72)	Recommended	Rsd (%)	Element	Measured (n=44)	Recommended	Rsd (%)
V	39.35	39.22	3.5	V			
Cr	40.10	39.88	4.3	Cr			
Co	35.37	35.26	3.3	Co			
Ni	38.91	38.44	10.5	Ni			
Rb	31.74	31.63	3.8	Rb	31.73	31.63	3.9
Y	38.34	38.25	3.3	Y	38.43	38.25	4.2
Zr	36.09	35.99	3.6	Zr			
Nb	38.18	38.06	3.8	Nb			
Ba	37.86	37.74	3.1	Ba	37.85	37.74	4.2
La	35.88	35.77	3.4	La	35.88	35.77	4.6
Ce	38.47	38.35	3.7	Ce	38.46	38.35	4.7
Pr	37.27	37.16	2.9	Pr	37.23	37.16	4.0
Nd	35.28	35.24	2.9	Nd	35.30	35.24	4.1
Sm	36.83	36.72	3.0	Sm	36.76	36.72	3.8
Eu	34.50	34.44	2.8	Eu	34.47	34.44	3.8
Gd	37.00	36.95	3.2	Gd	36.99	36.95	4.1
Tb	35.98	35.92	3.1	Tb	35.95	35.92	4.1
Dy	36.02	35.97	2.9	Dy	35.99	35.97	4.0
Ho	37.93	37.87	3.0	Ho	37.89	37.87	3.9
Er	37.48	37.43	3.0	Er	37.45	37.43	4.0
Tm	37.61	37.55	3.0	Tm	37.57	37.55	4.0
Yb	39.98	39.95	3.1	Yb	39.96	39.95	3.9
Lu	37.74	37.71	3.0	Lu	37.73	37.71	4.1
Hf	34.82	34.77	3.2	Hf			
Ta	39.84	39.77	3.2	Ta			
Pb	39.15	38.96	4.1	Pb	38.87	38.96	5.3
Th	37.26	37.23	3.1	Th			
U	37.21	37.15	2.4	U			
Sr				Sr	76.30	76.15	2.9

Table 3.2 Trace (ppm) element concentrations and significant element ratios for hornblende.

	508974			508973			508983			508931		
Rock type	Gabbro			Hornblendite			Hornblendite			Gabbro		
Unit	LGU			LGU			UU			MGU		
Group	Suite A			Suite A			Suite A			Suite B		
	Average (n=8)	Std	Rsd	Average (n=8)	Std	Rsd	Average (n=8)	Std	Rsd	Average (n=8)	Std	Rsd
V	321	28	8.8	248	15	6.2	196	10	5.1	315	32	10.1
Cr	309	37	12.0	712	94	13.2	1629	190	11.6	2681	403	15.0
Co	77	4	5.1	73	3	3.5	84	4	4.4	57	3	5.8
Ni	158	10	6.0	173	8	4.5	443	47	10.6	237	13	5.6
Rb	5.76	0.43	7.5	6.08	0.47	7.7	8.55	1.47	17.2	2.58	0.22	8.4
Y	23.62	3.21	13.6	15.15	0.32	2.1	9.31	0.40	4.3	8.44	0.43	5.1
Zr	36.95	2.91	7.9	26.97	0.92	3.4	11.97	0.65	5.4	5.12	0.26	5.2
Nb	3.70	0.62	16.8	2.29	0.14	6.1	0.42	0.15	35.6	0.21	0.01	3.7
Ba	43.14	5.06	11.7	37.83	2.16	5.7	24.25	5.22	21.5	8.89	0.40	4.5
La	6.62	0.37	5.5	4.39	0.41	9.3	1.60	0.07	4.7	0.28	0.01	3.4
Ce	18.43	1.03	5.6	11.33	0.20	1.8	5.18	0.24	4.6	0.95	0.03	3.5
Pr	2.80	0.27	9.7	1.68	0.03	1.9	0.86	0.05	6.3	0.17	0.01	3.9
Nd	14.32	1.67	11.7	8.65	0.18	2.0	4.71	0.25	5.4	1.07	0.03	2.6
Sm	4.05	0.47	11.7	2.62	0.08	3.2	1.46	0.12	8.1	0.53	0.05	8.5
Eu	1.30	0.11	8.5	0.91	0.02	2.2	0.55	0.02	4.2	0.28	0.01	3.6
Gd	4.42	0.59	13.4	2.92	0.11	3.6	1.74	0.10	5.5	0.91	0.05	5.5
Tb	0.72	0.09	13.2	0.45	0.01	3.3	0.27	0.02	6.7	0.18	0.02	8.3
Dy	4.67	0.61	13.2	3.05	0.06	2.0	1.89	0.07	3.6	1.46	0.11	7.3
Ho	0.94	0.12	13.3	0.61	0.01	1.9	0.36	0.01	4.1	0.33	0.03	7.6
Er	2.62	0.38	14.6	1.69	0.08	4.7	0.99	0.06	5.8	0.98	0.06	6.4
Tm	0.37	0.05	13.1	0.24	0.01	3.7	0.14	0.01	6.5	0.14	0.01	5.9
Yb	2.52	0.33	13.0	1.65	0.04	2.4	0.95	0.06	6.0	1.07	0.06	5.2
Lu	0.35	0.05	13.5	0.23	0.01	3.2	0.14	0.01	3.9	0.15	0.01	5.6
Hf	1.51	0.20	13.2	0.96	0.07	7.7	0.48	0.03	6.9	0.20	0.02	11.2
Ta	0.28	0.05	18.7	0.16	0.02	10.1	0.03	0.02	82.3	0.02	0.00	9.0
Pb	2.43	0.26	10.5	2.11	0.28	13.5	1.14	0.12	10.5	0.22	0.05	22.1
Th	0.21	0.07	34.2	0.12	0.02	13.6	0.03	0.00	16.8	0.01	0.00	15.9
U	0.15	0.10	66.2	0.09	0.01	9.1	0.07	0.01	15.0	0.06	0.00	6.9
La/Sm cn	1.04	0.08	7.9	1.06	0.10	9.0	0.69	0.03	4.2	0.33	0.02	7.3
Gd/Yb cn	1.42	0.05	3.3	1.43	0.04	2.8	1.49	0.08	5.6	0.69	0.03	4.6
Eu/Eu*	0.95	0.05	5.6	1.00	0.03	3.0	1.07	0.04	4.0	1.23	0.09	7.2
Nb/Nb*	0.80	0.21	25.7	0.77	0.08	10.6	0.51	0.17	33.3	0.81	0.10	12.0
Pb/Pb*	3.50	0.66	18.8	4.94	0.70	14.2	5.52	0.55	9.9	5.59	1.29	23.2
Zr/Zr*	0.30	0.03	10.7	0.35	0.01	3.0	0.28	0.01	3.5	0.42	0.01	3.3

cn: chondrite -normalized
LGU: Lower Gabbro Unit
UU: Ultramafic Unit
MGU: Middle Gabbro Unit

Table 3.2 (continued)

	508989			508988			508915			508925		
Rock type	Gabbro			Peridotite			Hornblendite			Leucogabbro		
Unit	MGU			MGU			MGU			ULGU		
Group	Suite B			Suite B			Suite B			Suite B		
	Average (n=8)	Std	Rsd	Average (n=8)	Std	Rsd	Average (n=8)	Std	Rsd	Average (n=6)	Std	Rsd
V	230	17	7.6	155	4	2.3	162	9	5.6	184	46	25.2
Cr	2848	405	14.2	541	209	38.6	761	294	38.6	1399	1972	140.9
Co	57	2	3.6	39	3	7.2	61	2	3.7	73	17	22.7
Ni	300	13	4.2	429	27	6.3	280	9	3.3	387	105	27.1
Rb	0.75	0.06	8.0	0.50	0.07	13.1	6.95	0.82	11.9	3.43	1.15	33.4
Y	6.53	0.44	6.7	5.18	0.24	4.5	11.03	0.42	3.8	7.82	0.60	7.6
Zr	3.30	0.20	6.0	5.77	0.14	2.4	9.41	0.59	6.3	9.77	0.58	6.0
Nb	0.03	0.00	14.7	0.11	0.01	7.2	0.47	0.04	8.8	0.39	0.03	7.3
Ba	1.58	0.24	15.0	0.10	0.01	12.8	2.01	0.37	18.7	4.21	0.51	12.2
La	0.16	0.01	5.3	0.19	0.01	5.0	0.26	0.01	4.8	0.25	0.01	4.9
Ce	0.60	0.03	5.6	0.61	0.03	4.8	0.95	0.05	4.8	1.40	0.09	6.2
Pr	0.12	0.00	2.4	0.10	0.00	4.6	0.18	0.01	4.5	0.25	0.01	4.1
Nd	0.76	0.06	7.3	0.62	0.03	4.4	1.23	0.05	4.5	1.49	0.08	5.2
Sm	0.38	0.04	9.8	0.28	0.04	12.8	0.66	0.04	6.8	0.62	0.06	9.6
Eu	0.20	0.01	6.1	0.04	0.01	23.4	0.19	0.01	5.9	0.47	0.02	3.9
Gd	0.69	0.06	9.2	0.49	0.03	6.7	1.19	0.08	6.8	0.96	0.11	11.9
Tb	0.14	0.01	9.1	0.10	0.01	11.9	0.24	0.01	5.8	0.19	0.02	8.2
Dy	1.13	0.10	8.6	0.81	0.07	9.1	1.87	0.08	4.5	1.39	0.15	10.9
Ho	0.25	0.02	7.4	0.19	0.01	4.4	0.40	0.02	5.8	0.32	0.03	10.4
Er	0.77	0.05	6.4	0.63	0.04	5.7	1.22	0.06	5.2	0.92	0.13	13.8
Tm	0.12	0.01	8.4	0.09	0.01	6.7	0.18	0.01	7.9	0.13	0.02	14.9
Yb	0.83	0.04	5.4	0.78	0.03	3.5	1.33	0.10	7.3	0.99	0.08	8.2
Lu	0.12	0.01	5.6	0.12	0.01	9.3	0.19	0.01	5.3	0.13	0.01	8.2
Hf	0.14	0.01	9.7	0.21	0.03	12.2	0.33	0.03	8.4	0.31	0.05	15.6
Ta	0.00	0.00	26.3	0.01	0.00	8.4	0.01	0.00	16.0	0.02	0.00	4.8
Pb	0.11	0.02	16.2	0.33	0.02	6.6	0.27	0.05	17.4	0.19	0.07	36.3
Th	0.01	0.00	26.2	0.02	0.00	24.4	0.06	0.00	5.9	0.09	0.02	20.4
U	0.00	0.00	11.3	0.01	0.00	10.6	0.23	0.02	7.7	0.05	0.01	12.1
La/Sm cn	0.26	0.03	10.1	0.43	0.07	16.0	0.24	0.02	6.3	0.26	0.02	6.2
Gd/Yb cn	0.67	0.03	5.2	0.51	0.04	7.6	0.72	0.05	7.4	0.79	0.07	8.8
Eu/Eu*	1.18	0.12	9.9	0.36	0.10	26.6	0.65	0.06	8.6	1.88	0.17	9.1
Nb/Nb*	0.23	0.04	17.8	0.51	0.07	13.3	0.91	0.07	8.0	0.64	0.09	14.1
Pb/Pb*	4.33	0.68	15.8	13.34	1.06	8.0	6.52	1.07	16.4	3.29	1.21	36.7
Zr/Zr*	0.38	0.03	6.9	0.87	0.07	7.5	0.65	0.03	4.8	0.63	0.02	3.4

cn: chondrite -normalized
MGU: Middle Gabbro Unit
ULGU: Upper Leucogabbro Unit

Table 3.2 (continued)

	508926			508903			508930			508916		
Rock type	Leucogabbro			Leucogabbro			Leucogabbro			Anorthosite		
Unit	ULGU			LLGU			LLGU			MGU		
Group	Suite B			Anomalous			Anomalous			Anomalous		
	Average (n=8)	Std	Rsd	Average (n=8)	Std	Rsd	Average (n=6)	Std	Rsd	Average (n=8)	Std	Rsd
V	99	15	15.6	79	12	15.0	305	51	16.7	227	10	4.4
Cr	3	2	58.7	328	149	45.3	2216	917	41.4	1597	571	35.8
Co	70	13	19.3	61	6	9.2	43	5	11.2	65	2	3.0
Ni	420	108	25.7	385	74	19.1	200	23	11.4	258	11	4.2
Rb	3.92	1.15	29.2	2.57	0.46	18.0	5.44	2.40	44.2	8.55	1.44	16.8
Y	6.79	0.61	8.9	6.57	0.97	14.8	34.73	4.22	12.1	14.59	0.28	1.9
Zr	8.40	0.83	9.9	11.80	2.36	20.0	24.95	2.58	10.3	13.59	1.70	12.5
Nb	0.40	0.06	14.0	2.36	0.95	40.1	12.70	0.84	6.6	7.15	1.88	26.3
Ba	2.94	0.38	13.0	7.78	3.11	40.0	45.74	4.28	9.4	5.18	0.65	12.5
La	0.30	0.01	4.1	0.62	0.06	9.1	7.48	0.67	9.0	1.39	0.25	17.7
Ce	1.41	0.13	9.1	2.50	0.27	10.9	37.08	2.63	7.1	5.78	1.38	23.9
Pr	0.27	0.01	5.6	0.41	0.05	12.6	5.83	0.32	5.4	0.95	0.23	24.0
Nd	1.58	0.10	6.1	1.90	0.26	13.9	22.76	1.69	7.4	4.45	0.95	21.4
Sm	0.62	0.04	6.7	0.65	0.09	13.2	5.57	0.39	7.1	1.58	0.25	15.7
Eu	0.43	0.02	5.5	0.41	0.03	8.4	0.69	0.04	5.2	0.51	0.03	5.5
Gd	0.89	0.09	10.7	0.83	0.14	16.5	5.37	0.47	8.8	2.04	0.18	8.7
Tb	0.16	0.01	8.4	0.16	0.02	14.5	0.91	0.09	9.9	0.37	0.03	7.8
Dy	1.16	0.09	7.3	1.15	0.20	17.1	6.00	0.74	12.4	2.64	0.12	4.6
Ho	0.25	0.02	9.4	0.24	0.04	15.2	1.22	0.15	12.5	0.54	0.01	1.6
Er	0.78	0.09	11.6	0.70	0.10	13.7	3.50	0.40	11.3	1.57	0.06	3.9
Tm	0.12	0.01	9.7	0.11	0.02	15.9	0.51	0.06	11.3	0.23	0.01	4.9
Yb	0.90	0.08	9.4	0.75	0.12	16.2	3.64	0.41	11.3	1.66	0.06	3.5
Lu	0.13	0.01	7.8	0.10	0.01	9.4	0.49	0.06	11.2	0.23	0.01	4.8
Hf	0.28	0.06	19.6	0.37	0.08	21.5	1.58	0.15	9.8	0.56	0.10	17.6
Ta	0.03	0.00	10.2	0.20	0.10	53.3	1.35	0.10	7.5	0.86	0.43	50.4
Pb	0.28	0.06	21.8	0.57	0.14	24.7	0.70	0.15	21.8	0.51	0.12	24.1
Th	0.08	0.01	14.1	0.38	0.04	11.1	0.83	0.09	11.2	0.27	0.02	7.1
U	0.07	0.02	25.6	0.38	0.03	8.4	0.26	0.03	12.6	0.36	0.01	2.3
La/Sm cn	0.31	0.02	7.0	0.60	0.05	8.2	0.84	0.02	2.7	0.55	0.03	6.1
Gd/Yb cn	0.81	0.08	10.2	0.89	0.04	4.7	1.20	0.05	4.6	1.00	0.10	10.4
Eu/Eu*	1.78	0.08	4.4	1.77	0.42	23.6	0.39	0.02	5.6	0.88	0.15	17.0
Nb/Nb*	0.61	0.11	18.6	1.17	0.40	34.5	1.25	0.08	6.2	2.81	0.56	19.8
Pb/Pb*	4.63	0.90	19.5	5.91	1.86	31.5	0.49	0.14	28.9	2.34	0.67	28.6
Zr/Zr*	0.53	0.07	12.4	0.65	0.06	9.6	0.14	0.01	5.6	0.32	0.03	10.8

cn: chondrite -normalized
ULGU: Upper Leucogabbro Unit
LLGU: Lower Leucogabbro Unit
MGU: Middle Gabbro Unit

Table 3.2 (continued)

	508939			508922 Type 1			508922 Type 2		
Rock type	Peridotite			Leucogabbro			Leucogabbro		
Unit	MGU			LLGU			LLGU		
Group	Anomalous			Anomalous			Anomalous		
	Average (n=8)	Std	Rsd	Average (n=5)	Std	Rsd	Average (n=3)	Std	Rsd
V	39	2	5.7	41	21	52.2	24	7.29	29.9
Cr	66	8	12.6	301	257	85.2	32	6.69	21.0
Co	44	2	5.1	68	12	17.8	79	9.60	12.1
Ni	484	29	6.0	471	108	23.0	516	35.21	6.8
Rb	2.60	0.32	12.3	2.24	0.67	29.9	2.16	0.16	7.3
Y	1.57	0.10	6.2	2.22	0.84	37.9	2.68	1.11	41.3
Zr	1.69	0.06	3.3	4.94	2.58	52.2	3.96	1.67	42.3
Nb	0.16	0.01	8.0	0.33	0.03	9.2	0.29	0.05	18.8
Ba	7.37	1.48	20.1	5.90	0.97	16.5	5.50	0.74	13.5
La	0.33	0.02	5.1	0.31	0.02	5.8	0.29	0.01	2.4
Ce	0.91	0.05	5.6	0.97	0.06	6.7	0.95	0.03	3.3
Pr	0.12	0.00	3.8	0.16	0.02	12.6	0.16	0.02	12.1
Nd	0.53	0.01	2.2	0.89	0.18	20.7	0.86	0.16	18.6
Sm	0.15	0.01	10.0	0.30	0.10	34.4	0.27	0.09	32.7
Eu	0.12	0.01	5.2	0.40	0.03	6.3	0.38	0.02	6.2
Gd	0.18	0.02	11.6	0.41	0.18	44.7	0.37	0.12	33.3
Tb	0.03	0.00	14.8	0.07	0.03	45.6	0.06	0.03	41.4
Dy	0.24	0.02	10.3	0.43	0.20	46.9	0.47	0.19	40.8
Ho	0.05	0.00	7.6	0.09	0.04	45.1	0.10	0.04	44.6
Er	0.17	0.01	8.5	0.25	0.11	42.4	0.31	0.14	44.8
Tm	0.03	0.00	10.4	0.03	0.01	40.6	0.05	0.02	35.2
Yb	0.27	0.04	13.3	0.25	0.10	38.0	0.35	0.12	34.4
Lu	0.05	0.00	7.4	0.04	0.02	39.5	0.05	0.02	34.0
Hf	0.05	0.01	19.7	0.23	0.17	76.7	0.11	0.04	40.0
Ta	0.00	0.00	15.9	0.02	0.00	22.7	0.01	0.00	42.0
Pb	0.52	0.05	10.2	0.22	0.02	7.5	0.23	0.03	12.9
Th	0.04	0.00	6.8	0.03	0.00	16.7	0.03	0.01	18.6
U	0.05	0.01	10.5	0.03	0.00	12.1	0.03	0.01	22.2
La/Sm cn	1.42	0.20	13.8	0.70	0.26	36.4	0.74	0.24	32.5
Gd/Yb cn	0.56	0.09	15.6	1.31	0.23	17.3	0.86	0.09	10.0
Eu/Eu*	2.29	0.18	7.7	4.02	1.88	46.7	4.00	1.47	36.7
Nb/Nb*	0.37	0.03	8.6	0.88	0.10	11.4	0.73	0.18	24.3
Pb/Pb*	16.16	1.27	7.8	5.61	0.82	14.6	5.98	1.10	18.4
Zr/Zr*	0.37	0.02	4.2	0.56	0.18	32.3	0.50	0.09	17.7

cn: chondrite -normalized
MGU: Middle Gabbro Unit
LLGU: Lower Leucogabbro Unit

Table 3.3

Trace (ppm) element concentrations and significant element ratios for clinopyroxene.

	508974			508968			508969		
Rock type	Gabbro			Dunite			Peridotite		
Unit	LGU			UU			UU		
Group	Suite A			Suite A			Suite A		
	Average (n=4)	Std	Rsd	Average (n=8)	Std	Rsd	Average (n=8)	Std	Rsd
V	125	2.3	1.8	87	6	7.0	72	4	5.2
Cr	88	9.9	11.3	1839	135	7.3	1139	144	12.6
Co	43	0.5	1.2	37	1	3.3	41	1	3.1
Ni	69	1.5	2.2	740	32	4.3	728	17	2.4
Rb				0.90	0.23		2.42	0.41	17.1
Y	7.41	0.35	4.8	18.47	0.90	4.9	11.92	0.67	5.6
Zr	20.19	0.78	3.9	13.80	1.11	8.0	19.36	2.00	10.3
Nb	0.01	0.00	16.9	0.79	0.06	7.5	1.89	0.29	15.2
Ba	0.14	0.01	7.0	5.82	0.52	9.0	6.50	1.35	20.8
La	1.64	0.08	4.7	3.28	0.13	3.8	2.21	0.14	6.4
Ce	4.71	0.17	3.6	12.93	0.54	4.2	9.17	0.72	7.8
Pr	0.85	0.04	5.3	2.33	0.09	4.0	1.60	0.12	7.3
Nd	4.22	0.18	4.3	12.82	0.57	4.4	8.75	0.70	8.0
Sm	1.20	0.04	3.6	3.99	0.17	4.4	2.72	0.21	7.6
Eu	0.39	0.04	11.5	1.17	0.04	3.1	0.66	0.04	5.8
Gd	1.39	0.07	5.2	4.35	0.17	3.9	2.88	0.28	9.6
Tb	0.22	0.01	6.5	0.65	0.04	6.4	0.42	0.03	7.8
Dy	1.44	0.14	9.6	4.05	0.16	3.9	2.68	0.20	7.4
Ho	0.30	0.02	7.5	0.74	0.03	4.1	0.50	0.04	7.5
Er	0.84	0.06	7.2	1.89	0.11	5.8	1.33	0.09	6.7
Tm	0.12	0.01	5.5	0.24	0.02	6.7	0.17	0.02	9.3
Yb	0.97	0.05	5.0	1.51	0.06	4.3	1.14	0.06	5.1
Lu	0.16	0.01	7.1	0.19	0.02	10.2	0.14	0.01	9.4
Hf	0.78	0.05	6.9	0.76	0.06	7.5	0.80	0.10	12.7
Ta	0.004	0.002	51.5	0.04	0.00	7.3	0.11	0.03	24.0
Pb	0.79	0.15	18.8	0.53	0.05	10.0	0.60	0.06	10.2
Th	0.07	0.02	34.8	0.10	0.02	16.9	0.08	0.01	17.1
U	0.08	0.04	52.7	0.06	0.01	20.1	0.09	0.01	14.5
La/Sm cn	0.85	0.01	1.6	0.52	0.01	1.8	0.51	0.02	4.5
Gd/Yb cn	1.16	0.04	3.1	2.34	0.11	4.5	2.04	0.13	6.3
Eu/Eu*	0.92	0.12	13.0	0.86	0.03	3.6	0.73	0.03	4.3
Nb/Nb*	0.01	0.00	43.4	0.33	0.02	6.8	1.11	0.13	11.4
Pb/Pb*	4.03	0.72	17.8	0.99	0.08	7.9	1.59	0.19	11.7
Zr/Zr*	0.56	0.04	7.1	0.12	0.01	4.4	0.25	0.01	3.9

cn: chondrite -normalized

LGU: Lower Gabbro Unit

UU: Ultramafic Unit

Table 3.3 (continued)

	508978			508979		
Rock type	Peridotite			Pyroxenite		
Unit	UU			UU		
Group	Suite A			Suite A		
	Average (n=8)	Std	Rsd	Average (n=9)	Std	Rsd
V	94	5	5.0	87	15	16.7
Cr	1136	72	6.3	970	341	35.2
Co	43	2	5.6	53	6	11.9
Ni	667	42	6.2	976	286	29.3
Rb	1.24	0.10	7.8	0.69	0.16	
Y	13.86	0.55	3.9	11.44	1.14	10.0
Zr	19.58	1.47	7.5	12.06	1.95	16.2
Nb	1.40	0.06	4.6	1.15	0.19	16.5
Ba	4.37	0.40	9.3	0.32	0.06	18.9
La	3.88	0.15	3.9	4.40	0.40	9.1
Ce	13.62	0.58	4.3	10.55	1.10	10.4
Pr	2.13	0.06	2.6	1.46	0.10	6.7
Nd	10.95	0.30	2.7	6.97	0.44	6.3
Sm	3.15	0.20	6.4	2.09	0.20	9.5
Eu	1.03	0.03	3.4	0.73	0.04	5.9
Gd	3.39	0.15	4.6	2.36	0.19	8.0
Tb	0.48	0.02	3.3	0.38	0.03	7.3
Dy	2.94	0.09	3.1	2.33	0.21	9.0
Ho	0.53	0.01	2.1	0.43	0.03	8.0
Er	1.36	0.04	3.0	1.10	0.08	7.4
Tm	0.18	0.01	3.8	0.15	0.01	6.9
Yb	1.11	0.07	6.5	0.91	0.06	6.2
Lu	0.15	0.01	6.0	0.12	0.01	11.7
Hf	0.78	0.06	8.1	0.53	0.09	17.7
Ta	0.07	0.01	12.5	0.18	0.03	15.2
Pb	0.51	0.06	12.0	0.38	0.06	16.5
Th	0.11	0.01	9.3	0.10	0.01	9.0
U	0.10	0.01	6.7	0.03	0.00	13.7
La/Sm cn	0.78	0.04	5.3	1.32	0.05	3.6
Gd/Yb cn	2.47	0.17	6.9	2.10	0.13	6.2
Eu/Eu*	0.97	0.05	4.9	1.00	0.05	4.9
Nb/Nb*	0.51	0.03	6.0	0.42	0.05	11.6
Pb/Pb*	0.96	0.11	11.1	0.97	0.11	11.8
Zr/Zr*	0.21	0.01	5.9	0.20	0.02	11.1

cn: chondrite -normalized
UU: Ultramafic Unit

Table 3.4 Trace (ppm) element concentrations for plagioclase.

	508974			508973			508916		
Rock type	Gabbro			Hornblendite			Anorthosite		
Unit	LGU			LGU			MGU		
Group	Suite A			Suite A			Suite A		
	Average (n=8)	Std	Rsd	Average (n=8)	Std	Rsd	Average (n=8)	Std	Rsd
Rb									
Sr	1039	64.6	6.2	868	16.7	1.9	101.75	2.3	2.3
Y	0.03	0.02	65.9				0.02	0.01	26.5
Ba	140	19.3	13.8	193	10.8	5.6	7.37	0.2	3.0
La	1.24	0.0770	6.2	1.11	0.0733	6.6	0.77	0.0850	11.0
Ce	1.23	0.1121	9.1	0.96	0.0412	4.3	1.20	0.0867	7.2
Pr	0.07	0.0081	11.0	0.05	0.0035	6.4	0.08	0.0090	11.0
Nd	0.18	0.0315	17.0	0.13	0.0172	13.5	0.21	0.0250	12.0
Sm	0.02	0.0064	26.2		0.0051		0.02	0.0060	28.7
Eu	0.23	0.0170	7.3	0.23	0.0110	4.8	0.13	0.0090	6.9
Gd	0.02	0.0038	18.3	0.01	0.0008	5.3			
Tb									
Dy									
Ho									
Er									
Tm									
Yb									
Lu									
Pb	13.3	2.40	18.1	12.9	0.50	3.8	1.95	0.13	6.9
La/Sm cn	32.8	6.10	18.6	41.7	10.28	24.6			
Gd/Yb cn									
Eu/Eu*	33.8	6.27	18.6						

cn: chondrite -normalized
LGU: Lower Gabbro Unit
MGU: Middle Gabbro Unit

Table 3.4 (continued)

	508998			508903			508930		
Rock type	Anorthosite			Leucogabbro			Leucogabbro		
Unit	AU			LLGU			LLGU		
Group	Suite A			Suite B			Suite B		
	Average (n=8)	Std	Rsd	Average (n=9)	Std	Rsd	Average (n=9)	Std	Rsd
Rb	0.38	0.6	166.8	54.64	163.0	298.3	0.58	1.1	185.8
Sr	70	3.6	5.1	133.92	9.4	7.0	76.15	3.0	4.0
Y	0.09	0.02	21.7				0.06	0.01	14.7
Ba	12	1.5	12.7	11.67	3.3	28.1	61.04	4.1	6.7
La	1.467	0.1842	12.6	0.60	0.0660	11.0	3.63	0.2274	6.3
Ce	2.996	0.1003	3.3	0.73	0.0803	11.0	6.06	0.2454	4.1
Pr	0.282	0.0222	7.9	0.04	0.0081	18.9	0.43	0.0183	4.3
Nd	0.827	0.0834	10.1	0.10	0.0234	23.9	0.91	0.0262	2.9
Sm	0.113	0.0117	10.4				0.07	0.0078	11.0
Eu	0.137	0.0097	7.0	0.10	0.0147	15.1	0.16	0.0073	4.5
Gd	0.056	0.0116	20.7				0.04	0.0072	16.8
Tb	0.005	0.0013	24.6				0.00	0.0008	26.5
Dy	0.018	0.0050	27.4				0.01	0.0035	30.2
Ho	0.002	0.0010	39.0						
Er	0.005	0.0013	27.9						
Tm									
Yb									
Lu									
Pb	2.75	0.38	14.0	3.58	0.38	10.5	2.49	0.19	7.4
La/Sm cn	8.21	0.63	7.7						
Gd/Yb cn									
Eu/Eu*	5.38	0.69	12.9						

cn: chondrite -normalized
AU: Anorthosite Unit
LLGU: Lower Leucogabbro Unit

Table 3.4 (continued)

	508922			508931			508989		
Rock type	Leucogabbro			Gabbro			Gabbro		
Unit	LLGU			MGU			MGU		
Group	Suite B			Suite B			Suite B		
	Average (n=8)	Std	Rsd	Average (n=8)	Std	Rsd	Average (n=8)	Std	Rsd
Rb							0.13	0.2	138.2
Sr	98.19	1.7	1.8	107.06	41.9	39.2	86.73	0.7	0.9
Y				0.39	0.2	62.7			
Ba	4.89	1.1	21.7	6.45	3.1	48.7	5.46	0.3	4.6
La	0.25	0.0080	3.3	0.06	0.0168	29.3	0.07	0.0034	4.9
Ce	0.28	0.0295	10.6	0.09	0.0403	43.2	0.09	0.0125	13.9
Pr	0.02	0.0021	13.9	0.01	0.0071	53.5	0.01	0.0016	19.9
Nd	0.05	0.0160	35.1	0.07	0.0406	58.8	0.03	0.0063	23.9
Sm				0.03	0.0154	45.8			
Eu	0.07	0.0038	5.3	0.06	0.0524	83.2	0.09	0.0065	7.0
Gd				0.04	0.0274	62.6			
Tb				0.01	0.0053	61.5			
Dy				0.07	0.0454	66.9			
Ho				0.01	0.0090	62.2			
Er				0.04	0.0263	59.5			
Tm				0.01	0.0033	50.0			
Yb				0.06	0.0343	60.1			
Lu				0.01	0.0049	59.9			
Pb	1.30	0.16	12.0	0.58	0.44	75.7	0.80	0.07	8.4
La/Sm cn				1.24	0.35	28.1			
Gd/Yb cn				0.63	0.15	23.7			
Eu/Eu*				5.17	3.18	61.5			

cn: chondrite -normalized
LLGU: Lower Leucogabbro Unit
MGU: Middle Gabbro Unit

Table 3.4 (continued)

	508925			508926		
Rock type	Leucogabbro			Leucogabbro		
Unit	ULGU			ULGU		
Group	Suite B			Suite B		
	Average (n=9)	Std	Rsd	Average (n=6)	Std	Rsd
Rb	0.10	0.1	113.8	0.13	0.1	103.9
Sr	80.83	3.3	4.1	85.36	1.6	1.9
Y						
Ba	7.28	1.3	18.2	3.53	0.5583	15.8
La	0.24	0.0142	5.9	0.29	0.0071	2.4
Ce	0.38	0.0199	5.2	0.40	0.0233	5.8
Pr	0.03	0.0022	8.3	0.03	0.0043	15.8
Nd	0.07	0.0097	13.4	0.08	0.0115	13.7
Sm		0.0020				
Eu	0.08	0.0098	11.7	0.08	0.0092	11.0
Gd		0.0030				
Tb						
Dy						
Ho						
Er						
Tm						
Yb						
Lu						
Pb	0.98	0.15	15.3	1.43	0.15	10.3
La/Sm cn						
Gd/Yb cn						
Eu/Eu*						

cn: chondrite -normalized

ULGU: Upper Leucogabbro Unit

CHAPTER 4

Origin of the Archean tonalite–trondhjemite–granodiorite (TTG) suites and granites in the Fiskenæsset region, southern West Greenland: implication for the continental growth

4.1. Introduction

Tonalite–trondhjemite–granodiorite (TTG) suites, constituting up to 90% of the juvenile continental crust, are the dominant intrusive rocks in Archean terranes (Martin et al., 2005). Studies of these rocks can provide significant information on the origin and chemical evolution of the continental crust (Drummond and Defant, 1990; Rudnick, 1995; Condie, 2005; Martin et al., 2005). Given that TTGs are important in determining the processes by which continental crust forms and understanding the mode of the evolution of the Earth during the Archean, they have been extensively studied over the last four decades (Barker and Arth 1976; Jahn et al. 1981; Drummond and Defant, 1990; Rudnick, 1995; Condie, 2005; Martin et al., 2005). Mineralogically, these rocks are composed typically of quartz, plagioclase, and biotite, and locally also contain hornblende. The major element geochemistry of Archean TTGs is characterized by high SiO_2 (averaging >68 wt.%), Al_2O_3 (>15.0 wt.%), high Na_2O (>3.0 wt.%), and $Na_2O/K_2O>2$ (Martin, 1994; Martin et al., 2005). Archean TTGs are also characterized by steep rare-earth element (REE) patterns and low heavy rare-earth element (HREE) contents (Jahn et al. 1981; Martin 1994; Martin et al. 2005; and references therein). The trace element concentrations of typical TTGs exhibit enrichments in incompatible elements and negative Nb–Ta anomalies (Martin, 1994, 1999; Martin et al., 2005).

Archean TTGs are generally considered to be the products of melting of hydrous metabasalts on the basis of their geochemical characteristics and compositional similarities with experimental high-pressure partial melts of hydrous basaltic material (Winther and Newton, 1991; Martin, 1994; Sen and Dunn, 1994; Rapp and Watson,

1995; Martin, 1999; Rapp et al., 1999; Foley et al., 2002; Rapp et al., 2003; Martin et al., 2005; Foley, 2008; Moyen, 2009). However, it is difficult to distinguish melting between garnet-bearing amphibolite and eclogite in terms of major and trace element chemistry (Martin, 1994; Sen and Dunn, 1994; Rapp and Watson, 1995; Martin, 1999; Rapp et al., 1999; Foley et al., 2002; Klemme et al., 2002; Rapp et al., 2003; Xiong, 2006; Foley, 2008; Hoffmann et al., 2011). In addition, the geodynamic setting of TTG petrogenesis still remains controversial. Three main hypotheses persist: (1) TTGs were formed by partial melts of subducting oceanic crust; (2) TTGs were generated by partial melting of amphibolite/eclogite at the base of thickened arc crust; and (3) TTGs resulted from partial melting of wet mafic roots of an oceanic plateau (see Jahn et al., 1981; Albarède, 1998; Martin, 1994; Rapp and Watson, 1995; Martin, 1999; Smithies, 2000; Foley et al., 2002; Whalen et al., 2002; Rapp et al., 2003; Martin et al., 2005; Bédard, 2006; Moyen and Stevens, 2006; Rollinson, 2010).

A substantial portion of the North Atlantic craton of southern West Greenland is made up of amphibolite to granulite facies Archean (ca. 3.07 – 2.82 Ga) granitoid gneisses that contain many conformable layers of mainly basic volcanic (now amphibolite) and gabbroic rocks and associated leucogabbro-anorthosite complexes, both of which are up to ca. 2 km thick, and rare metasedimentary rocks (Bridgwater et al., 1976; Steenfelt et al., 2005; Friend and Nutman, 2005). This study focuses on the Fiskenæsset region, which consists of granitoid orthogneiss, with minor amphibolites and layered anorthosite complexes comprising anorthosites, peridotites, pyroxenites, hornblendites, gabbros, and leucogabbros.

The layered anorthosite-peridotite-pyroxenite-hornblendite-gabbro-leucogabbro association is known as the Fiskenæsset Complex (Fig. 4.1; Myers, 1985). The granitoid gneisses were derived from tonalite, trondhjemite, granodiorite and granite by deformation and metamorphism. The protoliths of the gneisses were intruded syntectonically as sheets into sequences of mainly metavolcanic amphibolite and the

Fiskenæsset Complex. The Fiskenæsset Complex has been intensively investigated (Windley et al., 1973 ; Windley and Smith, 1974; Myers and Platt, 1977; Myers, 1985; Polat et al., 2009; 2010; 2011a), however, the widespread granitoid gneisses bordering the Fiskenæsset Complex have been understudied in recent years. Despite their widespread exposures and well-preserved igneous structures, the geochemical characteristics of the granitoid gneisses have not been studied in detail using modern analytical methods. Therefore, little is known about their geodynamic setting, petrogenesis, and their role in the growth of continental crust in the Fiskenæsset region. In this paper, we present new major and high-precision ICP-MS trace element data for the TTG gneisses and granites in the Fiskenæsset region (Fig. 4.1). The main objectives are: (1) to gain new insights into the petrogenesis of TTGs; (2) to assess the possible petrogenetic link between TTGs and granites; (3) to understand the tectonic setting of the TTGs and granites; and (4) to provide new constraints on the formation of Archean continental crust in the Fiskenæsset region.

4.2. Regional geology

4.2.1. Field characteristics

The Fiskenæsset region is composed of ~85% TTG orthogneisses, ~10% amphibolites, and ~5% of rocks of the anorthosite-leucogabbro-gabbro-ultramafic association as in the Fiskenæsset Complex (Kalsbeek and Myers, 1973; Windley and Smith, 1974; Myers, 1985). All these rocks were variably affected by granulite facies metamorphism and retrogressed under upper-amphibolite facies conditions (Myers, 1985; McGregor and Friend, 1992; Windley and Garde, 2009). The Fiskenæsset region is dominated by tonalite and granodiorite gneisses (Windley and Garde, 2009). The geological history of the Fiskenæsset region is complicated given that it has undergone complex folding and faulting. Three major fold phases, with axial surfaces approximately perpendicular to each other resulted in spectacular km scale fold interference patterns and

each episode of deformation gave rise to a complex sequence of fold and fabric development (Kalsbeek and Myers, 1973; Windley and Smith, 1974; Myers, 1985; Windley and Garde, 2009).

Field observations suggest that the oldest rocks in the area are metavolcanic amphibolites, which locally contain remnants of pillow structures (Escher and Myers, 1975; Myers, 1985). The Fiskenæsset Complex is in stratigraphic contact with an overlying 1 km-thick pillow-bearing amphibolite and the Fiskenæsset Complex appears to intrude the metavolcanic amphibolites (Escher and Myers, 1975). The anorthosite contains roof pendants of pillow-bearing amphibolite at several meters beneath the contact, which suggests that the Fiskenæsset Complex intruded into the protoliths of the amphibolites (basalts), and that the anorthosites and the basaltic lavas were essentially coeval (Escher and Myers, 1975). In the Fiskenæsset region, intrusive relationships between the Fiskenæsset Complex and granitoid gneisses are best exposed in the Majorqap qâva and Sinarssuk areas (Fig. 4.1). Myers (1985) pointed out that the Fiskenæsset Complex is a sheet-like body and the protoliths of syntectonic granitoid gneisses were emplaced as sub-concordant sheets into the stratigraphic units of the Fiskenæsset Complex and associated basaltic rocks, generally adjacent to thrust faults.

A notable feature of the Fiskenæsset region is that a suite of leucocratic gneisses composed of granitic rocks occurs together with those of gray gneisses with TTG affinity, and the leucocratic gneisses appear to be younger than the TTGs. In the field, granitoid gneisses can be readily subdivided into gray and leucocratic suites according to color and intrusive relationship. Deformation of gray gneisses is heterogeneous (Fig. 4.2a and b). At a number of locations, it can be seen that the leucocratic gneisses are younger than the gray gneisses. The leucocratic gneisses always show relationships of (1) intruding the gray gneisses (Fig. 4.2c and d), (2) intruding amphibolites (Fig. 4.2e and f), and (3) sharp contact with gray gneisses (Fig. 4.2g). In some places, both gray and leucocratic gneisses are also interlayered with amphibolites (Fig. 4.2h) and they can be readily distinguished

from amphibolites by gneissic foliation in the gneisses that parallels the elongation of the amphibolite enclaves.

4.2.2. Geochronology

Molybdenites occurring in the Fiskenæsset anorthosites yielded a Re–Os age of 3080±70 Ma (Herr et al., 1967). Gancarz (1976) reported a Pb–Pb isochron age of 2750 Ma from plagioclase and hornblende which were separated from Fiskenæsset anorthosites and leucogabbros. Ashwal et al. (1989) argued that a five point mixed whole-rock and mineral Sm-Nd isochron age of 2.86 ±0.05 Ga represents the time of primary crystallization of the Fiskenæsset Complex. Anorthosites, leucogabbros, gabbros and ultramafic rocks of the Fiskenæsset Complex have 2973±28 Ma (MSWD=33) and 2945±36 Ma (MSWD=44) Sm-Nd and Pb-Pb isotope regression ages, respectively (Polat et al., 2010). The hornblenditic pegmatite pipe cutting across the part of the Fiskenæsset Complex at Majorqap qâva has a $^{207}Pb/^{206}Pb$ zircon age of 2.87 Ga (Keulen et al., 2009). The oldest zircon grains from that hornblenditic pegmatite pipe are c. 2.95 Ga, which is in agreement with the intrusion age of the anorthosite complex inferred from Sm-Nd and Pb-Pb systematics.

Orthogneisses intruding the Fiskenæsset Complex have a Rb/Sr whole-rock age of 2.88 Ga (Moorbath and Pankhurst, 1976). Two orthogneiss samples for this study in the Sinarssuk area were dated as 2.95 Ga by zircon U-Pb method and these rocks also contain inherited zircons with older ages from 3.2 to 3.0 Ga and zircons of overgrowth and recrystallization with younger ages between 2.94 and 2.65 Ga (Polat et al., 2010).

Peak granulite facies conditions have been dated at 2.81–2.79 Ga and were associated with the intrusion of the Ilivertalik granite (Riciputi et al., 1990; McGregor and Friend, 1992). A muscovite granite has a zircon U-Pb age of 2660±20 Ma, which was interpreted as the end of the low grade amphibolite facies metamorphism because the rock exhibited the low amphibolite facies mineralogy typical of many rocks in the

southern part of the Fiskenæsset area (Pidgeon and Kalsbeek, 1978).

4.3. Petrography

Tonalitic and trondhjemitic gneisses are of variable grain sizes between fine- and medium-grained. They are made of 50-60% plagioclase, 25-30% quartz, 10-15% biotite, and minor interstitial K-feldspar. Magnetite, ilmenite, titanite, and zircon are accessory phases. Grain boundaries are highly irregular. Plagioclase is subhedral to euhedral (Fig. 4.3a). Plagioclase crystals contain patches of very fine mica and clay minerals. Several samples are variably altered, with epidote partially replacing plagioclase (Fig. 4.3b). Occasionally two morphologically different phases of quartz have been observed, suggesting grain-size reduction had started to take place (Fig. 4.3c). Biotite is normally the only mafic mineral, but hornblende is also rarely present (Fig. 4.3d).

Granodioritic gneisses generally have a heterogranular, granoblastic texture. The granodiorite gneisses are fine- to medium-grained, containing 30-40% plagioclase, 20-30% quartz, 10-15% biotite and 5-10% K-feldspar with accessory magnetite, ilmenite, titanite, apatite, and zircon. In plane-polarized light the areas that are clear are mostly quartz and K-feldspar. Quartz ranges from interstitial to coarse polygonized patches (Fig. 4.3e). Biotites occur mainly as interstitial grains around larger crystals of plagioclase, K-feldspar and quartz (Fig. 4.3e). Mica and clay minerals occur as tiny crystals in the plagioclases (Fig. 4.3f). In some samples, the appearance of many triple junctions in the felsic phases provides evidence of a closer approach to an equilibrium texture (Fig. 4.4a).

Granitic gneisses are generally medium-grained and biotite-bearing. Major phases are quartz (35-40%), plagioclase (25-30%), K-feldspar (25-30%), and biotite (5-10%) (Fig. 4.4b). Titanite, apatite, zircon, magnetite, and ilmenite are common accessory minerals. Garnet rarely occurs as an accessory phase (Fig. 4.4c). Quartz occurs as aggregates of large grains, or as small droplets either in plagioclase or along some grain boundaries (Fig. 4.4d). Plagioclase grains are subhedral to euhedral and commonly

twinned. Large amounts of tiny mica and clay minerals occur inside the plagioclase. Myrmekitic development occasionally occurs around the edges of plagioclase (Fig. 4.4e), while interstitial biotite has been partially altered to chlorite (Fig. 4.4f).

4.4. Sampling and analytical methods

Samples for this study were collected from the least-altered outcrops in the Fiskenæsset region. Weights of the samples varied between 5 and 6 kg. Seventy-six rock samples were collected from six areas including Camp 1, Camp 2, Camp 3, Base camp, Majorqap qâva and Sinarssuk in the Fiskenæsset region (Fig. 4.1) in order to cover a wide range of rock types and to give a meaningful distribution of samples throughout the study area.

Samples analyzed for this study have grain sizes between 1 mm and 1 cm. Accordingly, to be representative of the whole rocks, pulverized samples ranged from 300 to 500 g. Samples were powdered using an agate mill at Activation Laboratories Ltd. (ACTLABS), Canada. Major elements and some trace elements (Sc, Zr, and V) were analyzed on a Thermo Jarrel-Ash ENVIRO II ICP-OES at ACTLABS, Canada. Samples were fused at 1000°C in an induction furnace with a flux of lithium metaborate and lithium tetraborate. The molten beads were dissolved in a solution of 5% HNO_3 containing an internal standard, and mixed continuously until complete dissolution. Loss on ignition (LOI) was determined by measuring weight loss upon heating to 1100℃ over a three hour period. Totals of major element oxides are 100±1 wt.% with an analytical precision of 1–2% for most major elements. The analytical precision for Sc, Zr and V is better than 10%.

Trace elements including transition metals (Ni, Co, and Cr), REE, HFSE, and LILE were analyzed by a high-sensitivity Thermo Elemental X7 Series II ICP-MS in the Great Lakes Institute for Environmental Research (GLIER), University of Windsor, Canada, following the protocols of Jenner et al. (1990). Sample dissolution was conducted under

clean lab conditions with doubly distilled acids. Approximately 100 – 130 mg of sample powder was used for acid digestion. Samples were dissolved in Teflon bombs in a concentrated mixture of HF-HNO_3 at a temperature of 120°C for 4 days and then further attacked with 50% HNO_3 until no solid residue was left. International standards BHVO-2 and BCR-2 were used as reference materials to estimate analytical precision. The results of standard analyses and recommended values are given in Table 4.1. Analytical precision was estimated to be as follows: 3 – 10% for REE, Y, Nb, Rb, Sr, Cs, Ba, and Co; 10 – 30% for Ni, Ta, and Th; and 30 – 80% for U, Pb, and Cr (Table 4.1).

Mg-numbers (Mg#) were calculated as the molar ratio of $Mg^{2+}/(Mg^{2+}+Fe^{2+})$, alumina saturation indexes (A/CNK) were calculated as the molar ratio of $Al_2O_3/(CaO+Na_2O+K_2O)$. Samples are normalized to chondrite and normal mid-ocean ridge basalt (N-MORB) and the normalization values are from Taylor and McLennan (1985) and Hofmann (1988), respectively. Europium (Eu/Eu*), Ce (Ce/Ce*), Nb (Nb/Nb*), Ti (Ti/Ti*), Zr (Zr/Zr*), Pb (Pb/Pb*) and Sr (Sr/Sr*) anomalies were calculated with respect to the neighboring immobile elements, following the method of Taylor and McLennan (1985).

4.5. Geochemical results

In terms of normative An–Ab–Or (wt.%) composition, following the classification of Barker (1979), 38 samples of gray gneiss in the Fiskenæsset region plot in the field of tonalite – trondhjemite, 14 samples of gray gneiss plot in the field of granodiorite, and 24 samples of the leucocratic gneisses plot in the field of granite (Fig. 4.5). This classification is largely consistent with the field and petrographic observations.

4.5.1. Tonalites – trondhjemites

The tonalite – trondhjemites have SiO_2 contents ranging from 63.7 to 77.3 wt.% and high Al_2O_3 contents (Al_2O_3=15 – 18.2 wt.%) with samples 509016 and 509703 as

outliers (Fig. 4.6). They have relatively low MgO (0.55–1.47 wt.%, Mg#=28–51), Ni, and Cr contents (Ni=7 – 51 ppm, Cr=7 – 41 ppm). They are sodium rich (Na_2O=3.4 – 5.13 wt.%) and have low K_2O contents resulting in Na_2O/K_2O greater than 1.9. Four of the samples are metaluminous (A/CNK=0.97–0.99) and the others are peraluminous (A/CNK =1.00–1.15).

These rocks have strongly fractionated REE patterns (La/Yb_{cn}=14 – 664) and display positive to negative Eu anomalies (Eu/Eu*=0.54 – 6.14) and negative to positive Ce anomalies (Ce/Ce*=0.62 – 1.39) (Fig. 4.7). They are also characterized by high Sr/Y (26 – 519).

On N-MORB-normalized trace element diagrams, they have the following characteristics: (1) enrichment of Th and U relative to LREE; (2) positive Pb anomalies (Pb/Pb*=1.4 – 25.3); (3) positive Sr anomalies (Sr/Sr*=1.0 – 6.4) with three outliers; and (4) negative anomalies of Nb (Ta) (Nb/Nb* = 0.01–0.18) and Ti (Ti/Ti*= 0.21–0.89) (Fig. 4.7; Table 4.2).

4.5.2. Granodiorites

Granodiorites have moderate ranges of SiO_2 (65.2 – 74.7 wt.%), Al_2O_3 (14.2 – 18.6 wt.%), MgO (0.25 – 0.93 wt.%), CaO (2.17 – 4.43 wt.%), Na_2O (3.46 – 4.29 wt.%), K_2O (2.17 – 3.74 wt.%) and Na_2O/K_2O (0.9 – 2) (Fig. 4.6). They have low Mg–numbers (31–48). They have exclusively peraluminous (A/CNK=1.00–1.05) compositions. The REE patterns are strongly fractionated (La/Yb_{cn} =17 – 135), with low heavy REE contents (Yb=0.05 – 0.8 ppm). Europium anomalies are negative to positive (Eu/Eu*= 0.6 – 3.6) and Ce anomalies are minor to absent (Ce/Ce*= 0.91 – 1.04) although two samples have positive Ce anomalies (Fig. 4.8). They have high Sr/Y (29 – 597) ratios. N-MORB-normalized trace-element patterns are characterized by enrichment of Th and U, negative Nb (Ta) and Ti anomalies (Nb/Nb*= 0.04–0.34, Ti/Ti*=0.3 – 0.8), positive Pb anomalies (Pb/Pb*=7.1 – 34.9), and negative to positive Sr anomalies (Sr/Sr*=0.6 –

15.9) (Fig. 4.8; Table 4.3).

4.5.3. Granites

Granites are characterized by SiO_2 around 73 wt.%, have high K_2O contents around 4.6 wt.% and low Na_2O/K_2O (Na_2O/K_2O=0.5 – 1.1) (Fig. 4.6).They have low MgO (0.01 – 0.78 wt.%) and they have relatively low Al_2O_3 contents, ranging from 13 to 15.1 wt.%. They are mainly peraluminous (A/CNK=1.01–1.05). They are Ni- and Cr-poor (Ni=4–21 ppm, Cr=6–21 ppm). They exhibit significant variations in REE patterns, both in terms of fractionation and the magnitude of the europium anomaly (Fig. 4.9). Three samples have negative Ce anomalies (Ce/Ce*=0.72 – 0.75) and one samples has a minor positive Ce anomaly (Ce/Ce*= 1.14). The majority of samples have high Sr/Y (35 – 709) ratios but five samples have low Sr/Y (6 – 20) ratios. The N-MORB-normalized trace element patterns of granites are characterized by elevated Th and U, negative Nb (Ta) anomalies (Nb/Nb*=0.01 – 0.09), positive Pb anomalies (Pb/Pb*=2.1 – 122.2), negative to positive Sr anomalies (Sr/Sr*=0.3 – 14.7), and negative Ti anomalies (Ti/Ti* = 0.1 – 0.6) (Fig. 4.9; Table 4.4).

4.6. Discussion

4.6.1. Alteration and element mobility

The granitoid gneisses in the Fiskenæsset region are extensively recrystallised and deformed as a result of several phases of deformation and upper amphibolite to granulite facies regional metamorphism (Windley et al., 1973 ; Windley and Smith, 1974; Myers and Platt, 1977; Myers, 1985; Polat et al., 2009). Accordingly, it is necessary to take account of the effects of post-magmatic alteration on the geochemistry of granitoid gneisses in the Fiskenæsset region, given that post-magmatic alteration can modify the primary magmatic composition to a large extent (Alderton et al., 1980; Ward et al., 1992; Condie and Sinha, 1996).

Although samples analysed for this study are relatively unaltered, post-magmatic alteration may have affected the geochemistry of the granitoid gneisses. To assess the effect of alteration on the original chemistry of the TTGs and granites, we adopt the alteration criteria of Polat and Hofmann (2003). All the samples have loss on ignition (LOI) values < 1.33 wt.%, which suggests that the rocks have not been strongly hydrated or carbonated. However, dehydration of the granitoid gneisses during granulite facies metamorphism cannot be ruled out. Samples having large Ce anomalies ($Ce/Ce^* < 0.9$ and $Ce/Ce^* > 1.1$) are considered as variably altered.

REE and HFSE are relatively immobile during alteration and metamorphism, which is indicated by the coherent N-MORB-normalized and chondrite-normalized patterns for the TTGs and granites (Figs. 4.7, 4.8 and 4.9). LILE (Rb, Ba, Th, Pb and Sr) can be mobilized during metamorphism and hydrothermal alteration (Alderton et al., 1980; Ward et al., 1992; Condie and Sinha, 1996; Polat and Hofmann, 2003). However, on the N-MORB-normalized trace element diagrams, they display a limited variation, suggesting these elements were relatively immobile on the whole-rock scale (Figs. 4.7, 4.8 and 4.9).

4.6.2. Petrogenetic origin of TTGs

The tonalities and trondhjemites have all the key geochemical characteristics of Archean TTGs including: ≥15 wt.% $A1_2O_3$ at 70 wt.% SiO_2, CaO (< 4.46 wt.%), Na_2O(> 3.4 wt.%), K_2O (<2.08 wt.%), Na_2O/K_2O (>1.9) and Y (< 14.4 ppm) (Martin, 1994; Martin et al., 2005; Moyen, 2009). The TTG affinity of the tonalities and trondhjemites in the Fiskenæsset region indicates that they might have been derived by partial melting of hydrous basaltic rocks. In the field, there is no geological evidence that the TTGs were derived from older sialic material and certainly no evidence that they were derived by melting of the older gneisses (see Myers, 1985, and references therein). Additionally, Sr isotopic studies show that the tonalites from the Fiskenæsset area were originally

juvenile magmas whose source materials had been extracted from the mantle only shortly before melting occurred (Moorbath and Pankhurst, 1976). These two lines of evidence rule out the possibility of tonalities and trondhjemites being mainly derived from the melting of the preexisting TTG gneisses and further confirm a basaltic precursor for the tonalities and trondhjemites.

The presence of negative Eu anomalies in some samples could reflect residual plagioclase in the source or minor plagioclase fractionation (Fig.4.7), whereas the majority of samples with positive or no Eu anomalies accompanied by positive Sr anomalies (Fig. 4.7) could reflect melting at pressures above the plagioclase stability field or plagioclase accumulation. Similarly, the high Sr abundances (253 – 777 ppm) and low Y (1.15 – 14.4 ppm) and correspondingly high Sr/Y (26 – 519) (Fig. 4.10a) indicate plagioclase was not in the residue. Moreover, they display steep, enriched LREE relative to HREE patterns with high La/Yb_{cn} (14 – 664) and low Yb_{cn} (0.31 – 3.15) (Fig. 4.10b), which are consistent with garnet in the residue (e.g. Martin et al. 2005). The tonalities and trondhjemites all exhibit strong depletion in Nb, Ta and Ti on the N-MORB normalized diagrams, which is attributed to rutile in the residue (Martin et al., 2005).

The tonalities and trondhjemites have typical Archean TTG signatures, e.g., strongly fractionated REE patterns, positive Sr–Pb anomalies, and negative Nb–Ta–Ti anomalies. Such TTG characteristics are commonly explained by melting of subducted oceanic crust (see Tappe et al., 2011and references therein), but could also originate by melting the base of thickened crust or by melting of the root of the oceanic plateau (Smithies, 2000; Whalen et al., 2002; Rapp et al., 2003; Condie, 2005; Martin et al., 2005; Bédard, 2006). In comparison with silica-rich rocks in arc settings, the tonalities and trondhjemites have MgO contents lower than those of low-SiO_2 adakites but similar to those of high-SiO_2 adakites (Smithies, 2000; Condie, 2005; Martin et al., 2005) (Fig. 4.11a). Similarly, low Mg-numbers of the Fiskenæsset tonalities and trondhjemites, which are in the range of experimental melts produced by dehydration-melting of amphibolites (Rapp et al., 1999),

are consistent with them being melts produced by melting of a basaltic crustal source in one stage (Fig. 4.11b). In addition, they have low Ni and Cr contents (Ni=7 – 51 ppm, Cr=7 – 41 ppm). These features have therefore been taken to reflect an absence of interaction of TTG magmas with peridotite in the mantle wedge (see Rapp et al., 1999; Smithies, 2000; Condie, 2005; Martin et al., 2005). These facts seem to argue against slab melting and it appears reasonable to suggest that the initial tonalitic-trondhjemitic magmas in the Fiskenæsset formed by partial melting of hydrous basaltic material at the base of thickened lower crust. In fact, the chemical composition of the Fiskenæsset TTGs is similar to that of Phanerozoic Na-rich granitoids generated by melting hydrous basaltic material at the base of lower crust in many overthickened continental arcs, such as in the Mesozoic batholiths of the western North American Cordillera (Atherton and Petford, 1993; Petford and Atherton, 1996; Kay et al., 1999; Kay et al., 2005), Antarctica (Wareham et al., 1997) and New Zealand (Muir et al., 1995). Given that the lack of evidence for plume activity in the Fiskenæsset region, the possibility of melting of root of the oceanic plateau for the production of the tonalities and trondhjemites can be ruled out (Bridgwater et al., 1974; Myers, 1976; Myers, 1985; Polat et al., 2009; 2010; 2011a, Windley and Garde, 2009).

The granodiorites share some geochemical characteristics of the tonalities and trondhjemites (Fig. 4.7 and 4.8). Both suites have high Na_2O, commonly $Na_2O/K_2O>1$ and low Ni, Cr, Y and Yb contents, with strongly fractionated REE patterns. Thus, we suggest a similar petrogenetic origin for their formation.

4.6.3. Geochemical modeling constraints on the source mineralogy of TTGs

Previous partial melting experiments on low-K tholeiitic basalts have shown that tonalitic to trondhjemitic melts can be produced, coexisting with garnet-amphibolite or eclogite restites (Rapp et al., 1991; Winther and Newton, 1991; Sen and Dunn, 1994; Rapp and Watson, 1995; Clemens et al., 2006). Recently, Polat et al. (2009) and Polat et

al. (2011b) reported new major and trace element data for amphibolites associated with the Fiskenæsset Complex from the Qeqertarssuatsiaq, Majorqap qâva, Sinarssuk, Bjørnesund, Qagsse, and Nunatak areas in the Fiskenæsset region and they found that the protoliths of amiphibolites have a tholeiitic affinity with low-K content, which suggests that the amphibolites or their high-grade metamorphic counterparts (e.g., eclogites) might have been the source of tonalities and trondhjemites. In the field, most of the amphibolites occur as concordant layers or as inclusions within the TTG gneisses. Field relationships and geochronology (Figs. 4.1, 4.2e and f) indicate that the amphibolites are the oldest rocks in the Fiskenæsset region and suggest a further possible genetic link between them.

The hypothesis that the Fiskenæsset TTGs were formed by partial melting of a hydrous basaltic source was evaluated using trace element modeling. Modeling of batch melting was done using an amphibolite, 497122, with the lowest-K content from the Bjørnesund area as the source rock, and the typical TTGs as the partial melt. Two models have been chosen: (1) partial melting of hydrous basalts (amphibolites), producing TTG melts in equilibrium with a garnet-amphibolite residue containing with 20% garnet and 80% amphibole; and (2) partial melting of hydrous basalts (amphibolites), generating TTG melts in equilibrium with a rutile-bearing eclogite residue consisting of 49% clinopyroxene, 50% garnet and 1% rutile (cf., Drummond and Defant,1990; Rapp and Watson, 1995). The results for amphibolite restite (Fig. 4.12) show that the Fiskenæsset TTGs could not be modeled successfully with pure amphibolite residue (Fig. 4.12), since it yields a pattern with HREEs and Nb (Ta) that are too high. For 20% batch partial melting of amphibolite leaving a rutile-bearing eclogite residue, the calculated melts show strongly fractionated REE patterns (La/Yb_{cn}=35 for 20% partial melting), depletions in Nb (Ta) and heavy REE, and high Sr concentrations remarkably similar to Fiskenæsset TTGs (Fig. 4.12). The second model does provide support for the lower crust melting model, since it shows that it is plausible to generate the Fiskenæsset TTGs

by 20% melting of the most common tholeiitic basalt in the Fiskenæsset region, and that a rutile-bearing eclogitic residue is required (see Fig. 4.12).

Experimental melting of metabasalts under fluid-absent conditions (Rapp et al. 1991, Rapp and Watson 1995) indicates that the stability of garnet has its minimum at pressures >0.8 GPa (about 30 km) and garnet thoroughly replaces plagioclase at pressures $\geqslant$1.2 GPa (about 40 km). Rutile occurs at pressures higher than approximate 1.5 GPa (about 50 km) during partial melting of hydrated basalt (Xiong et al., 2005; Xiong, 2006). Therefore, the depth for melting of over-thickened lower crust to yield those tonalitic-trondhjemitic magmas must be more than about 50 km based on the minimum pressure for rutile-bearing eclogite residue. The rutile-bearing eclogite is stable at temperature 1000°C based on its mineral composition (Drummond and Defant, 1990). Moyen and Stevens (2006) proposed that the likely P–T range for the production of TTG melts are 15 kbar and 900–1,100°C following a reassessment of the experimental data for basalt melting. The estimated P–T condition for the partial melting of the rutile-bearing eclogite in the Fiskenæsset region is consistent with the P–T regime for the generation of TTG melts as suggested by Moyen and Stevens (2006).

4.6.4. Petrogenesis of granites

The compositional differences between granites and TTGs are remarkable. Granites have higher K_2O and lower Na_2O, Al_2O_3 and Sr contents than the TTGs. In contrast to the TTGs, the majority of granites have LREE-enriched and HREE-depleted patterns with negative Eu anomalies. Several experimental studies have shown that partial melting of metatonalites under fluid absent conditions within the middle or lower crust could produce granitic melts (Rutter and Wyllie, 1988; Skjerlie et al., 1993; Patiño and Alberto, 2005; Watkins et al., 2007). Additionally, Watkins et al (2007) emphasized that typical amphibolite-facies sodic TTGs with low K_2O/Na_2O=~0.3 in many Archean terranes could not generate melts with sufficient K_2O to account for the voluminous, late, potassic

granites in Archean terranes, and they argued that the source of the melts that formed the potassic granites must have had higher K_2O/Na_2O. The Fiskenæsset tonalities and trondhjemites have an average K_2O/Na_2O =0.31, whereas the granodiorites have an average K_2O/Na_2O=0.74. It is more likely that the granodiorites were the source for the granites than the tonalities and trondhjemites. As expected, the majority of granites have large negative europium anomalies. The depleted HREE and Y of the granites require garnet as a residual phase, suggesting formation in the middle-lower crust. The granites have high Sr/Y and La/Yb_{cn}, which were most likely inherited from the granodiorites in the source region (Fig. 4.10).

4.6.5. Magmatic and tectonic evolution processes

The geochemistry of the Fiskenæsset TTGs and the trace element modeling suggest that the most reasonable mechanism for the origin of these rocks is the partial melting of hydrous basalts (amphibolite) in the stability field of rutile-bearing eclogites at the base of an overthickened magmatic arc. Three compelling lines of evidence in favor of tectonic thickening include: (1) the intrusion of TTGs along active thrust fault zones; (2) the trace element modeling shows that spatially associated amphibolite is a viable source rock for the Fiskenæsset TTGs; and (3) the paucity of co-magmatic mantle-derived rocks associated with the Fiskenæsset TTGs (see Bridgwater et al., 1974; Myers, 1976; Myers, 1985 for crustal thickening). Tectonic thickening can be achieved by shallow subduction of a thick oceanic crust or by arc-arc and arc-continent collisions (Smithies et al., 2003; Lee et al., 2007; Schwartz et al., 2011). The Fiskenæsset mafic volcanic rocks (now amphibolites) show geochemical characteristics of MORB-Island-Arc-Basalt affinity and the geochemistry of the Fiskenæsset Complex indicates that it originated in an intra-oceanic island arc (Polat et al., 2009; 2010; 2011a; 2011b). Shallow subduction of a thick oceanic crust without involvement of a thick mantle wedge could not be the viable mechanism for the crust thickening, given that the amphibolites and the Fiskenæsset

Complex which formed shortly before the emplacement of the Fiskenæsset TTGs need a mantle source that has been overprinted by subduction components to produce the arc-signature (Smithies et al., 2003). Windley and Garde (2009) pointed out that there were no major continents in existence, however, Windley and Garde (2009) suggested there were many island arcs available to mutually accrete and amalgamate into microcontinents in the Meso- to Neoarchean in West Greenland. Therefore, the lower crust thickening might have resulted from an arc-arc collision as a result of horizontal tectonic regime (Bridgwater et al., 1974; Myers, 1976, 1985). Collectively, melting of hydrous basalts (amphibolites) in the eclogite facies at the base of an overthickened magmatic arc could have resulted in the formation of the Fiskenæsset TTGs (cf., Rapp et al., 2003; Hofmann et al., 2011).

The origin of the Fiskenæsset granites can also be linked to the crustal thickening in the arc via foundering of the eclogite residue to the sub-arc mantle. The foundering of the dense eclogite residue might have led to the basaltic underplating causing the emplacement of late high-K granites and the regional granulite metamorphism. In the Fiskenæsset region, the occurrence of the late Ilivertalic granite which marked regional granulite metamorphism is the evidence supporting the injection of large volumes of magma into the lower crust (Riciputi et al., 1990; McGregor and Friend, 1992). The heat source for the granitic magma generation and regional high grade metamorphism came from the basalt underplating as a result of the foundering of the dense eclogite residue into the mantle (cf., Kay and Mahlburg-Kay, 1991; Gao et al., 2004; Lustrino, 2005).

4.6.6. Continental growth in the Fiskenæsset region

The Archean craton of SW Greenland is dominated by Eoarchean to Neoarchean (ca. 3.8–2.7 Ga) orthogneisses with TTG compositions (Nutman et al., 1993; Nutman et al., 1996; Garde, 1997; Steenfelt et al., 2005; Friend et al., 2009; Windley and Garde, 2009). Previous studies of Eoarchean to Neoarchean TTG-gneisses in SW Greenland have

indicated that they formed from magmas derived by slab melts interacting with the mantle wedge to variable extent in oceanic and continental arc settings on the basis of field observations and geochemistry (Nutman et al., 1993; Nutman et al., 1996; Garde, 1997; Steenfelt et al., 2005; Friend et al., 2009; Windley and Garde, 2009; Tappe et al., 2011). The field relationships and geochemistry of the Fiskenæsset TTGs suggest they are juvenile continental crust and they were generated by basaltic melting at the base of thickened crust. This study shows that crustal thickening might have led to the partial melting of the lower part of the overthickened island arc crust, leaving rutile-bearing residual eclogites behind. The residual eclogites in the lower crust, owing to their high densities, were eventually foundered into the mantle, leaving behind a more felsic crust. This mechanism might have played an important role in the transformation of oceanic island arc crust to continental crust in the Fiskenæsset region.

It is generally believed that slab melting played a significant role in the formation of continents in SW Greenland (Nutman et al., 1993; Nutman et al., 1996; Garde, 1997; Steenfelt et al., 2005; Friend et al., 2009; Windley and Garde, 2009; Tappe et al., 2011); this study, however, suggests that, in addition to slab melting, the melting of amphibolites in the eclogite facies at the base of overthickened arc may also have played an important role in the production of Mesoarchean continental crust in SW Greenland (see also Hoffmann et al. (2011).

4.7. Conclusions

1. The Archean granitoid gneisses in the Fiskenæsset region, which occupy ca. 80% of the region, consist mostly of older TTGs and lesser amounts of younger high-K granites.
2. Field relationships suggest that the Fiskenæsset TTGs were emplaced into the spatially associated amphibolites and the Fiskenæsset Complex during regional-scale thrusting.
3. The Fiskenæsset TTGs with steep REE patterns and low HREE share the mineralogical and geochemical characteristics of typical Archean TTGs. The lack of

geological evidence of ancient crust and their lower initial $^{87}Sr/^{88}Sr$ excludes an origin of partial melting of preexisting TTG gneisses.

4. Major and trace element characteristics of the Fiskenæsset TTGs suggest that they were produced by partial melting amphibolite sources at the base of a thickened arc.

5. Field relationships, geochronology and trace element modeling provide a genetic link between the TTGs and spatially associated metavolcanic amphibolites occurring as inclusions in the granitoid gneisses. The geochemistry of the parental magma of the Fiskenæsset TTGs can be modeled by 20% partial melting of hydrous basalts (amphibolites), leaving a rutile-bearing eclogite residue. Denser residual eclogites might have been foundered into the underlying sub-arc mantle.

6. There are marked compositional differences between the TTGs and high-K granites. The granites have higher K_2O and lower Na_2O, Al_2O_3 and Sr contents than the TTGs. The granodiorites with relatively high K_2O/Na_2O are a possible source for the high-K granites. The granodiorites were partially melted, perhaps with heat provided by underplating basaltic magma, following the foundering of the eclogite residue, to generate the high-K granites.

7. The formation of the Fiskenæsset TTGs, the foundering of the eclogite residue into the mantle, and the intrusion of high-K granites mark the growth of the Archean continental crust in the Fiskenæsset region, SW Greenland.

4.8. Acknowledgments

Reviewers K.C. Condie and J.E. Hoffmann are acknowledged for their constructive comments, which have resulted in significant improvements to the paper. This contribution is supported by NSERC grants 250926 to A. Polat and 83117 to B. Fryer. Field work was supported by the Bureau of Minerals and Petroleum in Nuuk and the Geological Survey of Denmark and Greenland (GEUS). B.F. Windley is acknowledged

for discussions of geological and geochemical problems in various contexts. Zhaoping Yang is acknowledged for her help with the trace element analyses.

4.9. References

Albarède, F., 1998.The growth of continental crust. Tectonophysics 296, 1-14.

Alderton, D.H.M., Pearce, J.A., Potts, P.J., 1980. Rare earth element mobility during granite alteration: Evidence from southwest England. Earth and Planetary Science Letters, 49(1), 149-165.

Ashwal, L.D., Jacobsen, S.B., Myers, J.S., Kalsbeek, F., Goldstein, S.J., 1989. Sm-Nd age of the Fiskenæsset Anorthosite Complex, West Greenland. Earth and Planetary Science Letters 91, 261-270.

Atherton, M.P., Petford, N., 1993. Generation of sodium-rich magmas from newly underplated basaltic crust. Nature 362, 144-146.

Barker, F., Arth, J. G. 1976. Generation of trondhjemitic–tonalitic liquids and Archean bimodal trondhjemite–basalt suites. Geology 4, 596-600.

Barker, F., 1979. Trondhjemites: definition, environment and hypotheses of origin, In: Barker, F. (Ed.), Trondhjemites, Dacites and related rocks. Elsevier, Amsterdam, pp. 1-12.

Barth, M.G., Foley, S.F., Horn, I., 2002. Partial melting in Archean subduction zones: constraints from experimentally determined trace element partition coefficients between eclogitic minerals and tonalitic melts under upper mantle conditions. Precambrian Research 113(3-4), 323-340.

Bédard, J.H., 2006. A catalytic delamination-driven model for coupled genesis of Archaean crust and sub-continental lithospheric mantle. Geochimica et Cosmochimica Acta, 70(5): 1188-1214.

Bridgwater, D., McGregor, V.R., Myers, J.S., 1974. A horizontal tectonic regime in the Archaean of Greenland and its implications for early crustal thickening. Precambrian

Research 1, 179-197.

Bridgwater, D., Keto, L., McGregor, V.R., Myers, J.S., 1976. Archaean gneiss complex of Greenland, In: Escher, A., Watt, W.S. (Eds.), Geology of Greenland. Geological Survey of Greenland, Copenhagen, pp. 19-75.

Clemens, J.D., Yearron, L.M., Stevens, G., 2006. Barberton (South Africa) TTG magmas: Geochemical and experimental constraints on source-rock petrology, pressure of formation and tectonic setting. Precambrian Research 151, 53-78.

Condie, K.C., Sinha, A.K., 1996. Rare earth and other trace element mobility during mylonitization: A comparison of the Brevard and Hope Valley shear zones in the Appalachian Mountains, USA. Journal of Metamorphic Geology 14, 213-226.

Condie, K.C., 2005. TTGs and adakites: are they both slab melts? Lithos 80, 33-44.

Drummond, M.S., Defant, M.J., 1990. A model for trondhjemite-tonalite-dacite genesis and crustal growth via slab melting: Archean to modern comparisons. Journal of Geophysics Research 95, 21503-21521.

Escher, J.C., Myers, J.S., 1975. New evidence concerning the original relationships of early Precambrian volcanics and anorthosites in the Fiskenæsset region, southern West Greenland. Bulletin Grønlands Geologiske Undersøgelse 75, 72-76.

Foley, S., Tiepolo, M., Vannucci, R., 2002. Growth of early continental crust controlled by melting of amphibolite in subduction zones. Nature 417, 837-840.

Foley, S., 2008. A trace element perspective on Archean crust formation and on the presence or absence of Archean subduction. Geological Society of America Special Papers 440, 31-50.

Friend, C.R.L., Nutman, A.P., 2005. New pieces to the Archean jigsaw puzzle in the Nuuk region, southern West Greenland: steps in transforming a simple insight into a complex regional tectonothermal model. Journal of the Geological Society, London 162,147-162.

Friend, C.R.L., Nutman, A.P., Baadsgaard, H., Duke, M.J.M., 2009. The whole rock

Sm-Nd 'age' for the 2825 Ma Ikkattoq gneisses (Greenland) is 800 Ma too young: Insights into Archaean TTG petrogenesis. Chemical Geology 261, 61-75.

Gancarz, A.J., 1976. Isotopic systematics in Archean rocks, west Greenland. California Institute of Technology, Pasadena, p. 378.

Gao, S., Rudnick, R.L., Yuan, H.-L., Liu, X.-M., Liu, Y.-S., Xu, W.-L., Ling, W.-L., Ayers, J., Wang, X.-C., Wang, Q.-H., 2004. Recycling lower continental crust in the North China craton. Nature 432, 892-897.

Garde, A.A., 1997. Accretion and evolution of an Archaean high-grade grey gneissamphibolite complex: the Fiskefjord area, southern West Greenland. Geology of Greenland Survey Bulletin 177, 115 pp.

Herr, W., Wolfle, R., Eberhardt, P., Kopp, E., 1967. Development and recent application of the Re/Os dating method, Radioactive Dating and Methods of Low-Level Counting, International Atomic Energy Agency, Vienna 499-508.

Hoffmann, J.E., Münker, C., Næraa, T., Rosing, M.T., Herwartz, D., Garbe-Schönberg, D., Svahnberg, H., 2011. Mechanisms of Archean crust formation inferred from high-precision HFSE systematics in TTGs. Geochimica et Cosmochimica Acta 75, 4157-4178.

Hofmann, A.W., 1988. Chemical differentiation of the Earth: the relationship between mantle, continental crust, and oceanic crust. Earth and Planetary Science Letters 90, 297-314.

Jahn, B.M., Glikson, A.Y., Peucat, J.J., Hickman, A.H., 1981. REE geochimistry and isotopic data of Archean silicic volcanics and granitoids from the Pilbara Block, Western Australia: implications for the early crustal evolution. Geochimica et Cosmochimica Acta 45, 1633-1652.

Jenner, G.A., Longerich, H.P., Jackson, S.E., Fryer, B.J., 1990. ICP-MS - A powerful tool for high-precision trace-element analysis in Earth sciences: Evidence from analysis of selected U.S.G.S. reference samples. Chem. Geol. 83, 133-148.

Kalsbeek, F., Myers, J.S., 1973. The geology of the Fiskenæsset region. Rapport GrønlandsGeologiske Undersøgelse 51, 5-18.

Kay, R., Mahlburg-Kay, S., 1991. Creation and destruction of lower continental crust. Geologische Rundschau 80, 259-278.

Kay, S.M., Mpodozis, C., Coira, B., 1999. Magmatism,tectonism, and mineral deposits of the Central Andes (22°–33°S latitude), In: Skinner, B. (Ed.), Geology and ore deposits of the Central Andes. Society of Economic Geologists Special Publication pp. 27–59.

Kay, S.M., Godoy, E., Kurtz, A., 2005. Episodic arc migration, crustal thickening, subduction erosion, and magmatism in the south-central Andes. Geological Society of America Bulletin 117, 67-88.

Keulen, N., Schersten, A., Schumacher, J.C., Næraa, T., Windley, B.F., 2009. Geological observations in the southern West Greenland basement from Ameralik to Frederikshab Isblink in 2008. Geological Survey of Denmark and Greenland bulletin 17, 49-52.

Klemme, S., Blundy, J.D., Wood, B.J., 2002. Experimental constraints on major and trace element partitioning during partial melting of eclogite. Geochimica et Cosmochimica Acta 66, 3109-3123.

Lee, C.T.A., Morton, D.M., Kistler, R.W., Baird, A.K., 2007. Petrology and tectonics of Phanerozoic continent formation: From island arcs to accretion and continental arc magmatism. Earth and Planetary Science Letters, 263(3-4): 370-387.

Lustrino, M., 2005. How the delamination and detachment of lower crust can influence basaltic magmatism. Earth-Science Reviews 72, 21-38.

Martin, H., 1994. Chapter 6 The Archean Grey Gneisses and the Genesis of Continental Crust, In: Condie, K.C. (Ed.), Developments in Precambrian Geology. Elsevier, pp. 205-259.

Martin, H., 1999. Adakitic magmas: modern analogues of Archaean granitoids. Lithos 46, 411-429.

Martin, H., Smithies, R.H., Rapp, R., Moyen, J.F., Champion, D., 2005. An overview of

adakite, tonalite-trondhjemite-granodiorite (TTG), and sanukitoid: relationships and some implications for crustal evolution. Lithos 79, 1-24.

McGregor, V.R., Friend, C.R.L., 1992. Late Archean Prograde Amphibolite- to Granulite-Facies Relations in the Fiskenæsset Region, Southern West Greenland. The Journal of Geology 100, 207-219.

Moorbath, S., Pankhurst, R.J., 1976. Further rubidium-strontium age and isotope evidence for the nature of the late Archaean plutonic event in West Greenland. Nature 262, 124-126.Moyen, J.-F., 2009. High Sr/Y and La/Yb ratios: The meaning of the "adakitic signature". Lithos 112, 556-574.

Moyen, J.F., Stevens, G., 2006. Experimental constraints on TTG petrogenesis: Implications for Archean geodynamics. In: Benn, K., Mareschal, J.C., Condie, K.C. (Eds.), Archean Geodynamics and Environments. Geophysical Monograph Series, pp. 149-175.

Muir, R.J., Weaver, S.D., Bradshaw, J.D., Eby, G.N., Evans, J.A., 1995. The Cretaceous Separation Point batholith, New Zealand: granitoid magmas formed by melting of mafic lithosphere. Journal of the Geological Society 152, 689-701.

Myers, J.S., 1976. Granitoid sheets, thrusting, and Archean crustal thickening in West Greenland. Geology 4, 265-268.

Myers, J.S., Platt, R.G., 1977. Mineral chemistry of layered Archaean anorthosite at Majorqap qava, near Fiskenæsset, southwest Greenland. Lithos 10, 59-72.

Myers, J.S., 1985. Stratigraphy and structure of the Fiskenæsset complex, southernWest Greenland. Bulletin Grønlands Geologiske Undersøgelse 150.

Nutman, A.P., Friend, C.R.L., Kinny, P.D., McGregor, V.R., 1993. Anatomy of an Early Archean gneiss complex: 3900 to 3600 Ma crustal evolution in southern West Greenland. Geology 21, 415-418.

Nutman, A.P., McGregor, V.R., Friend, C.R.L., Bennett, V.C., Kinny, P.D., 1996. The Itsaq Gneiss Complex of southern West Greenland; the world's most extensive record

of early crustal evolution (3900-3600 Ma). Precambrian Research 78, 1-39.

Patiño, D., Alberto, E., 2005. Vapor-Absent Melting of Tonalite at 15–32 kbar. Journal of Petrology 46, 275-290.

Petford, N., Atherton, M., 1996. Na-rich partial melts from newly underplated basaltic crust: The Cordillera Blanca Batholith, Peru. Journal of Petrology 37, 1491-1521.

Pidgeon, R.T., Kalsbeek, F., 1978. Dating of igneous and metamorphic events in the Fiskenaesset region of southern west Greenland. Canadian Journal of Earth Sciences 15, 2021-2025.

Polat, A., Hofmann, A.W., 2003. Alteration and geochemical patterns in the 3.7-3.8 Ga Isua greenstone belt, West Greenland. Precambrian Res. 126, 197-218.

Polat, A., Appel, P.W.U., Fryer, B., Windley, B., Frei, R., Samson, I.M., Huang, H., 2009. Trace element systematics of the Neoarchean Fiskenæsset anorthosite complex and associated meta-volcanic rocks, SW Greenland: Evidence for a magmatic arc origin. Precambrian Research 175, 87-115.

Polat, A., Frei, R., Schersten, A., Appel, P.W.U., 2010. New age (ca. 2970Ma), mantle source composition and geodynamic constraints on the Archean Fiskenæsset anorthosite complex, SW Greenland. Chemical Geology 277, 1-20.

Polat, A., Fryer, B.J., Appel, P.W.U., Kalvig, P., Kerrich, R., Dilek, Y., Yang, Z., 2011a. Geochemistry of anorthositic differentiated sills in the Archean (~ 2970 Ma) Fiskenæsset Complex, SW Greenland: Implications for parental magma compositions, geodynamic setting, and secular heat flow in arcs. Lithos 123, 50-72.

Polat, A., Appel, P.W.U., Fryer, B.J., 2011b. An overview of the geochemistry of Eoarchean to Mesoarchean ultramafic to mafic volcanic rocks, SW Greenland: Implications for mantle depletion and petrogenetic processes at subduction zones in the early Earth. Gondwana Research 20, 255-283.

Rapp, R.P., Watson, E.B., Miller, C.F., 1991. Partial melting of amphibolite/eclogite and the origin of Archean trondhjemites and tonalites. Precambrian Research 51, 1-25.

Rapp, R.P., Watson, E.B., 1995. Dehydration melting of metabasalt at 8-32 kbar: Implications for continental growth and crust-mantle recycling. Journal of Petrology 36, 891-931.

Rapp, R.P., Shimizu, N., Norman, M.D., Applegate, G.S., 1999. Reaction between slab-derived melts and peridotite in the mantle wedge: Experimental constraints at 3.8 GPa. Chemical Geology 160, 335-356.

Rapp, R.P., Shimizu, N., Norman, M.D., 2003. Growth of early continental crust by partial melting of eclogite. Nature 425, 605-609.

Riciputi, L.R., Valley, J.W., McGregor, V.R., 1990. Conditions of Archean granulite metamorphism in the Godthab-Fiskenæsset region, southern West Greenland. Journal of Metamorphic Geology 8, 171-190.

Rollinson, H., 2010. Coupled evolution of Archean continental crust and subcontinental lithospheric mantle. Geology 38, 1083-1086.

Rudnick, R.L., 1995. Making continental crust. Nature 378, 571-578.

Rutter, M.J., Wyllie, P.J., 1988. Melting of vapour-absent tonalite at 10 kbar to simulate dehydration-melting in the deep crust. Nature 331, 159-160.

Schwartz, J.J., Johnson, K., Miranda, E.A., Wooden, J.L., 2011. The generation of high Sr/Y plutons following Late Jurassic arc-arc collision, Blue Mountains province, NE Oregon. Lithos, 126(1-2): 22-41.

Sen, C., Dunn, T., 1994. Dehydration melting of a basaltic composition amphibolite at 1.5 and 2.0 GPa: implications for the origin of adakites. Contributions to Mineralogy and Petrology 117, 394-409.

Skjerlie, K.P., Patiño Douce, A.E., Johnston, A.D., 1993. Fluid absent melting of a layered crustal protolith: implications for the generation of anatectic granites. Contributions to Mineralogy and Petrology 114, 365-378.

Smithies, R.H., 2000. The Archaean tonalite-trondhjemite-granodiorite (TTG) series is not an analogue of Cenozoic adakite. Earth and Planetary Science Letters 182,

115-125.

Smithies, R.H., Champion, D.C., Cassidy, K.F., 2003. Formation of Earth's early Archaean continental crust. Precambrian Research 127, 89-101.

Steenfelt, A., Garde, A.A., Moyen, J.-F., 2005. Mantle wedge involvement in the petrogenesis of Archaean grey gneisses in West Greenland. Lithos 79, 207-228.

Tappe, S., Smart, K.A., Pearson, D.G., Steenfelt, A., Simonetti, A., 2011. Craton formation in Late Archean subduction zones revealed by first Greenland eclogites. Geology 39, 1103–1106.

Taylor, S.R., McLennan, S.M., 1985. The Continental Crust: Its Composition and Evolution. Blackwell,Oxford, 312 pp.

Whalen, J.B., Percival, J.A., Mcnicoll, V.J., Longstaffe, F.J., 2002. A Mainly Crustal Origin for Tonalitic Granitoid Rocks, Superior Province, Canada: Implications for Late Archean Tectonomagmatic Processes. Journal of Petrology, 43(8): 1551-1570.

Ward, C.D., McArthur, J.M., Walsh, J.N., 1992. Rare Earth Element Behaviour During Evolution and Alteration of the Dartmoor Granite, SW England. Journal of Petrology 33, 785-815.

Wareham, C.D., Millar, I.L., Vaughan, A.P.M., 1997. The generation of sodic granite magmas, western Palmer Land, Antarctic Peninsula. Contributions to Mineralogy and Petrology 128, 81-96.

Watkins, J., Clemens, J., Treloar, P., 2007. Archaean TTGs as sources of younger granitic magmas: melting of sodic metatonalites at 0.6–1.2 GPa. Contributions to Mineralogy and Petrology 154, 91-110.

Windley, B.F., Herd, R.K., Bowden, A.A., 1973. The Fiskenæsset complex, West Greenland, Part I: A preliminary study of the stratigraphy, petrology, and whole-rock chemistry from Qeqertarssuatsiaq. Bulletin Grønlands Geologiske Undersøgelse 106, 80 pp.

Windley, B.F., Smith, J.V., 1974. The Fiskenæsset Complex, West Greenland,Part II:

General mineral chemistry from Qeqertarssuatsiaq. Bulletin Grønlands Geologiske Undersøgelse 108, 54 pp.

Windley, B.F., Garde, A.A., 2009. Arc-generated blocks with crustal sections in the North Atlantic craton of West Greenland: Crustal growth in the Archean with modern analogues. Earth-Science Reviews 93, 1-30.

Winther, K.T., Newton, R.C., 1991. Experimental melting of hydrous low-K tholeiite: evidence on the origin of Archaean cratons. Bulletin of the Geological Society of Denmark 39, 213-228.

Xiong, X.-L., 2006. Trace element evidence for growth of early continental crust by melting of rutile-bearing hydrous eclogite. Geology 34, 945-948.

Xiong, X.L., Adam, J., Green, T.H., 2005. Rutile stability and rutile/melt HFSE partitioning during partial melting of hydrous basalt: Implications for TTG genesis. Chemical Geology 218, 339-359.

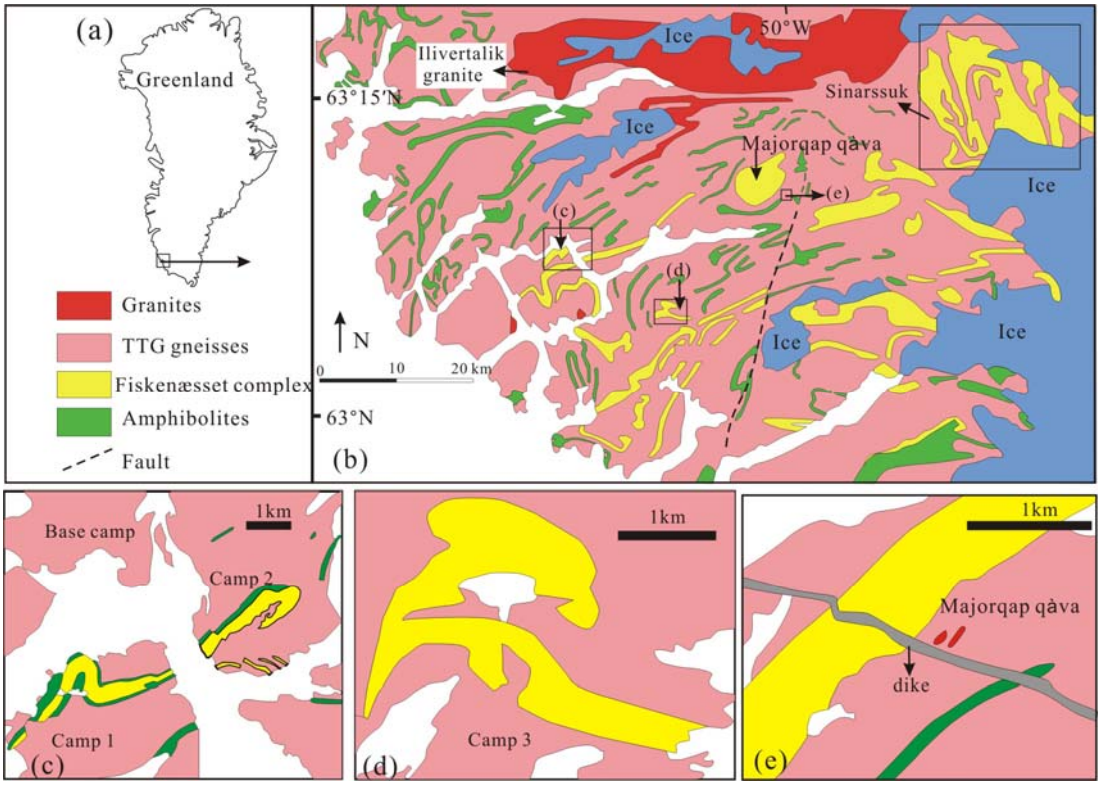

Fig 4.1. (a) General location of the study area in Greenland. (b) Simplified geological maps of the Fiskenæsset region (after Myers, 1976). (c) Simplified geological maps of Camp 1, Camp 2 and Base Camp. (d) Simplified geological maps of Camp 3. (e) Simplified geological maps of Majorqap qâva.

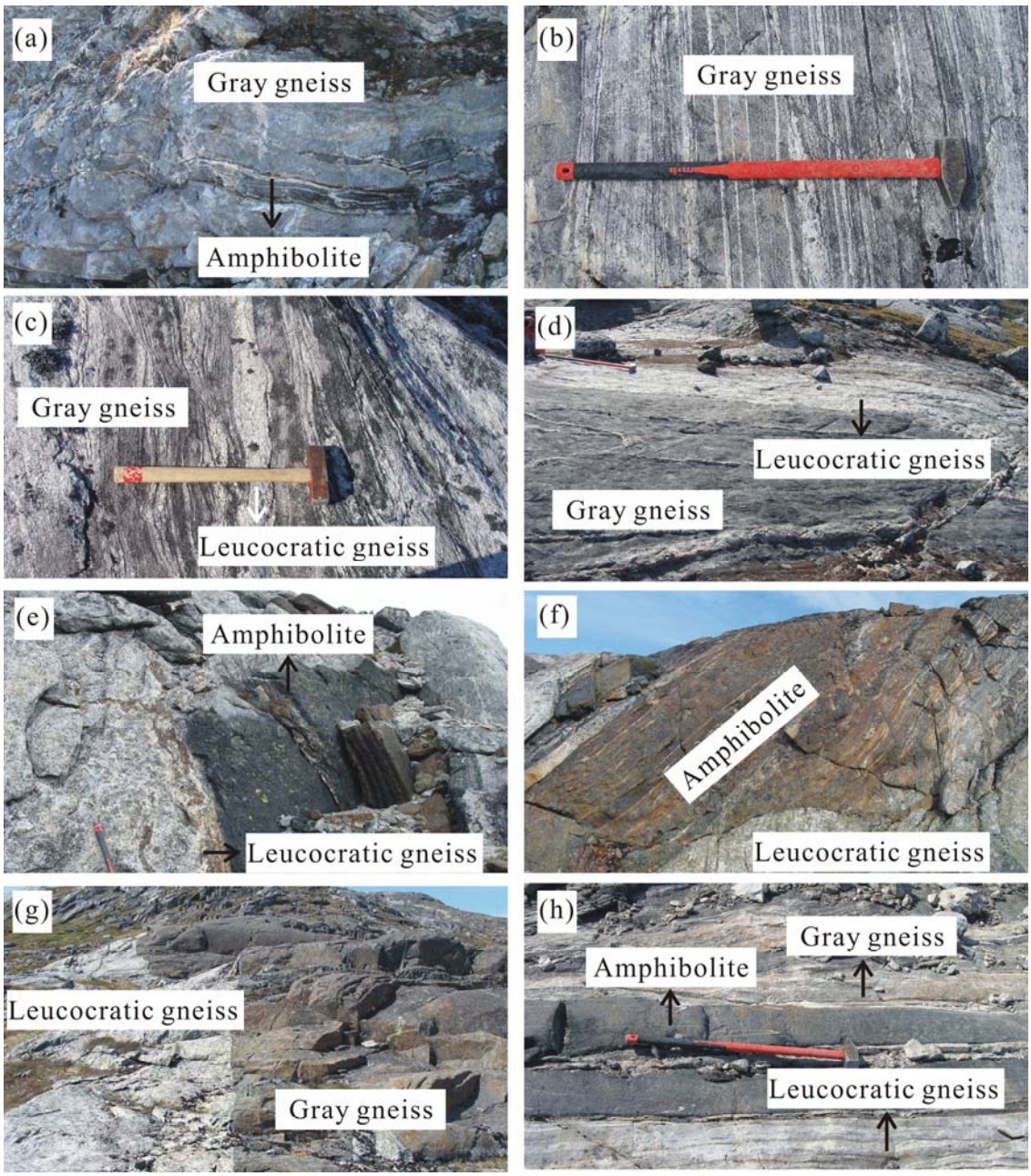

Fig 4.2. Field photographs illustrating lithological characteristics and field relationships in the Fiskenæsset area. (a) Little deformed gray gneisses containing inclusions of amphibolite. (b) Very strongly deformed gray gneisses. (c) Leucocratic gneisses intruding gray gneisses. (d) Leucocratic gneisses intruding gray gneisses. (e) Leucocratic gneisses intruding amphibolite. (f) Leucocratic gneisses intruding amphibolite. (g) Sharp contact between leucocratic gneisses and gray gneisses. (h) Intercalated leucocratic gneisses, gray gneisses and amphibolites.

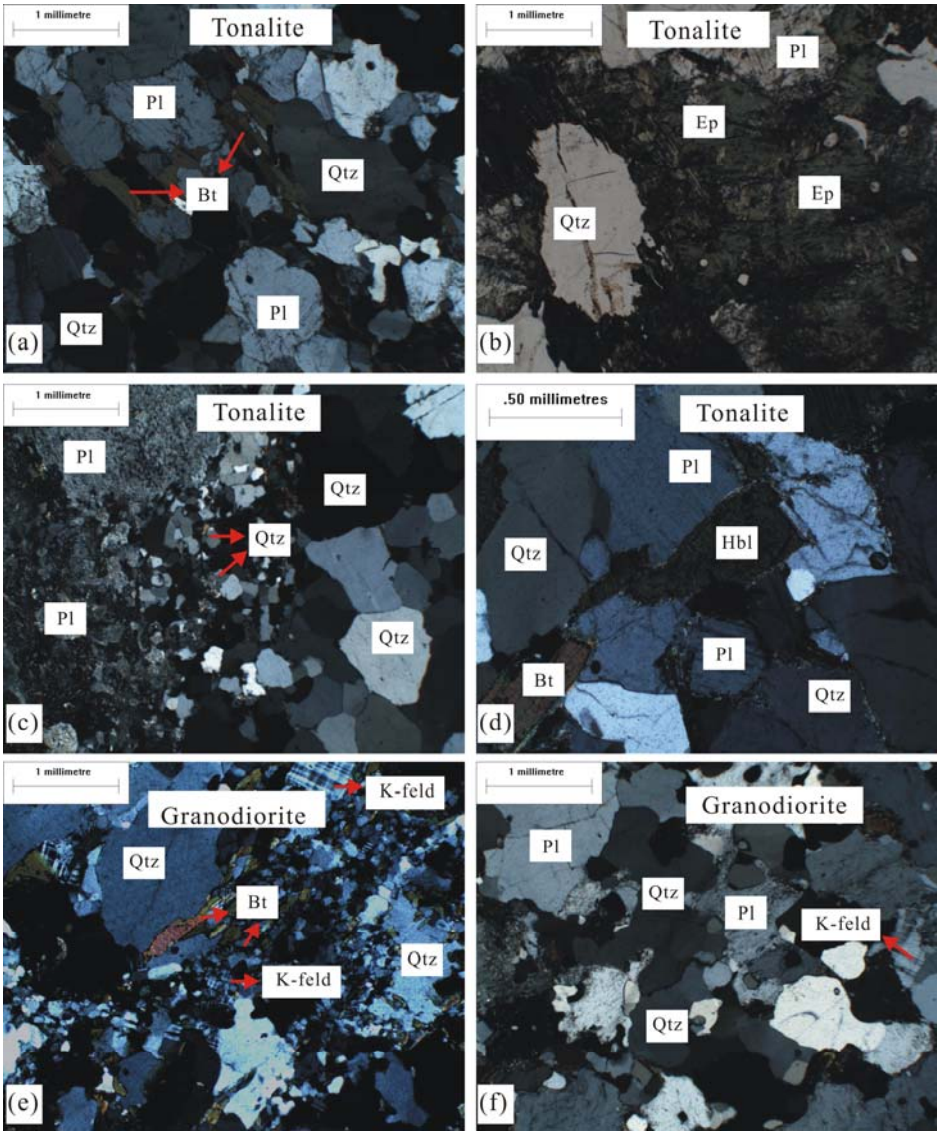

Fig 4.3. Photomicrographs of the rocks in the Fiskenæsset area. (a) Tonalite with quartz, plagioclase and biotite. (b) Tonalite with quartz and plagioclase (epidote). (c) Tonalite with quartz and plagioclase. (d) Tonalite with quartz, plagioclase and hornblende. (e) Granodiorite with quartz, K-feldspar and biotite. (f) Granodiorite with quartz and plagioclase. (Pl: plagioclase; Qtz: quartz; Bt: biotite; K-feld: K-feldspar; Hbl: Hornblende).

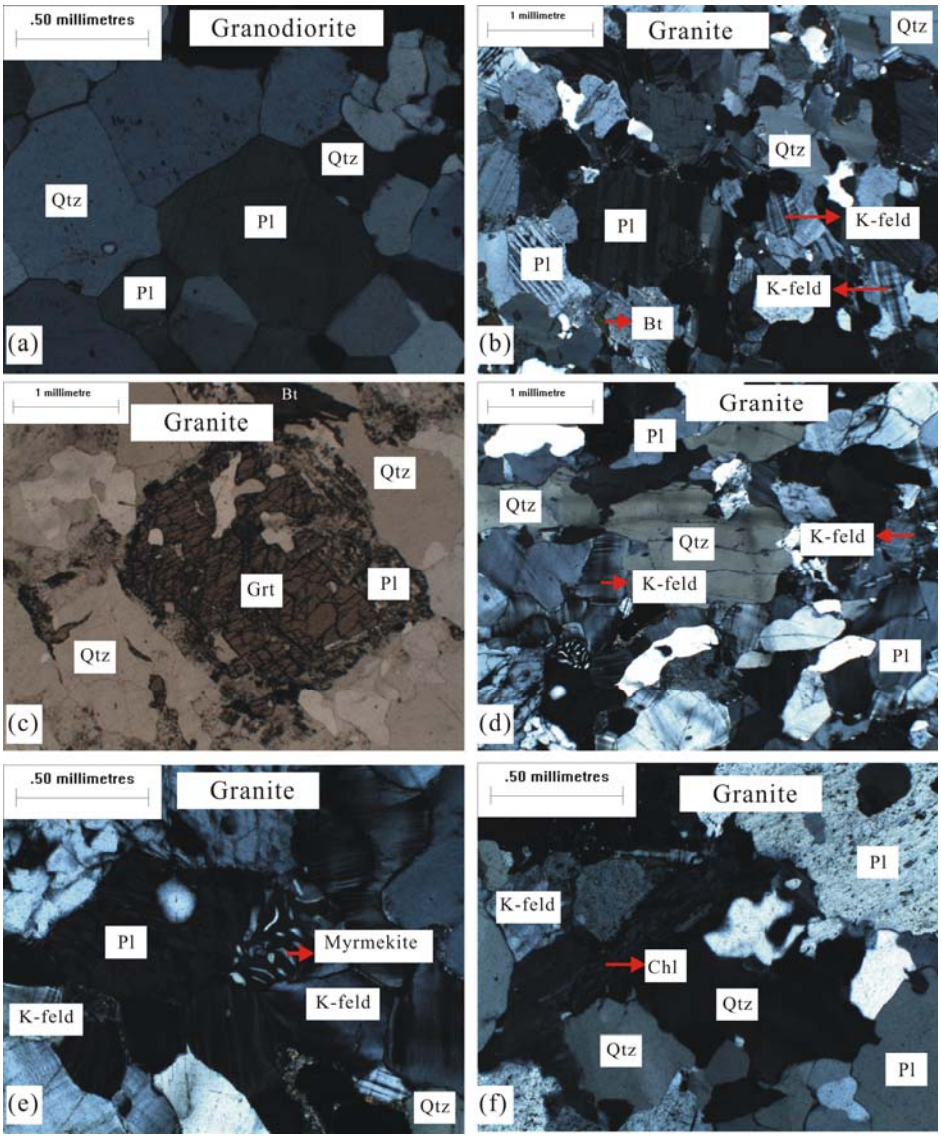

Fig 4.4. Photomicrographs of the rocks in the Fiskenæsset area. (a) Granodiorite with quartz and plagioclase. (b) Granite with quartz, plagioclase and K-feldspar. (c) Granite with quartz and garnet. (d) Granite with quartz, plagioclase and K-feldspar. (e) Granite with quartz, plagioclase and K-feldspar (Myrmekitie). (f) Granite with quartz, plagioclase, K-feldspar and biotite (chlorite). (Pl: plagioclase; Qtz: quartz; Bt: biotite; K-feld: K-feldspar; Chl: chlorite).

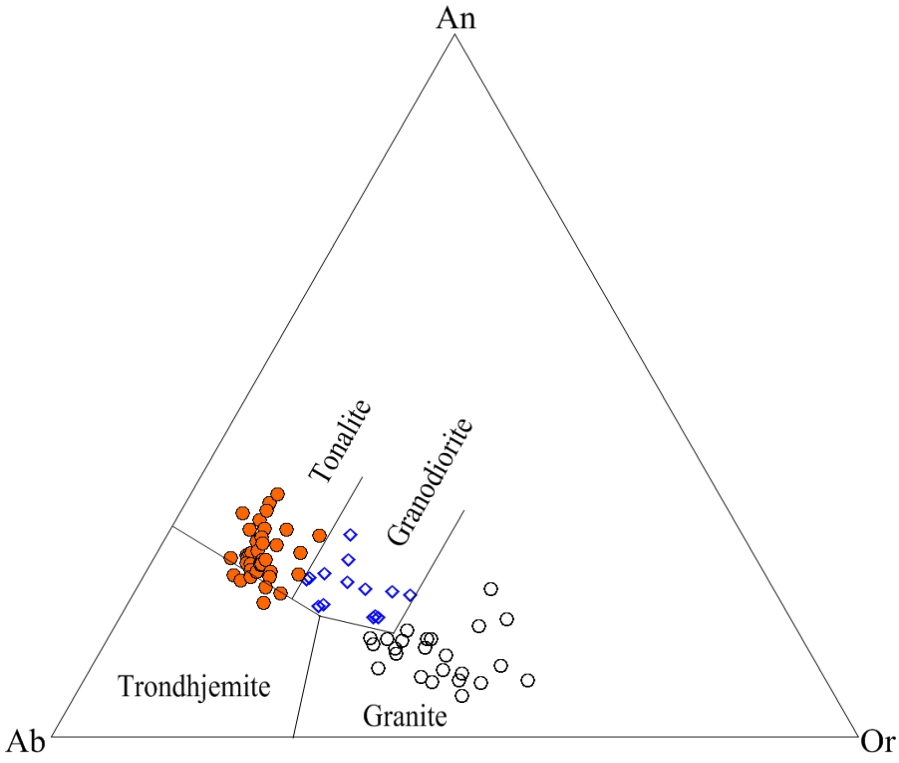

Fig 4.5. Classification of the granitoid gneisses using normative anorthite (an), albite (ab) and orthoclase (or), with fields defined by Barker (1979).

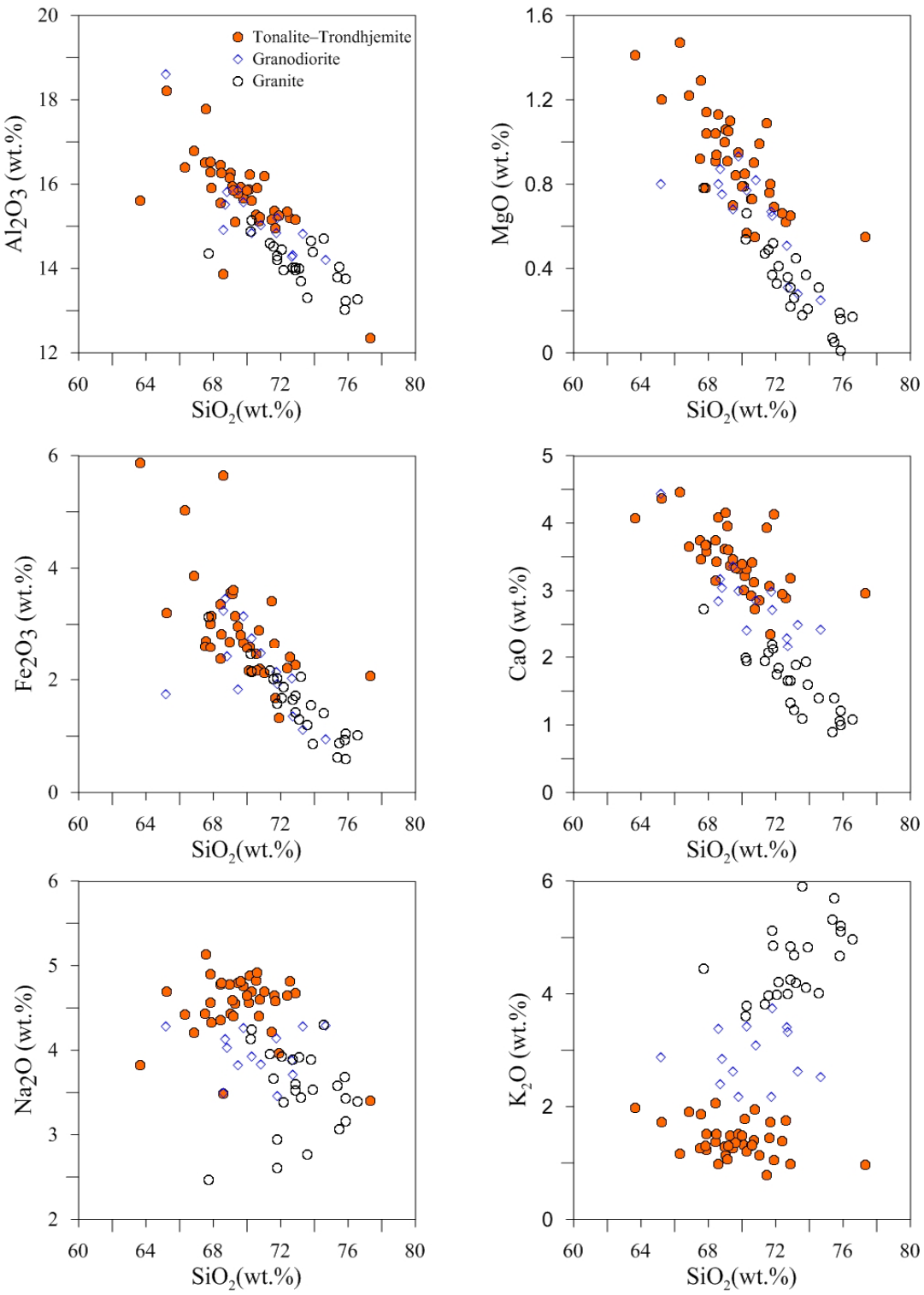

Fig 4.6. Major-element Harker diagrams for the TTGs and granites.

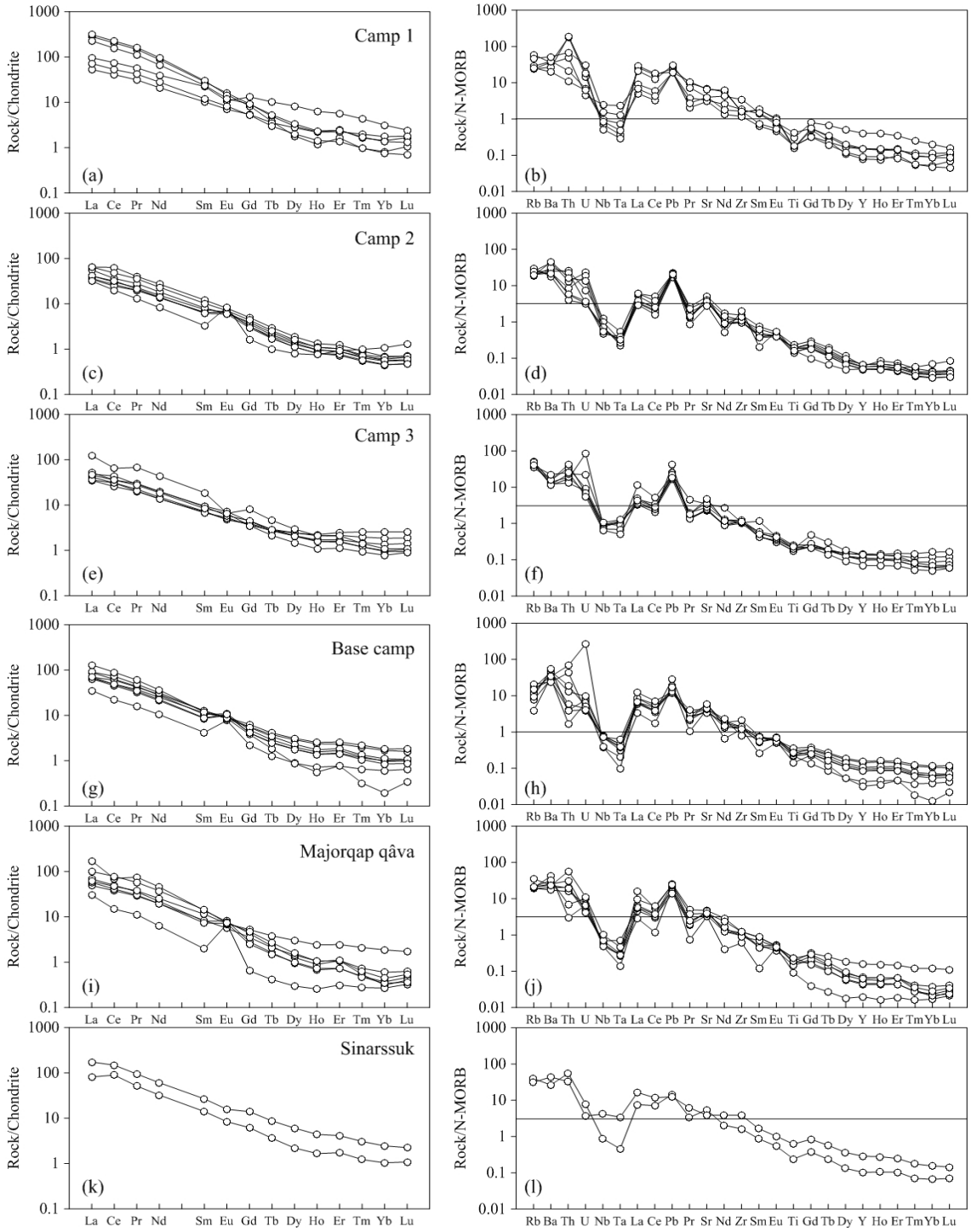

Fig 4.7. Whole-rock REE and trace-element concentrations for tonalities and trondhjemites, normalized to C1 chondrite (Taylor and McLennan, 1985) and N-MORB (Hofmann, 1988).

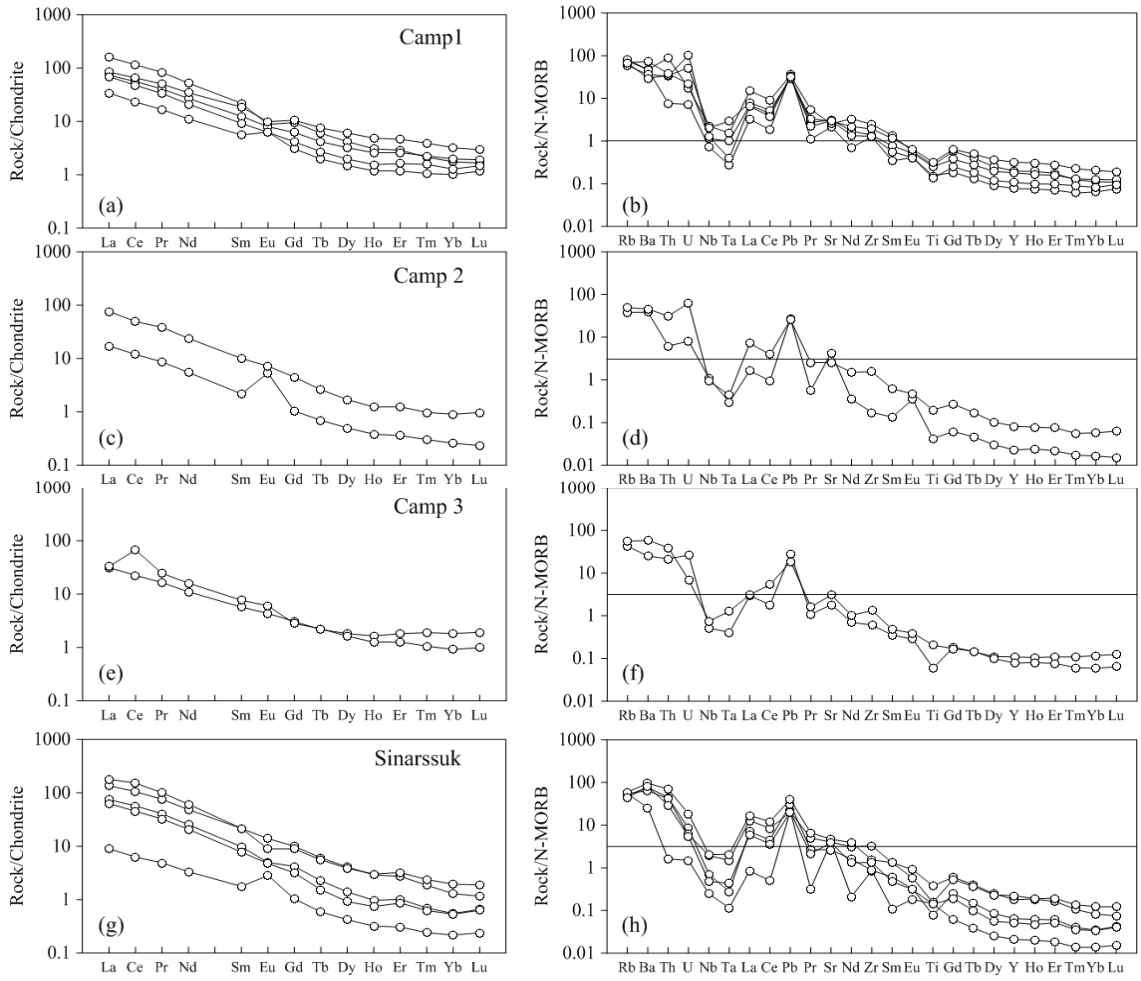

Fig 4.8. Whole-rock REE and trace-element concentrations for granodiorites, normalized to C1 chondrite (Taylor and McLennan, 1985) and N-MORB (Hofmann, 1988).

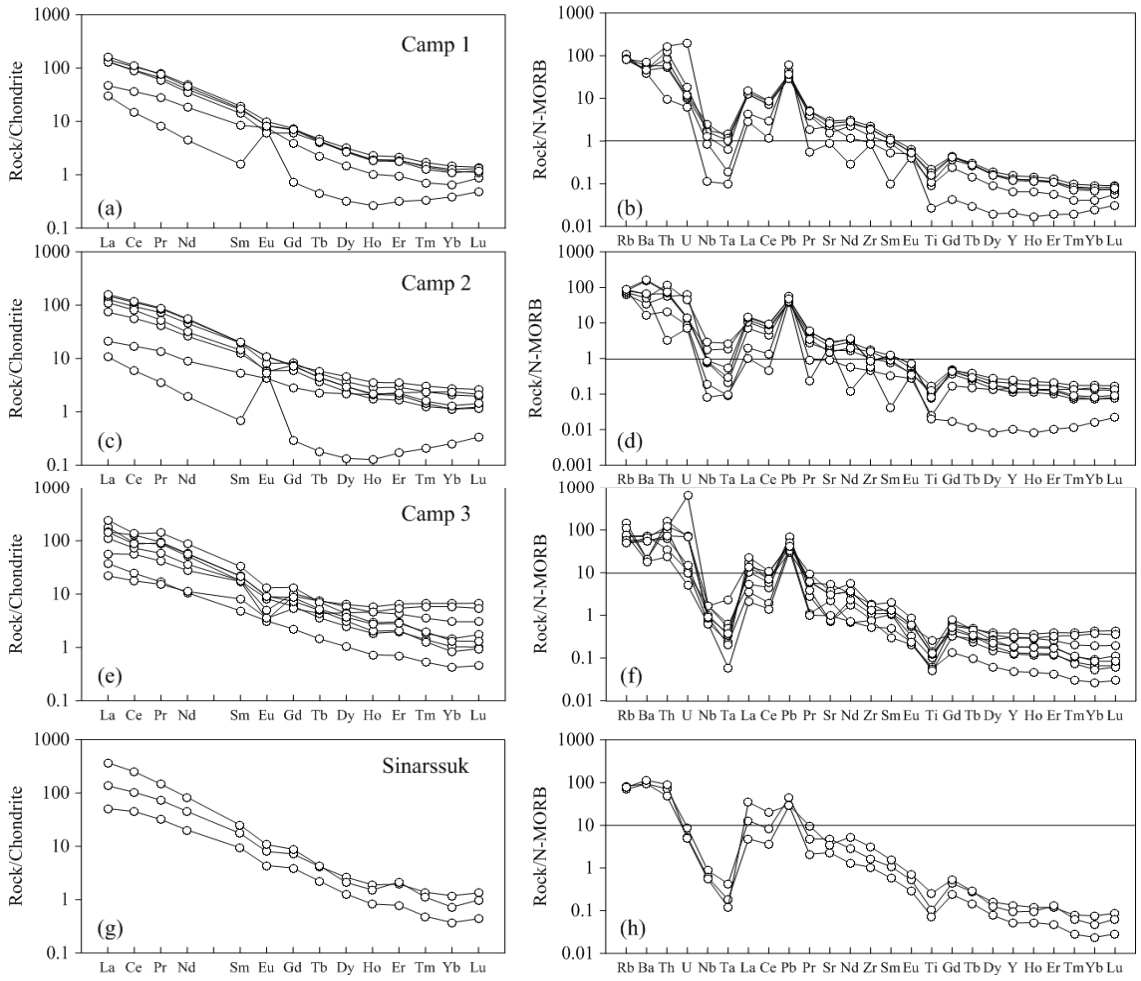

Fig 4.9. Whole-rock REE and trace-element concentrations for granites, normalized to C1 chondrite (Taylor and McLennan, 1985) and N-MORB (Hofmann, 1988).

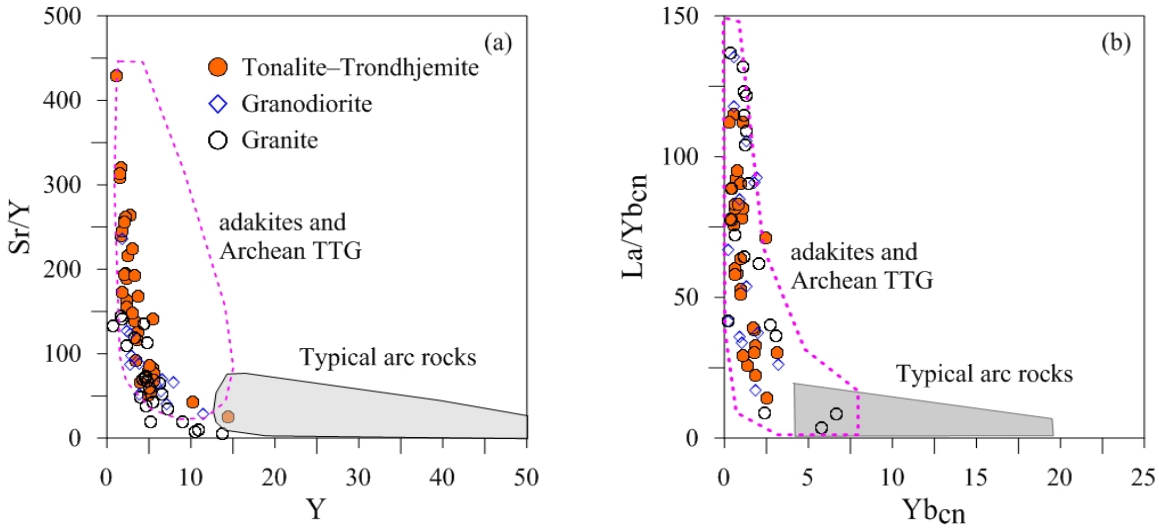

Fig 4.10. (a) La/Yb_{cn}–Yb_{cn} for the TTGs and granites adapted from Martin et al., (2005) and (b) Sr/Y–Y diagrams for the TTGs and granites adapted from Martin (1999).

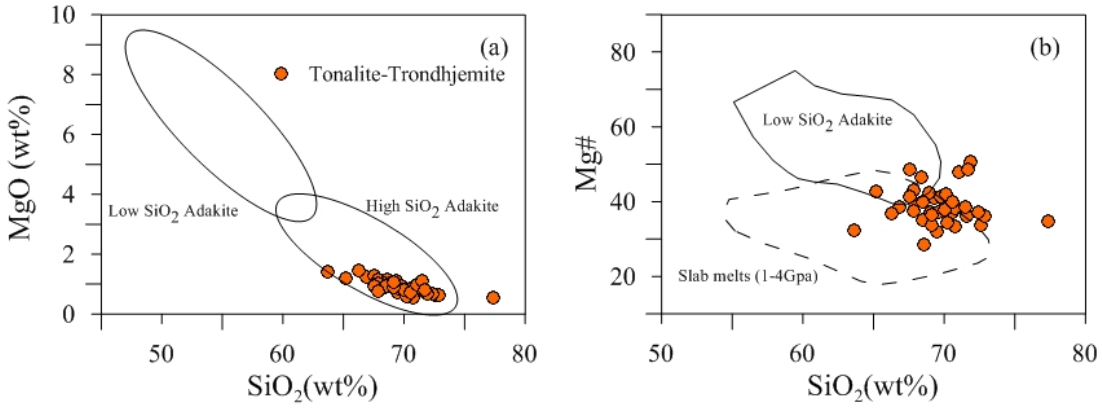

Fig 4.11. (a) SiO_2 vs. MgO for the tonalities and trondhjemites adapted from Martin (2005) and (b) SiO_2 vs. Mg# for the tonalities and trondhjemites adapted from Rapp et al. (1999) and Smithies (2000).

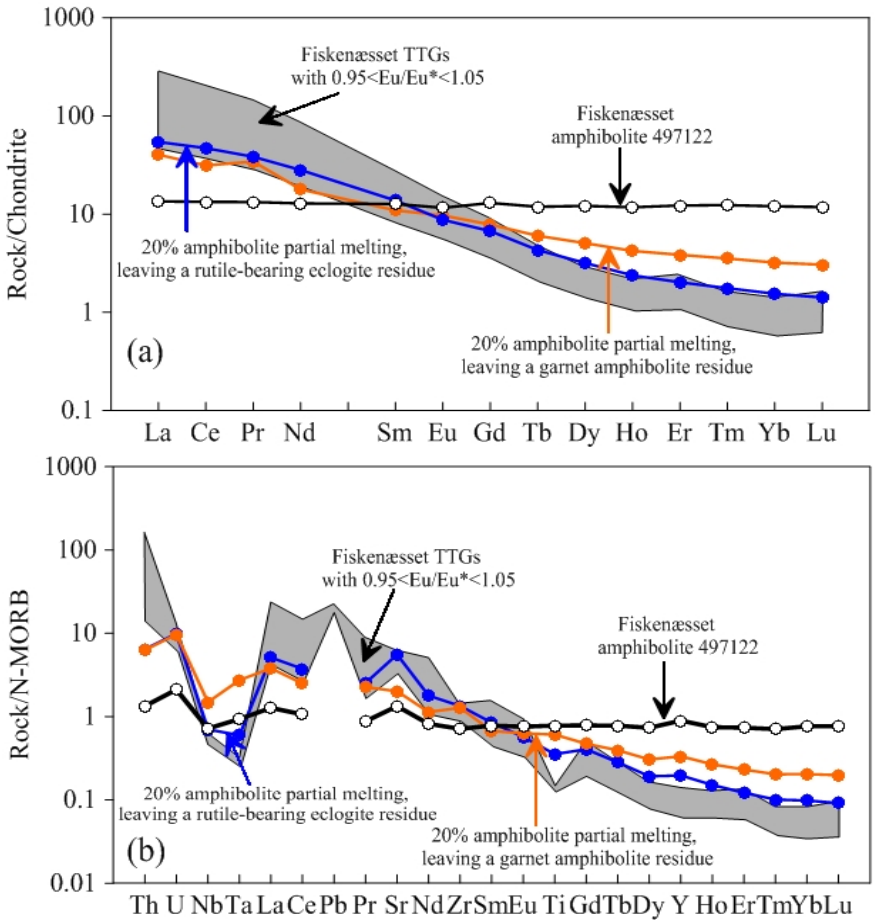

Fig 4.12. Results of 20% batch partial melting of a hydrous basaltic protolith compared to the tonalite average. The partition coefficients employed were mainly compiled from Barth et al. (2002) (garnet and clinopyroxene), Foley, (2008) (amphibole) and Xiong, (2006) (rutile).

Table 4.1

Measured and recommended trace element concentrations (ppm) for USGS BHVO-2 and BCR-2.

	BHVO-2			BCR-2		
Element	Measured (n=34)	Recommended	RSD (%)	Measured (n=9)	Recommended	RSD (%)
Cr	226	280	76.1	27	18	88.9
Co	46	45	9.0	36	37	24.5
Ni	186	119	23.6	91	18	37.3
Rb	8.90	9.8	4.9	40.83	48	35.8
Sr	388	389	9.1	350	346	22.6
Y	23	26	6.2	30	37	20.8
Zr	159	172	8.0	177	188	5.5
Nb	13.9	18	9.2	9.2	12.6	4.6
Ba	126	130	6.1	669	683	14.8
La	15	15	4.9	24	25	12.0
Ce	36	38	4.8	51	53	9.3
Pr	5.1	5.35	5.5	6.3	6.7	5.8
Nd	23	25	5.4	26	28	5.5
Sm	5.8	6.2	5.3	5.9	6.58	9.7
Eu	2.0	2.07	4.2	1.7	2	11.1
Gd	6.1	6.3	4.6	6.0	6.8	14.5
Tb	0.89	0.9	4.9	0.92	1.07	17.5
Dy	5.07	5.31	4.2	5.56	6.41	19.6
Ho	0.93	1.04	4.1	1.11	1.28	20.3
Er	2.49	2.54	5.1	3.24	3.66	20.7
Tm	0.32	0.33	5.7	0.45	0.54	21.2
Yb	1.9	2	5.7	2.9	3.5	21.4
Lu	0.27	0.28	13.2	0.43	0.503	21.5
Ta	0.9	1.4	18.6	0.5	1.07	21.1
Pb	3.3	1.6	80.9	12.0	11	45.6
Th	1.5	1.2	20.7	6.1	6.2	10.5
U	0.48	0.403	66.3	1.46	1.69	23.4

Table 4.2
Major (wt.%) and trace (ppm) element concentrations and significant element ratios for tonalite–trondhjemite.

	Camp 1						Camp 2		
	509009	509012	509016	509019	509022	509030	509033	509036[a]	509037
SiO_2	72.9	68.5	77.3	72.6	69.5	66.9	70.6	68.4	70.8
Al_2O_3	15.2	15.6	12.4	15.2	15.8	16.8	15.9	16.5	15.2
Fe_2O_3	2.3	3.4	2.1	2.4	3.0	3.9	2.2	2.4	2.2
MnO	0.027	0.051	0.02	0.037	0.038	0.037	0.031	0.03	0.027
MgO	0.65	0.91	0.55	0.62	0.7	1.22	0.73	1.04	0.55
CaO	3.18	3.15	2.96	2.89	3.46	3.65	3.42	3.74	2.73
Na_2O	4.67	4.36	3.4	4.81	4.8	4.21	4.92	4.78	4.6
K_2O	0.98	2.06	0.96	1.75	1.26	1.91	1.32	1.38	1.95
TiO_2	0.261	0.483	0.255	0.289	0.293	0.673	0.247	0.372	0.223
P_2O_5	0.05	0.13	0.03	0.07	0.1	0.22	0.1	0.17	0.09
LOI	0.47	0.21	0.13	0.09	0.39	0.2	0.23	0.32	0.17
Total	100.6	98.72	100	100.7	99.24	99.62	99.64	99.1	98.49
Mg#	36	35	35	34	32	39	40	47	33
Sc	2	5	1	4	3	4	3	4	3
Zr	164	190	157	123	171	358	108	159	102
V	5	49	7	25	28	45	17	26	16
Cr	12	15	12	13	18	27	13	15	15
Co	2	7	2	5	7	10	4	8	4
Ni	8	13	9	9	12	51	9	18	10
Rb	30	76	30	36	32	60	27	31	32
Sr	777	368	744	348	453	451	525	570	398
Y	5.52	14.41	2.82	5.34	3.27	5.46	2.05	2.17	2.05
Nb	2.46	8.58	1.80	3.33	2.98	5.47	2.46	4.39	3.49
Ba	519	485	376	543	273	721	326	350	598
La	102.95	35.16	114.19	19.50	26.32	82.68	13.26	23.43	15.16
Ce	195.32	71.88	214.35	39.17	50.62	149.52	25.24	60.74	28.62
Pr	20.16	7.90	22.11	4.28	5.74	15.15	2.74	5.48	3.11
Nd	62.25	28.22	68.64	14.97	19.81	47.58	9.66	19.30	10.96
Sm	6.55	5.17	6.89	2.37	2.79	5.47	1.48	2.79	1.73
Eu	1.39	0.93	1.27	0.61	0.71	1.05	0.58	0.69	0.57
Gd	2.82	4.05	2.55	1.65	1.60	2.80	0.97	1.52	1.10
Tb	0.28	0.59	0.22	0.21	0.17	0.31	0.11	0.17	0.12
Dy	1.13	3.18	0.69	1.05	0.77	1.28	0.49	0.72	0.52
Ho	0.19	0.54	0.10	0.19	0.12	0.20	0.08	0.11	0.08
Er	0.61	1.42	0.41	0.56	0.34	0.60	0.22	0.31	0.22
Tm	0.06	0.15	0.03	0.07	0.03	0.06	0.02	0.03	0.02
Yb	0.35	0.78	0.20	0.44	0.19	0.34	0.15	0.17	0.14
Lu	0.06	0.09	0.04	0.07	0.03	0.05	0.03	0.03	0.02
Ta	0.07	0.45	0.06	0.14	0.09	0.25	0.05	0.10	0.06
Pb	12.11	9.27	9.55	9.68	9.33	14.76	10.78	10.42	10.80
Th	33.79	9.09	35.39	3.96	2.03	12.90	1.04	4.74	2.45
U	1.03	0.31	1.29	0.48	0.44	2.13	0.23	0.53	1.65
A/CNK	1.04	1.03	1.03	1.01	1.01	1.07	1.01	1.02	1.04
Na_2O/K_2C	4.8	2.1	3.5	2.7	3.8	2.2	3.7	3.5	2.4
Sr/Y	141	26	264	65	139	83	256	262	194
La/Yb_{cn}	196	30	378	30	95	165	60	92	76
Eu/Eu*	0.99	0.62	0.93	0.94	1.03	0.82	1.48	1.03	1.27
Ce/Ce*	1.00	1.01	1.00	1.00	0.96	0.99	0.98	1.26	0.98
Yb_{cn}	1.43	3.15	0.82	1.75	0.75	1.36	0.60	0.69	0.55
Nb/Nb*	0.01	0.12	0.01	0.09	0.10	0.04	0.16	0.10	0.14
Zr/Zr*	0.50	0.98	0.45	1.28	1.43	1.38	1.78	1.35	1.46
Pb/Pb*	2.0	4.0	1.4	7.6	5.6	3.2	13.2	5.8	11.7
Sr/Sr*	1.0	1.0	0.8	1.9	1.8	0.8	4.5	2.8	3.1
Ti/Ti*	0.21	0.40	0.23	0.46	0.44	0.63	0.53	0.58	0.45
North	63°10′15.2″	63°10′29.5″	63°10′17.1″	63°10′8.4″	63°10′44.6″	63°11′25.8″	63°12′29.9″	63°12′26″	63°12′23.5″
West	50°35′44.9″	50°35′23″	50°35′8.4″	50°35′51.9″	50°35′20.1″	50°35′45.9″	50°30′51.1″	50°30′48.5″	50°30′56.8″

Table 4.2 (continued)

	Camp 2					Majorqap qâva			
	509042	509043	509048	509049	509061	509064	509065[a]	509066	509067[a]
SiO_2	70.0	70.7	70.6	69.6	71.9	71.0	70.1	72.4	71.7
Al_2O_3	15.9	15.1	15.3	15.9	15.3	16.2	15.9	15.4	15.0
Fe_2O_3	2.6	2.9	2.5	2.8	1.3	2.1	2.2	2.2	1.7
MnO	0.023	0.037	0.029	0.032	0.011	0.027	0.024	0.027	0.024
MgO	0.79	0.9	0.73	0.84	0.69	0.99	0.79	0.66	0.8
CaO	3.39	3.13	2.93	3.33	4.13	2.86	3.01	2.95	2.35
Na_2O	4.65	4.4	4.82	4.81	3.96	4.69	4.56	4.65	4.58
K_2O	1.48	1.4	1.3	1.36	1.05	1.13	1.32	1.39	1.72
TiO_2	0.31	0.308	0.301	0.311	0.263	0.29	0.268	0.232	0.146
P_2O_5	0.09	0.1	0.1	0.1	0.09	0.05	0.07	0.09	0.02
LOI	0.23	0.1	0.23	0.04	0.07	0.92	0.76	0.1	0.71
Total	99.38	99.12	98.74	99.16	98.76	100.3	98.94	100	98.64
Mg#	38	38	37	37	51	48	42	37	49
Sc	3	4	3	3	2	3	3	2	3
Zr	100	125	114	140	210	120	128	100	63
V	26	28	27	29	22	19	21	16	15
Cr	19	19	21	19	23	29	31	24	41
Co	6	7	6	7	5	5	5	4	4
Ni	12	14	12	15	16	17	12	10	12
Rb	38	26	23	31	24	24	27	25	26
Sr	441	372	448	418	312	472	534	393	368
Y	1.80	2.40	2.37	1.74	1.81	1.53	2.07	2.41	0.71
Nb	2.12	2.53	2.47	1.63	1.90	2.47	2.06	1.91	1.72
Ba	242	310	434	293	637	283	352	240	586
La	12.71	20.20	23.71	14.92	11.54	25.16	62.92	17.91	11.08
Ce	23.35	34.69	45.51	30.46	19.06	47.43	67.07	36.09	14.12
Pr	2.69	3.82	4.86	2.93	1.77	4.88	10.30	3.94	1.54
Nd	9.69	12.95	16.44	9.99	5.85	15.56	32.36	13.79	4.44
Sm	1.50	1.87	2.36	1.42	0.76	1.85	3.18	1.92	0.45
Eu	0.56	0.52	0.61	0.51	0.74	0.71	0.68	0.49	0.60
Gd	0.98	1.20	1.33	0.90	0.50	0.86	1.32	1.08	0.20
Tb	0.10	0.13	0.15	0.10	0.06	0.09	0.13	0.12	0.02
Dy	0.43	0.57	0.61	0.42	0.30	0.37	0.48	0.55	0.11
Ho	0.07	0.09	0.09	0.07	0.06	0.06	0.08	0.09	0.02
Er	0.18	0.26	0.25	0.19	0.23	0.18	0.27	0.27	0.08
Tm	0.02	0.03	0.03	0.02	0.04	0.02	0.02	0.03	0.01
Yb	0.11	0.16	0.14	0.11	0.27	0.09	0.08	0.15	0.07
Lu	0.02	0.03	0.02	0.02	0.05	0.02	0.02	0.02	0.01
Ta	0.06	0.04	0.05	0.08	0.06	0.06	0.05	0.06	0.05
Pb	8.33	10.45	10.56	9.92	10.14	8.68	12.38	9.34	10.04
Th	0.74	1.57	4.21	1.10	3.05	3.81	5.85	2.96	0.56
U	0.23	1.33	0.23	0.26	0.97	0.35	0.32	0.50	0.48
A/CNK	1.03	1.05	1.04	1.03	1.01	1.15	1.10	1.06	1.09
Na_2O/K_2C	3.1	3.1	3.7	3.5	3.8	4.2	3.5	3.3	2.7
Sr/Y	245	155	189	240	173	308	258	163	519
La/Yb_{cn}	78	83	115	89	29	186	547	82	112
Eu/Eu*	1.40	1.07	1.05	1.39	3.66	1.72	1.01	1.04	6.14
Ce/Ce*	0.94	0.92	0.99	1.08	0.99	1.00	0.62	1.01	0.27
Yb_{cn}	0.45	0.66	0.56	0.46	1.08	0.37	0.31	0.60	31.8
Nb/Nb*	0.17	0.11	0.06	0.10	0.08	0.06	0.03	0.06	0.17
Zr/Zr*	1.63	1.58	1.14	2.31	6.19	1.39	0.78	1.21	2.75
Pb/Pb*	10.7	9.3	7.2	10.7	17.8	5.8	4.8	8.0	22.0
Sr/Sr*	3.7	2.2	2.1	3.4	4.1	2.4	1.3	2.4	6.4
Ti/Ti*	0.68	0.63	0.54	0.74	0.70	0.60	0.46	0.51	0.68
North	63°12′11.5″	63°12′4.8″	63°11′59.1″	63°11′59.5″	63°11′55.9″	63°15′35.4″	63°15′34.5″	63°15′33.5″	63°15′31.3″
West	50°29′43.4″	50°29′35.3″	50°29′36.3″	50°29′55.3″	50°31′7.8″	50°1′0.5″	50°1′2.6″	50°1′2.3″	50°1′20.6″

Table 4.2 (continued)

	Majorqap qâva			Camp 3					
	509068	509069	509070	509073	509076	509078[a]	509082[a]	509089	509093[a]
SiO_2	69.2	67.9	67.6	71.6	69.8	67.9	69.0	69.3	70.2
Al_2O_3	15.9	16.3	17.8	15.4	15.7	15.9	16.2	15.1	16.2
Fe_2O_3	3.6	3.0	2.7	2.7	2.7	3.1	2.7	3.1	2.6
MnO	0.035	0.038	0.033	0.047	0.04	0.044	0.027	0.042	0.034
MgO	1.05	1.14	1.29	0.76	0.95	1.04	1	1.1	0.85
CaO	3.6	3.68	3.46	3.07	3.32	3.58	3.62	3.37	3.22
Na_2O	4.4	4.56	5.13	4.65	4.76	4.33	4.78	4.55	4.88
K_2O	1.31	1.24	1.86	1.45	1.51	1.52	1.29	1.49	1.78
TiO_2	0.381	0.309	0.369	0.284	0.283	0.326	0.402	0.328	0.328
P_2O_5	0.11	0.09	0.07	0.08	0.08	0.1	0.13	0.12	0.1
LOI	0.88	0.47	0.5	0.01	0.11	0.13	0.13	0.08	0.27
Total	100.4	98.67	100.8	100	99.17	98.02	99.18	98.65	100.4
Mg#	37	43	49	36	41	40	42	41	39
Sc	3	5	4	4	5	4	4	5	4
Zr	115	93	127	121	105	117	113	127	110
V	38	37	27	25	28	30	34	40	27
Cr	28	22	18	11	11	11	11	12	9
Co	8	8	7	5	6	7	6	7	5
Ni	13	17	18	10	13	13	14	15	8
Rb	27	27	45	56	57	64	44	54	60
Sr	526	431	448	253	262	286	424	320	388
Y	1.65	5.63	2.30	4.93	4.00	5.21	3.63	3.49	4.89
Nb	1.72	2.42	3.53	3.10	3.25	2.85	3.47	3.69	2.46
Ba	441	324	320	158	169	191	217	162	218
La	21.03	22.52	36.60	15.26	12.86	13.20	17.78	19.14	44.92
Ce	39.37	45.06	75.11	29.34	24.42	29.29	41.82	33.97	61.95
Pr	4.14	5.13	7.88	3.06	2.75	2.80	3.96	4.10	9.28
Nd	13.81	17.93	26.50	10.63	9.71	9.83	14.13	14.18	30.96
Sm	1.68	2.63	3.29	1.68	1.63	1.56	2.19	2.14	4.32
Eu	0.63	0.62	0.63	0.42	0.41	0.46	0.62	0.51	0.57
Gd	0.77	1.60	1.45	1.19	1.15	1.09	1.33	1.38	2.45
Tb	0.09	0.22	0.16	0.17	0.15	0.16	0.16	0.17	0.26
Dy	0.38	1.16	0.60	0.93	0.80	0.92	0.81	0.78	1.12
Ho	0.06	0.21	0.09	0.18	0.14	0.19	0.14	0.13	0.18
Er	0.18	0.61	0.27	0.54	0.43	0.62	0.39	0.38	0.52
Tm	0.02	0.08	0.02	0.07	0.05	0.09	0.04	0.04	0.05
Yb	0.08	0.46	0.11	0.46	0.34	0.64	0.23	0.24	0.27
Lu	0.01	0.07	0.02	0.07	0.05	0.10	0.04	0.04	0.04
Ta	0.03	0.14	0.09	0.21	0.22	0.21	0.17	0.25	0.13
Pb	6.79	11.31	11.74	12.66	20.32	8.02	9.98	9.24	10.86
Th	1.31	3.66	10.70	3.17	2.44	3.52	6.36	4.32	7.92
U	0.72	0.29	0.79	6.05	0.56	0.52	0.65	1.58	0.50
A/CNK	1.04	1.05	1.06	1.04	1.01	1.04	1.02	0.99	1.03
Na_2O/K_2C	3.4	3.7	2.8	3.2	3.2	2.8	3.7	3.1	2.7
Sr/Y	320	76	195	51	66	55	117	92	79
La/Yb_{cn}	168	33	225	22	26	14	51	53	112
Eu/Eu*	1.68	0.92	0.89	0.90	0.92	1.07	1.11	0.90	0.54
Ce/Ce*	0.99	0.98	1.04	1.01	0.96	1.13	1.17	0.90	0.71
Yb_{cn}	0.34	1.87	0.44	1.86	1.36	2.56	0.95	0.98	1.09
Nb/Nb*	0.08	0.06	0.04	0.11	0.14	0.10	0.08	0.10	0.03
Zr/Zr*	1.48	0.84	0.84	1.78	1.64	1.86	1.26	1.43	0.59
Pb/Pb*	5.4	7.6	4.9	13.6	25.3	9.0	7.9	8.0	4.6
Sr/Sr*	3.1	2.0	1.4	2.0	2.2	2.3	2.5	1.8	1.1
Ti/Ti*	0.89	0.50	0.62	0.65	0.66	0.74	0.71	0.63	0.45
North	63°15′29.4	63°15′30″	63°15′30.7″	63°6′59.6″	63°6′56.7″	63°6′57.3″	63°6′52.2″	63°7′9.4″	63°7′5.4″
West	50°1′13″	50°1′11.9″	50°1′7.8″	50°15′51.9″	50°15′50.2″	50°15′53.7″	50°16′12″	50°17′31.9″	50°17′32.6″

Table 4.2 (continued)

	Camp 3	Base Camp							
	509094	509098	509099	509100	509703	509704	509706	509707	509708
SiO_2	68.5	66.3	71.5	69.1	68.6	67.5	69.0	70.3	67.8
Al_2O_3	16.3	16.4	15.2	15.9	13.9	16.5	16.3	15.6	16.5
Fe_2O_3	2.8	5.0	3.4	3.5	5.6	2.6	3.6	2.1	2.6
MnO	0.034	0.052	0.038	0.047	0.054	0.03	0.033	0.018	0.025
MgO	0.94	1.47	1.09	0.91	1.13	0.92	1.06	0.57	0.78
CaO	3.43	4.46	3.93	3.96	4.08	3.75	4.15	3.32	3.67
Na_2O	4.8	4.42	4.22	4.59	3.49	4.43	4.43	4.69	4.9
K_2O	1.51	1.17	0.78	1.07	0.98	1.26	1.13	1.21	1.3
TiO_2	0.374	0.489	0.35	0.353	0.584	0.372	0.427	0.231	0.443
P_2O_5	0.1	0.16	0.1	0.11	0.24	0.12	0.14	0.02	0.13
LOI	0.13	-0.01	0.4	-0.07	0.96	1.33	0.35	0.59	0.22
Total	98.9	99.93	101	99.56	99.58	98.84	100.6	98.64	98.4
Mg#	40	37	39	34	28	41	37	35	37
Sc	4	6	4	4	4	4	5	2	3
Zr	116	132	124	140	217	143	145	81	126
V	32	54	36	30	62	23	44	22	37
Cr	9	17	10	9	19	9	7	7	11
Co	6	12	7	7	11	5	9	4	5
Ni	11	24	15	13	22	13	30	7	14
Rb	50	20	10	5	15	21	27	18	12
Sr	538	436	479	451	386	649	475	493	674
Y	2.49	5.10	1.53	3.04	5.61	3.37	3.78	1.15	3.01
Nb	2.29	2.74	1.33	2.50	2.65	2.49	2.55	1.39	2.57
Ba	307	371	407	462	583	638	332	477	748
La	16.87	24.12	12.94	23.48	25.61	32.20	33.23	47.39	25.86
Ce	34.07	46.83	20.99	43.13	57.04	59.61	69.68	85.97	46.20
Pr	3.75	5.08	2.16	4.40	5.75	6.00	6.68	8.24	4.72
Nd	13.28	17.84	7.37	14.98	20.54	19.67	22.31	25.87	15.92
Sm	1.94	2.60	0.97	1.97	2.91	2.43	2.90	2.71	2.03
Eu	0.56	0.78	0.67	0.87	0.79	0.95	0.73	0.75	0.92
Gd	1.07	1.70	0.68	1.26	1.93	1.46	1.67	1.17	1.26
Tb	0.12	0.22	0.07	0.15	0.24	0.17	0.20	0.11	0.14
Dy	0.56	1.10	0.34	0.69	1.19	0.76	0.88	0.33	0.68
Ho	0.09	0.20	0.06	0.12	0.22	0.13	0.15	0.05	0.12
Er	0.28	0.58	0.19	0.37	0.65	0.42	0.46	0.19	0.36
Tm	0.03	0.07	0.02	0.04	0.08	0.04	0.05	0.01	0.04
Yb	0.19	0.42	0.15	0.25	0.45	0.24	0.27	0.05	0.21
Lu	0.03	0.06	0.02	0.04	0.07	0.04	0.04	0.01	0.03
Ta	0.10	0.09	0.04	0.06	0.09	0.07	0.12	0.02	0.08
Pb	9.15	6.69	9.36	14.07	6.10	5.77	5.88	6.27	8.35
Th	4.78	0.75	0.32	1.09	2.41	3.56	8.09	12.77	0.72
U	0.40	0.55	0.46	0.32	0.69	0.37	0.27	19.07	0.29
A/CNK	1.03	0.98	1.01	1.00	0.97	1.07	1.01	1.04	1.02
Na_2O/K_2C	3.2	3.8	5.4	4.3	3.6	3.5	3.9	3.9	3.8
Sr/Y	216	86	313	149	69	193	126	429	224
La/Yb_{cn}	59	39	58	64	39	90	82	664	83
Eu/Eu*	1.20	1.14	2.53	1.68	1.01	1.54	1.02	1.28	1.76
Ce/Ce*	1.00	0.99	0.93	0.99	1.10	1.00	1.10	1.02	0.98
Yb_{cn}	0.78	1.69	0.61	1.00	1.81	0.97	1.11	0.19	0.85
Nb/Nb*	0.06	0.16	0.16	0.12	0.08	0.06	0.04	0.01	0.14
Zr/Zr*	1.42	1.21	2.88	1.60	1.74	1.28	1.12	0.60	1.38
Pb/Pb*	8.3	4.4	14.2	10.4	3.4	3.1	2.8	2.4	5.8
Sr/Sr*	3.4	2.1	5.7	2.5	1.6	2.7	1.8	1.5	3.4
Ti/Ti*	0.77	0.68	0.83	0.55	0.76	0.51	0.62	0.40	0.66
North	63°7′5.4″	63°13′36″	63°13′37.8″	63°13′38.5″	63°12′56.1″	63°12′59.3″	63°13′0.8″	63°13′1.4″	63°13′1.9″
West	50°17′33.4″	50°34′6.2″	50°34′12.1″	50°34′7.7″	50°34′36.3″	50°34′25.6″	50°33′48.9″	50°33′49.3″	50°33′49.7″

Table 4.2 (continued)

	Sinarsuuk	
	508138[a]	508193[a]
SiO_2	65.2	63.7
Al_2O_3	18.2	15.6
Fe_2O_3	3.2	5.9
MnO	0.04	0.068
MgO	1.2	1.41
CaO	4.36	4.07
Na_2O	4.69	3.82
K_2O	1.73	1.98
TiO_2	0.389	0.998
P_2O_5	0.11	0.38
LOI	0.25	0.33
Total	99.42	98.2
Mg#	43	32
Sc	3	6
Zr	170	402
V	38	58
Cr	10	20
Co	9	13
Ni	24	45
Rb	50	39
Sr	618	442
Y	3.69	10.26
Nb	3.05	14.64
Ba	366	611
La	29.69	63.69
Ce	85.49	141.05
Pr	7.00	12.88
Nd	23.02	43.14
Sm	3.24	6.17
Eu	0.73	1.37
Gd	1.89	4.27
Tb	0.21	0.51
Dy	0.84	2.30
Ho	0.14	0.37
Er	0.43	1.03
Tm	0.04	0.11
Yb	0.26	0.61
Lu	0.04	0.09
Ta	0.09	0.66
Pb	7.10	6.15
Th	10.34	6.08
U	0.57	0.26
A/CNK	1.04	0.99
Na_2O/K_2O	2.7	1.9
Sr/Y	168	43
La/Yb_{cn}	78	71
Eu/Eu*	0.90	0.81
Ce/Ce*	1.39	1.15
Yb_{cn}	1.04	2.44
Nb/Nb*	0.04	0.18
Zr/Zr*	1.22	1.53
Pb/Pb*	3.0	1.5
Sr/Sr*	2.1	0.8
Ti/Ti*	0.53	0.67
North	63o 20' 53.7"	63o 20' 24.2"
West	49o 15' 34.7"	49o 15' 53.3"

cn: chondrite -normalized. [a] Altered

Table 4.3
Major (wt.%) and trace (ppm) element concentrations and significant element ratios for granodiorite.

	Camp 1					Camp 2	
	509002	509004	509011	509014	509017	509032	509050
SiO_2	71.8	70.3	69.8	68.7	72.7	74.7	71.7
Al_2O_3	15.2	14.8	15.6	15.5	14.3	14.2	14.9
Fe_2O_3	1.9	2.8	3.1	3.5	2.0	0.9	2.1
MnO	0.019	0.056	0.047	0.041	0.033	0.021	0.021
MgO	0.65	0.77	0.93	0.87	0.51	0.25	0.67
CaO	2.72	2.41	3	3.17	2.3	2.42	2.98
Na_2O	3.46	3.93	4.26	4.13	3.88	4.29	4.14
K_2O	3.74	3.42	2.18	2.4	3.41	2.53	2.17
TiO_2	0.247	0.44	0.406	0.52	0.22	0.068	0.321
P_2O_5	0.08	0.15	0.11	0.12	0.06	0.04	0.12
LOI	0.36	0.13	0.19	0.2	0.22	0.24	0.12
Total	100.2	99.18	99.6	99.12	99.64	99.7	99.29
Mg#	40	36	37	33	33	35	38
Sc	3	5	5	5	3	1	3
Zr	131	257	143	199	134	18	161
V	20	30	42	49	19		22
Cr	18	27	17	13	14	12	22
Co	4	5	7	7	3	2	5
Ni	9	12	14	14	8	16	14
Rb	94	102	75	86	86	48	62
Sr	242	288	359	329	339	487	286
Y	2.77	7.08	6.44	11.47	3.85	0.82	2.93
Nb	2.57	7.85	4.01	7.10	4.41	3.84	3.31
Ba	660	656	499	412	1012	538	633
La	12.55	58.54	27.03	30.97	25.34	6.33	28.02
Ce	22.23	110.39	53.39	62.80	45.64	11.44	47.22
Pr	2.29	11.43	5.59	6.88	4.57	1.18	5.27
Nd	7.94	37.22	19.13	24.51	15.06	3.90	16.94
Sm	1.29	5.06	2.89	4.30	2.12	0.50	2.31
Eu	0.55	0.77	0.69	0.86	0.54	0.47	0.63
Gd	0.94	2.92	1.90	3.23	1.27	0.31	1.37
Tb	0.11	0.35	0.24	0.44	0.16	0.04	0.15
Dy	0.57	1.60	1.23	2.32	0.75	0.19	0.65
Ho	0.10	0.26	0.22	0.41	0.13	0.03	0.10
Er	0.29	0.72	0.65	1.16	0.41	0.09	0.31
Tm	0.04	0.08	0.08	0.14	0.06	0.01	0.03
Yb	0.25	0.44	0.49	0.80	0.32	0.06	0.22
Lu	0.04	0.06	0.07	0.11	0.06	0.01	0.04
Ta	0.05	0.30	0.19	0.56	0.08	0.06	0.08
Pb	18.07	16.73	15.50	14.27	15.55	13.42	12.42
Th	1.43	16.55	6.21	6.44	7.19	1.16	5.85
U	0.51	1.24	7.30	3.69	1.55	0.58	4.47
A/CNK	1.034	1.020	1.050	1.023	1.002	1.000	1.019
Na_2O/K_2C	0.9	1.1	2.0	1.7	1.1	1.7	1.9
Sr/Y	88	41	56	29	88	597	98
La/Yb_{cn}	34	91	37	26	54	67	85
Eu/Eu*	1.53	0.61	0.91	0.71	1.02	3.58	1.08
Ce/Ce*	0.97	1.00	1.02	1.01	0.99	0.98	0.91
Yb_{cn}	1.01	1.76	1.98	3.23	1.28	0.26	0.90
Nb/Nb*	0.15	0.06	0.08	0.12	0.08	0.34	0.06
Zr/Zr*	2.55	1.16	1.19	1.20	1.47	0.80	1.60
Pb/Pb*	25.85	4.80	9.16	7.00	10.98	37.21	8.03
Sr/Sr*	2.58	0.61	1.48	1.07	1.72	9.48	1.33
Ti/Ti*	0.55	0.47	0.57	0.50	0.43	0.29	0.56
North	63°10′16.8″	63°10′17.7″	63°10′29.8″	63°10′28.3″	63°10′20.6″	63°12′29.7″	63°11′58.4″
West	50°36′59.5″	50°36′49.2″	50°35′16.2″	50°35′47.9″	50°36′36.9″	50°30′57.3″	50°31′13.2″

Table 4.3 (continued)

	Camp 3		Sinarsuuk				
	509079	509085[a]	508135	508136	508139	508152[a]	508158
SiO_2	73.3	70.8	65.2	72.7	68.6	68.8	69.5
Al_2O_3	14.8	15.0	18.6	14.3	14.9	15.8	15.9
Fe_2O_3	1.1	2.5	1.8	1.4	3.3	2.4	1.8
MnO	0.025	0.035	0.023	0.018	0.045	0.044	0.022
MgO	0.28	0.82	0.8	0.31	0.8	0.75	0.68
CaO	2.49	2.86	4.43	2.17	2.84	3.04	3.36
Na_2O	4.28	3.83	4.28	3.71	3.5	4.03	3.82
K_2O	2.62	3.08	2.87	3.33	3.38	2.84	2.62
TiO_2	0.096	0.331	0.231	0.127	0.612	0.249	0.227
P_2O_5	0.05	0.11	0.08	0.04	0.18	0.1	0.08
LOI	0.03	-0.06	0.39	0.18	0.3	0.14	0.14
Total	99.1	99.33	98.61	98.28	98.42	98.24	98.09
Mg#	33	40	48	31	33	38	42
Sc	2	4	2	1	4	3	2
Zr	63	138	89	91	342	160	139
V	6	26	21	7	38	22	23
Cr	11	12	9	7	13	14	9
Co	2	6	6	2	7	5	5
Ni	5	14	17	6	28	17	16
Rb	53	70	69	63	69	75	55
Sr	205	347	465	296	453	530	438
Y	3.90	2.80	0.76	2.33	6.53	7.96	1.86
Nb	1.81	2.62	0.87	2.50	6.80	7.16	1.69
Ba	347	814	355	1072	892	1333	1121
La	11.52	12.13	3.29	27.31	49.94	66.07	23.09
Ce	21.53	64.13	6.00	54.48	100.98	146.03	43.30
Pr	2.26	3.36	0.67	5.58	10.37	13.75	4.45
Nd	7.86	11.44	2.37	17.96	34.55	43.64	14.73
Sm	1.32	1.78	0.41	2.27	4.96	4.98	1.79
Eu	0.38	0.52	0.25	0.43	1.21	0.77	0.41
Gd	0.94	0.86	0.31	1.28	3.05	2.72	0.97
Tb	0.13	0.13	0.03	0.13	0.35	0.32	0.09
Dy	0.69	0.62	0.16	0.53	1.55	1.47	0.35
Ho	0.14	0.11	0.03	0.08	0.25	0.26	0.06
Er	0.45	0.32	0.08	0.25	0.68	0.80	0.21
Tm	0.07	0.04	0.01	0.02	0.07	0.08	0.02
Yb	0.45	0.23	0.05	0.14	0.32	0.48	0.13
Lu	0.07	0.04	0.01	0.03	0.04	0.07	0.02
Ta	0.08	0.25	0.02	0.05	0.29	0.40	0.08
Pb	13.72	9.12	10.50	14.96	9.91	19.49	9.90
Th	4.03	7.35	0.30	8.31	7.76	13.10	5.46
U	1.87	0.49	0.11	0.60	0.43	1.32	0.39
A/CNK	1.030	1.013	1.022	1.049	1.023	1.038	1.041
Na_2O/K_2C	1.6	1.2	1.5	1.1	1.0	1.4	1.5
Sr/Y	53	124	614	127	69	67	236
La/Yb_{cn}	17	36	41	135	105	93	118
Eu/Eu*	1.04	1.29	2.10	0.77	0.95	0.64	0.96
Ce/Ce*	0.99	2.35	0.95	1.03	1.04	1.14	1.00
Yb_{cn}	1.83	0.92	0.22	0.55	1.29	1.94	0.53
Nb/Nb*	0.06	0.07	0.21	0.04	0.08	0.06	0.04
Zr/Zr*	1.22	1.90	5.62	0.89	1.62	0.67	1.68
Pb/Pb*	20.09	6.34	53.52	8.76	3.12	4.44	7.28
Sr/Sr*	2.21	2.46	15.93	1.27	1.02	0.94	2.24
Ti/Ti*	0.26	0.79	1.34	0.28	0.51	0.28	0.58
North	63°6′56.9″	63°7′11.2″	63o 20' 57"	63o 20' 56.6"	63o 20' 58.8"	63o 20' 50.7"	63o 20' 56.7"
West	50°16′11.6″	50°17′20.6″	49o 15' 19"	49o 15' 21"	49o 15' 47.5"	49o 15' 43.1"	49o 16' 17.2"

cn: chondrite -normalized. [a] Altered

Table 4.4

Major (wt.%) and trace (ppm) element concentrations and significant element ratios for granite.

	Camp 1						Camp 2		
	509006	509008	509023	509024	509026	509029	509039	509044	509046
SiO_2	72.9	75.46	70.21	71.36	72.09	71.82	73.21	73.78	72.73
Al_2O_3	13.96	14.03	14.88	14.59	14.44	14.2	13.7	14.66	14.01
Fe_2O_3	1.42	0.87	2.46	2.16	1.67	2.03	2.05	1.55	1.64
MnO	0.026	0.01	0.03	0.034	0.034	0.025	0.033	0.028	0.038
MgO	0.22	0.05	0.54	0.47	0.33	0.52	0.45	0.37	0.36
CaO	1.33	1.4	1.99	1.95	1.74	2.13	1.89	1.93	1.65
Na_2O	3.6	3.07	4.13	3.95	3.93	2.94	3.44	3.89	3.89
K_2O	4.84	5.69	3.6	3.81	3.99	4.86	4.19	4.11	4
TiO_2	0.149	0.043	0.36	0.289	0.176	0.254	0.272	0.164	0.201
P_2O_5	0.06	0.03	0.1	0.09	0.07	0.08	0.1	0.07	0.08
LOI	0.42	0.12	0.3	0.24	0.06	0.39	0.06	0.08	0.02
Total	98.91	100.8	98.58	98.94	98.52	99.27	99.38	100.6	98.62
Mg#	23.49	10.22	30.31	30.12	28.13	33.66	30.31	32.11	30.31
Sc	2		3	3	2	2	3	3	3
Zr	96	86	233	205	136	194	179	105	161
V	6	10	23	19	7	14	18	11	10
Cr	13	15	13	17	13	15	15	21	16
Co	2	1	4	4	2	3	3	3	3
Ni	4	4	11	11	10	12	10	9	11
Rb	101	135	105	103	105	104	109	80	90
Sr	252	99	330	237	175	294	248	194	170
Y	2.32	0.74	4.57	5.54	4.63	4.21	7.21	3.98	8.97
Nb	3.02	0.40	6.19	8.72	5.72	4.42	6.08	2.72	10.10
Ba	628	544	814	664	646	992	887	478	698
La	17.16	11.07	52.64	48.10	48.28	60.36	47.16	27.13	40.69
Ce	34.80	14.01	101.11	87.67	85.09	105.61	90.19	54.41	76.98
Pr	3.83	1.14	10.72	9.01	8.22	10.36	9.90	5.59	7.15
Nd	13.12	3.16	34.98	28.45	25.03	31.90	32.42	18.55	22.30
Sm	1.96	0.37	4.49	3.86	3.29	4.07	4.51	2.86	3.33
Eu	0.66	0.58	0.87	0.73	0.53	0.72	0.71	0.52	0.49
Gd	1.20	0.22	2.26	2.18	1.86	2.12	2.51	1.83	2.30
Tb	0.13	0.03	0.25	0.27	0.24	0.25	0.30	0.21	0.34
Dy	0.56	0.12	1.06	1.21	1.05	1.01	1.40	0.91	1.75
Ho	0.09	0.02	0.16	0.19	0.16	0.16	0.24	0.15	0.30
Er	0.23	0.08	0.47	0.54	0.46	0.44	0.72	0.41	0.87
Tm	0.03	0.01	0.05	0.06	0.05	0.04	0.09	0.04	0.11
Yb	0.16	0.10	0.29	0.36	0.31	0.27	0.51	0.28	0.68
Lu	0.03	0.02	0.04	0.05	0.05	0.05	0.07	0.05	0.10
Ta	0.04	0.02	0.28	0.23	0.20	0.12	0.35	0.04	0.51
Pb	21.35	30.61	14.14	14.31	18.20	17.95	18.42	19.98	19.09
Th	9.95	1.78	10.94	15.67	23.60	30.98	12.43	10.41	22.08
U	0.71	0.45	0.77	0.85	1.29	14.09	0.94	4.37	3.16
A/CNK	1.03	1.02	1.04	1.03	1.04	1.02	1.01	1.02	1.02
Na_2O/K_2O	0.7	0.5	1.1	1.0	1.0	0.6	0.8	0.9	1.0
Sr/Y	109	133	72	43	38	70	34	49	19
La/Yb_{cn}	72	78	123	90	104	151	62	65	40
Eu/Eu*	1.33	6.23	0.84	0.76	0.65	0.75	0.65	0.69	0.54
Ce/Ce*	1.01	0.92	1.00	0.99	1.00	0.99	0.98	1.04	1.06
Yb_{cn}	0.65	0.39	1.16	1.45	1.26	1.09	2.07	1.15	2.75
Nb/Nb*	0.06	0.02	0.06	0.08	0.04	0.02	0.06	0.04	0.08
Zr/Zr*	1.17	4.95	1.16	1.22	0.93	1.06	0.92	0.90	1.16
Pb/Pb*	18.87	78.17	4.38	5.20	7.02	5.54	6.29	11.69	8.30
Sr/Sr*	1.51	2.22	0.76	0.65	0.54	0.74	0.61	0.86	0.59
Ti/Ti*	0.27	0.19	0.41	0.37	0.29	0.33	0.33	0.27	0.30
North	63°10′30.5″	63°10′20.6″	63°11′12.3″	63°11′12.3″	63°11′20.4″	63°11′25.7″	63°12′2.5″	63°11′55.8″	63°12′18.5″
West	50°36′26.6″	50°35′53.4″	50°35′13.6″	50°35′17.8″	50°35′38.7″	50°35′49.5″	50°31′9.3″	50°30′25.5″	50°30′13.9″

Table 4.4 (continued)

	Camp 2				Camp 3				
	509051	509052	509056	509057	509062[a]	509063	509071	509075[a]	509080
SiO_2	75.36	76.58	75.86	75.87	73.57	72.87	73.9	70.27	75.83
Al_2O_3	13.8	13.27	13.75	13.23	13.31	14.02	14.39	15.14	13.03
Fe_2O_3	0.62	1.02	0.6	1.04	1.19	1.72	0.86	2.15	0.93
MnO	0.049	0.026	0.007	0.019	0.036	0.031	0.013	0.03	0.064
MgO	0.07	0.17	0.01	0.16	0.18	0.31	0.21	0.66	0.19
CaO	0.89	1.08	1.21	1	1.09	1.65	1.59	1.95	1.05
Na_2O	3.58	3.39	3.43	3.16	2.77	3.52	3.53	4.24	3.68
K_2O	5.32	4.97	5.1	5.21	5.91	4.25	4.82	3.78	4.67
TiO_2	0.04	0.124	0.032	0.131	0.098	0.161	0.091	0.414	0.081
P_2O_5	0.08	0.04	0.02	0.02	0.04	0.03	0.03	0.13	0.03
LOI	0.02	0.01	0	-0.03	0.08	0.07	0.06	-0.02	0.02
Total	99.82	100.7	100	99.82	98.26	98.64	99.5	98.75	99.59
Mg#	18.28	24.82	3.20	23.36	23.06	26.31	32.60	37.82	28.81
Sc	1	2		2	3	4	2	3	4
Zr	47	83	60	89	84	113	79	192	55
V						10		25	
Cr	13	16	17	14	17	17	10	12	10
Co	1	1	1	1	1	2	1	5	1
Ni	6	7	6	7	6	7	4	10	4
Rb	107	100	102	113	181	140	90	90	94
Sr	101	328	264	304	80	84	249	600	111
Y	5.22	4.85	0.37	5.12	13.81	10.53	1.72	4.43	10.96
Nb	0.68	2.81	0.28	3.03	5.87	5.85	2.38	5.76	2.22
Ba	234	2108	906	2236	290	290	971	1023	252
La	7.68	54.39	3.91	58.36	21.00	40.64	13.76	65.72	8.10
Ce	16.27	107.30	5.63	112.73	53.15	69.50	23.41	86.41	16.93
Pr	1.88	11.68	0.49	12.16	5.68	7.99	2.32	11.94	2.09
Nd	6.34	38.28	1.37	39.63	19.70	25.69	7.51	36.66	7.94
Sm	1.24	4.59	0.16	4.64	3.99	4.17	1.12	4.09	1.88
Eu	0.37	0.95	0.47	0.94	0.29	0.43	0.27	0.71	0.31
Gd	0.87	2.25	0.09	2.21	2.82	3.14	0.68	1.81	1.63
Tb	0.13	0.25	0.01	0.26	0.43	0.44	0.08	0.21	0.25
Dy	0.84	1.14	0.05	1.13	2.44	2.20	0.39	0.95	1.70
Ho	0.18	0.18	0.01	0.19	0.49	0.39	0.06	0.16	0.39
Er	0.57	0.51	0.04	0.55	1.63	1.06	0.18	0.49	1.35
Tm	0.08	0.05	0.01	0.06	0.24	0.13	0.02	0.05	0.21
Yb	0.59	0.28	0.06	0.32	1.66	0.76	0.10	0.26	1.44
Lu	0.08	0.04	0.01	0.05	0.26	0.12	0.02	0.04	0.21
Ta	0.02	0.06	0.02	0.10	0.12	0.10	0.04	0.45	0.01
Pb	27.41	22.39	19.86	22.71	31.82	34.06	19.01	14.58	15.80
Th	3.93	13.39	0.60	14.32	30.25	21.22	6.56	18.05	4.39
U	0.60	1.01	0.50	0.99	4.98	45.22	0.79	0.70	0.36
A/CNK	1.04	1.03	1.03	1.05	1.03	1.05	1.03	1.04	1.00
Na_2O/K_2O	0.7	0.7	0.7	0.6	0.5	0.8	0.7	1.1	0.8
Sr/Y	19	68	709	59	6	8	145	135	10
La/Yb_{cn}	9	132	42	122	9	36	89	173	4
Eu/Eu*	1.08	0.91	12.00	0.89	0.26	0.37	0.96	0.80	0.54
Ce/Ce*	1.00	1.00	0.95	0.99	1.14	0.90	0.97	0.72	0.96
Yb_{cn}	2.38	1.12	0.26	1.31	6.69	3.06	0.42	1.04	5.81
Nb/Nb*	0.03	0.03	0.05	0.03	0.06	0.05	0.06	0.04	0.09
Zr/Zr*	1.04	0.39	8.01	0.41	0.59	0.68	1.69	0.97	0.88
Pb/Pb*	50.52	6.45	122.16	6.26	18.68	14.74	26.32	4.63	27.12
Sr/Sr*	1.30	0.72	14.74	0.61	0.36	0.27	2.66	1.25	1.20
Ti/Ti*	0.11	0.14	0.25	0.15	0.18	0.22	0.34	0.59	0.18
North	63°11′46.7″	63°11′45.3″	63°11′46.8″	63°11′47.7″	63°6′39.4″	63°6′35.5″	63°6′59.4″	63°6′58.2″	63°6′56.5″
West	50°31′17.8″	50°31′14.3″	50°31′14.3″	50°31′11.4″	50°18′11″	50°18′9.1″	50°15′45.4″	50°15′50.4″	50°16′12.3″

Table 4.4 (continued)

	Camp 3			Sinarsuuk		
	509090	509091[a]	509092[a]	508134	508137[a]	508141
SiO_2	73.1	72.18	74.54	71.56	71.79	67.75
Al_2O_3	13.99	13.96	14.71	14.52	14.29	14.35
Fe_2O_3	1.3	1.87	1.41	2.01	1.57	3.13
MnO	0.019	0.021	0.022	0.039	0.018	0.028
MgO	0.26	0.41	0.31	0.49	0.37	0.78
CaO	1.22	1.84	1.4	2.07	2.2	2.73
Na_2O	3.92	3.38	4.3	3.66	2.61	2.47
K_2O	4.68	4.21	4.01	3.97	5.12	4.44
TiO_2	0.197	0.233	0.204	0.169	0.118	0.413
P_2O_5	0.06	0.07	0.07	0.08	0.05	0.14
LOI	-0.02	0.33	-0.1	0.19	0.2	0.31
Total	98.72	98.51	100.9	98.75	98.33	96.55
Mg#	28.38	30.28	30.34	32.57	31.83	33.05
Sc	2	2	2	2	1	3
Zr	137	184	136	171	108	327
V	7	16	7	15		25
Cr	6	8	7	6	20	8
Co	2	5	2	3	2	5
Ni	5	8	6	11	9	21
Rb	72	62	62	88	104	98
Sr	346	416	345	539	259	397
Y	4.71	6.37	6.64	4.79	1.83	3.35
Nb	3.55	3.10	3.21	3.08	2.13	1.92
Ba	787	906	764	1295	1303	1580
La	53.95	88.80	53.15	50.00	18.71	135.33
Ce	122.26	130.28	82.83	98.54	43.03	240.09
Pr	12.93	19.27	12.46	10.01	4.36	20.10
Nd	40.97	62.00	40.56	32.02	14.35	58.99
Sm	5.04	7.60	5.02	4.03	2.17	5.80
Eu	0.79	1.14	0.78	0.70	0.38	0.94
Gd	2.24	4.09	2.64	2.21	1.20	2.70
Tb	0.29	0.41	0.30	0.24	0.13	0.25
Dy	1.19	1.64	1.40	1.01	0.49	0.80
Ho	0.17	0.25	0.23	0.16	0.07	0.13
Er	0.52	0.75	0.70	0.49	0.20	0.53
Tm	0.05	0.07	0.07	0.05	0.02	0.04
Yb	0.21	0.36	0.33	0.29	0.09	0.18
Lu	0.04	0.07	0.05	0.05	0.02	0.04
Ta	0.07	0.04	0.07	0.08	0.03	0.02
Pb	24.00	20.57	20.18	21.78	14.09	14.43
Th	11.56	22.92	13.63	13.30	9.05	16.85
U	1.06	5.27	4.91	0.63	0.37	0.35
A/CNK	1.02	1.04	1.05	1.03	1.03	1.04
Na_2O/K_2O	0.8	0.8	1.1	0.9	0.5	0.6
Sr/Y	73	65	52	112	141	118
La/Yb_{cn}	176	165	109	115	137	506
Eu/Eu*	0.72	0.63	0.66	0.71	0.72	0.72
Ce/Ce*	1.08	0.74	0.75	1.03	1.12	1.08
Yb_{cn}	0.84	1.46	1.33	1.19	0.37	0.73
Nb/Nb*	0.03	0.02	0.03	0.03	0.04	0.01
Zr/Zr*	0.59	0.53	0.59	0.93	1.20	1.10
Pb/Pb*	6.16	4.19	6.41	7.07	10.50	2.12
Sr/Sr*	0.66	0.53	0.70	1.32	1.41	0.49
Ti/Ti*	0.24	0.17	0.23	0.22	0.28	0.42
North	63°7′7.7″	63°7′4.7″	63°7′8″	63o 20' 52.3"	63o 20' 55.5"	63o 21' 24.8"
West	50°17′32.2″	50°17′33.2″	50°17′33.2″	49o 14' 52.3"	49o 15' 28.5"	49o 16' 42.1"

cn: chondrite -normalized. [a] Altered

CHAPTER 5

Conclusions and Implications

5.1. Formation of the Fiskenæsset Complex

The Fiskenæsset Complex has very fresh cumulative rocks and displays original magmatic stratigraphy. In addition, petrographic analyses show that these rocks preserve their original igneous textures and geochemical data illustrate that these rocks also retain their primary magmatic signatures. A notable feature of the Fiskenæsset Complex was the early fractionation of olivine, pyroxene and hornblende and the late appearance of plagioclase as a major cumulus phase. This sequence of crystallization is similar to cumulate rocks from the Onion Valley Complex of the Sierra Nevada batholiths and the Alaskan-type complex on Duke Island (Irvine, 1974; Sisson et al., 1996). Moreover, experiments by Sisson and Grove (1993a, b) and Müntener et al. (2001) have demonstrated that high water content in the basic magmas suppresses the liquidus volume of plagioclase and enhances those of olivine and pyroxene, concomitantly, increases in the Al_2O_3 content in the residual melt allowing crystallization of late calcic plagioclase. It is therefore likely that the Fiskenæsset Complex crystallized from hydrous magmas, in which plagioclase crystallization was suppressed and only occurred in evolved liquid. Two distinct suites of magmas (Suites A and B) have been identified based on both whole rock and hornblende trace element geochemical compositions. The earlier Suite A is characterized by HREE-depletion whereas the later Suite B is characterized by HREE-enrichment. Fractionation and in situ crystallization of mafic magmas with elevated H_2O contents may explain the petrogenesis of the Fiskenæsset Complex. In hydrous magmas of Suite A, the overall increase in water promoted the early crystallization of olivine, pyroxene and hornblende, and most of the olivine pyroxene and hornblende formed during the ensuing period of crystallization were carried down to the bottom of the chamber where they were deposited as the Ultramafic

Unit consisting of dunite, peridotite, pyroxenite and hornblendite. The fractionation of olivine, pyroxene and hornblende led to a gradual build-up Al_2O_3 of in the residual liquid, so that eventually plagioclase began to precipitate and the Anorthosite Unit was produced. At about this time, intrusive activity was resumed, stimulated possibly by the injection of the late-stage water-rich gabbroic magmas of the Suite B which intruded into the partially solidified anorthosite magmas. Magma mixing between the gabbroic magmas of the Suite B and the anorthositic magmas produced part of the Upper Leucogabbro and Lower Leucogabbro Units.

5.2. Tectonic setting for the Fiskenæsset Complex

On the N-MORB-normalized diagrams, the rocks from the Fiskenæsset Complex at Majorqap qâva are characterized by Nb-Ta depletions. Polat et al. (2009, 2010, 2011a, 2012) noted that least-altered anorthosites, gabbros, leucogabbros, and peridotites of the Fiskenæsset Complex on Qeqertarssuatsiaq island and in the Sinarssuk area exhibit negative Nb anomalies on the N-MORB-normalized diagrams and argued the Nb depletion is a primary mantle source characteristic. However, Hoffmann et al. (2012) attributed negative Nb anomaly of the Naajat Kuuat Anorthosite Complex to the igneous fractionation processes. In addition, whole-rock trace elements of the Fiskenæsset Complex at Majorqap qâva exhibit enrichment in LILE (Pb and Sr), which is another typical feature of subduction-related magmatism. Experimentally, Brenan et al. (1995) provided good explation for the Pb enrichment in convergent-margin magmas. The common occurrence of hornblende and plagioclase with high An content point to the hydrous nature of the magma. In addition, anorthite-rich plagioclase is commonly found in island arc basalts on the volcanic front, which has been interpreted as crystallization from H_2O-rich basalt based on hydrous melting experiments (Arculus and Wills, 1980; Sisson and Grove, 1993a, 1993b; Takagi et al., 2005). Moreover, the striking similarity between the Fiskenæsset Complex and the cumulate rocks from the Onion Valley

Complex of the Sierra Nevada batholiths and the Alaskan-type complex on Duke Island further strengthen the Fiskenæsset Complex were produced in an island arc setting.

5.3. Formation of the Orthogneisses

The Archean orthogneisses in the Fiskenæsset region consist mostly of older TTGs and lesser amounts of younger high-K granites. The Fiskenæsset TTGs with enrichment of Th, U, Sr and Pb and fractionated REE patterns and low HREE are comparable to typical Archean TTGs (Martin et al., 2005 and references therein). It was unlikely for the Fiskenæsset TTGs deriving from the partial melting of preexisting TTG gneisses on the basis of the lack of geological evidence of ancient crust and their lower initial $^{87}Sr/^{88}Sr$ (Moorbath and Pankhurst, 1976; Myers, 1985). A genetic link between the TTGs and spatially associated metavolcanic amphibolites were established through field relationships, geochronology and trace element modeling. Geochemical characteristics of the Fiskenæsset TTGs suggest that they were produced by 20% partial melting of amphibolite with residual rutile-bearing eclogite at the base of a thickened arc. Compared with the Fiskenæsset TTGs, the granites have relative high K_2O and low Na_2O, Al_2O_3 and Sr contents. Based on the conclusion of experiments of Watkins et al. (2007), the granodiorites with relatively high K_2O/Na_2O are a possible source for the high-K granite. Following the foundering of the eclogite residue, the granodiorites were heated by underplating basaltic magma and partially melted to generate the high-K granites.

5.4. Tectonic Setting for the TTG Gneisses

Geochemical characteristics and modeling of trace element composition suggest that the production of the Fiskenæsset TTG-type melts requires magma generation to occur at P >15 kbar. In comparison with typical subduction induced adakites, the Fiskenæsset TTGs have relatively low MgO, Ni and Cr contents. Such typical signatures of the Fiskenæsset TTGs are explained by partial melting of hydrous basaltic material at the

base of thickened lower crust. On the basis of the lack of evidence for plume activity in the Fiskenæsset region, it can be argued against the possibility of melting of root of the oceanic plateau for the production of the Fiskenæsset TTGs (Bridgwater et al., 1974; Myers, 1976; Myers, 1985; Polat et al., 2009, 2010, 2011a, Windley and Garde, 2009). A shallow subduction driven tectonic thickening was ruled out as the amphibolites show geochemical characteristics of MORB-Island-Arc-Basalt affinity and the geochemistry of the Fiskenæsset Complex indicates that it originated in an intra-oceanic island arc (Polat et al., 2009, 2010, 2011a, 2011b, 2012). Given the availability of many island arcs to mutually accrete and amalgamate into microcontinents and the lack of major continents in existence in the Meso- to Neoarchean in West Greenland, an arc-arc collision as a consequence of horizontal tectonic regime was preferred for the lower crust thickening (Bridgwater et al., 1974; Myers, 1976, 1985).

5.5. Implication for the Archean Anorthosites

Traditionally, the generation of the Archean anorthosites is favored by a two-stage crystallization/emplacement model involving mantle-derived anhydrous magmas ponding and fractionation probably at the crust-mantle boundary, followed by shallow level emplacement of plagioclase-rich melts (Ashwal, 1993; Ashwal et al., 1994; Phinney et al., 1988). In addition, Phinney et al. (1988) also proposed a multistage petrogenetic model for the formation of the Archean anorthosites. Phinney et al. (1988) emphasized that the initial fractionation of large amounts of olivine and/or orthopyroxene of anhydrous mafic or ultramafic melt in a high-pressure magma chamber, the ensuing rise of the residual melt and the final crystallization of plagioclase in the residual magma in a low-pressure magma chamber. The processes related to the formation of the Fiskenæsset Complex serve as a proxy to refine the crystallization model of the Archean anorthosites and explain the occurrence of plagioclase with high An content. The Archean anorthosites, therefore, can be interpreted as the product of the igneous

differentiation of relatively hydrous basaltic magmas in the crust of island arcs (Irvine, 1974; Sisson et al., 1996).

5.6. Implication for the Growth of Continental Crust

Eoarchen to Neoarchean (ca. 3.8–2.7 Ga) TTG gneisses are extensively distributed in the Archean craton of SW Greenland (Nutman et al., 1993; Nutman et al., 1996; Garde, 1997; Steenfelt et al., 2005; Friend et al., 2009; Windley and Garde, 2009). The field observations and geochemistry of the Eoarchean to Neoarchean TTG-gneisses in SW Greenland were generally attributed to slab melting and the following interaction between the slab melts and the overlying mantle wedge to variable extent in oceanic and continental arc settings (Nutman et al., 1993; Nutman et al., 1996; Garde, 1997; Steenfelt et al., 2005; Friend et al., 2009; Windley and Garde, 2009; Tappe et al., 2011). According to the field relationships and geochemistry of the Fiskenæsset TTGs, partial melting of amphibolites under amphibolite to granulite facies at the base of a tectonically thickened crust is a feasible explanation for their origin. This study shows that crustal thickening might have led to the partial melting of the lower part of the overthickened island arc crust, leaving rutile-bearing residual eclogites behind. The residual eclogites in the lower crust, owing to their high densities, were eventually foundered into the mantle, leaving behind a more felsic crust. As for the results of this study, the melting of mafic volcanic rocks (amphibolites) in the eclogite facies at the base of overthickened arc may also have played an important role in the production of Mesoarchean continental crust in SW Greenland.

5.7. References

Arculus, R.J., Wills, K.J.A., 1980. The Petrology of Plutonic Blocks and Inclusions from the Lesser Antilles Island Arc. Journal of Petrology 21(4): 743-799.

Ashwal, L.D., 1993. Anorthosites. Minerals and Rocks Series, 21. Springer-Verlag,

Berlin, 422 pp.

Ashwal, L.D., Myers, J.S., Condie, K.C., 1994. Chapter 8 Archean anorthosites, Developments in Precambrian Geology. Elsevier, pp. 315-355.

Brenan, J.M., Shaw, H.F., Ryerson, F.J., 1995. Experimental evidence for the origin of lead enrichment in convergent-margin magmas. Nature 378(6552): 54-56.

Bridgwater, D., McGregor, V.R., Myers, J.S., 1974. A horizontal tectonic regime in the Archaean of Greenland and its implications for early crustal thickening. Precambrian Research 1(3): 179-197.

Friend, C.R.L., Nutman, A.P., Baadsgaard, H., Duke, M.J.M., 2009. The whole rock Sm-Nd 'age' for the 2825 Ma Ikkattoq gneisses (Greenland) is 800 Ma too young: Insights into Archaean TTG petrogenesis. Chemical Geology 261(1-2): 61-75.

Garde, A.A., 1997. Accretion and evolution of an Archaean high-grade grey gneissamphibolite complex: the Fiskefjord area, southern West Greenland. Geology of Greenland Survey Bulletin 177.

Hoffmann, J.E., Svahnberg, H., Piazolo, S., Scherstén, A., Münker, C., 2012. The geodynamic evolution of Mesoarchean anorthosite complexes inferred from the Naajat Kuuat Complex, southern West Greenland. Precambrian Research 196–197(0): 149-170.

Irvine, T.N., 1974. Petrology of the Duke Island Ultramafic Complex, Southeastern Alaska. Geological Society of America, Memoirs,138, 240 pp.

Martin, H., Smithies, R.H., Rapp, R., Moyen, J.F., Champion, D., 2005. An overview of adakite, tonalite-trondhjemite-granodiorite (TTG), and sanukitoid: relationships and some implications for crustal evolution. Lithos 79(1-2): 1-24.

Moorbath, S., Pankhurst, R.J., 1976. Further rubidium-strontium age and isotope evidence for the nature of the late Archaean plutonic event in West Greenland. Nature 262(5564): 124-126.

Müntener, O., Kelemen, P., Grove, T., 2001. The role of H_2O during crystallization of

primitive arc magmas under uppermost mantle conditions and genesis of igneous pyroxenites: an experimental study. Contributions to Mineralogy and Petrology 141(6): 643-658.

Myers, J.S., 1976. Granitoid sheets, thrusting, and Archean crustal thickening in West Greenland. Geology 4(5): 265-268.

Myers, J.S., 1985. Stratigraphy and structure of the Fiskenæsset complex, southernWest Greenland. Bulletin Grønlands Geologiske Undersøgelse 150: 1-72.

Nutman, A.P., Friend, C.R.L., Kinny, P.D., McGregor, V.R., 1993. Anatomy of an Early Archean gneiss complex: 3900 to 3600 Ma crustal evolution in southern West Greenland. Geology 21(5): 415-418.

Nutman, A.P., McGregor, V.R., Friend, C.R.L., Bennett, V.C., Kinny, P.D., 1996. The Itsaq Gneiss Complex of southern West Greenland; the world's most extensive record of early crustal evolution (3900-3600 Ma). Precambrian Research 78(1-3): 1-39.

Phinney, W.C., Morrison, D.A., Maczuga, D.E., 1988. Anorthosites and related megacrystic units in the evolution of Archean crust. Journal of Petrology 29(6): 1283-1323.

Polat, A., Appel, P.W.U., Fryer, B., Windley, B., Frei, R., Samson, I.M., Huang, H., 2009. Trace element systematics of the Neoarchean Fiskenæsset anorthosite complex and associated meta-volcanic rocks, SW Greenland: Evidence for a magmatic arc origin. Precambrian Research 175(1-4): 87-115.

Polat, A., Frei, R., Scherstén, A., Appel, P.W.U., 2010. New age (ca. 2970 Ma), mantle source composition and geodynamic constraints on the Archean Fiskenæsset anorthosite complex, SW Greenland. Chemical Geology 277(1-2): 1-20.

Polat, A., Fryer, B.J., Appel, P.W.U., Kalvig, P., Kerrich, R., Dilek, Y., Yang, Z., 2011a. Geochemistry of anorthositic differentiated sills in the Archean (~ 2970 Ma) Fiskenæsset Complex, SW Greenland: Implications for parental magma compositions, geodynamic setting, and secular heat flow in arcs. Lithos 123(1-4): 50-72.

Polat, A., Appel, P.W.U., Fryer, B.J., 2011b. An overview of the geochemistry of Eoarchean to Mesoarchean ultramafic to mafic volcanic rocks, SW Greenland: Implications for mantle depletion and petrogenetic processes at subduction zones in the early Earth. Gondwana Research 20(2-3): 255-283.

Polat, A., Fryer, B.J., Samson, I.M., Weisener, C., Appel, P.W.U., Frei, R., Windley, B.F., 2012. Geochemistry of ultramafic rocks and hornblendite veins in the Fiskenæsset layered anorthosite complex, SW Greenland: Evidence for hydrous upper mantle in the Archean. Precambrian Research doi:10.1016/j.precamres.2011.11.013.

Sisson, T.W., Grove, T.L., 1993a. Experimental investigations of the role of H_2O in calc-alkaline differentiation and subduction zone magmatism Contributions to Mineralogy and Petrology 113(2): 143-166.

Sisson, T.W., Grove, T.L., 1993b. Temperatures and H_2O contents of low-MgO high-alumina basalts. Contributions to Mineralogy and Petrology 113(2): 167-184.

Sisson, T.W., Grove, T.L., Coleman, D.S., 1996. Hornblende gabbro sill complex at Onion Valley, California, and a mixing origin for the Sierra Nevada batholith. Contributions to Mineralogy and Petrology 126(1-2): 81-108.

Steenfelt, A., Garde, A.A., Moyen, J.-F., 2005. Mantle wedge involvement in the petrogenesis of Archaean grey gneisses in West Greenland. Lithos 79(1-2): 207-228.

Takagi, D., Sato, H., Nakagawa, M., 2005. Experimental study of a low-alkali tholeiite at 1–5 kbar: optimal condition for the crystallization of high-An plagioclase in hydrous arc tholeiite. Contributions to Mineralogy and Petrology 149(5): 527-540.

Tappe, S., Smart, K.A., Pearson, D.G., Steenfelt, A., Simonetti, A., 2011. Craton formation in Late Archean subduction zones revealed by first Greenland eclogites. Geology 39(12): 1103-1106.

Watkins, J., Clemens, J., Treloar, P., 2007. Archaean TTGs as sources of younger granitic magmas: melting of sodic metatonalites at 0.6–1.2 GPa. Contributions to Mineralogy and Petrology 154(1): 91-110.

Windley, B.F., Garde, A.A., 2009. Arc-generated blocks with crustal sections in the North Atlantic craton of West Greenland: Crustal growth in the Archean with modern analogues. Earth-Science Reviews 93(1-2): 1-30.

Vita Auctoris

Hua Huang was born in 1981 in P.R.China. He studied Geology at the China University of Geosciences (Wuhan), P.R.China, where he obtained his B.Sc. in geology in 2004. The same year he went on China University of Geosciences (Wuhan), P.R.China, where he continued studying geochemistry as a P.h.D student. In May 2008, he moved on to the University of Windsor in Canada, where he started his Ph.D. and is currently a doctoral candidate. He hopes to graduate in May.